THE UNIVERSITY
OF BIRMINGHAM

# The Modelling of Ferrite-Loaded Helical Devices

by Omar Qureshi

January 2011

# Acknowledgement

I would like to take this opportunity to express my gratitude to all the people who have aided me in the completion of this investigation. Dr P. Smith, Dr S. Stephen and Dr D. Leppinen have all supervised me throughout the duration of this research. I am very grateful for their continual encouragement, support and assistance throughout this work. I also wish to thank EPSRC for funding me throughout the period of this study.

# Abstract

Helical devices are employed in the area of microwave technology. Applications such as filters and travelling-wave tubes are some of these in which helical devices are used. Ferrite loaded helical devices have been of interest to scientists and engineers throughout the last half century.

The structure that is considered in this thesis is of a helix surrounded by a ferrite tube, both of which are enclosed in a cylindrical waveguide. Maxwell's equations for electromagnetism are employed in order to derive the expressions for the electric and magnetic fields. The parameters of the structure are varied in order to observe how certain factors will affect the dispersiveness, loss and phase shift of the structure. The investigation considers the effect of varying the applied magnetic field. The investigation also incorporates an air gap between the ferrite and helix and between the ferrite and metal waveguide. For the first time, the affects of these air gaps are analysed.

# Contents

# List of Figures

# List of Tables

# Chapter 1

# Introduction

## 1.1 Chapter Overview

This investigation deals with the modelling of ferrite loaded helical devices. This chapter provides an introduction to ferrites. It looks at their magnetic properties and their applications in microwave devices. Concepts of magnetisaion that are used in explaining the ferrite behavior are also introduced and explained. The previous work that has been done in closely related areas of study is also analysed. Helical structures have been modelled differently by various authors, each model having different assumptions. These procedures and assumptions are studied and the validity of these are examined. The chapter concludes with a discussion concerning what the thesis intends to investigate and how the previous work will be extended.

## 1.2 Introduction to Magnetism

A magnetic field is a force field that is produced by moving electric charges and by time varying electric fields. It is represented by two vector fields: the **B**-field and the **H**-field. The **B**-field will be referred to as the *magnetic flux density* and the **H**-field by the *magnetic field intensity*. Maxwell's

equations describe the relationship between the electric and magnetic fields together with the charges and currents that create them.

A magnetic field can be visualised by the use of *field lines*. This method can be used to show that the magnetic **B**-field lines neither start nor end. Therefore, a B-field entering a region must leave it - it can not have an end point. This leads to the conclusion that magnetic poles always comes in N and S pairs, and cutting a magnet in half will produce two separate magnets each having N and S poles. Mathematically, this can be expressed as,

$$\oint_S \mathbf{B} \cdot d\mathbf{A} = 0. \tag{1.1}$$

Applying the divergence theorem to this relation gives rise to one of Maxwell's equation,

$$\nabla \cdot \mathbf{B} = 0. \tag{1.2}$$

This property of the **B**-field gives rise to it being a *solenoidal* vector field[1].

In a vacuum, the **B**-field and **H**-field are related to each other by the relation

$$\mathbf{B} = \mu_0 \mathbf{H}, \tag{1.3}$$

where $\mu_0$ is the permeability of free space and is given by $4\pi \times 10^{-7}$ H/m. A genealised expression of (1.3) is given by,

$$\mathbf{B} = \mu_r \mu_0 \mathbf{H}, \tag{1.4}$$

where $\mu_r$ is denoted as the relative permeability of a material. Inside a material, **B** and **H** are related by,

$$\mathbf{B} = \mu_0 \left( \mathbf{M} + \mathbf{H} \right), \tag{1.5}$$

where **M** is the magnerisation of the material.

When a material is subjected to an applied **B**-field, it produces its own magnetisation (**M**-field), and thus its own **B**-field. This only exists in the presence of an applied magnetic field and

[1] A solenoidal vector field is one which has a divergence of 0.

is very weak. Depending on a material's magnetic behaviour, materials can be classified into the following categories: Diamagnetic materials, Paramagnetic materials and Ferromagnetic materials. A diamagnetic material produces a magnetisation that is in the opposite direction to the applied magnetic field, whilst a paramagnetic material produces a magnetisation that is in the same direction to the applied magnetic field.

The magnetisation $\mathbf{M}$ of a material is defined by the following equation,

$$\mathbf{M} = \frac{N}{V}\,\mathbf{m} = n\mathbf{m}, \tag{1.6}$$

where $\mathbf{m}$ is the magnetic moment, $N$ represents the number of magnetic moments in the material and V is the volume. N/V is replaced by n and is referred to as the number density of magnetic moments. The $\mathbf{M}$ field is measured in Amperes per metre (A/m). The magnetic moment $\mathbf{m}$ is equal to the sum of two different moments: one due to electron spin, and the other due to its electrical charge. Many materials (those which have a filled electron shell), the total moment is zero due to the electron spins occurring in up/down pairs. The net magnetic moment due to electron spin depends on the number of spins in each direction. If all the spins are up (or down), the net moment is equal to the sum of moments due to each spin. If some of the spins are up whilst others are down, the difference in the number of spins in each direction will determine the net magnetic moment. Hund's rule states that electrons entering a subshell will spread out over all available orbitals with their spin in the same direction. These unpaired magnetic moments align parallel to an applied magnetic field. This is called paramagnetism. In ferromagnetism, the unpaired magnetic moments tend to align spontaneously without an applied field. Antiferromagnetism is the complete cancellation of all the unpaired magnetic moments. Ferrimagnetism is a hybrid of ferromagnetism and antiferromagnetism - there is an incomplete cancellation of all the magnetic moments.

In many materials, $\mathbf{M}$ and $\mathbf{H}$ are related by the equation,

$$\mathbf{M} = \chi\mathbf{H} \tag{1.7}$$

where $\chi$ called the magnetic susceptibility. In ferrites, $\chi$ is a tensor matrix. Substituting (1.7) into (1.5) gives,

$$\mathbf{B} = \mu_0 (1 + \chi) \mathbf{H} = \underline{\mu}\mathbf{H}, \tag{1.8}$$

where

$$\underline{\mu} = \mu_0 (1 + \chi), \tag{1.9}$$

where $\underline{\mu}$ is called the tensor permeability matrix and was introduced by Polder in 1949 [5].

A permanent magnet is an object that produces its own magnetic field. If an external field is applied to it, the magnetic moments will align themselves in the direction of the applied magnetic field. When the applied field is removed, part of this alignment is retained and the material is said to be magnetised. If the relationship between the magnetic field strength **H** and flux density **B** is plotted, figure 1.1 is obtained. By increasing the applied field, the flux density will reach a maximum value, (referred to as the *saturation magnetisation*, $M_s$). Removing the applied magnetic field the flux density will decrease to a value called the *remanence magnetisation*. After the saturation magnetisation is obtained, the intensity of the magnetic field that is required to reduce the magnetisation of the material to zero is called the *coercivity*. This is an example of hysteresis and is shown in figure 1.1.

## 1.3 Introduction to Ferrites

Whilst ferrite materials were known approximately three thousand years ago, it was World War II that saw the development of usable ferrites by Snoek at the Gloeilampenfabriken research laboratories in The Netherlands [1]. Although the original intention was to use these ferrites at low frequencies, it was soon discovered that the materials had many possibilities for use at microwave frequencies. In the 1950s, a new class of ferrites, the garnets, were produced by Néel and by workers at Bell Laboratories [1].

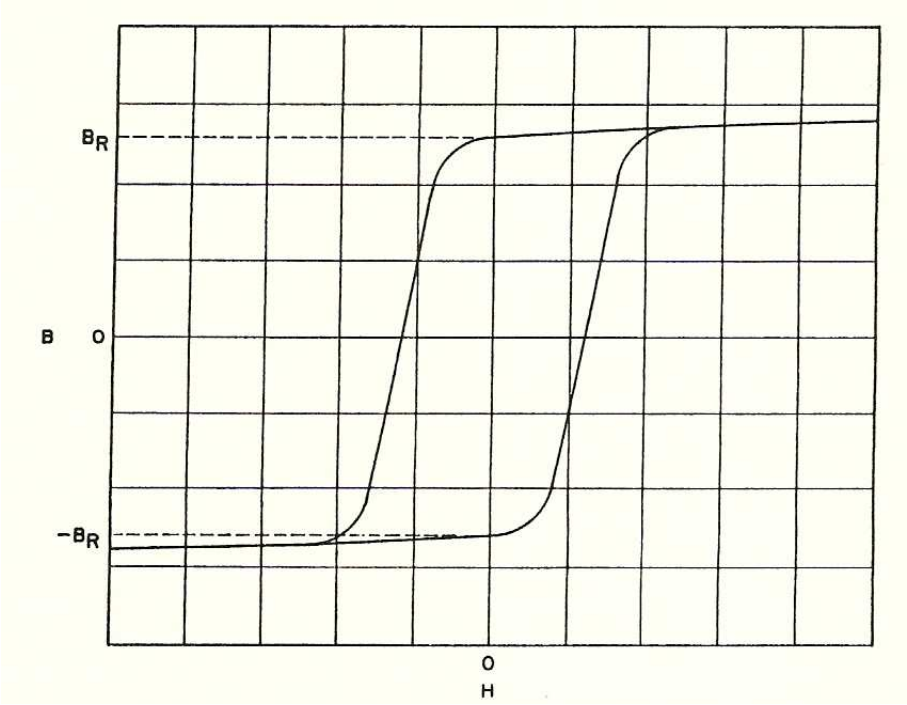


Figure 1.1: A typical hysteresis curve. $B_R$ is the remanence magnetisation [1].

Ferrites are classified into three main groups, the spinels, the garnets, and the hexagonal ferrites. The names of these classes describe the crystal structure of the materials [1]. The ferrites used in the applications that will be discussed in the thesis are mainly from the garnets and spinels.

## 1.4 Transmission Lines and Slow-Wave Structures

A transmission line is the material medium that forms all or part of a path from one place to another for the purpose of directing the transmission of energy, such as electromagnetic waves [10]. If the transmission line is uniform along its length, then its behaviour is largely described by a parameter called the *characteristic impedance*, denoted by $Z_0$ [10]. When sending power down a transmission line, it is desirable that as much power as possible will be absorbed by the load and as little to be reflected back to the source. This can be ensured by making the source and load impedances $Z_L$ equal to $Z_0$, in which case the transmission line is said to be *matched* [10].

The reflection coefficient $\Gamma$ is related to $Z_L$ and $Z_0$ in the following way,

$$\Gamma = \frac{Z_0 - Z_L}{Z_0 + Z_L}. \tag{1.10}$$

Therefore, by calculating the characteristic impedance $Z_0$, and using a load of suitable impedance, $Z_L$, the reflection coefficient, $\Gamma$ can be minimised.

The phase velocity $v_p$ is given by,

$$v_p = \frac{\lambda}{T}, \tag{1.11}$$

where $\lambda$ and $T$ denote the wavelength and time period of the wave respectively. In some devices, it is possible for the phase velocity to exceed the velocity of light in a vacuum, c. An example of this are X-rays through most glasses. However, such waves do not convey any information. A slow wave structure is one where the velocity of a wave passing through it is much less than that of the velocity of light. The propagation constant $\beta$ of a signal is given by,

$$\beta = \frac{\omega}{v}, \tag{1.12}$$

where $\omega$ is the angular frequency and $v$ is the velocity of the wave. Letting $\beta_0$ be the propagation constant of an EM wave in air with speed c, a slow wave structure fulfils the condition

$$v < c, \tag{1.13}$$

therefore

$$\frac{1}{v} > \frac{1}{c}, \qquad \Rightarrow \qquad \frac{\omega}{v} > \frac{\omega}{c}, \qquad \Rightarrow \qquad \beta > \beta_0. \tag{1.14}$$

This condition $\beta > \beta_0$ is a condition that is used extensively in the analysis of slow-wave structures.

## 1.5 Gyromagnetic Resonance and the Nonreciprocal Effect

This section introduces concepts in electromagnetism that will be used throughout this investigation. As stated above, the **B** and **H** fields in a ferrite are related by a matrix equation involving

the tensor permeability matrix. The tensor permeability matrix will depend on how the ferrite is biased. Theoretically, a ferrite can be biased in any direction. However, three directions are generally employed. Firstly, *longitudinal biasing*, where the biasing field is in the direction of the propagation wave and is shown in figure 1.2. The **B** and **H** fields are related by equation (1.15). Longitudinal biasing is where the direction of biasing is parallel to the direction of wave propagation. If the direction of biasing is antiparallel to the the direction of wave propagation (i.e. parallel, but in the opposite direction), the **B** and **H** fields are related by equation (1.16), ($\kappa$ is replaced by -$\kappa$). Secondly, *transverse biasing*, where the biasing field is perpendicular to the direction of the propagation wave and is shown in figure 1.3. The **B** and **H** fields are related by equation (1.17). Thirdly, *azimuthal biasing*, where the biasing field is circumferential. The **B** and **H** fields are related by equation (1.18) and is shown in figure 1.4. The orientation of the magnetic field is shown by the crosses and dots. The crosses show the field entering the page (at the top of the ferrite) and the dots show the field coming out of the page (at the bottom of the ferrite).

$$\begin{bmatrix} B_x \\ B_y \\ B_z \end{bmatrix} = \begin{bmatrix} \mu & -i\kappa & 0 \\ i\kappa & \mu & 0 \\ 0 & 0 & \mu_0 \end{bmatrix} \begin{bmatrix} H_x \\ H_y \\ H_z \end{bmatrix}. \tag{1.15}$$

$$\begin{bmatrix} B_x \\ B_y \\ B_z \end{bmatrix} = \begin{bmatrix} \mu & i\kappa & 0 \\ -i\kappa & \mu & 0 \\ 0 & 0 & \mu_0 \end{bmatrix} \begin{bmatrix} H_x \\ H_y \\ H_z \end{bmatrix}. \tag{1.16}$$

$$\begin{bmatrix} B_x \\ B_y \\ B_z \end{bmatrix} = \begin{bmatrix} \mu & 0 & -i\kappa \\ 0 & \mu_0 & 0 \\ i\kappa & 0 & \mu \end{bmatrix} \begin{bmatrix} H_x \\ H_y \\ H_z \end{bmatrix}. \tag{1.17}$$

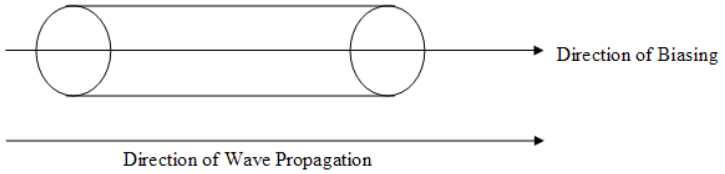


Figure 1.2: Longitudinal Biasing

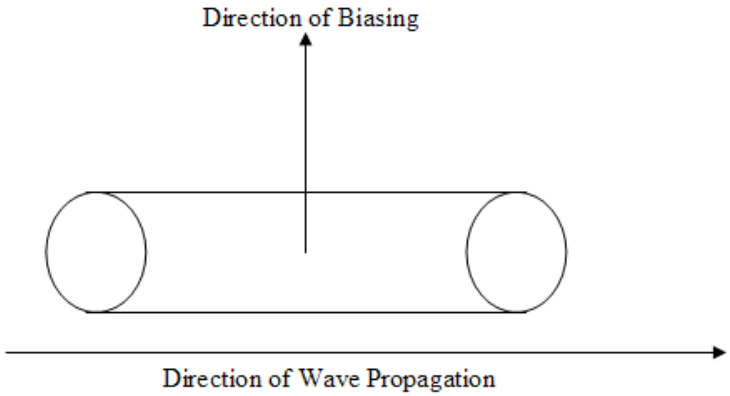


Figure 1.3: Transverse Biasing

$$\begin{bmatrix} B_r \\ B_\theta \\ B_z \end{bmatrix} = \begin{bmatrix} \mu & 0 & -i\kappa \\ 0 & \mu_0 & 0 \\ i\kappa & 0 & \mu \end{bmatrix} \begin{bmatrix} H_r \\ H_\theta \\ H_z \end{bmatrix}. \tag{1.18}$$

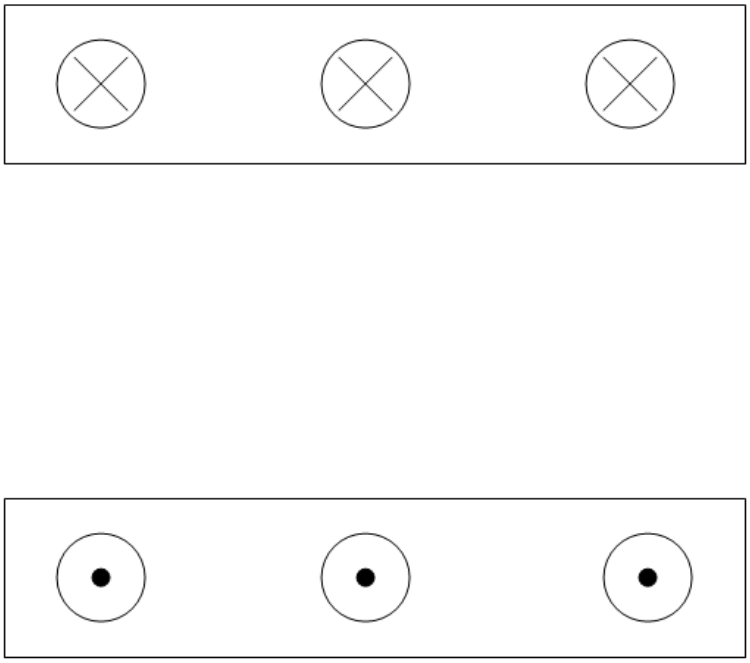

Figure 1.4: Azimuthal Biasing

In order to introduce some important ideas, it is assumed that the direction of propagation and applied magnetic field are both in the $z$ direction and the microwave field is in the x-y plane, (transverse plane). The propagation is governed by Maxwell's equations:

$$\nabla \wedge \mathbf{E} = -i\omega[\mu]\mathbf{H}, \tag{1.19}$$

$$\nabla \wedge \mathbf{H} = i\omega\varepsilon_0\varepsilon_r\mathbf{E}, \tag{1.20}$$

$$\nabla \cdot \mathbf{E} = 0, \tag{1.21}$$

$$\nabla \cdot \mathbf{H} = 0, \tag{1.22}$$

where $[\mu]$ is the tensor permeability matrix and is given by,

$$[\mu] = \begin{bmatrix} \mu & -i\kappa & 0 \\ i\kappa & \mu & 0 \\ 0 & 0 & \mu_0 \end{bmatrix}. \tag{1.23}$$

By taking the curl of (1.20) gives,

$$\nabla \wedge \nabla \wedge \mathbf{H} = i\omega\varepsilon_0\varepsilon_r \left(\nabla \wedge \mathbf{E}\right), \tag{1.24}$$

and replacing $(\nabla \wedge \mathbf{E})$ by (1.19) gives,

$$\nabla \wedge \nabla \wedge \mathbf{H} - \omega^2\varepsilon_0\varepsilon_r[\mu]\mathbf{H} = 0. \tag{1.25}$$

The alternating magnetic field in the transverse plane is given by,

$$\mathbf{h} = \begin{bmatrix} H_x \\ H_y \\ 0 \end{bmatrix}. \tag{1.26}$$

By assuming the wave has propagation of the form $\mathrm{e}^{-i\beta z}$ and has no variation of the fields in the xy plane. Applying this situation in (1.25) in the xy plane leads to the following equation,

$$\beta^2 \begin{bmatrix} H_x \\ H_y \end{bmatrix} = \omega^2\varepsilon_r\varepsilon_0 \begin{bmatrix} \mu & -i\kappa \\ i\kappa & \mu \end{bmatrix} \begin{bmatrix} H_x \\ H_y \end{bmatrix}. \tag{1.27}$$

The roots of the eigenvalues of (1.27) give

$$\begin{vmatrix} \mu - \frac{\beta^2}{\omega^2 \varepsilon_0 \varepsilon_r} & -i\kappa \\ i\kappa & \mu - \frac{\beta^2}{\omega^2 \varepsilon_0 \varepsilon_r} \end{vmatrix} = 0. \tag{1.28}$$

Solving (1.28) gives,

$$\beta_{\pm}^2 = \omega^2 \varepsilon_0 \varepsilon_r \left(\mu \pm \kappa\right). \tag{1.29}$$

The magnetic fields that correspond to $\beta_{\pm}$ can be obtained by substituting $\beta_{\pm}$ into (1.27) to give,

$$H_y^{\pm} = \pm\, i\, H_x^{\pm}. \tag{1.30}$$

The solutions (in the transverse plane) are two plane circularly polarised magnetic waves rotating in opposite directions. These waves have propagation constants $\beta_{\pm}$ [6]. The $\pm$ indicates the sense of circular polarisation, the plus sign refers to clockwise rotation (when observed in the direction of the propagating wave), and the minus sign indicates anticlockwise rotation [6]. If the direction of the applied magnetic field is reversed, the propagation constants of the two normal modes are interchanged [6]. Figure 1.5 shows the different situations. This is an example of *Faraday Rotation*. When plane wave travels through a magnetised ferrite, it separates into a circularly clockwise and anticlockwise sense of rotation, and travels through the medium with different propagation constants. They recombine at the emergence of the medium with a phase shift offset to the phase angle of the wave at the entry of the medium.

The phase shift can be thought of in different ways. If an electromagnetic wave propagates through a ferrite medium of length $L$, a phase shift will occur. The angle of this phase shift can be denoted $\phi_F$. If an electromagnetic wave travels through a transmission line of the same length $L$, a phase shift will also occur. This angle can be denoted by an angle $\phi_T$. The phase shift that will be calculated in this investigation, denoted by $\psi$ can be considered by,

$$\psi = \phi_F - \phi_T. \tag{1.31}$$

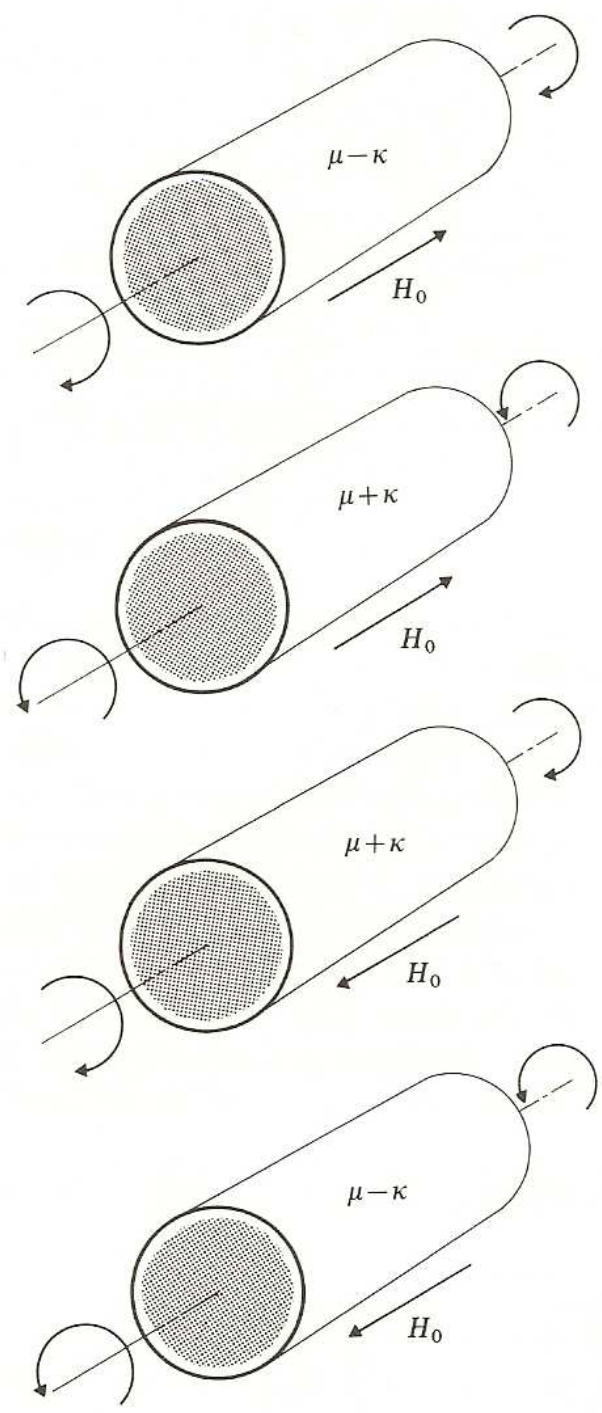


Figure 1.5: Normal modes of propagation in longitudinally magnetised ferrite medium. $H_0$ is the applied magnetic field [6].

This angle $\psi$ can be thought of as the increase in phase angle that an EM wave is rotated in a ferrite medium than a corresponding transmission line of the same length.

Another way of thinking of the phase shift is by relating it to Faraday rotation. When a wave travels down a biased ferrite medium, the wave decomposes into two circularly polarized components which propagate at different speeds through the material. The clockwise rotation has a propagation constant of $\beta_+$ and the anticlockwise rotation has a propagation constant of $\beta_-$. The components re-combine upon emergence from the medium. As there is a difference in propagation speed they do so with a net phase offset, resulting in a rotation of the angle of linear polarization. Therefore, as the wave travels in the forward wave direction.

The difference in propagation constants is given by,

$$\Delta\beta = \left|\beta^+ - \beta^-\right|. \tag{1.32}$$

The phase shift is given by,

$$\triangle\Phi = \triangle\beta\, P\, L\, \sqrt{\varepsilon_f}, \tag{1.33}$$

where $\Phi$ is given in radians per length. P is the polarising function and is calculated by,

$$P(\omega) = \sin\left(\frac{\omega}{c}\sqrt{\varepsilon_f}\, l_0\right) \qquad \text{with} \qquad l_0 \approx 2\pi r_0, \tag{1.34}$$

where $c$ is the velocity of light in free space, $\varepsilon_f$ is the effective relative dielectric constant for the ferrite. $L$ is the length over which the phase shift is measured and $r_0$ is the radius of the innermost region of the structure [27].

If a wave travels down a non-reciprocal medium and is rotated by $\theta$ in the positive $z$ direction, it is rotated by a further $\theta$ degrees in the negative $z$ direction. Therefore, the total phase shift of a wave travelling in the forward direction, and then reflected in the reverse direction, (so the wave returns to the initial position), it does so with a phase difference of $2\theta$. In a reciprocal medium, if a wave is rotated through $\theta$ degrees in the forward direction, it is rotated by $-\theta$ degrees in the

reverse direction, (or $\theta$ in the reverse rotational direction). Therefore, if a wave travels in the forward direction, and then reflected in the reverse direction, (so the wave returns to its initial position), there is no phase difference [6].

The differential phase shift in a magnetised ferrite is given by,

$$\Phi = \triangle\beta PL\sqrt{\varepsilon} \tag{1.35}$$

where P is the polarising function, L is the lengthover which the phase shift is measured, and $\triangle\beta$ is given by,

$$\triangle\beta = \left|\beta^{+} - \beta_{-}\right|. \tag{1.36}$$

As stated earlier, $\beta^{+}$ and $\beta_{-}$ can refer to the clockwise and anticlockwise rotation respectively, or $\beta^{+}$ and $\beta_{-}$ can refer to the propagation constant in the forward and backward direction respectively.

Section (1.6) describes the two models that are chosen to model helices. Although the sheath helix model assumes a helix to be of infinite length, authors such as Suhl and Walker [17] (amongst many others) have considered both a forward and backward wave. Therefore, although the sheath helix model will be used extensively, forward and backward waves can be modelled, for two reasons (amongst others),

• The assumption of a helix being of infinite length simplifies the modelling of the helical structure. However, this does not detract from the fact that a helix will always have a finite length.

• Authors (such as Suhl and Walker [8]) have used the sheath helix model and considered both the forward and the backward wave.

• Many authors have used the sheath helix model to model real-life situations which have helical structures of finite length. Quantities such as insertion loss are dependent on length (i.e. dB/m) and have been calculated using the sheath helix model.

• The tape helix model does not assume an infinitely long helix. However, (as will be shown in chapter 3), the results generated from the the present research (which used this sheath helix model

assumption) agree well with those of the tape helix model as presented in published papers.

The tensor permeability matrices have $\mu$ and $\kappa$ in their entries. $\mu$ and $\kappa$ depend on the applied magnetic field $H_0$ and the saturation magnetisation $M_s$. The equations are given below:

$$\frac{\mu}{\mu_0} = 1 - \frac{\gamma^2 H_0 M_0}{\gamma^2 H_0^2 - \omega^2} \qquad \text{and} \qquad \frac{\kappa}{\mu_0} = \frac{\gamma\omega M_0}{\gamma^2 H_0^2 - \omega^2}, \tag{1.37}$$

where

$$\mu_0 = 4\pi \times 10^{-7}\ H/m \qquad \text{and} \qquad \gamma = 2.21 \times 10^5\ m/C.$$

These equations give the values of $\kappa$ and $\mu$ is S.I. units, ($M_s$ in Teslas and $H_0$ in Amps per metre). Some textbooks use the Gaussian representations.

$$\frac{\mu}{\mu_0} = \frac{1 - p\sigma - \sigma^2}{1 - \sigma^2}, \quad \frac{\kappa}{\mu_0} = \frac{p}{1 - \sigma^2}, \tag{1.38}$$

where $\sigma$ is the ratio of the precession frequency to the signal frequency [7],

$$\sigma = \frac{\frac{|\gamma| H_0}{2\pi}}{f}. \tag{1.39}$$

$p$ is the ratio of the frequency associated with the saturation magnetization to the signal frequency

$$p = \frac{\frac{|\gamma| M_0}{2\pi\mu_0}}{f}. \tag{1.40}$$

Substituting (1.40) and (1.39) into (1.38) give,

$$\mu = \mu_0 + \frac{\gamma^2 H_0 M_0}{\gamma^2 H_0^2 - \omega^2} \qquad \text{and} \qquad \kappa = \frac{|\gamma|\,\omega M_0}{\omega^2 - \gamma^2 H_0^2}. \tag{1.41}$$

In Gaussian units, $\mu_0 = 1$, $H_0$ is measured in Oesteds and $M_s$ is in Gauss.

The equations for $\mu$ and $\kappa$ (in both cases whether SI units or Gaussian units are considered), the denominator will become 0 if

$$\omega = \gamma H_0. \tag{1.42}$$

At the frequency corresponding to $\omega = \gamma H_0$, the values of $\mu$ and $\kappa$ become infinite. The particular frequency at which this arises and where $\mu$ and $\kappa$ become infinite, Gyro-Magnetic Resonance (GMR) occurs.

Due to angular momentum each electron of a ferrite behaves as if it were a magnetic spinning top with its magnetic moment lying along the axis of rotation. When an electron is in equilibrium and a magnetic field is applied to the ferrite, the electron spin aligns itself with the magnetic field to create minimum potential energy. If a disturbance occurs and the electron is moved from its equilibrium point, instead of immediately moving back to equilibrium the electron begins to rotate about the magnetic field. This is known as *procession* [3].

The above description can be employed when considering the behaviour of electrons in a ferrite. If a magnetic field H is applied that saturates the ferrite - thus all the electrons align themselves. If an alternating magnetic field acts in a perpendicular plane to H is superimposed onto the field H, this produces a resultant field. This field will alternate between A and B. If the direction of H is suddenly altered to A, the electrons precess about the axis A along the path a-b. When the electron reaches b, if H changes to B, the electrons will precess about b-c. When the electron reaches c, if H returns to A, the electrons will precess about c-d. By H moving between A and B, the precessional angle will continue increasing. Theoretically, this may occur indefinitely. Physically, an equilibrium will occur between the losses in the ferrite and the effect of alternating H. Thus a maximum precessional angle will occur. When this is attained, power is transferred from the alternating magnetic field to the electrons in the ferrite which are processing. Energy is dissipated from these electrons which increases the temperature in the material. This energy transfer only occurs if the frequency of the alternative magnetic field is the same as that of the procession frequency of the electrons inside the ferrite, this phenomenon is known as *resonance absorption* or Gyro-Magnetic Resonance (GMR) [4].

The H field in figure 1.6 is in the $\hat{\mathbf{z}}$ direction, (with reference to figure 1.7). The above explanation of procession assumes that a wave with $H_{RF}$ is perpendicular to H. Therefore, $H_{RF}$ *must* be in the x-y plane. Therefore, letting

$$H_{RF} = X\hat{\mathbf{x}} + Y\hat{\mathbf{y}} \tag{1.43}$$

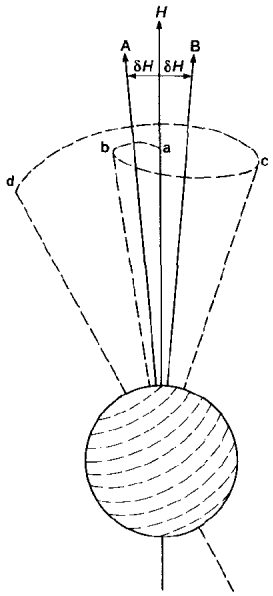


Figure 1.6: Processional motion of a spinning electron in a magnetic field which oscillates between the directions A and B [3].

where $X$ and $Y$ are constant, and

$$H = Z\hat{\mathbf{z}} \tag{1.44}$$

where $Z$ is a constant. Taking the dot product (scaler product) of H and $\mathrm{H}_{RF}$ gives

$$H_{RF} \cdot H = (X\hat{\mathbf{x}} + Y\hat{\mathbf{y}}) \cdot (Z\hat{\mathbf{z}}) = 0. \tag{1.45}$$

When the scaler product of two vectors are 0, then they are perpendicular to each other. Therefore, $\mathrm{H}_{RF}$ can be solely in the $\hat{\mathbf{y}}$ direction, or in the $\hat{\mathbf{x}}$direction, or any vector in the x-y plane. Any of these are perpendicular to H and are possible for the above explanation of procession.

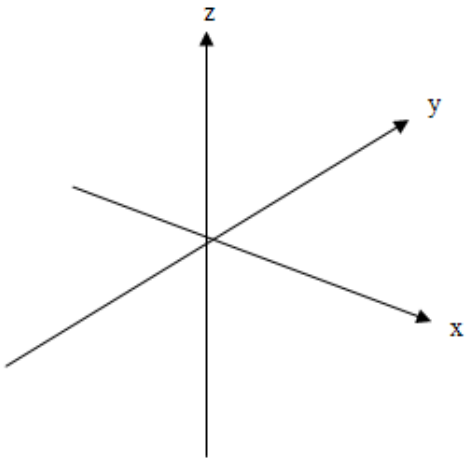


Figure 1.7: Cartesian x-y-z axis.

## 1.6 Application of Ferrites

### 1.6.1 Circulators and Isolators

Circulators are the most widely used ferrite device today. An ideal circulator usually has three or four ports, and a signal entering port 1 is transmitted to port 2 without loss and nothing comes out of the other ports. Figure 1.8 shows a stripline Y-junction circulator.

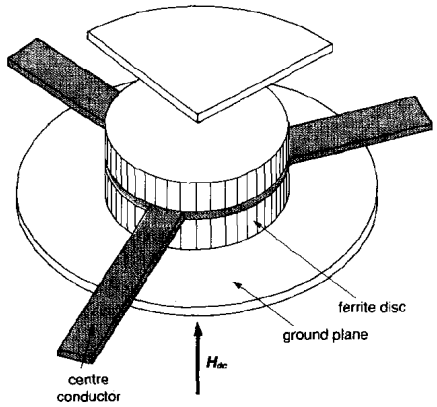


Figure 1.8: Stripline Y-junction circulator [3].

Another common application of the nonreciprocal properties of ferrites is in providing isolation. An isolator can be constructed from a circulator by adding a matched termination absorber to the third port of a three-port circulator. In an ideal isolator, the forward wave is transmitted without loss whereas any reverse wave is absorbed in the load. Such devices are commonly used in circuits where devices such as amplifiers require protection.

### 1.6.2 Phase Shifters

An important application of the use of ferrites came when ferrite phase shifters came into use. Ferrite phase shifters are able to control the permeability throughout the waveguide. This modifies the phase velocity of a microwave signal moving through the medium [12].

### Types of Phase Shifters

Ferrite phase shifters can be classified into different types as follows,

• Reciprocal/ Nonreciprocal

The phase shift in a reciprocal phase shifter is the same for signals propagating in either direction. It is different in the two directions in nonreciprocal types [12].

• Driven/Latching

Driven phase shifters require continuous control current. Latched types have a closed magnetic path and require only a momentary pulse of current [12].

• Analogue/Digital

Analogue types allow the insertion phase to be continuously varied by an external control current. Digital types generally comprise discrete phase shift sections [12].

### Applications

Ferrite phase shifters are most commonly used in electrically steered antenna systems, known as phased-array antenna systems. Ideally, a phase shifter is required to have the full range of 360°. It is important to chose the correct type of phase shifter. The choice of phase shifter can be determined by the following:

• Frequency

At lower frequencies, Transverse Electromagnetic Wave (TEM) devices are more common. A waveguide containing a simpler geometrical structure is easier to create for small sizes needed at high frequencies [12].

• Phase accuracy

The insertion phase varies significantly with frequency in some designs. In many types the phase shift is a function of the remnant magnetisation, which varies with temperature [12].

• Switching time and energy

If a nonreciprocal device is used in a radar application, the phase shifter has to be switched between two different states, referred to as transmit and receive. Continuously driven phasers are generally very slow compared to latching types [12]. The power from a continuously driven phase shifter may be adequate if a few phase shifters are needed. However, a latched device is adopted in a phased array antenna which may consist of hundreds or thousands of phase shifters [12].

• Power handling

In general, ferrite phase shifters can usually deal with higher power than other technological devices. Designs in which the ferrite is in direct contact with the waveguide wall will conduct heat dissipated in the ferrite away more readily, permitting higher power handling [12].

### 1.6.3 Travelling Wave Tubes

A travelling wave tube (TWT) is a device that is used in the amplification of radio frequency signals to a higher power. The main components of this device are a vacuum tube, a helical wire and a focusing magnetic field. An electron gun is placed at one end of the vacuum tube - the electrons that are emitted are focused into a beam by the magnetic field that is around the tube. A helical wire is placed between the input and output down which the electron beam travels before striking the output. The signal which will be amplified is fed into a coupler which is near the emitter, thus inducing a current into the helix. The purpose of the helix is to act as a delay line so that the signal travels at approximately the same speed as the electron beam. The interaction between the EM field due to the signal and the electron beam cause the electrons to bunch (also referred to as *velocity modulation*). The EM field due to the beam current induces more current into the helix thus amplifying the current. Near the collector, a coupler receives the amplified signal. The reflected wave needs to be suppressed (or attenuated) to prevent it returning to the electron gun and thus an attenuator is positioned between the input and output [14].

**The property of a ferrite having low loss in the forward direction and substantial loss**

**in the reverse, lends itself to this application. The necessity of an attenuator for the reflected wave can be achieved with the use of ferrite. However, due to the magnetic focusing field, substantial future work will have to be undertaken to ensure that the magnetic focusing field for the electron beam will not be affected by the presence of the ferrite material. This could distort the applied field and hence cause defocusing of the electron beam. Two possible ways of overcoming this are, either to have a separate biasing field for the ferrite, or to use the focusing field of the electron beam to bias the ferrite.**

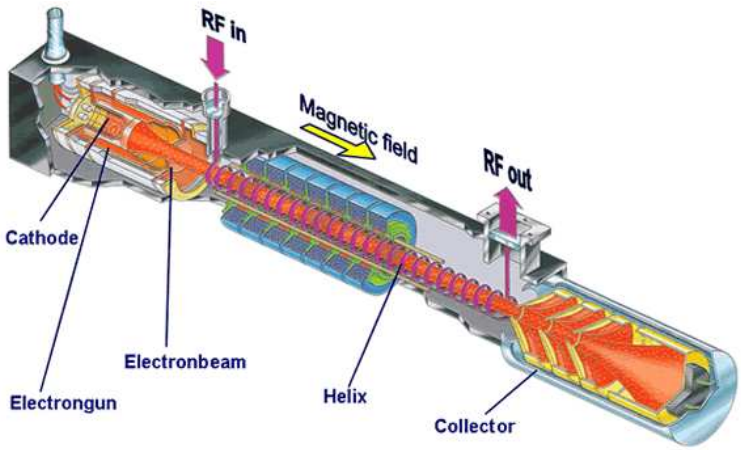


Figure 1.9: A Travelling-Wave Tube (TWT) [15].

Of all the periodic slow wave structures, the helix stands out in both importance and geometrical simplicity. It is employed in all low and medium-power travelling wave tubes and in low-power backward wave oscillators [16]. The next section deals with different ways that a helix can be modelled.

## 1.7 Helical Models

Different helical models have been employed in the analysis of electromagnetic waves propagating through helical structures. Two standard helical models have been used, the *sheath helix* model and the *tape helix* model [17].

### 1.7.1 The Sheath Helix Model

Figure 1.10 shows a perfect conducting wire which is wound into a helix. The axis of the helix is along the $z$-direction of the circular cylindrical co-ordinate system. A developed view is shown in figure 1.11, where the unit vectors $\vec{a}_{||}$ and $\vec{a}_{\perp}$ are drawn. Letting the radius of the helix be denoted by $r$, the pitch of the helix by $p$, the pitch angle by $\psi$, the following expression is obtained:

$$\tan(\psi) = \frac{p}{2\pi r}. \tag{1.46}$$

The model assumes the wave to be of harmonic dependence. The sheath helix model assumes the following,

- the helix is infinitely long,
- the helical wire is infinitely thin,
- the helical wire conducts only in the direction of the windings,
- the conductivity normal to the helical path is taken to be zero,
- the conductivity in the direction of the helical path is taken to be infinite,
- the helical pitch is significantly less than the wavelength of the wave ($p << \lambda$).

This model is idealized as an anisotropically conducting cylindrical surface that conducts only in the helical direction. The conductivity normal to the helical path is taken to be zero.

**Boundary Conditions**

At the surface of the sheath helix, there are three boundary conditions that are established. At the surface, the tangential electric field must vanish (since the conductivity in this direction is assumed to be infinite). This can be expressed as

$$\mathbf{E}^i_{\parallel}(a) = \mathbf{E}^o_{\parallel}(a) = 0. \tag{1.47}$$

The conductivity perpendicular to the windings is assumed to be zero. Thus, the electric field on the cylindrical surface in this direction is continuous across this boundary. This is expressed as

$$\mathbf{E}^i_{\perp}(a) = \mathbf{E}^o_{\perp}(a). \tag{1.48}$$

Finally, the magnetic field on the cylindrical surface are continuous along the wire. This is expressed as

$$\mathbf{H}^i_{\parallel}(a) = \mathbf{H}^o_{\parallel}(a). \tag{1.49}$$

Here, the superscripts $i$ and $o$ represent the interior and exterior of the helix, respectively [18]. Also, parallel and perpendicular in this context are with reference to the helical windings as shown in figure 1.11.

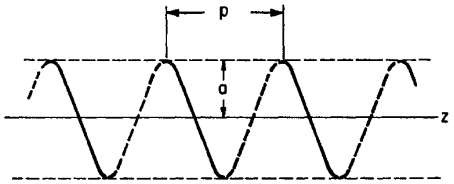


Figure 1.10: The sheath helix [17].

## 1.7.2 The Tape Helix Model

Due to the assumptions of the sheath helix model, the helix is modelled as a cylinder. Thus the air gaps between the windings are not taken into consideration. The sheath helix also does not model

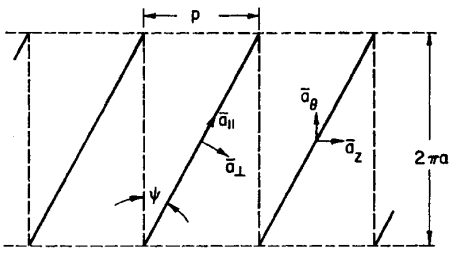


Figure 1.11: Developed sheath helix [17].

the periodic character of the helix. The tape helix *does* incorporate these into the model and was analysed by Sensiper [17]. The tape helix consists of a thin ribbon of metal wound into a helical structure [13]. The tape is of width $\delta$ and gap width $\delta'$ [17] as shown in figure 1.12. It is considered to be perfectly conducting in all directions [16]. The helical radius is $a$ and

$$\tan(\psi) = \frac{p}{2\pi a}, \tag{1.50}$$

where $p$ is the pitch.

If a helix is situated as shown in figure 1.11, and the helix is displaced by a distance $p$ along the $z$ axis, the helix will coincide with itself. Also, if the helix is rotated through an angle $\theta$ and then translated by a distance $p\theta/2\pi$, the helix will again coincide with itself. These periodic properties of the helix create some restrictions as to the nature of the solutions. Cylindrical polar coordinates are taken in the usual context. If $\mathbf{E}_1(r, \phi, z)$ is a solution for the electric field, then $e^{-i\beta(p\theta/2\pi)}\,\mathbf{E}_1(r, \phi + \theta, z + p\theta/2\pi)$ is also a solution. This is can be shown as the points $(r, \phi, z)$ and $(r, \phi+\theta, z+p\theta/2\pi)$ cannot be distinguished from each other (due to the periodic nature of the wave). The term $e^{-i\beta(p\theta/2\pi)}$ represent the propagation factor of the wave. The solution $\mathbf{E}_1(r, \phi, z)$ must be periodic in $\phi$. It must also be periodic in the $z$ direction with period $p$ (apart from the propagation factor $e^{-i\beta z}$). Therefore, $\mathbf{E}_1$ can be expressed as a double Fourier series,

$$\mathbf{E}_1(r, \phi, z) = \sum_{m=-\infty}^{\infty} \sum_{n=-\infty}^{\infty} \mathbf{E}_{1,mn}(r) e^{-im\phi - i2n\pi z/p} e^{-i\beta z}, \tag{1.51}$$

where $\mathbf{E}_{1,mn}(r)$ are vector functions of $r$. It is required that $\mathrm{e}^{i\beta z}\mathbf{E}_1(r, \phi, z)$ does not change when $\phi$

and $z$ are replaced by $\phi + \theta$ and $z + p\theta/2\pi$. Therefore, in equation (1.7.2), it is required that

$$e^{-im\phi - i2n\pi z/p} = e^{-im(\phi+\theta) - i2n\pi(z+p\theta/2\pi)/p}. \tag{1.52}$$

The condition is fulfilled if $m = -n$. Therefore, the Fourier series can be reduced to a single summation,

$$\mathbf{E}_1(r, \phi, z) = \sum_{n=-\infty}^{\infty} \mathbf{E}_{1,n}(r) e^{-in(2\pi z/p - \phi)} e^{-i\beta z}. \tag{1.53}$$

The solutions for the electric and magnetic field components for a helix can be obtained by expanding the fields in the regions $r < a$ and $r > a$ into an infinite series of E and H modes expressed in cylindrical coordinates [13]. For a helix that is immersed in free-space, the region $r > a$ will be represented by the modified Bessel function of $nth$ order $K_n(v_n r)$, where

$$v_n^2 = \left[\beta + \frac{2n\pi}{p}\right]^2 - \omega^2 \varepsilon_0 \mu_0. \tag{1.54}$$

For real values of $v_n$, $K_n$ will decay exponentially as $r$ tends to infinity [2]

The tape helix ensures that it excludes solutions that are nonexistant. Therefore, any particular frequency value will only generate such propagation constants, say $\beta_M$, that are physically possible. The field corresponding to each value of $\beta_M$ is expressed by the Fourier series

$$\mathbf{E}_M(r, \phi, z) = \sum_{n=-\infty}^{\infty} \mathbf{E}_{M,n}(r) e^{-in(2nz/p - \phi) - i\beta_M z}. \tag{1.55}$$

In this summation, each term is called a **spatial harmonic** and has a propagation constant of $\beta_M + 2n\pi/p$. The radially propagation constant $v_n$ in the $z$ direction must always remain real, as an imaginary $v_n$ will correspond to a phase velocity in the z-direction greater than the velocity of light [16]. Also, the $n = 0$ spatial harmonic will not decay for imaginary valued $v_n$. For these reasons, certain regions are called *forbidden regions*. On a graph where $kp$ is plotted against $\beta p$, the regions above $k = \pm\beta$ represent the forbidden region. In these regions, the propagation constant is complex

[2] It can be shown that the function $K_n$ asymptotes to $\sqrt{\pi/2v_n r}\, e^{-v_n r}$ [13].

rather than purely real. Figure 1.13 shows an example of a usual diagram corresponding to the behaviour of the wave in a tape helix [17]. $\psi$ denotes the pitch angle, $a$ denotes the helical radius and $\beta_0 = \omega/c$. By considering the cases of when $r < a$ and $r > a$ (corresponding to the interior and exterior of the helix), and applying the relevant boundary conditions, a solution can be sought.

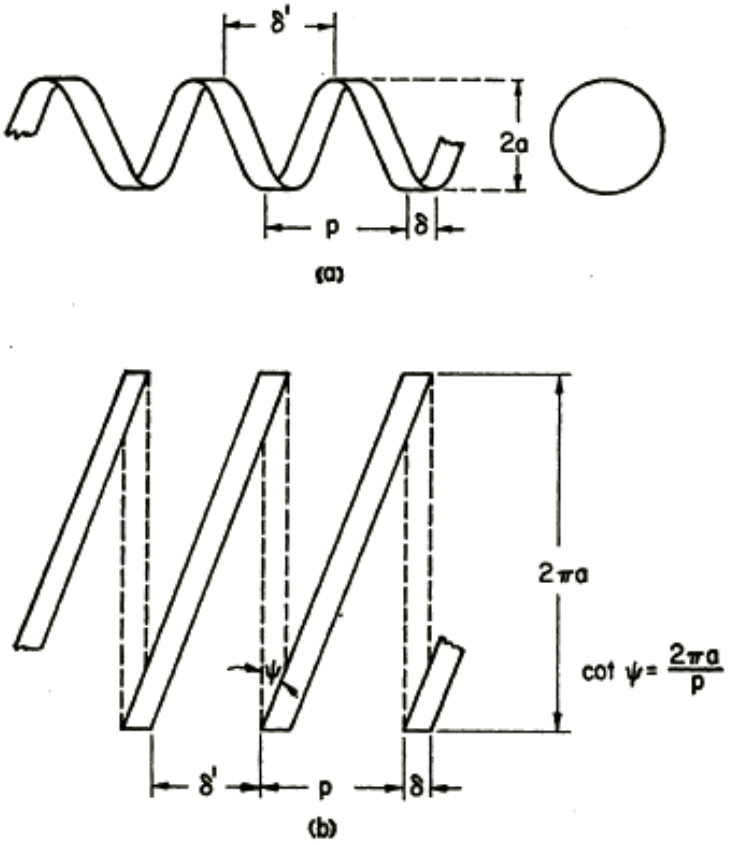


(a) Tape helix; (b) Developed tape helix.

Figure 1.12: Tape Helix [17].

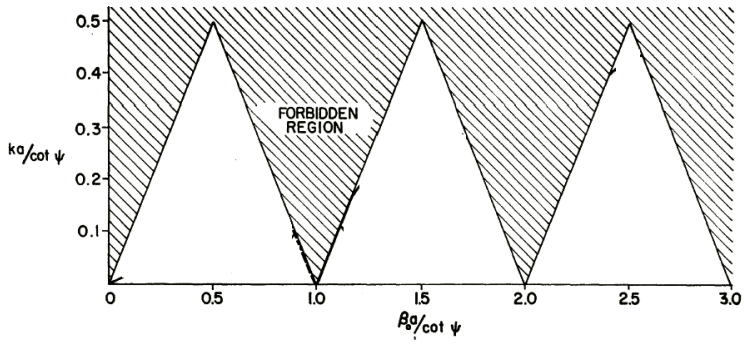


Figure 1.13: Forbidden-region diagram fora single tape helix. Values of $\beta$ in the shaded regions are not allowed because such a solution would correspond to one of the space harmonics having a velocity greater than the velocity of light. $k = \omega/c$. [17].

## 1.8 Literature Review

Previous authors have investigated different helical structures and different authors have made various assumptions in an attempt to make an accurate analysis of the structure. This section introduces some of the work that has previously been done on helical structures surrounded by ferrite or dielectric. These papers will be made use of when the reliability and accuracy of the model is to be investigated (section 2.9).

Gilmour et al [19] considered the case of a helix supported by dielectric rods inside a waveguide. These rods were modelled as a single dielectric tube with an effective permittivity, see figure 1.14. The dielectric layer was assumed to be in contact with the metal helix and the barrel. No angular dependance was assumed (i.e. the axisymmetric case was considered). The sheath helix model was employed and a method for calculating the loss from the metal helix and the barrel was described in detail, relying on some equations that were obtained from Bryant and White [20]. The paper plotted the loss against frequency for variation in helical radius, barrel radius, helical pitch and helical resistivity. The barrel-helix ratio is given by,

$$\text{barrel-helix ratio} = \frac{\text{radius of barrel}}{\text{radius of helix}}.$$

The paper attempted to measure the losses in the structure experimentally. These experimental results were compared to the theoretical ones. The paper concluded by stating that in order to minimise the loss in the structure, it is necessary to:

1. maximise helix pitch
2. minimise helix radius
3. maximise barrel - helix ratio
4. minimise helix resistivity

5. minimise support rod cross-sectional area and dielectric constant.

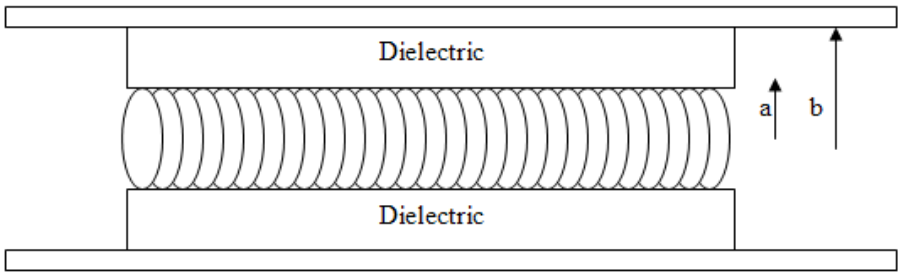


Figure 1.14: Model of helix used in analysis, (dielectric).

Lopes and Motta [21] calculated the losses in a similar structure, but use of the tape helix model was made. Loss against frequency was plotted for variation in helical radius, barrel-helix ratio, helical pitch, helical resistivity and dielectric permittivity. The paper concluded by stating that in order to reduce loss in the tape-helix structure, at least in the frequency range under investigation, it is necessary to,

1. maximise helix pitch;
2. minimise helix radius;
3. maximise guide-to-helix diameter ratio;
4. minimise helix resistivity;
5. minimise support rod cross-sectional area; and
6. minimise dielectric constant of the support rods, [21].

These are in agreement with [19].

Duan et al [22] considered the case of a helix supported by dielectric rods surrounded by a metal waveguide, see figure 1.15. These rods are modelled as a single dielectric tube with an effective

permittivity, $\varepsilon_{eff}$, see figure 1.16. If $\varepsilon_r$ is the relative permittivity of each rod, then the effective permittivity of the dielectric layer is given by,

$$\varepsilon_{eff} = 1 + m\,(\varepsilon_r - 1)\,\frac{A_s}{A}, \tag{1.56}$$

where $A_s$ is the cross-sectional area of a single dielectric rod, $A$ is the cross-sectional area of the region $b_1 < r < b$ and $m$ is the number of dielectric support rods.

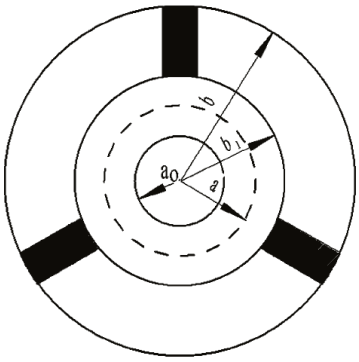


Figure 1.15: Cross - section of structure [22].

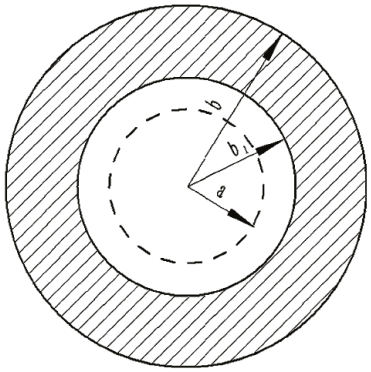


Figure 1.16: Equivalent cross - section of structure [22]

The paper compares the sheath helix model, the tape helix model and experimental results from [23] and computes the propagation constant $\beta$. The sheath helix model is used with the assumptions given in [24]. Duan et al [25] extended this further by considering the support rods not as a single layer, but multiple layered dielectric tubes, in the region between the helix and the waveguide. The

dielectric loss was considered by assuming the permittivity was a complex-valued constant, of the form

$$\varepsilon_r' = \varepsilon_r \left(1 - \tan(\delta)\, i\right), \tag{1.57}$$

where $\tan(\delta)$ is referred to as the loss tangent. The loss tangent was in the range of

$$-4 \leq \log_{10}\left(\tan(\delta)\right) \leq -1. \tag{1.58}$$

The value of $\beta$ was also a complex value.[3]

An electromagnetic wave passing down a structure comprising of a metal helix surrounded by a ferrite tube was considered by Cook, Kompfner and Suhl [26]. When a wave passes through any device, some of this wave is reflected. It is always desirable to minimise the extent of this reflected wave. This reflected wave can oscillate backwards and forwards in a TWT. A standard method of reducing these oscillations is to place lossy dielectric materials on the dielectric supports. A backward wave will therefore undergo twice the loss of the forward wave. However, this has some disadvantages, as it can lead to a reduction in tube efficiency. If the dielectric tube is replaced with a ferrite one, the backward wave will be severely reduced, if not completely eliminated. However, this has a problem, an electron beam in travelling wave tubes is usually focused by an axial B field. A ferrite tube surrounding the helix would severely reduce the field inside. By dividing the ferrite into a succession of relatively narrow rings spaced apart, it is found the the axial field is substantially the same as would exist in the absence of the ferrite rings [26]. The idea of using a ferrite helix as an alternative to a tube was first considered by Cook, Kompfner and Suhl [26]. Figure 1.17 shows the experimental results of this structure. At about 4500 megacycles, the loss in the backward direction is substantially more than in the forward direction.

Swifthook et al [24] analysed a helix surrounded by a dielectric tube. They modelled an air gap between the helix and the dielectric. The equations in each region and the boundary conditions were

[3]Section 2.7 gives further details of the loss calculations.

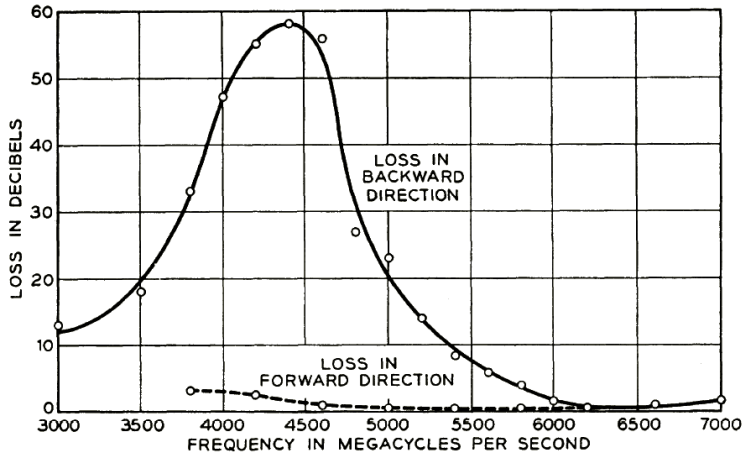


Figure 1.17: Loss in a metal helix surrounded by ferrite helix [26]

formed. The equations were written in matrix form and a zero determinant was sought. This will be explained in detail in the chapter 2. The paper considered different variations of the structure; the cases where, the permittivity of the dielectric was taken to be 1 (i.e. the dielectric is modelled as an air region), the structure is considered as a free-space helix (a helix in air), the structure replaces the air gap with dielectric, the structure considers the glass tube to have infinite thickness.

Suhl and Walker [8] considered the case of a metal helix surrounded by a ferrite toroid of infinite thickness, see figure 1.18. The following assumptions were made:

1. The helix and the ferrite toroid were infinitely long;

2. The helix was infinitely thin, directly on the ferrite surface and could be treated as a sheath helix;

3. Helix and ferrite and the whole device in general were lossless;

4. The propagation constant $\beta$ for axial direction, the quantity to be found, was very large compare with all other propagation constants;

5. All fields are independent of the circumferential angle, i.e. only the zero-order mode of propagation on a helix is present;

6. The ferrite was azimuthally magnetised;

7. The ferrite wall was infinitely thick [27].

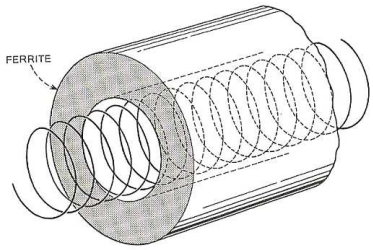


Figure 1.18: Cylindrical helix surrounded by a ferrite [8].

The paper derives the dispersion relation, but due to the inability of programs to solve such an equation (having been written in the 1950s), many mathematical simplifications were made. A determinental equation was derived and various functional analysis was carried out on the equation to ascertain its behaviour. Dispersions curves were produced.

The structure of a helix surrounded by a finite ferrite tube which has azimuthal biasing has been considered by certain authors. Ivanov and Koster [28] and [29] analysed a shielded thin wire helix which was inhomogeneously loaded with a latching ferrite and magnetised azimuthally to resonance. The ferrite was assumed to be lossless and the electromagnetic wave had no angular dependance. Orlando [30] considered the case of angular dependance. Both used the sheath helix model and dispersion curves were produced.

Kai and Chakraboti [31] considered the case of a helix surrounded by a ferrite tube (which the paper referred to as an "inverted helix"), and the case of a helix wound around a ferrite tube (which the paper referred to as an "normal helix"), see figure 1.19. The ferrite was biased azimuthally and the structure was analysed using the finite-element method (FEM). The differential phase shift was calculated and dispersion curves were plotted for variations in the pitch angle ($\psi$). The results showed that the phase shift was larger in the case of a normal helix compared to that of an inverted

helix. Despite this, the ferrite loaded helical structure, or "inverted helix", will be investigated in this thesis due to the structure lending itself more easily for modification and adaptation in TWT applications.

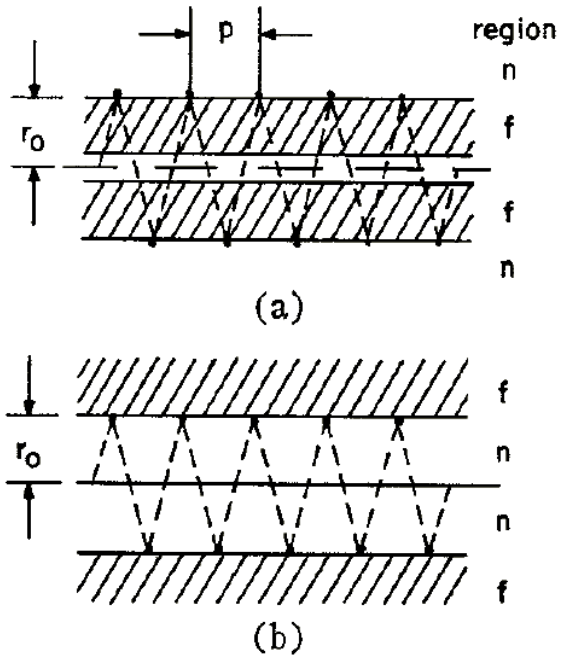


Figure 1.19: Helical Structures: (a) normal helix, (b) inverted helix [27].

Secklemann [27] considered the case of a metal helix surrounded by a ferrite toroid, enclosed in a metal waveguide, see figure 1.20. The ferrite was assumed to be lossless and biased azimuthally. Both the 'normal helix' and 'inverted helix' were analysed. Dispersion curves and graphs showing the variation of phase shift with frequency were produced. In addition to the assumptions that have been mentioned earlier, additional ones that were assumed were:

• The device works at remnant magnetisation.

• The remnant magnetisation is equal to the saturation magnetisation.

If a ferrite material is magnetised to saturation and the magnetising field is then removed, the ferrite will remain in a state of **remnant magnetisation** which is close to the saturation magnetisation [4]. The two assumptions above imply that the latched device works at saturation magnetisation.

However, as mentioned earlier, a more accurate assumption would have been to model the magnetic field as 80% or 90% of the saturation magnetisation. The paper concluded by stating that the normal helix type phase shifter was superior to inverted helix type ones as they have a higher differential phase shift per unit length. Some experimental results were conducted which had a good agreement with the theoretical model.

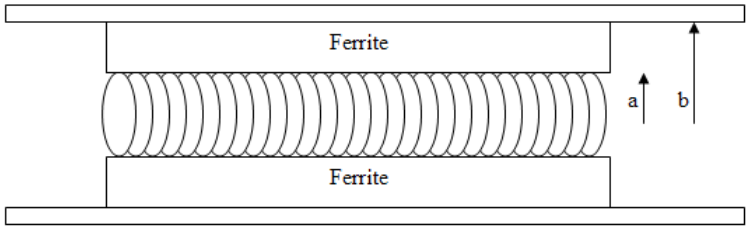


Figure 1.20: Model of helix used in analysis, (ferrite).

## 1.9 An Overview of the Thesis

This thesis aims at extending the analysis of the work that has been done on ferrite loaded helical structures. The previous section gave an insight into what has been considered in past and present papers. Whilst the loss ($\alpha$) of a helix surrounded by dielectric and the propagation constant ($\beta$) of a helix surrounded by ferrite or dielectric have been considered by previous authors, the loss of ferrite loaded helical structures have yet to be investigated. This thesis uses the sheath helix to model the structure, to calculate the loss and to consider how this is affected by varying certain parameters within the structure (e.g. helical radius, ferrite thickness, pitch angle). The model is not restricted to the examination of the saturated case, but also considers the case of an unsaturated ferrite. The dielectric and magnetic loss of the ferrite are also calculated. The model considers the effects of air gaps in the structure in an attempt to improve the accuracy and reliability of the model. The propagation constants of the forward and backward wave are calculated and dispersion curves are produced. The model also calculates the differential phase shift of the structure.

Chapter 2 takes a detailed look at the model that will be employed. The problem is formulated and the governing equations, boundary conditions and field solutions are presented. The modelling assumptions are discussed in detail. A quantitive analysis of the loss in the structure is also formulated. Chapter 3 assesses the accuracy and reliability of the model. This is achieved by a comparison with results that have been published in the previous papers[4]. Chapter 4 examines certain situations that have not been considered before. For example, calculating the attenuation coefficient of a wave travelling through a structure consisting of a helix surrounded by a ferrite tube enclosed inside a metal a waveguide. Dispersion curves are produced, the phase shift and attenuation coefficient are plotted. Chapter 5 concludes the investigation and considers how the current study can be extended.

[4]Section 1.5 introduced the previously published results that will be used for comparisons in chapter 3.

# Chapter 2

# The Model

This chapter contains a description of the problem that was investigated. The modelling assumptions are taken into consideration together with the governing equations, boundary conditions and the field solutions. The procedure for calculating the loss in the structure is illustrated.

## 2.1 Problem Formulation

A uniform helix is described by its radius ($r = a$), its pitch ($p$), and its pitch angle ($\psi$), which is the angle that the tangent to the helix makes with a plane perpendicular to the axis of the structure ($z$). Figure 2.1 shows a view of the helical structure and figure 2.2 shows the the pitch angle ($\psi$) and the vectors parallel and perpendicular to the helical windings. Geometrically, $\cot(\psi) = \frac{2\pi a}{p}$. The helical structure supports propagation along the longitudinal ($z$) axis with travelling wave variations of the form $e^{i(\omega t - \beta z)}$, where $\beta$ is to be determined.

Figure 2.3 shows the structure that is analysed in the current study - a metal helix surrounded a ferrite tube. This is further enclosed within a waveguide wall. The structure is modelled with an air gap between the helix and the ferrite tube and also between the ferrite tube and the metal waveguide. The metal helix is of radius $a$, the ferrite tube has inner and outer radii $b$ and $c$ respectively. The

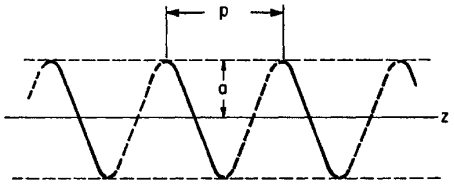


Figure 2.1: Helix [17].

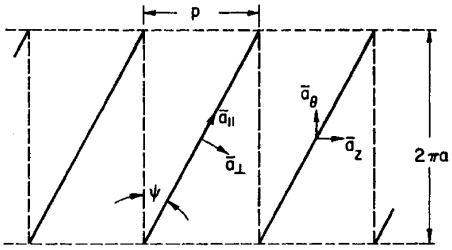


Figure 2.2: Developed helix [17].

metal waveguide is at a length $d$ from the centreline, where $a < b < c < d$ are with reference to figure 2.3.

Region 1 refers to the air inside the metal helix, region 2 refers to the air gap between the helix and the ferrite, region 3 refers to the region inside the ferrite and region 4 refers to the air gap between the ferrite and the metal waveguide.

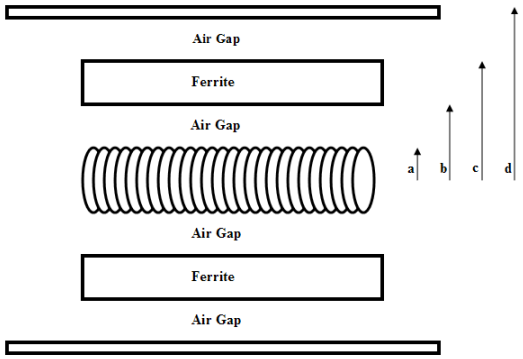


Figure 2.3: Helical structure.

## 2.2 The Wave Equation

The governing equations for the electromagnetic wave in the structure are given by Maxwell's equations:

$$\nabla \cdot \mathbf{E} = 0, \quad \nabla \cdot \mathbf{B} = 0, \quad \nabla \wedge \mathbf{E} = -\frac{\partial \mathbf{B}}{\partial t}, \quad \nabla \wedge \mathbf{H} = \varepsilon \frac{\partial \mathbf{E}}{\partial t}.$$

In materials other then ferrites, $\mathbf{B}$ and $\mathbf{H}$ are related by the equation

$$\mathbf{B} = \mu \mathbf{H},$$

where $\mu$ is the permeability. Maxwell's equations become

$$\nabla \cdot \mathbf{E} = 0, \quad \nabla \cdot \mathbf{H} = 0, \quad \nabla \wedge \mathbf{E} = -\mu \frac{\partial \mathbf{H}}{\partial t}, \quad \nabla \wedge \mathbf{H} = \varepsilon \frac{\partial \mathbf{E}}{\partial t}.$$

By using vector identities, these equations can be rearranged to give the wave equation[1]

$$\nabla^2 \begin{bmatrix} \mathbf{E} \\ \mathbf{H} \end{bmatrix} = \frac{1}{c^2} \frac{\partial^2}{\partial t^2} \begin{bmatrix} \mathbf{E} \\ \mathbf{H} \end{bmatrix}, \quad \text{where} \quad c = \frac{1}{\sqrt{\mu\varepsilon}}. \tag{2.1}$$

## 2.3 Modelling Assumptions

The structure is modelled using the following assumptions.

1. The RF fields vary with time as $e^{i\omega t}$: This time variation is indicative of harmonic oscillation [17]. It can be derived by considering the time dependance in the wave equation, as will be shown in the next section.

2. The helix and the ferrite tube are of infinite length: This is a standard assumption used in the sheath helix model. Previous authors who have analysed helical structures using the sheath helix model have made this assumption [17]. Although this assumption would imply that the reflected wave can be ignored in the calculations and analysis, this is not unrealistic. By

[1] The equation is derived in Appendix A

calculating the characteristic impedance of the structure, it is possible to put a load of equal impedance and thus *match* the impedances so that the structure would behave as an infinitely long device without any reflected wave [32].

3. The helix is infinitely thin: This is another standard assumption in the sheath helix model, which has also been used by many authors when analysing helical structures [17].

4. The conductivity is infinite in the direction parallel to the windings, but zero perpendicular to the direction of windings: This is another standard assumption in the sheath helix model, which has also been used by many authors when analysing helical structures [17].

5. The magnetic field inside the structure is known. This assumption has been used by several authors; some of whom are Orlando [30], Suhl [8], and Ivanov [28].

## 2.4 The Electric and Magnetic Fields

The electric field **E** and magnetic flux density **B** are vector fields that have amplitude and direction that vary with spatial co-ordinates and time. Therefore, the electric field and magnetic flux density can be written as **E**(**x**,t) and **B**(**x**,t), respectively, where **x** is a position vector. As a cylindrical structure is considered, the spatial coordinates are represented in cylindrical polar coordinates. Therefore, letting **X** represent both fields **E** and **H**, such that **X**=X$(r, \theta, z, t)$, substituting into equation (2.1) gives

$$\frac{1}{r}\frac{\partial}{\partial r}\left(r\,\frac{\partial X}{\partial r}\right)+\frac{1}{r^2}\frac{\partial^2 X}{\partial \theta^2}+\frac{\partial^2 X}{\partial z^2}=\frac{1}{c^2}\frac{\partial^2 X}{\partial t^2}. \tag{2.2}$$

Equation (2.2) can be solved using the method of separation of variables. Initially, an axisymmetric solution is sought, with $X = R(r)Z(z)T(t)$ [33]. Therefore,

$$\frac{R''}{R}+\frac{1}{r}\frac{R'}{R}+\frac{Z''}{Z}=\frac{1}{c^2}\frac{T''}{T}=-\frac{\omega^2}{c^2}. \tag{2.3}$$

The choice of separation constant becomes apparent, when the equation $T'' + \omega^2 T = 0$ leads to

$$T = \exp(\pm i\omega t),$$

which represents harmonic oscillation. Rearranging (2.3) gives

$$\frac{R''}{R} + \frac{1}{r}\frac{R'}{R} = -\frac{\omega^2}{c^2} - \frac{Z''}{Z} = -\frac{\omega^2}{c^2} + \beta^2, \tag{2.4}$$

where the choice of separation constant leads to $Z'' + \beta^2 Z = 0$ and thus

$$Z = \exp(\pm i\beta z),$$

where the propagation constant $\beta$ indicates that the wave is travelling in the $z$-direction. Equation (2.4) becomes

$$R'' + \frac{R'}{r} - \left(\beta^2 - \omega^2\mu\varepsilon\right) R = 0, \tag{2.5}$$

which can be solved to give

$$R = \bar{a} I_0(kr) + \bar{b} K_0(kr), \tag{2.6}$$

where $k^2 = \beta^2 - \omega^2\mu\varepsilon$, $\bar{a}$ and $\bar{b}$ are constants and $I_0$ and $K_0$ are modified Bessel functions of zero order. Now, if the electric and magnetic fields are assumed to have angular dependance (i.e, the non-axisymmetric case), then letting $X = R(r)\Theta(\theta)\exp\left(i\left(\omega t - \beta z\right)\right)$ and substituting this into (2.4) gives

$$\frac{R''}{R} + \frac{1}{r}\frac{R'}{R} = -\frac{1}{r^2}\frac{\Theta''}{\Theta} = k^2. \tag{2.7}$$

The equation simplifies to

$$r^2\frac{R''}{R} + r\frac{R'}{R} - rk^2 = -\frac{\Theta''}{\Theta} = n^2. \tag{2.8}$$

The solutions of these equations are

$$R(r) = \bar{a} I_n(kr) + \bar{b} K_n(kr), \tag{2.9}$$

$$\Theta(\theta) = \bar{c}\cos(n\theta) + \bar{d}\sin(n\theta), \tag{2.10}$$

where $\bar{a}, \bar{b}, \bar{c}$ and $\bar{d}$ are constants. Therefore,

$$X = \left(\bar{a}\, I_n(kr) + \bar{b}\, K_n(kr)\right)\left(\bar{c}\, \cos(n\theta) + \bar{d}\, \sin(n\theta)\right) \exp\left(i\left(\omega t - \beta z\right)\right). \tag{2.11}$$

A change in $2p\pi$ where $p$ is an integer would generate the same value, as $\theta$ is $2\pi$ periodic. Therefore, $n$ must be an integer. The $\theta$ dependance of the wave is of the form $\exp(\pm in\theta)$. Therefore, the expressions for $\mathbf{E}$ and $\mathbf{B}$ take the form

$$\mathbf{B} = \left[B_r(r)\widehat{r} + B_\theta(r)\widehat{\theta} + B_z(r)\widehat{z}\right] e^{i(\omega t + n\theta - \beta z)}, \qquad \mathbf{E} = \left[E_r(r)\widehat{r} + E_\theta(r)\widehat{\theta} + E_z(r)\widehat{z}\right] e^{i(\omega t + n\theta - \beta z)}. \tag{2.12}$$

The term $e^{i(\omega t + n\theta - \beta z)}$ shows that the wave has an angular frequency $\omega$, the wave propagates in the $z$ - direction with the respect to the phase constant $\beta$ and the complex number $i$ signifies that there is a phase shift $\frac{\pi}{2}$. The following relations can also be derived:

$$\frac{\partial}{\partial t}\begin{pmatrix}\mathbf{E}\\ \mathbf{H}\end{pmatrix} = i\omega\begin{pmatrix}\mathbf{E}\\ \mathbf{H}\end{pmatrix}, \qquad \frac{\partial}{\partial \theta}\begin{pmatrix}\mathbf{E}\\ \mathbf{H}\end{pmatrix} = in\begin{pmatrix}\mathbf{E}\\ \mathbf{H}\end{pmatrix}, \qquad \frac{\partial}{\partial z}\begin{pmatrix}\mathbf{E}\\ \mathbf{H}\end{pmatrix} = -i\beta\begin{pmatrix}\mathbf{E}\\ \mathbf{H}\end{pmatrix}. \tag{2.13}$$

These expressions will be used when deriving the governing equations in each of the different regions.

## 2.5 The Equations in Air

The structure consists of three regions of air and one of ferrite. This section derives the governing equations in air and gives solutions to these equations.

### 2.5.1 The Governing Equations

In air $\mathbf{B} = \mu_0\mathbf{H}$, and substituting this into Maxwell's equations gives

$$\nabla \cdot \mathbf{H} = 0, \qquad \nabla \cdot \mathbf{E} = 0, \tag{2.14}$$

$$\nabla \wedge \mathbf{H} = i\omega\varepsilon_0\mathbf{E}, \qquad \nabla \wedge \mathbf{E} = -i\omega\mu_0\mathbf{H}. \tag{2.15}$$

By using vector identities, these equations can be rearranged to give the wave equation

$$\nabla^2 \begin{bmatrix} \mathbf{E} \\ \mathbf{H} \end{bmatrix} = \frac{1}{c^2}\frac{\partial^2}{\partial t^2} \begin{bmatrix} \mathbf{E} \\ \mathbf{H} \end{bmatrix}. \tag{2.16}$$

In cylindrical polar co-ordinates (2.16) becomes

$$\frac{d^2}{dr^2} \begin{bmatrix} \mathbf{E} \\ \mathbf{H} \end{bmatrix} + \frac{1}{r}\frac{d}{dr} \begin{bmatrix} \mathbf{E} \\ \mathbf{H} \end{bmatrix} - \left(\frac{n^2}{r^2} + \beta^2 - \omega^2\varepsilon_0\mu_0\right) \begin{bmatrix} \mathbf{E} \\ \mathbf{H} \end{bmatrix} = 0. \tag{2.17}$$

As shown in the previous subsection, this can be solved to give

$$E_z = \bar{a}\, I_n\left(\bar{k}_0 r\right) + \bar{b}\, K_n\left(\bar{k}_0 r\right), \qquad \text{and} \qquad H_z = \bar{c}\, I_n\left(\bar{k}_0 r\right) + \bar{d}\, K_n\left(\bar{k}_0 r\right), \tag{2.18}$$

where $\bar{k}_0^2 = \beta^2 - \omega^2\mu_0\varepsilon_0$, and $\bar{a}$, $\bar{b}$, $\bar{c}$, and $\bar{d}$ are constants. $I$ and $K$ refer to modified Bessel functions.

Expressing (2.15) in cylindrical polar co-ordinates give

$$\begin{aligned}
(\nabla \wedge \mathbf{H})_r &= \tfrac{1}{r}\tfrac{\partial H_z}{\partial \theta} - \tfrac{\partial H_\theta}{\partial z} &&= i\omega\varepsilon_0 E_r, \\
(\nabla \wedge \mathbf{H})_\theta &= \tfrac{\partial H_r}{\partial z} - \tfrac{\partial H_z}{\partial r} &&= i\omega\varepsilon_0 E_\theta, \\
(\nabla \wedge \mathbf{H})_z &= \tfrac{\partial H_\theta}{\partial r} + \tfrac{H_\theta}{r} - \tfrac{1}{r}\tfrac{\partial H_r}{\partial \theta} &&= i\omega\varepsilon_0 E_z, \\
(\nabla \wedge \mathbf{E})_r &= \tfrac{1}{r}\tfrac{\partial E_z}{\partial \theta} - \tfrac{\partial E_\theta}{\partial z} &&= -i\omega\mu_0 H_r, \\
(\nabla \wedge \mathbf{E})_\theta &= \tfrac{\partial E_r}{\partial z} - \tfrac{\partial E_z}{\partial r} &&= -i\omega\mu_0 H_\theta, \\
(\nabla \wedge \mathbf{E})_z &= \tfrac{\partial E_\theta}{\partial r} + \tfrac{E_\theta}{r} - \tfrac{1}{r}\tfrac{\partial E_r}{\partial \theta} &&= -i\omega\mu_0 H_z.
\end{aligned} \tag{2.19}$$

Rearranging (2.19) give

$$\bar{k}_0^2\, E_r = i\beta\frac{\partial E_z}{\partial r} + \frac{i\omega\mu_0}{r}\frac{\partial H_z}{\partial \theta}, \qquad \bar{k}_0^2\, E_\theta = -i\omega\mu_0\frac{\partial H_z}{\partial r} + \frac{i\beta}{r}\frac{\partial E_z}{\partial \theta}, \tag{2.20}$$

$$\bar{k}_0^2\, H_r = i\beta\frac{\partial H_z}{\partial r} - \frac{i\omega\varepsilon_0}{r}\frac{\partial E_z}{\partial \theta}, \qquad \bar{k}_0^2\, H_\theta = i\omega\varepsilon_0\frac{\partial E_z}{\partial r} + \frac{i\beta}{r}\frac{\partial H_z}{\partial \theta}. \tag{2.21}$$

By substituting (2.18) into equations (2.20) - (2.21), expressions for $E_r$, $E_\theta$, $H_r$ and $H_\theta$ can be written in terms of modified Bessel functions. This will be done in the next subsection.

### 2.5.2 Solutions

**The case when $n = 0$**

For $n = 0$, $\frac{\partial}{\partial\theta} = 0$ corresponding to the axisymmetric case. Substituting $n = 0$ into the expressions above gives:

$$E_z = \bar{a}\, I_0\left(\bar{k}_0 r\right) + \bar{b}\, K_0\left(\bar{k}_0 r\right), \qquad H_z = \bar{c}\, I_0\left(\bar{k}_0 r\right) + \bar{d}\, K_0\left(\bar{k}_0 r\right), \tag{2.22}$$

$$E_\theta = -\frac{i\omega\mu_0}{\bar{k}_0}\left[\bar{c}\, I_1\left(\bar{k}_0 r\right) - \bar{d}\, K_1\left(\bar{k}_0 r\right)\right], \qquad H_\theta = \frac{i\omega\varepsilon_0}{\bar{k}_0}\left[\bar{a}\, I_1\left(\bar{k}_0 r\right) - \bar{b}\, K_1\left(\bar{k}_0 r\right)\right], \tag{2.23}$$

$$E_r = \frac{i\beta}{\bar{k}_0}\left[\bar{a}\, I_0\left(\bar{k}_0 r\right) + \bar{b}\, K_0\left(\bar{k}_0 r\right)\right], \qquad H_r = \frac{i\beta}{\bar{k}_0}\left[\bar{c}\, I_0\left(\bar{k}_0 r\right) + \bar{d}\, K_0\left(\bar{k}_0 r\right)\right]. \tag{2.24}$$

These terms will be substituted into the boundary conditions in order to arrive at the full system of equations to be solved.

**The case when $n = 1$**

For $n = 1$, the following solutions are obtained:

$$E_z = \bar{a}\, I_1\left(\bar{k}_0 r\right) + \bar{b}\, K_1\left(\bar{k}_0 r\right), \qquad H_z = \bar{c}\, I_1\left(\bar{k}_0 r\right) + \bar{d}\, K_1\left(\bar{k}_0 r\right), \tag{2.25}$$

$$E_\theta = -\frac{i\omega\mu_0\left[\bar{c}\, I_0\left(\bar{k}_0 r\right) - \bar{d}\, K_0\left(\bar{k}_0 r\right)\right]}{\bar{k}_0} - \frac{\beta\left[\bar{a}\, I_1\left(\bar{k}_0 r\right) + \bar{b}\, K_1\left(\bar{k}_0 r\right)\right] - i\omega\mu_0\left[\bar{c}\, I_1\left(k_0 r\right) + \bar{d}\, K_1\left(\bar{k}_0 r\right)\right]}{\bar{k}_0^2 r}, \tag{2.26}$$

$$H_\theta = \frac{i\omega\varepsilon_0\left[\bar{a}\, I_0\left(\bar{k}_0 r\right) - \bar{b}\, K_0\left(\bar{k}_0 r\right)\right]}{\bar{k}_0} - \frac{\beta\left[\bar{c}\, I_1\left(\bar{k}_0 r\right) + \bar{d}\, K_1\left(\bar{k}_0 r\right)\right] + i\omega\varepsilon_0\left[\bar{a}\, I_1\left(\bar{k}_0 r\right) + \bar{b}\, K_1\left(\bar{k}_0 r\right)\right]}{\bar{k}_0^2 r}, \tag{2.27}$$

$$E_r = \frac{i\beta\left[\bar{a}\, I_0\left(\bar{k}_0 r\right) - \bar{b}\, K_0\left(\bar{k}_0 r\right)\right]}{\bar{k}_0} - \frac{i\beta\left[\bar{a}\, I_1\left(\bar{k}_0 r\right) + \bar{b}\, K_1\left(\bar{k}_0 r\right)\right] + \omega\mu_0\left[\bar{c}\, I_1\left(\bar{k}_0 r\right) + \bar{d}\, K_1\left(\bar{k}_0 r\right)\right]}{\bar{k}_0^2 r}, \tag{2.28}$$

$$H_r = \frac{i\beta\left[\bar{c}\, I_0\left(\bar{k}_0 r\right) - \bar{d}\, K_0\left(\bar{k}_0 r\right)\right]}{\bar{k}_0} - \frac{i\beta\left[\bar{c}\, I_1\left(\bar{k}_0 r\right) + \bar{d}\, K_1\left(\bar{k}_0 r\right)\right] - \omega\varepsilon_0\left[\bar{a}\, I_1\left(\bar{k}_0 r\right) + \bar{b}\, K_1\left(\bar{k}_0 r\right)\right]}{\bar{k}_0^2 r}. \tag{2.29}$$

The expression have been written using the Bessel function relations in Appendix C.

## 2.6 System of Equations

This section deals with how the system of equations is arrived at. Although, the case of $n = 0$ is described here, the method is applicable to the other cases, for n > 0.

### 2.6.1 Region 1

Region 1 refers to region of air inside the metal helix. This has the following solutions,

$$E_{z1} = a_1\, I_0\,(k_0 r) + b_1\, K_0\,(k_0 r)\,, \qquad H_{z1} = c_1\, I_0\,(k_0 r) + d_1\, K_0\,(k_0 r)\,, \tag{2.30}$$

where $a_1$, $b_1$, $c_1$ and $d_1$ are constants. Physically the fields must be finite at $r = 0$, therefore $b_1$ and $d_1$ must vanish. Therefore, in region 1,

$$E_{z1} = a_1\, I_0\,(k_0 r)\,, \quad E_{\theta 1} = -\frac{i\omega\mu_0}{k_0}\, c_1\, I_1\,(k_0 r)\,, \quad E_{r1} = \frac{i\beta}{k_0}\, a_1\, I_0\,(k_0 r)\,, \tag{2.31}$$

$$H_{z1} = c_1\, I_0\,(k_0 r)\,, \quad H_{\theta 1} = \frac{i\omega\varepsilon_0}{k_0}\, a_1\, I_1\,(k_0 r)\,, \quad H_{r1} = \frac{i\beta}{k_0}\, c_1\, I_0\,(k_0 r)\,, \tag{2.32}$$

where the subscript $_1$ indicates region 1.

### 2.6.2 Region 2

Region 2 refers to the air gap between the metal helix and the ferrite. This has the following solutions,

$$E_{z2} = a_2\, I_0\,(k_0 r) + b_2\, K_0\,(k_0 r)\,, \qquad H_{z2} = c_2\, I_0\,(k_0 r) + d_2\, K_0\,(k_0 r)\,, \tag{2.33}$$

$$E_{\theta 2} = -\frac{i\omega\mu_0}{k_0}\left[c_2\, I_1\,(k_0 r) - d_2\, K_1\,(k_0 r)\right], \qquad H_{\theta 2} = \frac{i\omega\varepsilon_0}{k_0}\left[a_2\, I_1\,(k_0 r) - b_2\, K_1\,(k_0 r)\right], \tag{2.34}$$

$$E_{r2} = \frac{i\beta}{k_0}\left[a_2\, I_0\,(k_0 r) + b_2\, K_0\,(k_0 r)\right], \qquad H_{r2} = \frac{i\beta}{k_0}\left[c_2\, I_0\,(k_0 r) + d_2\, K_0\,(k_0 r)\right], \tag{2.35}$$

where $a_2$, $b_2$, $c_2$ and $d_2$ are constants and the subscript $_2$ indicates region 2.

### 2.6.3 Region 3

Region 3 refers to the region of the ferrite. Due to the complexity of the equations in region 3, full details of the governing equations and solutions can be found in Appendix B.1. It can be noticed that each region has four constants associated with it, (region 1 has $a_1...d_1$ associated with it, region 2 has $a_2...d_2$ associated with it and region 4 have $a_4...d_4$ associated with it). Thus, region 3 has also four constants associated with it $a_3...d_3$. Therefore, each expression ($E_r$, $E_\theta$, $E_z$, $H_r$, $H_\theta$, $H_z$) can be expressed as a sum of four linearly independent radial expressions with constants $a_3...d_3$. Therefore, the expressions below are assumed.

$$E_{z3} = a_3 E_{z31}(r) + b_3 E_{z32}(r) + c_3 E_{z33}(r) + d_3 E_{z34}(r), \tag{2.36}$$

$$H_{z3} = a_3 H_{z31}(r) + b_3 H_{z32}(r) + c_3 H_{z33}(r) + d_3 H_{z34}(r), \tag{2.37}$$

$$E_{\theta 3} = a_3 E_{\theta 31}(r) + b_3 E_{\theta 32}(r) + c_3 E_{\theta 33}(r) + d_3 E_{\theta 34}(r), \tag{2.38}$$

$$H_{\theta 3} = a_3 H_{\theta 31}(r) + b_3 H_{\theta 32}(r) + c_3 H_{\theta 33}(r) + d_3 H_{\theta 34}(r), \tag{2.39}$$

$$E_{r3} = a_3 E_{r31}(r) + b_3 E_{r32}(r) + c_3 E_{r33}(r) + d_3 E_{r34}(r), \tag{2.40}$$

$$H_{r3} = a_3 H_{r31}(r) + b_3 H_{r32}(r) + c_3 H_{r33}(r) + d_3 H_{r34}(r). \tag{2.41}$$

where $a_3$, $b_3$, $c_3$ and $d_3$ are constants and the subscript $_3$ indicates region 3. Appendix B.1 give the expressions for all of the above terms.

### 2.6.4 Region 4

Region 4 refers to the air gap between the metal helix and the ferrite. This has the following solutions,

$$E_{z4} = a_4\, I_0\,(k_0 r) + b_4\, K_0\,(k_0 r)\,, \qquad H_{z4} = c_4\, I_0\,(k_0 r) + d_4\, K_0\,(k_0 r)\,, \tag{2.42}$$

$$E_{\theta 4} = -\frac{i\omega\mu_0}{k_0}\left[c_4\, I_1\,(k_0 r) - d_4\, K_1\,(k_0 r)\right], \qquad H_{\theta 4} = \frac{i\omega\varepsilon_0}{k_0}\left[a_4\, I_1\,(k_0 r) - b_4\, K_1\,(k_0 r)\right], \tag{2.43}$$

$$E_{r4} = \frac{i\beta}{k_0}\left[a_4\, I_0\,(k_0 r) + b_4\, K_0\,(k_0 r)\right], \qquad H_{r4} = \frac{i\beta}{k_0}\left[c_4\, I_0\,(k_0 r) + d_4\, K_0\,(k_0 r)\right], \tag{2.44}$$

where $a_4$, $b_4$, $c_4$ and $d_4$ are constants and the subscript $_4$ indicates region 4.

### 2.6.5 Boundary Conditions

#### Boundary Conditions between the air and metal helix

The boundary conditions between the air and metal helix at $r = a$ are given by

$$\mathbf{E}^i_\perp(a) = \mathbf{E}^o_\perp(a),\ \ \mathbf{E}^i_\parallel(a) = \mathbf{E}^o_\parallel(a) = 0,\ \ \mathbf{H}^i_\parallel(a) = \mathbf{H}^o_\parallel(a). \tag{2.45}$$

In these equations, parallel and perpendicular are in reference to the windings, and $^i$ and $^o$ indicate the inside and outside of the helix, respectively. As these equations are in reference to the windings, and *not* with respect to the surface, it is necessary to resolve $E_\theta$, $E_z$, $H_\theta$ and $H_z$ in these directions. Therefore, equations (2.45) can be written as

$$E_{\theta1}(a) + E_{z1}(a)\tan(\psi) = 0, \qquad E_{\theta2}(a) + E_{z2}(a)\tan(\psi) = 0,$$

$$E_{z1}(a) - E_{\theta1}(a)\tan(\psi) = E_{z2}(a) - E_{\theta2}(a)\tan(\psi), \qquad H_{\theta1}(a) + H_{z1}(a)\tan(\psi) = H_{\theta2}(a) + H_{z2}(a)\tan(\psi).$$

#### Boundary Conditions between the Air and Ferrite Tube

The boundary conditions between the air and ferrite tube at $r = b$ and $r = c$ are given by

$$\mathbf{E}^i_\parallel(b) = \mathbf{E}^o_\parallel(b), \quad \mathbf{H}^i_\parallel(b) = \mathbf{H}^o_\parallel(b), \tag{2.46}$$

$$\mathbf{E}^i_\parallel(c) = \mathbf{E}^o_\parallel(c), \quad \mathbf{H}^i_\parallel(c) = \mathbf{H}^o_\parallel(c). \tag{2.47}$$

In these equations, parallel and perpendicular are in reference to the ferrite tube, and $^i$ and $^o$ indicate the different sides of the boundary. These equations can also be written in terms of $E_\theta$, $E_z$, $H_\theta$ and $H_z$. Thus, the following expressions are obtained.

$$E_{z2}(b) = E_{z3}(b), \qquad E_{\theta2}(b) = E_{\theta3}(b), \qquad H_{z2}(b) = H_{z3}(b), \qquad H_{\theta2}(b) = H_{\theta3}(b),$$

$$E_{z3}(c) = E_{z4}(c), \qquad E_{\theta3}(c) = E_{\theta4}(c), \qquad H_{z3}(c) = H_{z4}(c), \qquad H_{\theta3}(c) = H_{\theta4}(c),$$

**Boundary Conditions between the Air and Metal Waveguide**

The boundary conditions between the air and metal waveguide at $r = d$ are given by:

$$\mathbf{E}_{\parallel}(d) = 0. \tag{2.48}$$

In this equation, parallel and perpendicular are in reference to the metal container. Writing this in terms of $E_\theta$ and $Ez$ gives

$$E_{z4}(d) = 0. \qquad E_{\theta 4}(d) = 0$$

The table below shows all the boundaries with the corresponding equations that were used.

| Boundary regions | Boundary condition | Equation |
|---|---|---|
| 1 and 2<br>air and metal helix<br>$r = a$ | $E_{\parallel 1} = 0$<br>$E_{\parallel 2} = 0$<br>$E_{\perp 1} = E_{\perp 2}$<br>$H_{\parallel 1} = H_{\parallel 2}$<br>($\parallel$ and $\perp$ to the windings) | $E_{\theta 1}(a) + E_{z1}(a)\tan(\psi) = 0$<br>$E_{\theta 2}(a) + E_{z2}(a)\tan(\psi) = 0$<br>$E_{z1}(a)$ - $E_{\theta 1}(a)\tan(\psi) =$<br>$E_{z2}(a)$ - $E_{\theta 2}(a)\tan(\psi)$<br>$H_{\theta 1}(a) + H_{z1}(a)\tan(\psi) =$<br>$H_{\theta 2}(a) + H_{z2}(a)\tan(\psi)$ |
| 2 and 3<br>air and ferrite<br>$r = b$ | $E_{\parallel 2} = E_{\parallel 3}$<br>$H_{\parallel 2} = H_{\parallel 3}$<br>($\parallel$ and $\perp$ to the surface) | $E_{z2}(b) = E_{z3}(b) \quad E_{\theta 2}(b) = E_{\theta 3}(b)$<br>$H_{z2}(b) = H_{z3}(b) \quad H_{\theta 2}(b) = H_{\theta 3}(b)$ |
| 3 and 4<br>ferrite and air<br>$r = c$ | $E_{\parallel 3} = E_{\parallel 4}$<br>$H_{\parallel 3} = H_{\parallel 4}$<br>($\parallel$ and $\perp$ to the surface) | $E_{z3}(c) = E_{z4}(c) \quad E_{\theta 3}(c) = E_{\theta 4}(c)$<br>$H_{z3}(c) = H_{z4}(c) \quad H_{\theta 3}(c) = H_{\theta 4}(c)$ |
| air and metal container<br>$r = d$ | $E_{\parallel 4} = 0$<br>($\parallel$ and $\perp$ to the surface) | $E_{z4}(d) = 0$<br>$E_{\theta 4}(d) = 0$ |

By substituting the expressions for each region into the boundary conditions, the system of simultaneous linear equations can be written as:

$$a_1\, I_0\,(k_0 a)\tan(\psi) - \frac{i\omega\mu_0}{k_0}\, c_1\, I_1\,(k_0 a) = 0, \tag{2.49}$$

$$(a_2\, I_0\,(k_0 a) + b_2\, K_0\,(k_0 a))\tan(\psi) - \frac{i\omega\mu_0}{k_0}\,[c_2\, I_1\,(k_0 a) - d_2\, K_1\,(k_0 a)] = 0, \tag{2.50}$$

$$\begin{aligned} a_1\, I_0\,(k_0 a) + \frac{i\omega\mu_0}{k_0}\, c_1\, I_1\,(k_0 r)\tan(\psi) - (a_2\, I_0\,(k_0 a) + b_2\, K_0\,(k_0 a)) \\ -\frac{i\omega\mu_0}{k_0}\,[c_2\, I_1\,(k_0 a) - d_2\, K_1\,(k_0 a)]\tan(\psi) = 0, \end{aligned} \tag{2.51}$$

$$\begin{aligned} \frac{i\omega\varepsilon_0}{k_0}\, a_1\, I_1\,(k_0 a) + c_1\, I_0\,(k_0 a)\tan(\psi) - \frac{i\omega\varepsilon_0}{k_0}\,[a_2\, I_1\,(k_0 a) - b_2\, K_1\,(k_0 a)] \\ -(c_2\, I_0\,(k_0 r) + d_2\, K_0\,(k_0 r))\tan(\psi) = 0, \end{aligned} \tag{2.52}$$

$$a_2\, I_0\,(k_0 b) + b_2\, K_0\,(k_0 b) - (a_3 E_{z31}(b) + b_3 E_{z32}(b) + c_3 E_{z33}(b) + d_3 E_{z34}(b)) = 0, \tag{2.53}$$

$$-\frac{i\omega\mu_0}{k_0}\,[c_2\, I_1\,(k_0 b) - d_2\, K_1\,(k_0 b)] - (a_3 E_{\theta 31}(b) + b_3 E_{\theta 32}(b) + c_3 E_{\theta 33}(b) + d_3 E_{\theta 34}(b)) = 0, \tag{2.54}$$

$$c_2\, I_0\,(k_0 b) + d_2\, K_0\,(k_0 b) - (a_3 H_{z31}(b) + b_3 H_{z32}(b) + c_3 H_{z33}(b) + d_3 H_{z34}(b)) = 0, \tag{2.55}$$

$$\frac{i\omega\varepsilon_0}{k_0}\,[a_2\, I_1\,(k_0 b) - b_2\, K_1\,(k_0 b)] - (a_3 H_{\theta 31}(b) + b_3 H_{\theta 32}(b) + c_3 H_{\theta 33}(b) + d_3 H_{\theta 34}(b)) = 0, \tag{2.56}$$

$$a_3 E_{z31}(c) + b_3 E_{z32}(c) + c_3 E_{z33}(c) + d_3 E_{z34}(c) - (a_4\, I_0\,(k_0 c) + b_4\, K_0\,(k_0 c)) = 0, \tag{2.57}$$

$$a_3 E_{\theta 31}(c) + b_3 E_{\theta 32}(c) + c_3 E_{\theta 33}(c) + d_3 E_{\theta 34}(c) + \frac{i\omega\mu_0}{k_0}\,[c_4\, I_1\,(k_0 c) - d_4\, K_1\,(k_0 c)] = 0, \tag{2.58}$$

$$a_3 H_{z31}(c) + b_3 H_{z32}(c) + c_3 H_{z33}(c) + d_3 H_{z34}(c) - (c_4\, I_0\,(k_0 c) + d_4\, K_0\,(k_0 c)) = 0, \tag{2.59}$$

$$a_3 H_{\theta 31}(c) + b_3 H_{\theta 32}(c) + c_3 H_{\theta 33}(c) + d_3 H_{\theta 34}(c) - \frac{i\omega\varepsilon_0}{k_0}\,[a_4\, I_1\,(k_0 c) - b_4\, K_1\,(k_0 c)] = 0, \tag{2.60}$$

$$a_4\, I_0\,(k_0 d) + b_4\, K_0\,(k_0 d) = 0, \tag{2.61}$$

$$c_4\, I_1\,(k_0 d) - d_4\, K_1\,(k_0 d) = 0. \tag{2.62}$$

These equations can be rewritten in the form

$$\mathbf{A}.\,(a_1, a_2, a_3, a_4, b_2, b_3, b_4, c_1, c_2, c_3, c_4, d_2, d_3, d_4)^T = \mathbf{0}, \quad \text{where} \quad \mathbf{A} = \begin{pmatrix} A_{11} & \cdots & A_{114} \\ \vdots & \ddots & \vdots \\ A_{141} & \cdots & A_{1414} \end{pmatrix}. \tag{2.63}$$

There are two possible solutions:

$$(a_1, a_2, a_3, a_4, b_2, b_3, b_4, c_1, c_2, c_3, c_4, d_2, d_3, d_4)^T = 0,$$

or

$$\begin{vmatrix} A_{11} & \cdots & A_{114} \\ \vdots & \ddots & \vdots \\ A_{141} & \cdots & A_{1414} \end{vmatrix} = 0.$$

Ignoring the trivial solution, it is necessary to determine a value of $\beta$ such that

$$\begin{vmatrix} A_{11} & \cdots & A_{114} \\ \vdots & \ddots & \vdots \\ A_{141} & \cdots & A_{1414} \end{vmatrix} = 0.$$

The numerical method that was employed to find a $\beta$ value is described in section 2.8.

## 2.7 Losses

The losses in the helical structure arise from two parts.

1. **The conductor loss**. This is due to the conductivity of the metal helix and tube.

2. **The dielectric or ferrite loss**. This is due to the loss of the dielectric or ferrite.

However, a calculation of the power flow through the structure is required - for which the *Poynting vector* needs to be introduced.

Electromagnetic waves carry energy through space. At any point in space, the flow of energy can be described by a *power density vector* $\mathbf{P}$. The vector $\mathbf{P}$ is called the *Poynting vector*, and is a cross product of electric and magnetic field vectors. The total power passing through a surface $S$, denoted by W, is obtained by integration over $S$, i.e

$$W = \int_S \mathbf{P} \cdot d\mathbf{S}. \tag{2.64}$$

The Poynting vector for complex phasor representation is defined as

$$\mathbf{P} = \frac{1}{2}\,\mathbb{R}\left(\mathbf{E} \wedge \mathbf{H}^{\star}\right), \tag{2.65}$$

where $\mathbf{H}^{\star}$ refers to the conjugate of $\mathbf{H}$ [13]. The total power flow $\Pi_T$ is obtained by the sum of the power flow in each region. Therefore,

$$\Pi_T = \Pi_1 + \Pi_2 + \Pi_3 + \Pi_4.$$

Letting

$$T_1 = E_{r1}H^{\star}_{\theta 1} - E_{\theta 1}H^{\star}_{r1},\ T_2 = E_{r2}H^{\star}_{\theta 2} - E_{\theta 2}H^{\star}_{r2},\ T_3 = E_{r3}H^{\star}_{\theta 3} - E_{\theta 3}H^{\star}_{r3},\ T_4 = E_{r4}H^{\star}_{\theta 4} - E_{\theta 4}H^{\star}_{r4},$$

then

$$\Pi_T = \frac{1}{2}\,\mathbb{R}\int_{S_1} T_1 \cdot dA + \frac{1}{2}\,\mathbb{R}\int_{S_2} T_2 \cdot dA + \frac{1}{2}\,\mathbb{R}\int_{S_3} T_3 \cdot dA + \frac{1}{2}\,\mathbb{R}\int_{S_4} T_4 \cdot dA. \tag{2.66}$$

In cylindrical polar coordinates, the area of a region $R$ is given by,

$$\int_R dA = \int r dr \int d\theta. \tag{2.67}$$

Substituting (2.67) into (2.66) leads to

$$\Pi_1 = \frac{1}{2}\int_0^{2\pi} d\theta \int_0^{a} T_1 r\ \mathrm{dr},\ \ \Pi_2 = \frac{1}{2}\int_0^{2\pi} d\theta \int_a^{b} T_2 r\ \mathrm{dr},\ \ \Pi_3 = \frac{1}{2}\int_0^{2\pi} d\theta \int_b^{c} T_3 r\ \mathrm{dr},\ \ \Pi_4 = \frac{1}{2}\int_0^{2\pi} d\theta \int_c^{d} T_4 r\ \mathrm{dr}.$$

Equations (2.49) - (2.62) represent the system of equations. Letting $a_1 = A$, the other coefficients can be written in terms of $A$. Therefore, equation (2.66) can be calculated in terms of a single constant, $A$.

### 2.7.1 The Conductor Loss

A general expression for a wave propagating in the direction of the positive z-axis is

$$e^{-i\beta z}.$$

Due to attenuation, the amplitude of the wave will decay exponentially. Therefore, letting $\alpha$ represent the attenuation coefficient, the wave will have the expression

$$e^{-i\beta z}e^{-\alpha z},$$

where the minus sign indicates a decay. If a wave is represented by the term $\Pi_0$, the modelling of attenuation can be included to give

$$\Pi_T = \Pi_0\, e^{-\alpha z},$$

where $\Pi_T$ is the expression of the wave with attenuation. Then

$$\alpha = -\frac{1}{\Pi_T}\frac{d}{dz}\Pi_T.$$

Letting

$$\frac{d}{dz}\,\Pi_T = \frac{d}{dz}\,\Pi_1 + \frac{d}{dz}\,\Pi_2,$$

such that

$$\frac{d}{dz}\,\Pi_1 = 2\pi a P_{L1} \text{ and } \frac{d}{dz}\,\Pi_2 = 2\pi b P_{L2},$$

where $P_{L1}$ and $P_{L2}$ are the power loss per unit area in the structure and are determined by the Poynting vectors $S_1$ and $S_2$. The expression $2\pi a$ is the circumference of the metal helix, and $2\pi d$ is the circumference of the metal waveguide. The expressions $2\pi a P_{L1}$ and $2\pi d P_{L2}$ correspond to the loss that is contributed by the metal helix and waveguide, respectively. Letting $\mathbf{n}$ be a unit vector normal to the direction of propagation, and $R_s$ be the surface resistance, then

$$\mathbf{E} = R_s(\mathbf{n} \wedge \mathbf{H}).$$

Hence,

$$E_z = R_s H_\theta \qquad \text{and} \qquad E_\theta = -R_s H_z.$$

Therefore[2],

$$P_L = \frac{1}{2}\, R_s \left(|H_\theta|^2 + |H_z|^2\right).$$

[2] [20], equation (4)

$R_s$ is given by

$$R_s = \sqrt{\pi \mu \rho f}.$$

$P_{L1}$ is the loss due to the helix. This is comprised of the loss from the inside and outside of the helix. This gives

$$P_L(\text{inside helix}) = \frac{1}{2} R_s \left( |H_{\theta 1}(a)|^2 + |H_{z1}(a)|^2 \right), \quad P_L(\text{outside helix}) = \frac{1}{2} R_s \left( |H_{\theta 2}(a)|^2 + |H_{z2}(a)|^2 \right).$$

Therefore,

$$P_{L1} = \frac{1}{2} R_s \left( |H_{\theta 1}(a)|^2 + |H_{z1}(a)|^2 \right) + \frac{1}{2} R_s \left( |H_{\theta 2}(a)|^2 + |H_{z2}(a)|^2 \right).$$

Letting $\rho_1$ be the resistivity of the helix and $R_{s1}$ be the surface resistance of the helix. Thus

$$R_{s1} = \sqrt{\pi \mu_0 \rho_1 f}.$$

Therefore,

$$P_{L1} = \frac{1}{2} R_{s1} \left( |H_{\theta 1}(a)|^2 + |H_{z1}(a)|^2 \right) + \frac{1}{2} R_{s1} \left( |H_{\theta 2}(a)|^2 + |H_{z2}(a)|^2 \right).$$

$P_{L2}$ is the loss due to the metal wall. This has the expression

$$P_{L2} = \frac{1}{2} R_s \left( |H_{\theta 4}(d)|^2 + |H_{z4}(d)|^2 \right).$$

Letting $\rho_2$ be the resistivity of the metal wall and $R_{s2}$ be the surface resistance of the metal wall. Thus,

$$Rs_2 = \sqrt{\pi \mu_0 \rho_2 f}.$$

Therefore,

$$P_{L2} = \frac{1}{2} R_{s2} \left( |H_{\theta 4}(d)|^2 + |H_{z4}(d)|^2 \right).$$

Therefore,

$$\alpha = -\frac{1}{\Pi_T} \frac{d}{dz} \Pi_T = -\frac{2\pi a P_{L1} + 2\pi d P_{L2}}{\Pi_T} = -\frac{2\pi \left( a P_{L1} + d P_{L2} \right)}{\Pi_1 + \Pi_2 + \Pi_3 + \Pi_4}.$$

Expanding the denominator gives,

$$\alpha = -\frac{2aP_{L1} + 2dP_{L2}}{\int_0^a rS_1 dr + \int_a^b rS_2 dr + \int_b^c rS_3 dr + \int_c^d rS_4 dr}.$$

Expanding the numerator gives,

$$\alpha = -\frac{\sqrt{\pi\mu_0 f}}{\Upsilon} \left[a \sqrt{\rho_1} \left(|H_{\theta 1}(a)|^2 + |H_{z1}(a)|^2 + |H_{\theta 2}(a)|^2 + |H_{z2}(a)|^2\right) + d \sqrt{\rho_2} \left(|H_{\theta 4}(d)|^2 + |H_{z4}(d)|^2\right)\right], \tag{2.68}$$

where

$$\Upsilon = \int_0^a rS_1 dr + \int_a^b rS_2 dr + \int_b^c rS_3 dr + \int_c^d rS_4 dr.$$

Equation (2.68) is important will be discussed further in chapter 4.

### 2.7.2 The Ferrite Loss

The loss from the ferrite (i.e. from region 3) can be obtained by assuming a complex valued propagation constant. Letting

$$\beta = \mathrm{R} - \mathrm{I}\, i$$

gives the expression $e^{-i\beta z}$ as

$$e^{-i\beta z} = e^{-i(\mathrm{R}-\mathrm{I}\ i\ i)z} = e^{-\mathrm{R}iz-\mathrm{I}z} = e^{-\mathrm{I}z} e^{-\mathrm{R}iz}.$$

The imaginary part of the propagation constant gives the loss in the ferrite.

The loss from the ferrite can be either the dielectric loss or the magnetic loss. The dielectric loss can be obtained by assuming a complex-valued permittivity constant.

$$\varepsilon = \varepsilon\left(1 - \tan(\delta)i\right),$$

where $\tan(\delta)$ is referred to as the dielectric loss tangent. The magnetic loss can be obtained by assuming a complex-valued permeability constant.

$$\mu = \mu\left(1 - \tan(\delta)i\right),$$

where $\tan(\delta)$ is referred to as the magnetic loss tangent. From the above, the total axial propagation constant

$$\alpha_0 + i\,\beta$$

can be obtained, where $\alpha_0$ and $\beta$ represent the attenuation constant resulting from the dielectric loss and the phase propagation constant, respectively [34]. If $\alpha_1$ denotes the attenuation coefficient resulting from the metal helix, $\alpha_2$ denotes the attenuation coefficient resulting from the metal waveguide, a total attenuation coefficient $\alpha$ can be obtained [34]. This is given by

$$\alpha = \alpha_0 + \alpha_1 + \alpha_2.$$

## 2.8 Numerical Methods

This section deals with the numerical methods that were employed in the numerical program to arrive at a value of $\beta$. The methods outlined below were particularly useful in showing certain properties of the helical structure.

### 2.8.1 Phase Propagation Constant

The derivation of equation (2.63) shows how establishing the governing equations in matrix form gives,

$$\mathbf{Ax} \;=\; \mathbf{0},$$

where $\mathbf{x}$ represents the column vector of constants and $\mathbf{0}$ represents the zero column vector. To obtain a non-trivial solution,

$$\det(\mathbf{A}) = 0.$$

However, the determinant of the matrix $\mathbf{A}$, is a function of $\beta$. Therefore, letting

$$\det(\mathbf{A}) = f(\beta),$$

a solution for the equation

$$f(\beta) = 0$$

is sought.

### 2.8.2 Real-Valued Constants

When $\varepsilon$ and $\mu$ of the dielectric are real-valued, or $\kappa$, $\varepsilon$ and $\mu$ of the ferrite are real-valued, this resulted in a real-valued propagation constant, i.e.

$$\text{if} \quad \varepsilon \,\epsilon\, \mathbb{R},\ \mu \,\epsilon\, \mathbb{R} \quad \text{and} \quad \kappa \,\epsilon\, \mathbb{R} \ \Rightarrow \beta \,\epsilon\, \mathbb{R}.$$

When $\varepsilon$, $\mu$ and $\kappa$ are all real quantities, $f(\beta)$ was purely imaginary. Therefore,

$$\text{if} \quad \beta \,\epsilon\, \mathbb{R}, \qquad f(\beta) = x\, i, \quad \text{where} \quad x \,\epsilon\, \mathbb{R}.$$

This shows that if $\varepsilon$, $\mu$ and $\kappa$ are all real, the structure does not model the ferrite loss. In order to seek a zero determinant, $\beta$ can be assumed to be real and an iterative technique was employed. The iterative technique that was used was the bisection method.

#### Bisection Method

A method of finding an approximation to a root of the equation $f(x) = 0$ is to find an interval $[a, b]$ in which the root lies and then to take the mid-point $\frac{a+b}{2}$ of the interval as a first approximation to the root [35]. When this is done, the root will either lie in the left-hand interval $\left[a, \frac{a+b}{2}\right]$ or in the right-hand interval $\left[\frac{a+b}{2}, b\right]$. By selecting the mid-point in the correct interval, the interval containing the root will decrease. By repeating this iterative method, the accuracy of the root can be improved.

### 2.8.3 Complex-Valued Constants

Until this point, $\varepsilon$, $\mu$, $\kappa$ and $\beta$ were assumed to be real. In order to calculate the losses in the dielectric or ferrite, the permittivity will take the form,

$$\varepsilon_r' = \varepsilon_r \left(1 - \tan(\delta)\, i\right),$$

thus $\varepsilon \,\epsilon\, \mathbb{C}$. This changes the determinant to a complex-valued number. Thus

$$f(\beta) = F(\beta) + G(\beta)\, i, \qquad \text{where F}(\beta)\,\epsilon\,\mathbb{R}, \quad \text{and} \quad \text{G}(\beta)\,\epsilon\,\mathbb{R}.$$

In order for $f(\beta) = 0$, it is necessary for both $F(\beta) = 0$ and $G(\beta) = 0$. Letting $\beta$ be a complex number of the form,

$$\beta = x + y\, i, \qquad \text{where x,y}\epsilon\mathbb{R},$$

and seeking a solution to the equations,

$$F(x, y) = 0 \qquad \text{and} \qquad G(x, y) = 0.$$

A method of solving these equations, *Newton's method* can be employed. The method is shown here. Using the Taylor Series,

$$0 = F(x + \delta_x, y + \delta_y) \approx F(x, y) + \delta_x \frac{\partial F}{\partial x} + \delta_y \frac{\partial F}{\partial y},$$
$$0 = G(x + \delta_x, y + \delta_y) \approx G(x, y) + \delta_x \frac{\partial G}{\partial x} + \delta_y \frac{\partial G}{\partial y},$$

and calculating the partial derivatives as follows,

$$F_x = \frac{F(x + X, y) - F(x - X, y)}{2X}, \qquad F_y = \frac{F(x, y + Y) - F(x, y - Y)}{2Y},$$
$$G_x = \frac{G(x + X, y) - G(x - X, y)}{2X}, \qquad G_y = \frac{G(x, y + Y) - G(x, y - Y)}{2Y}.$$

These expressions can be used to calculate the Jacobian matrix $J$.

$$J = \begin{pmatrix} F_x & F_y \\ G_x & G_y \end{pmatrix}$$

Therefore,

$$\begin{pmatrix} X \\ Y \end{pmatrix} = -J^{-1} \begin{pmatrix} F(x,y) \\ G(x,y) \end{pmatrix}.$$

Therefore, the following iterative formula is arrived at,

$$\begin{pmatrix} x_{n+1} \\ y_{n+1} \end{pmatrix} = \begin{pmatrix} x_n \\ y_n \end{pmatrix} + \begin{pmatrix} X_n \\ Y_n \end{pmatrix}.$$

The above method is referred to as Newton's method [36]. The resultant $x$ and $y$ are used to obtain the propagation constant given below.

$$\beta = x + y\, i.$$

$x$ is always positive and $y$ is always negative. Therefore, the propagation can be expressed as

$$\beta = \beta - \alpha\, i,$$

where $\beta$ and $\alpha$ are positive numbers. The **E** and **H** fields can be written as,

$$\mathbf{E} = \left[E_r(r)\hat{r} + E_\theta(r)\hat{\theta} + E_z(r)\hat{z}\right] e^{i(\omega t - \beta z)} = \left[E_r(r)\hat{r} + E_\theta(r)\hat{\theta} + E_z(r)\hat{z}\right] e^{i\omega t} e^{-i\beta z} e^{-\alpha z}.$$

$$\mathbf{H} = \left[H_r(r)\hat{r} + H_\theta(r)\hat{\theta} + H_z(r)\hat{z}\right] e^{i(\omega t - \beta z)} = \left[H_r(r)\hat{r} + H_\theta(r)\hat{\theta} + H_z(r)\hat{z}\right] e^{i\omega t} e^{-i\beta z} e^{-\alpha z}.$$

The additional term $e^{-\alpha z}$ represents exponential decay along the $z$-axis in the positive direction.

## 2.9 Computational Methods

The programs that are written in this investigation can be divided into two parts: the program that generates the propagation coefficient, $\beta$, which is done in MATLAB, and the program that generates the attenuation coefficient, $\alpha$, which is done in MAPLE. Both of these programs are given in Appendix D. A brief outline of the programs is given below.

### 2.9.1 MATLAB

The program begins by defining the constants, (e.g. $\mu_0$, $\mu$, $\kappa$, $\varepsilon$ etc). The $14 \times 14$ matrix, denoted by **A**, is then entered. Finally, the determinant is calculated. The bisection method is then used to improve the accuracy of the answer.

### 2.9.2 MAPLE

As in the previous case, this program begins by defining the constants. The program then formulates expressions to all of the constants in terms of $a_1$. This is achieved by using equations (2.49) - (2.62). After this, the Poynting vector is calculated and is expressed in terms of $a_1$. Equation (2.68) is calculated and the value of $\alpha$ is arrived at. Since both the numerator and denominator are expressed as a multiple of $a_1$, $\alpha$ is independent of $a_1$.

## 2.10 Summary

This chapter took a detailed look at the model considered in this study. The geometrical structure and modelling assumptions were examined closely. The governing equations, boundary conditions and field solutions were derived, and expressions formulating the methods for calculating the losses in the structure were calculated. Other expressions and ideas were introduced such as dielectric and magnetic loss tangents. Due to the complexity of the system of equations, some time was spent in obtaining a model that produced accurate and reliable results. However, as will be shown in the next chapter, the results that were produced from the current study compare very well with those that are present in the published literature.

# Chapter 3

# Verification of the Model

## 3.1 Introduction

Chapter 2 formulated the model used in this thesis.. This chapter compares the results from the model with those in the literature. Parameters that are used for comparison are the propagation constant and the attenuation coefficient. Although the attenuation coefficient has never before been calculated for a ferrite loaded helical device, a helix surrounded by a dielectric *has* been considered previously. When comparing the values of the attenuation coefficient against other results in the literature, it is necessary to model the ferrite as a dielectric. This is achieved by letting (i) $\kappa = 0$, and (ii) $\mu = \mu_0$. Condition (i) ensures that the non-reciprocal behaviour is removed, and condition (ii) models the ferrite as an isotropic substance of permeability $\mu_0$, (i.e. a dielectric).

Many authors have considered the case of a helix supported by dielectric rods surrounded by a metal waveguide. This was principally done in order to develop models to calculate propagation constants and losses in TWT's. In figure 3.1, $a_0$ is the inner radius of the metal helix, $a$ is the mean radius of the helix, $b_1$ is the outer radius of the helix, and $b$ is the radius of the waveguide. The three dielectric support rods are modelled as an equivalent dielectric-tube region of an effective relative permittivity, $\varepsilon_{eff}$, into which the discrete dielectric-supports are smoothed out, see figure 3.2. This

is divided into three regions: 1) the free space region inside the helix, $0 < r \leq a$; 2) the free space gap between the mean and outer helix radii, $a < r \leq b$; 3) the region between the outside of the helix and the metal waveguide, $b < r \leq b_1$. If the permittivity of a single dielectric rod is denoted by $\varepsilon_r$, the effective permittivity of the assumed dielectric tube is given by

$$\varepsilon_{eff} = 1 + m\,(\varepsilon_r - 1)\,\frac{A_s}{A}, \tag{3.1}$$

where $A_s$ is the cross-sectional area of a single dielectric rod, $A$ is the cross-sectional area of the region $b_1 < r < b$ and $m$ is the number of dielectric support rods. Figure 3.3 shows the structure that is modelled with the dielectric tube having a permittivity of $\varepsilon_{eff}$. This assumption has been used by many authors; Duan et al [22] and [25], Gilmour et al [19] and Lopes and Motta [21] are a few examples. In the following sections, the results generated from our model will be compared to results in previously published papers.

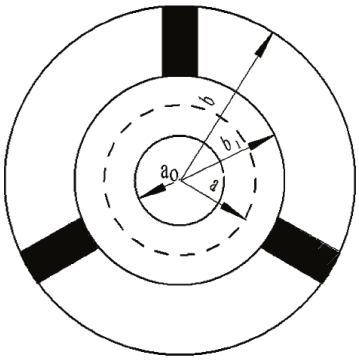


Figure 3.1: Cross-section of structure [22].

## 3.2 Comparison to a Dielectric

This section deals with comparison of results that are generated from the numerical program to previously published ones, where the model is of a helix surrounded by a dielectric tube. In most cases, the model is considered lossless by setting the permittivity to be a real number. Where the

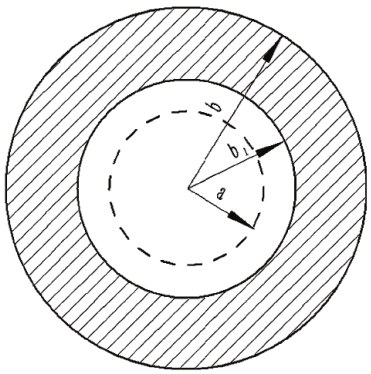


Figure 3.2: Equivalent cross-section of structure [22].

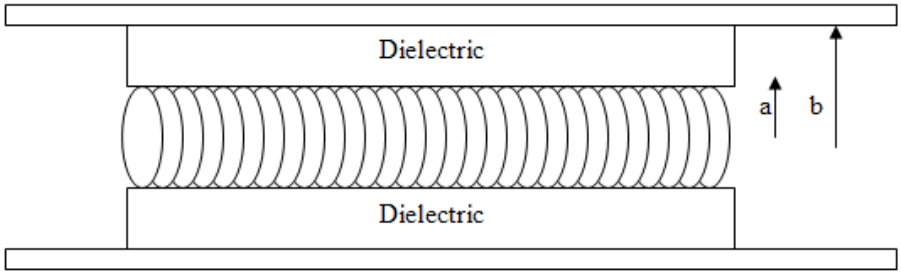


Figure 3.3: Model of helix used in analysis (dielectric).

dielectric loss is modelled, the permittivity is a complex value.

Firstly, the propagation constant is compared to previously published results. Duan et al [22] considered the case of a metal helix supported by three dielectric rods. These rods were modelled as a lossless dielectric tube between the helix and the waveguide. An effective permittivity for the tube was calculated by using equation (3.1). Duan's [22] model also included an air gap between the metal helix and the dielectric. The analysis in the paper used the tape and sheath helix models and considered experimental results. Table 3.1 gives the results that were presented in the paper together with results that are generated from the numerical program.

Although this model uses the sheath helix assumptions, the results agreed very well with those of the tape helix [22]. The final column shows that the difference between the tape helix and the current model is very small; the largest difference being less than 0.5%. This is an extremely good

Table 3.1: Comparison of results from Duan et al [22] with results generated from numerical program.

| f (GHz) | $\beta$ (Tape Helix) (Radian/m) [22] | $\beta$ (Experimental Results) (Radian/m) [22] | $\beta$ (Sheath Helix) (Radian/m) [22] | $\beta$ (Current Model) (Radian/m) | % difference between Current Model and Tape Helix |
|---|---|---|---|---|---|
| 4 | 479.57 | 480.2 | 577.86 | 481.76 | 0.457 |
| 6 | 746.52 | 753.9 | 903.43 | 749.20 | 0.359 |
| 8 | 1029.4 | 1051.2 | 1251.4 | 1030.48 | 0.105 |
| 10 | 1316.7 | 1343.2 | 1608.6 | 1314.94 | 0.134 |

agreement. Although the tape helix model is more sophisticated than the sheath helix, which yields a greater level of accuracy, the propagation constants in the case that is considered here agree very well. Table 3.1 shows that the tape helix, experimental results and results from the current model all give similar results to each other. However, the column based on the sheath helix model differs substantially from the others. This difference can be explained if the assumptions that are used in the sheath helix model are carefully examined. The sheath helix model in [37] was based on Swifthook's model [24]. Figure 3.4 shows the model that was used by Swifthook et al [24]. Region 1 refers to the region of air inside the metal helix, region 2 refers to the free space between metal helix and the dielectric, region 3 refers to the dielectric region and region 4 refers to the region outside the structure. One important assumption that was used in the sheath helix model used by Swifthook [24], is that the radial propagation constant was approximately the same in each region. The radial propagation constant in air is given by

$$k_0^2 = \beta^2 - \frac{\omega^2}{c^2},$$

and a general expression for the radial propagation constant in each region is given by

$$k_n^2 = \beta^2 - \varepsilon_n \frac{\omega^2}{c^2}.$$

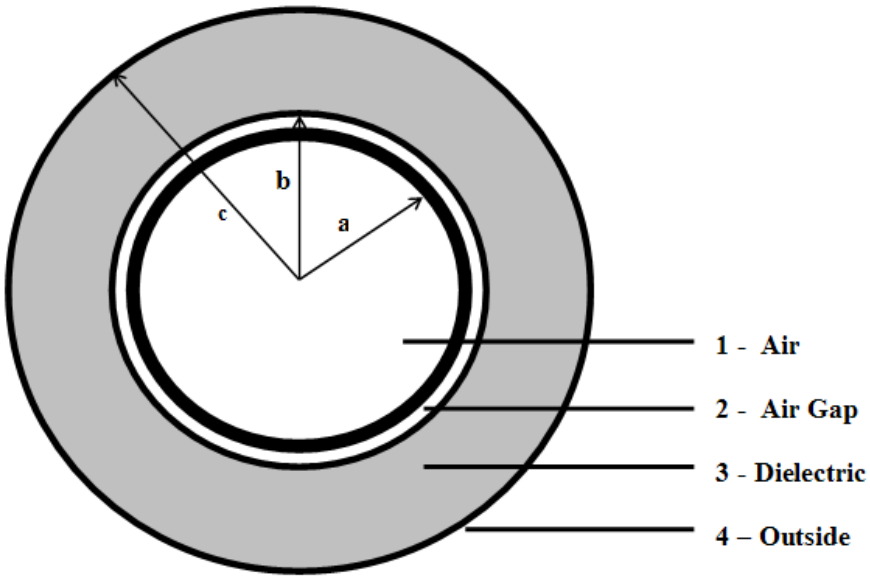


Figure 3.4: Cross-section of Swifthook's model [24] .

This assumption assumed that $k_n \approx k_0$. However, the current model assumes that every region has a different propagation constant. This could account for the large discrepancy between the results from the sheath helix [22] model and the other sets of results.

Secondly, the attenuation coefficient is considered. Gilmour et al [19] investigated the case of a metal helix supported by dielectric rods. The structure was enclosed inside a metal barrel. The rods were modelled as a lossless dielectric tube, see figure 3.3. The dimensions that were used in [19] are given in Table 3.2.

Figures 3.5 - 3.10 show how the loss in the structure is affected by varying certain parameters such as; helix radius, helix pitch, barrel to helix diameter ratio, helix resistivity, barrel resistivity and effective dielectric constant of support rods. All of these are compared with the results generated from the current model. The results show a good agreement with the maximum difference between the results of [19] and the current model being always less than 10%.

Table 3.2: Parameters for the model in [19]

| | |
|---|---|
| Helix pitch | 0.141 cm |
| Helix radius | 0.12 cm |
| Barrel to helix diameter ratio | 2.0 |
| Helix resistivity | $2.5 \times 10^{-6}$ Ω cm |
| Barrel resistivity | $2.5 \times 10^{-6}$ Ω cm |
| Effective relative dielectric constants of support rods ($\varepsilon_{eff}$) | 1.5 |

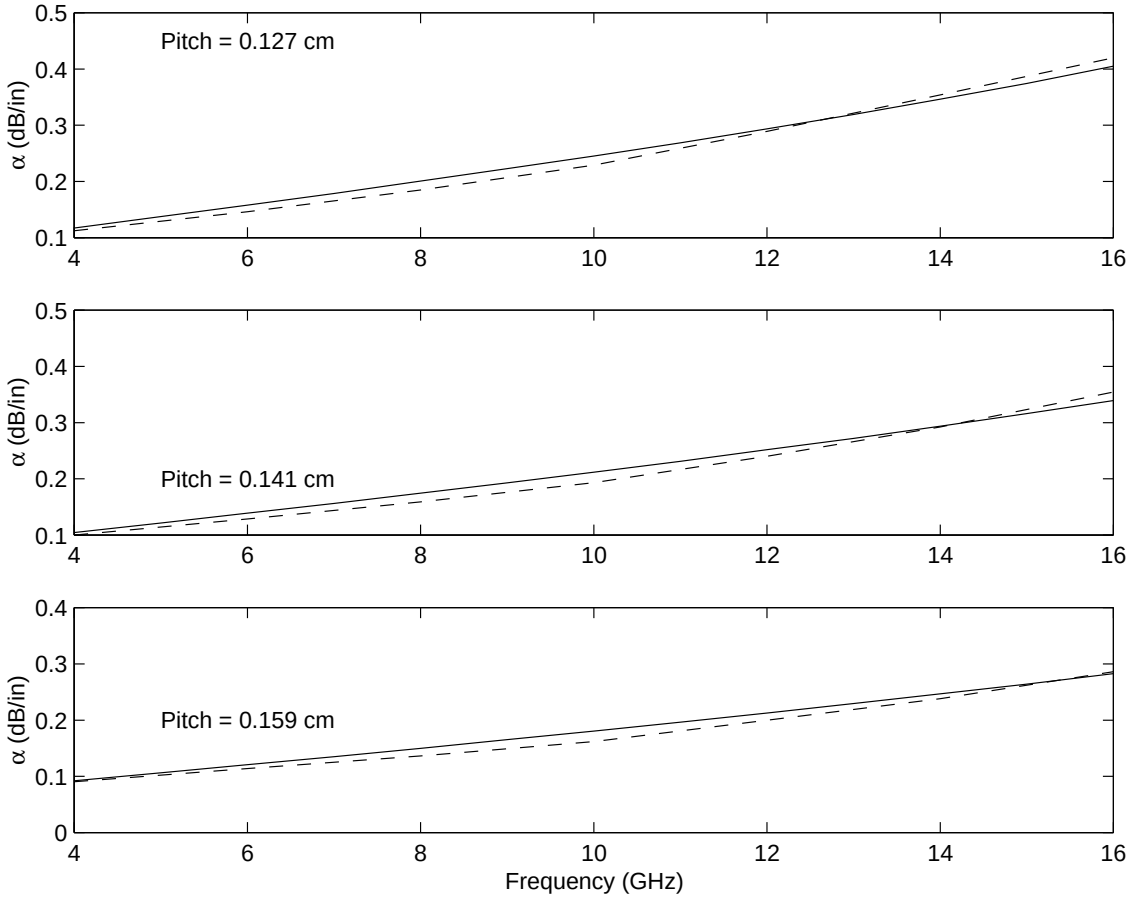


Figure 3.5: Loss against frequency for different values of pitch from model. A comparison of [19] (dashed line) with the model (solid line).

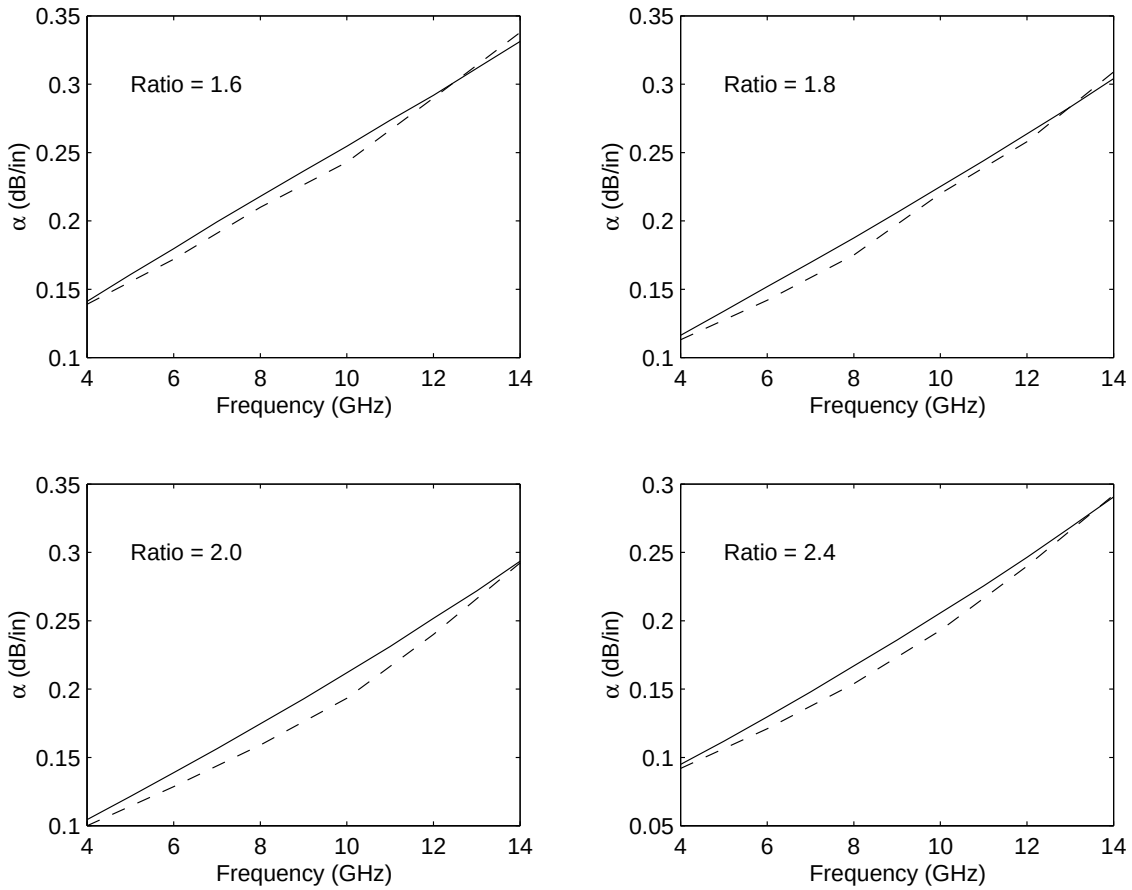


Figure 3.6: Loss against frequency for different values of barrel to helical diameter ratio from model. A comparison of [19] (dashed line) with the Model (solid line).

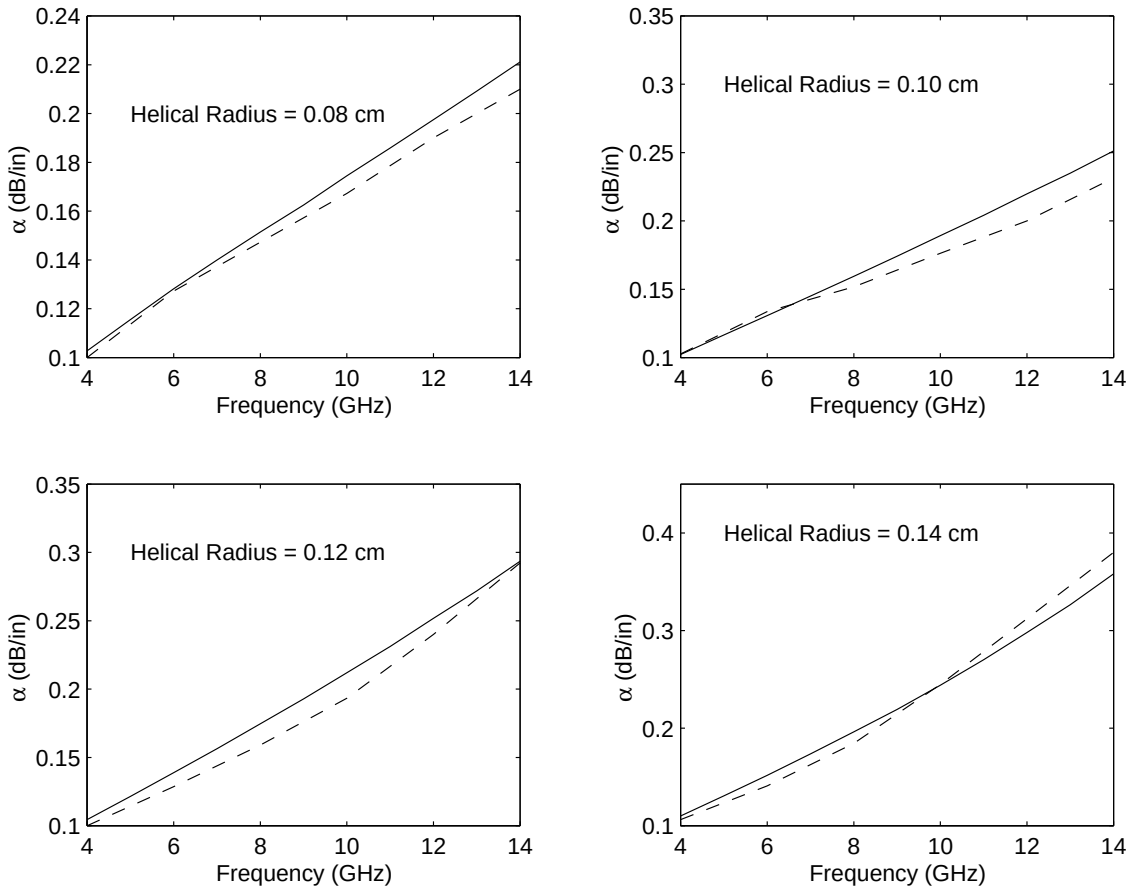


Figure 3.7: Loss against frequency for different values of helix radius from model. A comparison of [19] (dashed line) with the Model (solid line).

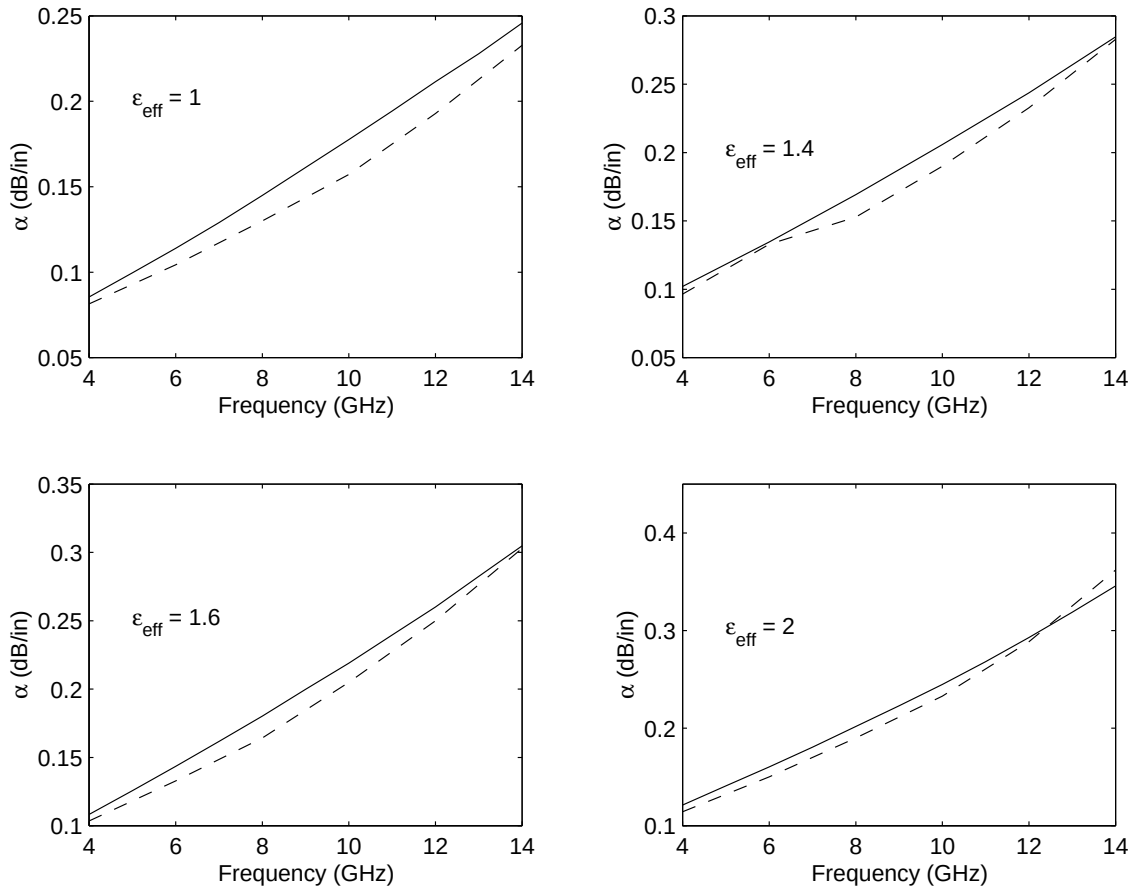


Figure 3.8: Loss against frequency for different values of effective relative dielectric constant of support rods from model, A comparison of [19] (dashed line) with the Model (solid line).

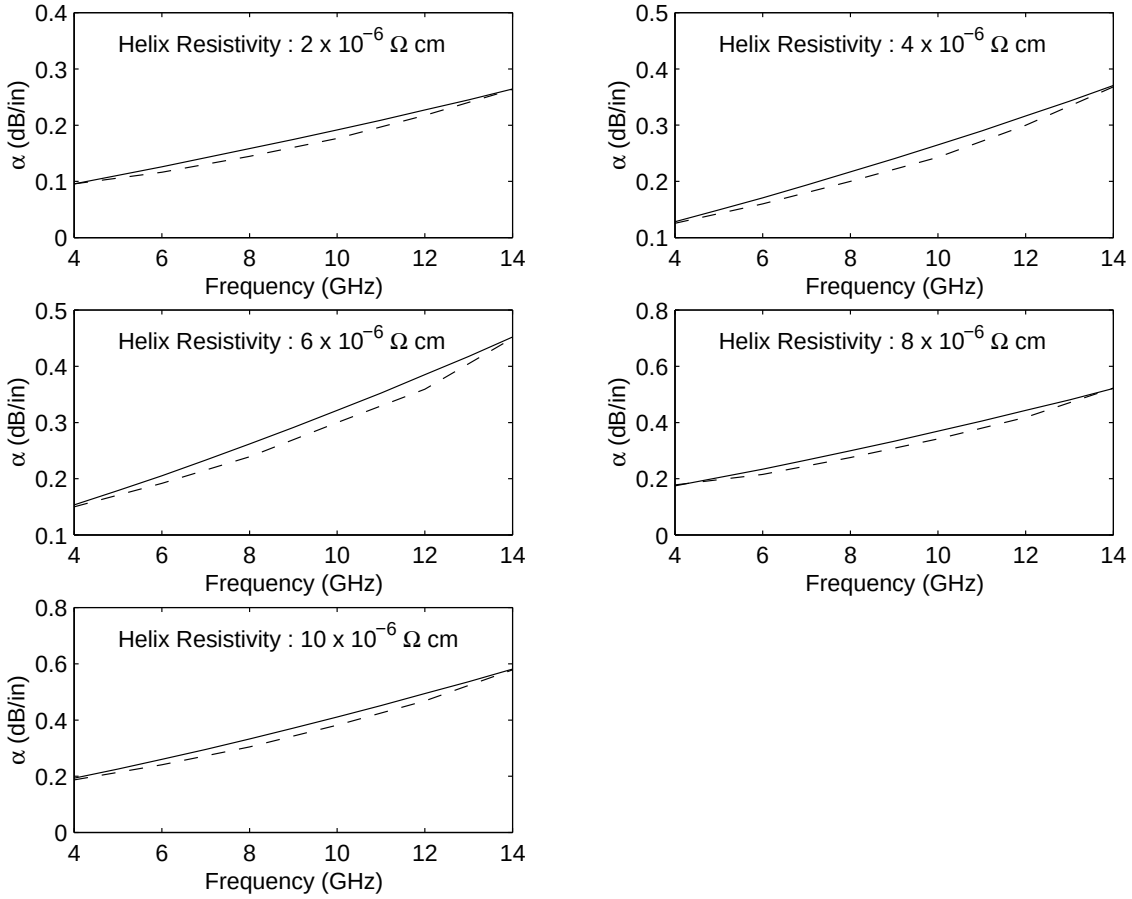


Figure 3.9: Loss against frequency for different values of helix resistivity from model. A comparison of [19] (dashed line) with the model (solid line).

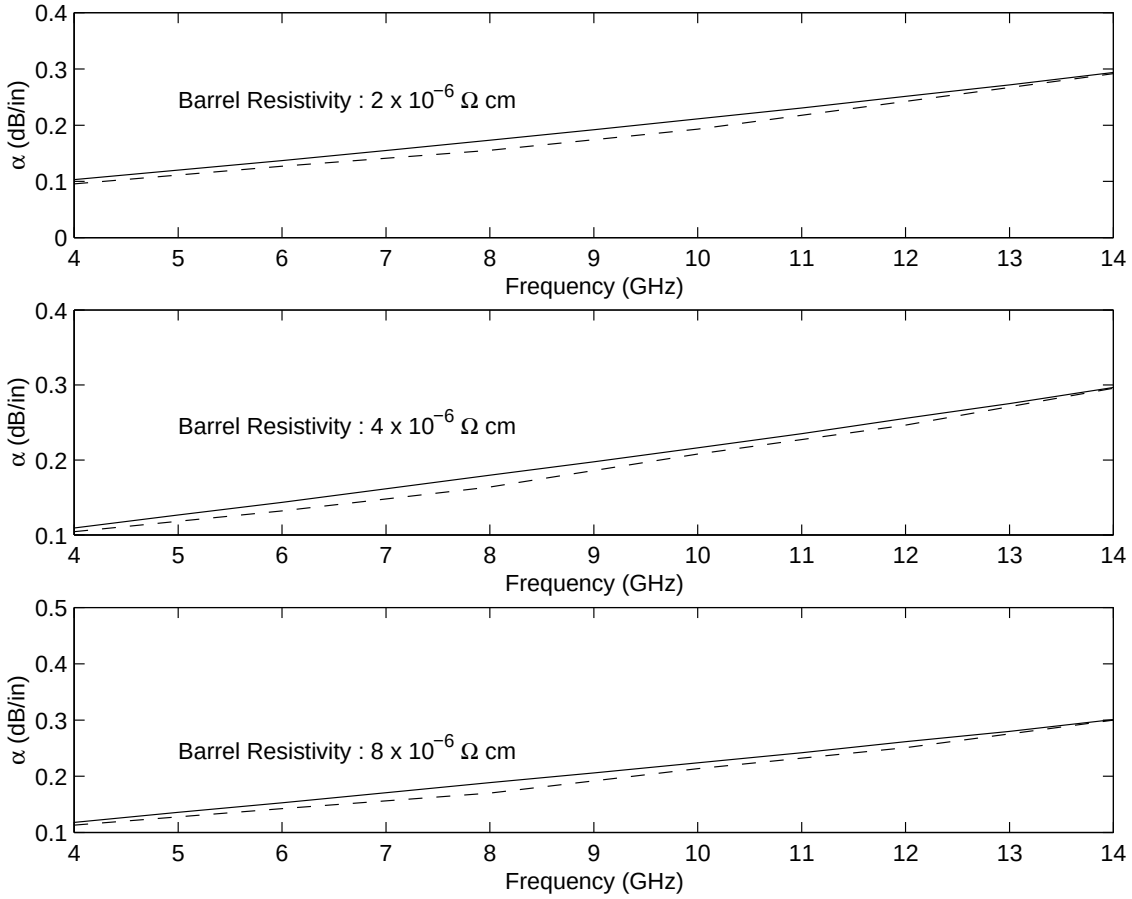


Figure 3.10: Loss against frequency for different values of waveguide resistivity from model. A comparison of [21] (dashed line) with the model (solid line).

Table 3.3: Parameters used in experimental results in [19]

| | |
|---|---|
| Helix pitch | 0.141 cm |
| Helix radius | 0.111 cm |
| Barrel-to-helix diameter ratio | 2.02 |
| Effective relative dielectric constant of support rods | 1.9 |

Gilmour et al [19] also produced experimental results for the losses in the structure. The helical structure that was used had the characteristics given in table 3.3. Gilmour commented that accurate experimental results were very difficult for two main reasons:

- The loss was relatively low ($\sim 0.5$ dB): Therefore, it was necessary to take precautions in order to eliminate even small losses in transmission lines, connectors and other equipment that were used to obtain measurements.

- The impedance of the helical structure was a function of frequency: Figure 3.11 shows how the impedance varies with frequency for this system, (where the effective dielectric constant of the structure was 1.9). The measurement apparatus had an impedance of 50 $\Omega$. This was matched at approximately 8 GHz, (see figure 3.11).

Gilmour et al [19] plotted the simulated and intrinsic loss. The *simulated* loss represented the loss that was measured experimentally. However, above and below 8 GHz, the impedance mismatched at the connections to the helix caused multiple reflections of signals in the structure and in some of the components in the measurement apparatus. This resulted in the simulated loss to be higher than expected. The loss that would have occurred in the absence of these reflections is referred to as the *intrinsic* loss. The simulated loss was compared with the intrinsic loss for a helical structure with a copper plated helix and barrel of resistivity $4 \times 10^{-6}$ $\Omega$ cm. In figure 3.12, the two curves

are tangential at 8 GHz because the impedances were matched. The graph also shows shows how these results compare with the results produced from the current model. The difference between the intrinsic results and current model is always less than 10%.

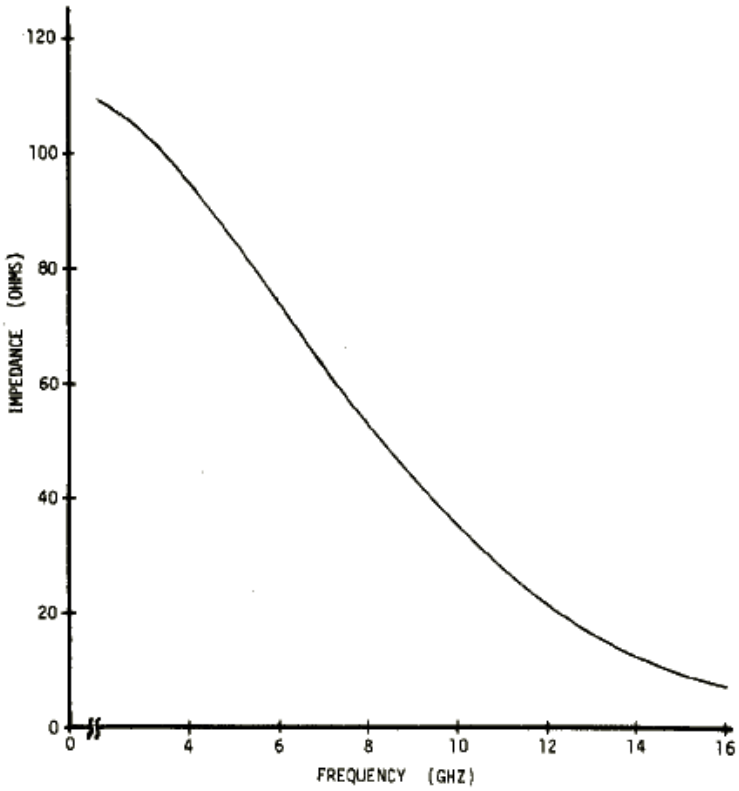


Figure 3.11: Impedance as a function of frequency [19].

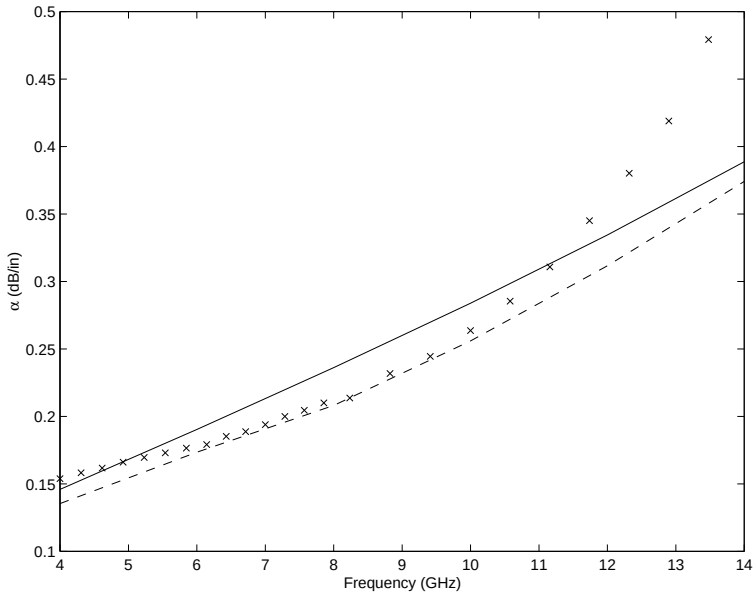


Figure 3.12: Loss as a function of frequency. A comparison of intrinsic loss (dashed line), simulated loss (crossed line) and loss from current model (solid line).

Lopes and Motta [21] used the tape helix to analyse the same structure and produced graphs showing how the loss in the structure varied with frequency when certain parameters within the model were varied. These parameters were: helical radius, helical pitch, guide-to-helix diameter ratio, helix resistivity, guide resistivity and effective relative dielectric constants of support rods. The dimensions that were used in [21] are given in table 3.4.

Table 3.4: Parameters for model in [21]

| Parameter | Symbol | Numeric Value |
|---|---|---|
| Helix pitch | p | 1.25 mm |
| Helix radius | a | 1.09 mm |
| Guide to helix diameter ratio | r = b/a | 1.63 |
| Helix resistivity | $\rho_1$ | $2.5 \times 10^{-5}$ $\Omega$ mm |
| Guide resistivity | $\rho_2$ | $2.5 \times 10^{-5}$ $\Omega$ mm |
| Effective relative dielectric constants of support rods | $\varepsilon_r$ | 1.78 |

When the same structure is analysed using the current model, the following results are produced, figure 3.13 - 3.18. Although there is a good agreement between the two sets of results, the current model generates results which are approximately 12% higher than [21]. Even though this is not a large difference, even this discrepancy can be explained. The current model uses the sheath helix assumptions, of which one is that the metal helix is modelled as a cylinder. The gaps between the winding are not taken into consideration, thus the helix is treated as a cylinder. A cylinder has a greater quantity of metal in comparison to a corresponding helix of the same radius and length. This results in the sheath helix giving a larger value for the conductor loss of the helix at a particular frequency then the actual metal helix. As the tape helix incorporates these gaps between the windings, a more accurate value for the conductor loss from the helix is generated. Therefore,

the sheath helix will give a larger value for the overall loss from the structure than the tape helix. As the frequency increased, the agreement decreases. This can be explained in the following way: Whilst the sheath helix agrees well at low frequencies, the accuracy of the model decreases as the frequency increases. This can be understood by considering the assumption that the helical pitch is significantly less than the wavelength ($p << \lambda$).

As,

$$\lambda = \frac{c}{f},$$

the inequality becomes

$$p << \frac{c}{f}.$$

As $f$ increases, the term on the right-hand side of the inequality will decrease, the strength of the inequality will also decrease. Therefore, an increase in frequency will lead to a decrease in the accuracy of the sheath helix model. If the graphs for both the sheath and tape helix were to be extended over a larger frequency range, it is expected that the two lines will diverge.

Figure 3.14, which considered the variation in helical pitch, also illustrates an example of this assumption. When the helical pitch increases from 1.25 mm to 1.454 mm, the agreement between the current results and the tape helix [21] slightly decreases. For example, at a frequency of 5 GHz, a helical pitch of 1.25 mm gives an error in agreement of 5.6%, whilst a helical pitch of 1.454 mm gives an error in agreement of 11%. This can also be explained by the the assumption that ($p << \lambda$). As the pitch increases, the left-hand side of the inequality will increase, thus the strength of the inequality will also decrease. Therefore, an increase in pitch will lead to a decrease in the accuracy of the sheath helix model.

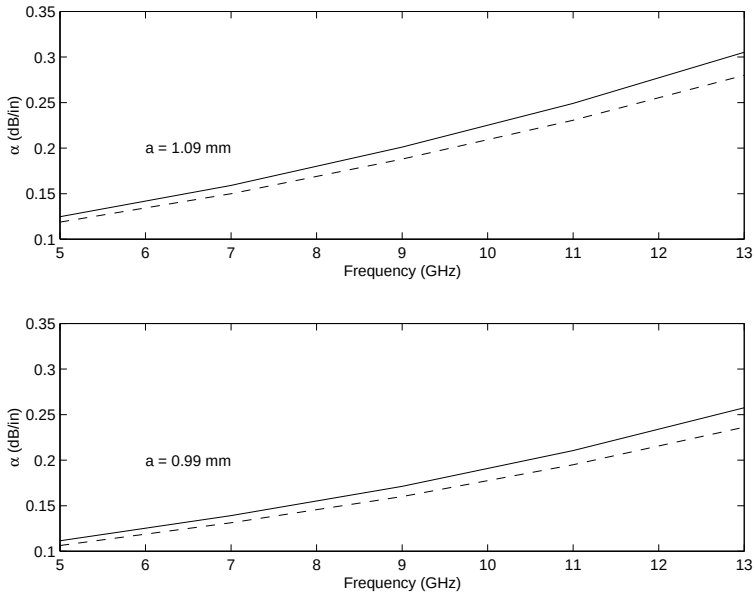


Figure 3.13: Loss against frequency for different values of helical radii from current model. A comparison of [21] (dashed line) with the current model (solid line).

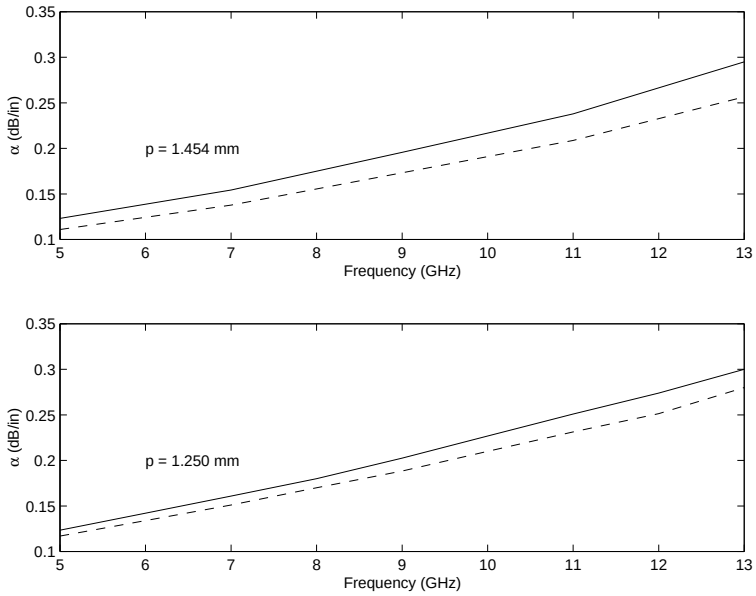


Figure 3.14: Loss against frequency for different values of helical pitches from current model. A comparison of [21] (dashed line) with the current model (solid line).

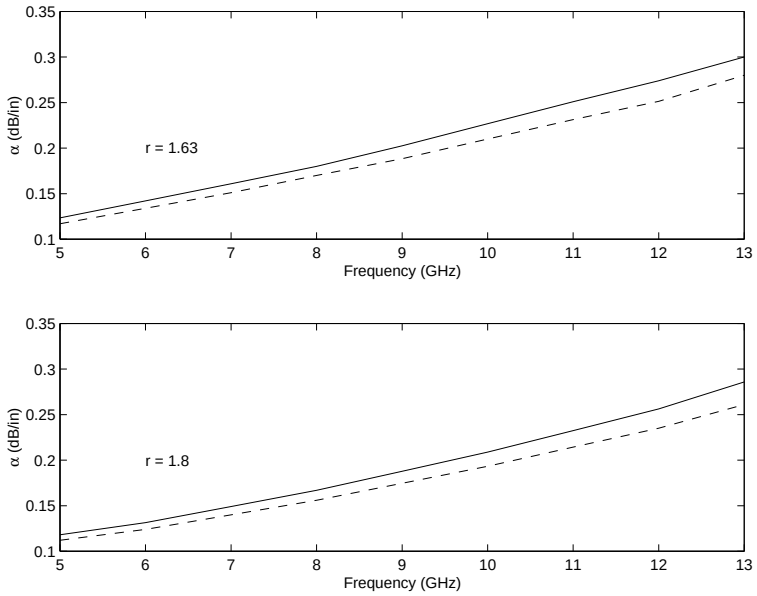


Figure 3.15: Loss against frequency for different values of guide to helical diameter ratio from current model. A comparison of [21] (dashed line) with the current model (solid line).

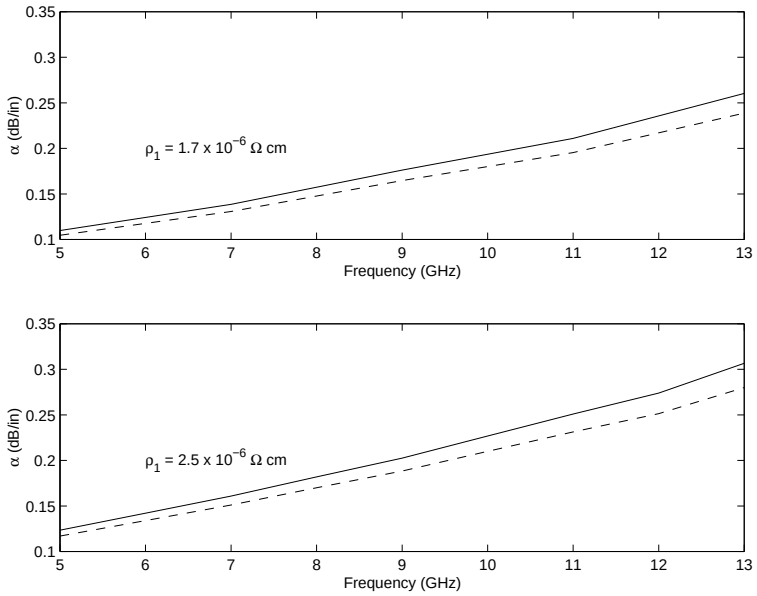


Figure 3.16: Loss against frequency for different values of barrel resistivity from current model. A comparison of [21] (dashed line) with the current model (solid line).

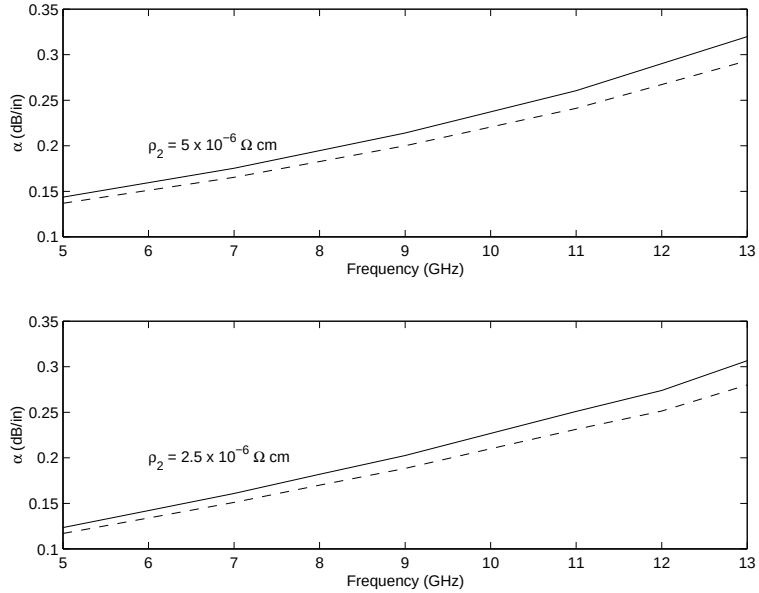


Figure 3.17: Loss against frequency for different values of helix resistivity from current model. A comparison of [21] (dashed line) with the current model (solid line).

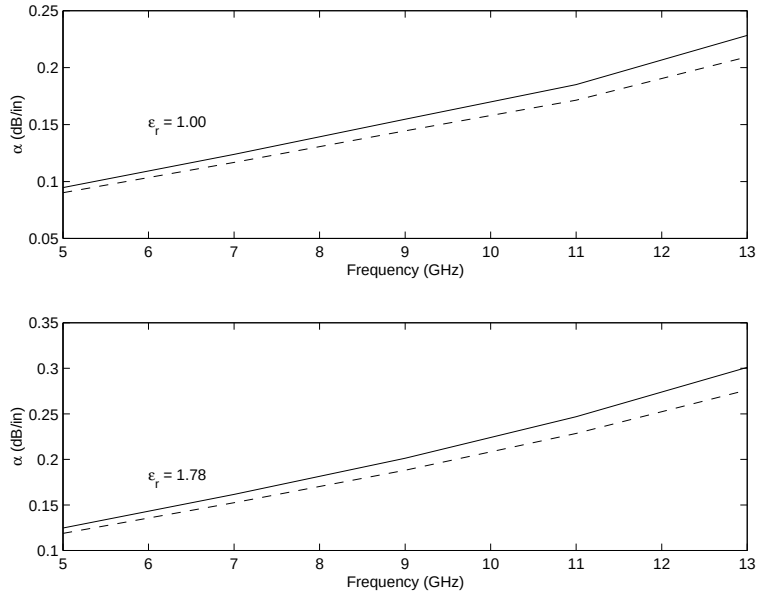


Figure 3.18: Loss against frequency for different values of effective relative dielectric constant of support rods from current model. A comparison of [21] (dashed line) with the current model (solid line).

Duan et al [25] considered the case of a metallic helix supported by dielectric support rods. In this paper, the dielectric support rods were modelled by continuous dielectric tubes into which the discrete supports were smoothed out, figure 3.19. The effective complex relative permittivity of the $k$-th layer can be expressed as

$$\varepsilon_{r,eff}^{(k)} = 1 + (\varepsilon_r^{\prime(k)} - 1)\, m\, \frac{A_s^{(k)}}{A^{(k)}},$$

where $A_s^{(k)}$ and $A^{(k)}$ denote cross-sectional area of the $k$-th layer of a single dielectric rod and the cross-sectional area of the k-th layer respectively. The complex relative permittivity of the discrete dielectric rods is given by

$$\varepsilon_r^{\prime(k)} = \varepsilon_r^{\prime(k)}(1 - i \tan\delta),$$

where $\varepsilon_r$ is the relative permittivity, $\tan\delta$ is the loss tangent and $m$ is the number of the dielectric rods, [25]. As the permittivity was complex, the propagation constant that was calculated by the model was also a complex-valued number.

Duan et al [25] calculated the attenuation coefficient for the same structure, see figure 3.19. In the case of $\tan(\delta) \to 0$, the results from Duan et al [25] compare well with Chernin et al [38]. The parameters of this structure are taken from Dayton et al [39]. Figure 3.20 shows a good agreement between the current model and [25]. At lower values of the loss tangent, the error in the agreement is less than 10%. At $\log_{10}(\tan(\delta)) = -1$, the difference is 18.6%. However, a $\tan(\delta)$ value of -1 would indicate a very lossy material. The results from the model were consistently higher than those in [25]. This can be understood by considering two assumptions in the model.

• The current model assumes a sheath helix structure: As mentioned earlier, this models the helix as a cylinder - thus modelling a greater quantity of metal. The conductor loss that is contributed from the metal helix will be less than that from a corresponding cylinder. Therefore, the attenuation coefficient from the current model is higher than that of the tape helix, [25].

• The model assumes the dielectric rods as a single layer, whereas [25] assumed many continuous layers: An increased number of layer will increase the accuracy of the model. However, increased

accuracy by the addition of a layer will decrease until subsequent layers will produce so small a difference, they can be dispensed with. Despite the presence of these two factors, the results from the model agree well with [25].

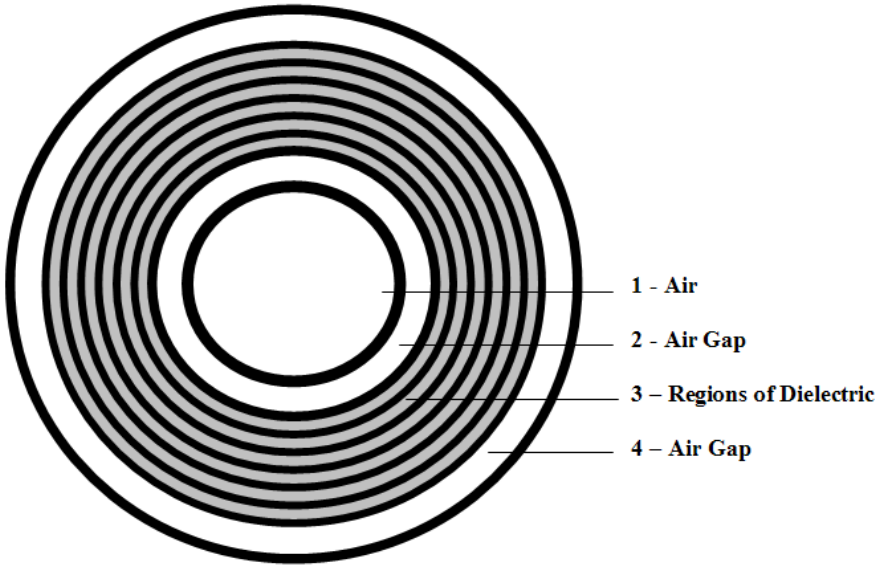


Figure 3.19: Cross-section of Helical Structure with regions of dielectric.

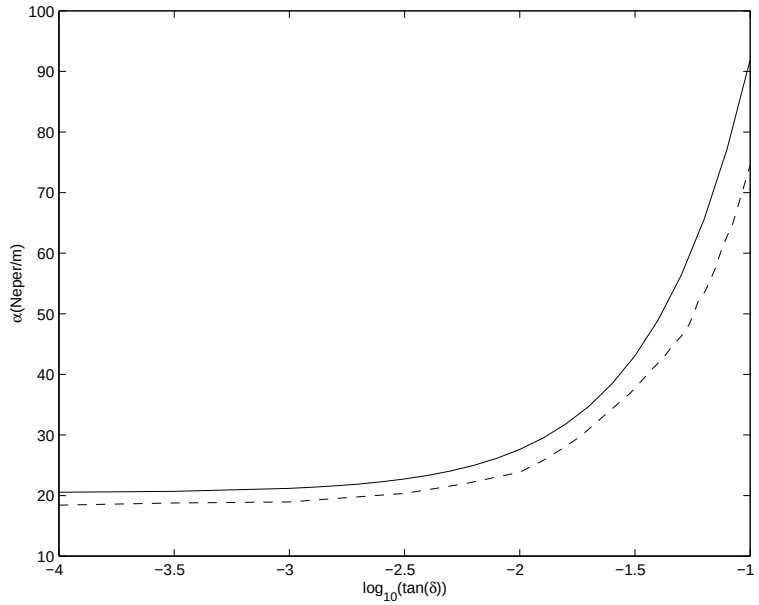


Figure 3.20: Attenuation constant versus loss tangent at f = 70 GHz. A comparison of [25] (dashed line) and current model (solid line).

## 3.3 Comparison to a Ferrite

A helix surrounded by a ferrite has not been considered by many authors. From the few authors that have, various assumptions were made that do not lend themselves for comparison with the current model. Suhl and Walker [8] modelled a helix surrounded by a ferrite of infinite thickness. The paper also made simplifying assumptions with reference to the mathematical expressions and equations. Ivanov and Koster [28] and [29] considered the case where $\mu = \mu_0$. This assumption is only valid for frequencies very far from that of GMR. However, for frequencies that far from that of GMR, the value of $\kappa$ is very small - thus the phase shift is minimal and the ferrite behaves like a dielectric. Therefore, only the work by Secklemann [27] is used to compare with the current model.

This section considers how the current model compares with a helix surrounded by ferrite. Secklemann [27] considered the case of a metal helix surrounded by a ferrite tube. The ferrite was assumed to be lossless and azimuthally biased. The comparison is displayed on a dispersion curve, see figure **??**. The results agree well. However, as the the values on the $x$-axis increase, the agreement becomes less strong. This relates to the sheath helix assumption $p << \lambda$. As $\tan(\psi) = p/2\pi r_0$, the assumption can be expressed as

$$\frac{r_0}{\cot(\psi)} << \lambda.$$

As $r_0/\cot(\psi)$ increases, the the inequality becomes less strong. Therefore, as the value on the x-axis increases, the accuracy of the sheath helix model decreases, thus the graphical agreement becomes less strong.

Secklemann [27] also provided some experimental results to verify the theoretical calculations. The graph containing experimental data has been reproduced in figure 3.22. The experimental data, which are shown as point on the graph, lie on the curve plotted using the theoretical calculations. As figure 3.21 shows a good agreement between the current study and Secklemann's model, and figure 3.22 shows a very good correlation between the theoretical and experimental results of Secklemann [27],

it can be concluded that the results of the current study compare well to the practical measurement plotted by Secklemann [27].

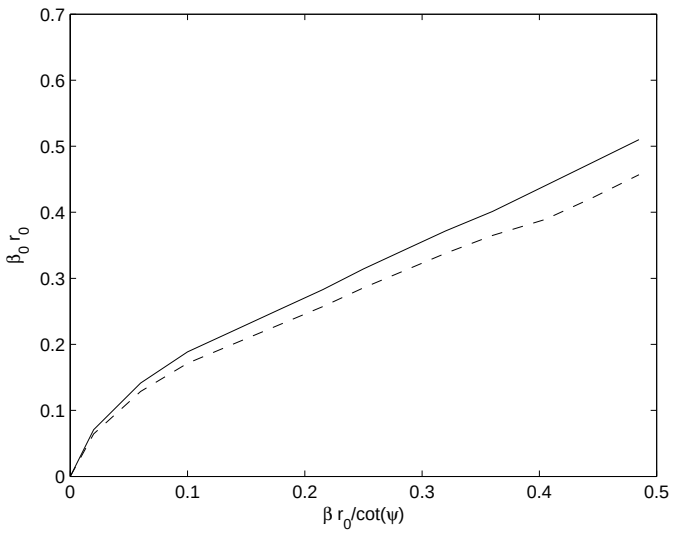


Figure 3.21: Dispersion curve. A comparison of [27] (solid line) with current model (dashed line).

## 3.4 Summary

This chapter investigated the accuracy and reliability of the model. This was achieved by comparing the model with results from previously published work. The propagation constant and attenuation coefficient for a helix surrounded by dielectric have been calculated before, and this served as comparative material with the model. The propagation constant for a helix surrounded by an azimuthally biased lossless ferrite have been calculated previously, and this was compared with the results from the model. Generally, the results agreed very well with those of the model, but any slight discrepancies between the model and previously published results have all been accounted for. Thus, having ascertained the accuracy and reliability of the model, the investigation can be extended to consider situations that have not been analysed previously. The next chapter does this and a full analysis of these new situations are investigated.

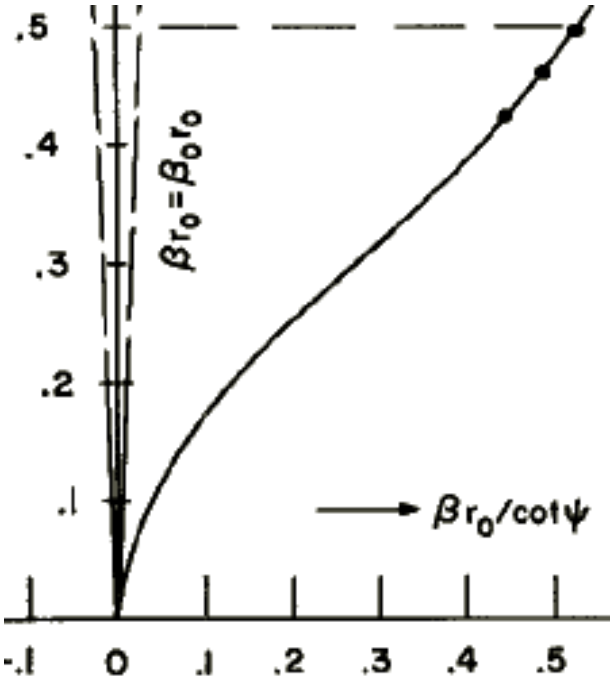


Figure 3.22: Dispersion curve [27].

# Chapter 4

# Results

## 4.1 Introduction

The previous chapter examined the accuracy and reliability of the current model. This chapter discusses how the the model can be used to calculate certain properties of the helical structure, such as; the attenuation coefficient ($\alpha$), the propagation constant ($\beta$) and other quantities. This chapter then investigates how these quantities are affected by changing certain parameters within the structure.

A quantity of particular interest in the structure is the phase shift[1]. The differential phase shift is given by

$$\triangle\Phi = \triangle\beta \; P \; L \; \sqrt{\varepsilon_f}, \tag{4.1}$$

where $\Phi$ is given in radians per length. P is the polarising function and is calculated by,

$$P(\omega) = \sin\left(\frac{\omega}{c}\sqrt{\varepsilon_f}\, l_0\right) \qquad \text{with} \qquad l_0 \approx 2\pi r_0,$$

where $c$ is the velocity of light in free space, $\varepsilon_f$ is the effective relative dielectric constant for the ferrite and $r_0$ is the radius of the helix. $L$ is the length over which the phase shift is measured. There

[1]Section **??** introduces the differential phase shift.

are different ways of considering this longitudinal quantity, one of which is the *quarter wavelength*. The wavelength can be expressed as either the free space wavelength; denoted by $\lambda$, or the electrical wavelength; denoted by $\lambda_g$. The free space wavelength $\lambda$ is defined by

$$\lambda = \frac{c}{f},$$

where $c$ is the velocity in free space. The electrical wavelength is given by

$$\lambda_g = \frac{c'}{f},$$

where $c'$ is the velocity of the wave in the structure. $\lambda_g$ can be obtained by the expression

$$\beta = \frac{2\pi}{\lambda_g}.$$

Another way of considering the longitudinal quantity $L$ is the length over which the wave is attenuated by 1 dB. Initially, this loss will be purely from the metal helix and the waveguide[2]. When the the loss in the ferrite is taken into consideration, the overall loss quantity will include both the metallic loss and the ferrite loss.

## 4.2 Application of Numerical and Computational Methods

This section illustrates how the model can be used to investigate certain properties of the structure. In this particular example, a commercially available ferrite is selected. This has a saturation magneisation of 680 Gauss and a relative permittivity of 14.5. The particular ferrite is available from Transtech[3] and the dimensions of the structure are those that have been adopted by Duan et

[2]The chapter progresses in the complexity of the model. Therefore, initially, only the metallic loss is considered. Here, the quantities $\mu$ and $\varepsilon_f$ are real quantities. Then the ferrite loss will be taken into consideration. Here, $\mu$ and $\varepsilon$ can take complex values. Although, as will be shown, the contribution made to the loss from the ferrite is very minimal.

[3]Transtech: Ceramics and Advanced Material

al [22]. A side view of the helical structure is shown in figure 4.1 and a cross-sectional view is shown in figure 4.2, where the innermost circle represents the helix. The parameters of the helical structure are given in table 4.1.

The selection of material with a suitable saturation magnetisation is dependent upon the microwave frequency, and three operational modes can be considered: below resonance, resonance and above resonance [1]. The terms *below resonance* and *above resonance* refer to the magnetic operating point relative to GMR [1]. The magnetic operating points are opposite in reference to the operating points in the frequency domain [1]. The region below resonance corresponds to frequencies higher than GMR, whilst the region above resonance corresponds to frequencies lower than GMR [1].

To avoid low field losses, the saturation frequency should be chosen such that the ferrite is fully biased. To meet this condition, the following inequality is required,

$$4\pi M_s < \frac{\omega}{\gamma} - H_\alpha, \tag{4.2}$$

where, $H_\alpha$ is the anisotrophy field associated with the particularly material that is selected [40]. Typically, $H_\alpha$ is on the order of 100 Oe [1]. The maximum usable value of $4\pi \mathrm{M}_s$ varies linearly with frequency [1]. Equation (4.2) can be used to determine the power handling and bandwidth of a device. For a given impedance-matching circuit, a lower $4\pi \mathrm{M}_s$ will lead to a narrower bandwidth. For a below resonance device, a lower $4\pi \mathrm{M}_s$ value will increase the peak power handling capability [1].

| Parameter | Symbol | Numerical Value |
|---|---|---|
| Helical radius | $a$ | 1.465 mm |
| Ferrite (inner radius) | $b$ | 1.59 mm |
| Ferrite (outer radius) | $c$ | 2.92 mm |
| Waveguide radius | $d$ | 2.921 mm |
| Pitch angle | $\psi$ | 9.5° |
| Relative permittivity of ferrite | $\varepsilon_r$ | 14.5 |
| Helical resistivity | $\rho_1$ | $2.5 \times 10^{-8}$ Ω m |
| Waveguide resistivity | $\rho_2$ | $2.5 \times 10^{-8}$ Ω m |
| Saturation Magnetisation | $4\pi M_s$ | 0.068 T |
| Applied Magnetic Field | $H_0$ | 55 kA $m^{-1}$ |

Table 4.1: Parameters of helical structure

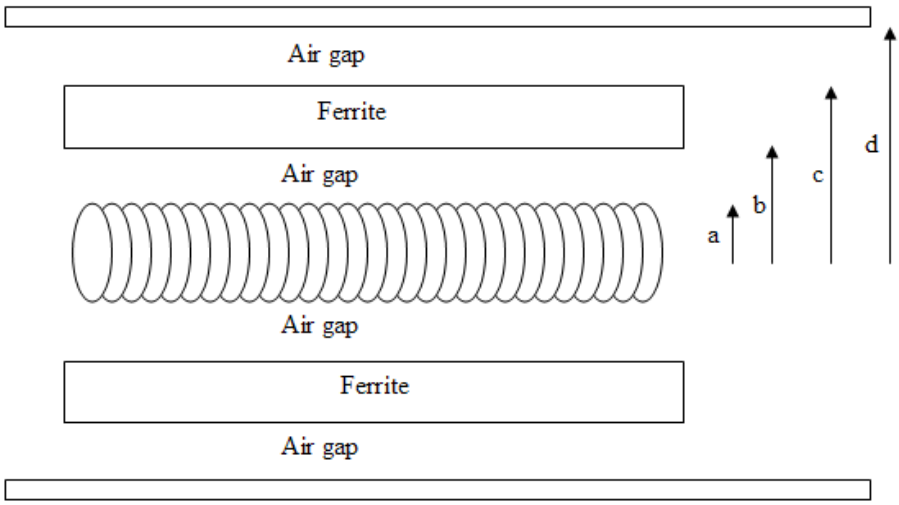


Figure 4.1: Helical structure

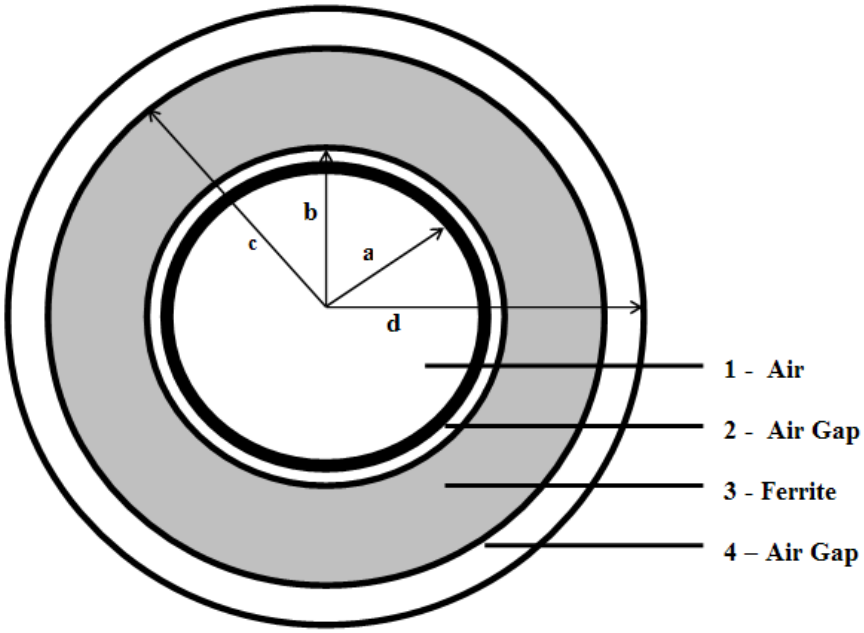


Figure 4.2: Cross-section of Helical Structure

The quantity referred to as *saturation magnetisation* can be used to determine the particular frequency at which GMR occurs in the ferrite. This value of GMR is dependant on saturation magnetisation and the degree of saturation of the ferrite, the latter is related to the applied magnetic field. Initially, the ferrite is assumed to be completely saturated. When the relative values of $\mu$ and $\kappa$ are plotted against frequency, the following graphs are obtained: figure 4.3 and 4.4. These graphs show that the GMR occurs at 1.9 GHz. These graphs are obtained using the expressions of $\mu$ and $\kappa$ given in chapter 1. Considering these expressions further,

$$\mu = 1 - \frac{\gamma^2 H_0 M_0}{\gamma^2 H_0^2 - \omega^2} \qquad \text{and} \qquad \kappa = \frac{|\gamma|\,\omega M_0}{\gamma^2 H_0^2 - \omega^2},$$

both $\mu$ and $\kappa$ approach a singularity at

$$\omega = \gamma H_0.$$

For the values given above, this frequency occurs at 1.9 GHz, (coinciding with the graphical representations of $\mu$ and $\kappa$). Letting $f_g$ denote the frequency at which GMR occurs, $f'$ represent a frequency below $f_g$ and $f''$ represent a frequency above $f_g$, then as

$$f' \to f_g, \;\; \mu \to \infty \;\text{ and }\; \kappa \to -\infty, \tag{4.3}$$

and as

$$f'' \to f_g, \;\; \mu \to -\infty \;\text{ and }\; \kappa \to \infty. \tag{4.4}$$

Figures 4.3 and 4.4 show how $\mu$ and $\kappa$ behave as the frequency approaches that of GMR. The graphs correspond to equations (4.3) - (4.4). Practically, the values of $\mu$ and $\kappa$ will not approach $\pm\infty$ but will approach a very large or very small value due to the losses that are present in the ferrite. As the frequency increases, the value of $\kappa$ also increases.

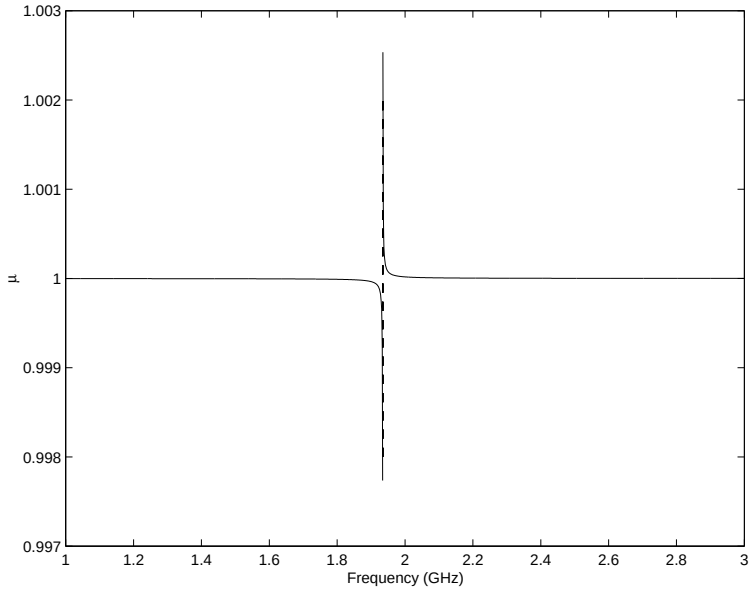


Figure 4.3: $\mu$ against frequency showing asymptotes at GMR

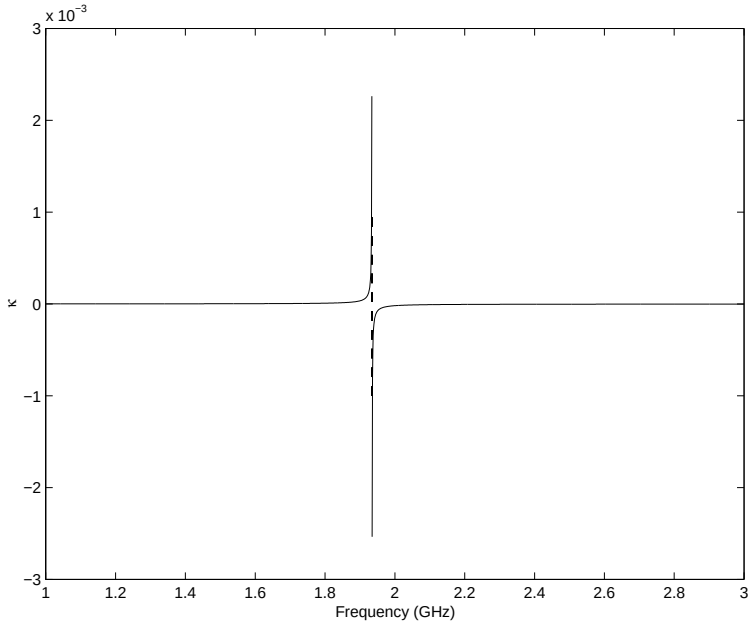


Figure 4.4: $\kappa$ against frequency showing asymptotes at GMR

**When a wave travels through a particular device, it is desirable to calculate how dispersive it is. The values of the dispersion of both the forward and backward directions are given in figure 4.6. The dispersion D for both of these waves can be calculated by using the dispersion formula,**

$$D = \frac{2\pi c}{\lambda^2}\frac{d^2\beta}{d\omega^2}. \tag{4.5}$$

**The second derivative of $\beta$ with respect to $\omega$ can be obtained numerically using the approximation.**

$$\left.\frac{d^2\beta}{d\omega^2}\right|_{\omega=\omega_n} \approx \frac{\beta_{n+1} + \beta_{n-1} - 2\beta_n}{\Delta\omega^2}. \tag{4.6}$$

**The dispersion is measured in nanosecond per radian square metre, (ns $m^{-2}$/rad).**

The attenuation coefficient $\alpha$ of the structure is shown in figure 4.7. The graph shows that as the frequency increases, the value of $\alpha$ increases[4]. From figure 4.7, it appears that $\alpha \propto \sqrt{f}$. The graph shows that at 0.5 GHz, $\alpha \approx 2.35$ db/m and that at 1.5 GHz, $\alpha \approx 4.13$ db/m. The increase in frequency from 0.5 GHz to 1.5 GHz is by a factor of 3; the square root of which is 1.732. The numerical results show that $\alpha$ increased by a factor of 1.757 over the same frequency range.

The phase shift in the structure is shown in figures 4.8 - 4.10. Figure 4.8 shows the phase shift in degrees per quarter wavelength - where the wavelength is free space is $\lambda$. Figure 4.9 shows the phase shift in degrees per quarter wavelength - where the wavelength is the electrical wavelength, $\lambda_g$. The values of $\alpha$ in figure 4.9 are consistently less than the corresponding values in figure 4.8. The length over which the phase shift is measured is different in each figure. Figure 4.11 shows the magnitude of the free space wavelength is approximately 11 times greater than that of the electrical wavelength. This coincides with the fact that the phase shift measured in (deg/($\lambda_g$/4)) is approximately 11 times less than the phase shift that is measured in (deg/($\lambda$/4)). This is shown in figures 4.8 and 4.9. Figure 4.10 express the phase shift in degrees per dB loss. This loss is the metallic loss from the helix and

[4]Initially, $\alpha$ is only metallic loss. It will be shown later that when $\alpha$ comprises of metallic and ferrite loss, the ferrite loss is very small compared to the metallic loss.

waveguide. All of these graphs show that an increase in frequency leads to an increase in phase shift. The phase shift in a structure is related to the magnitude of $\kappa$. Figure **??** shows that this increases as the frequency approaches that of GMR. Equation (4.1) shows that the phase shift depends on $\triangle\beta$. Figure 4.12 show that this increases with frequency. Both of these quantities contribute to the phase shift in the structure.

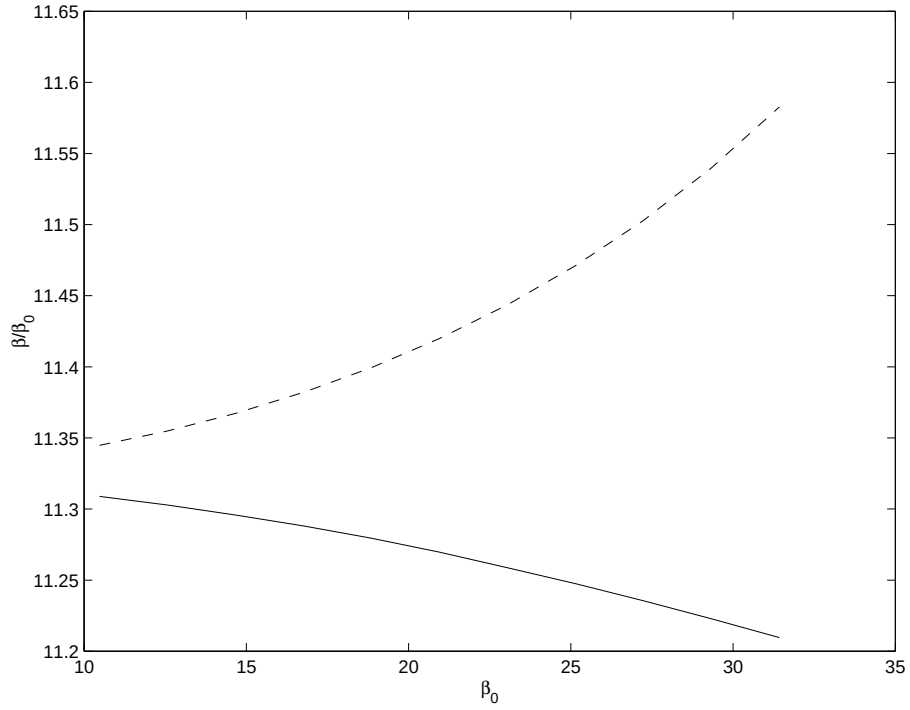


Figure 4.5: Dispersion Curves for a saturated ferrite. The propagation constant in the forward direction (solid line) and backward direction (dashed line) are shown.

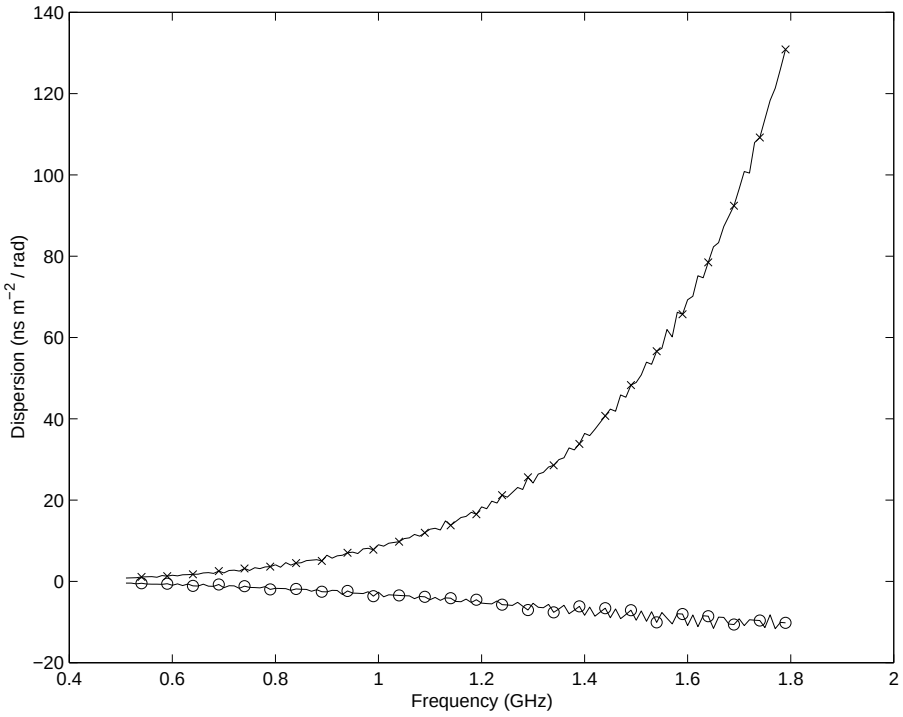


Figure 4.6: The dispersion of the forward (crossed) and backward wave (circled).

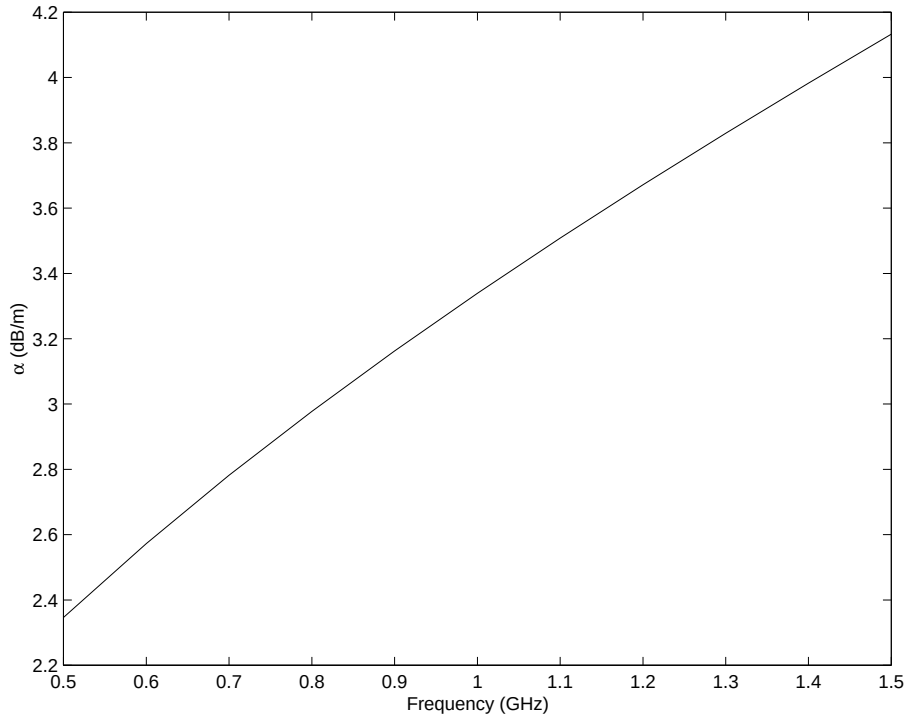


Figure 4.7: Attenuation coefficient of the structure. The attenuation, $\alpha$ (dB/m), consists solely of conductor loss.

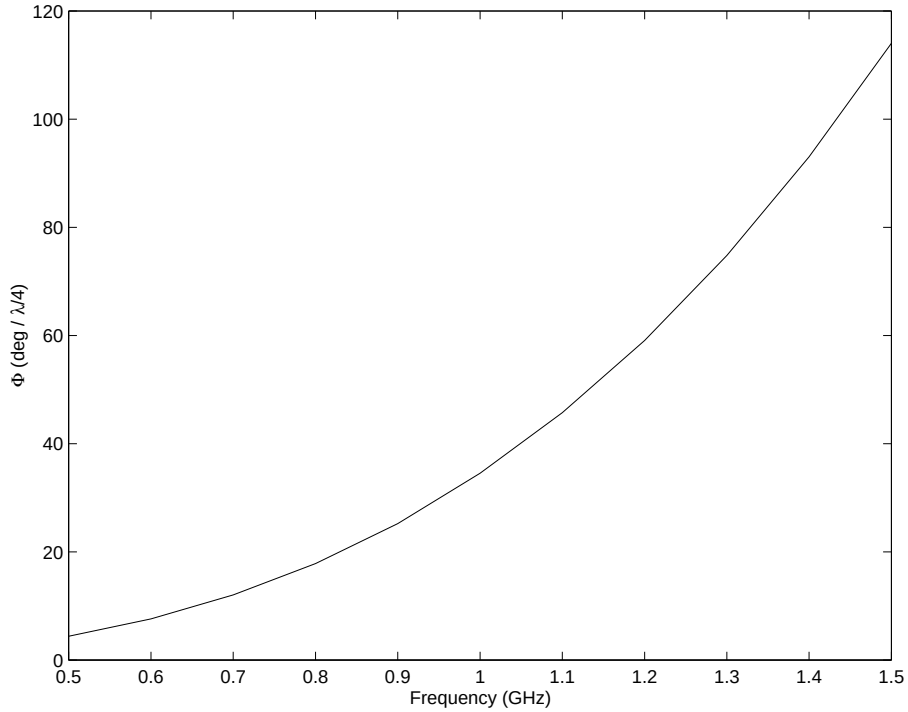


Figure 4.8: Phase Shift (degrees per quarter free space wavelength) for a saturated ferrite.

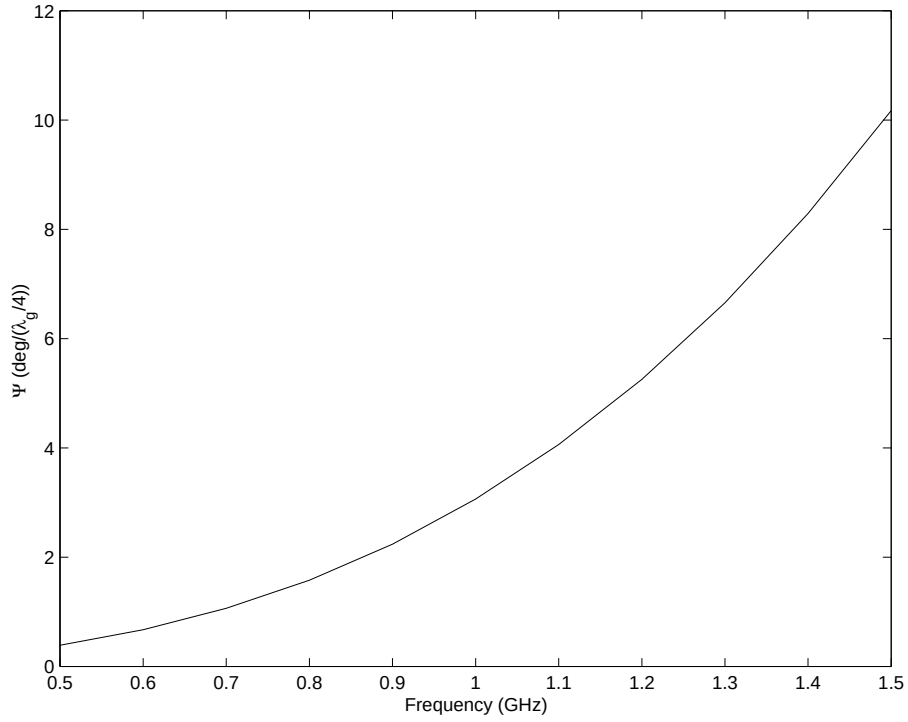


Figure 4.9: Phase Shift (degrees per quarter electrical space wavelength) for a saturated ferrite.

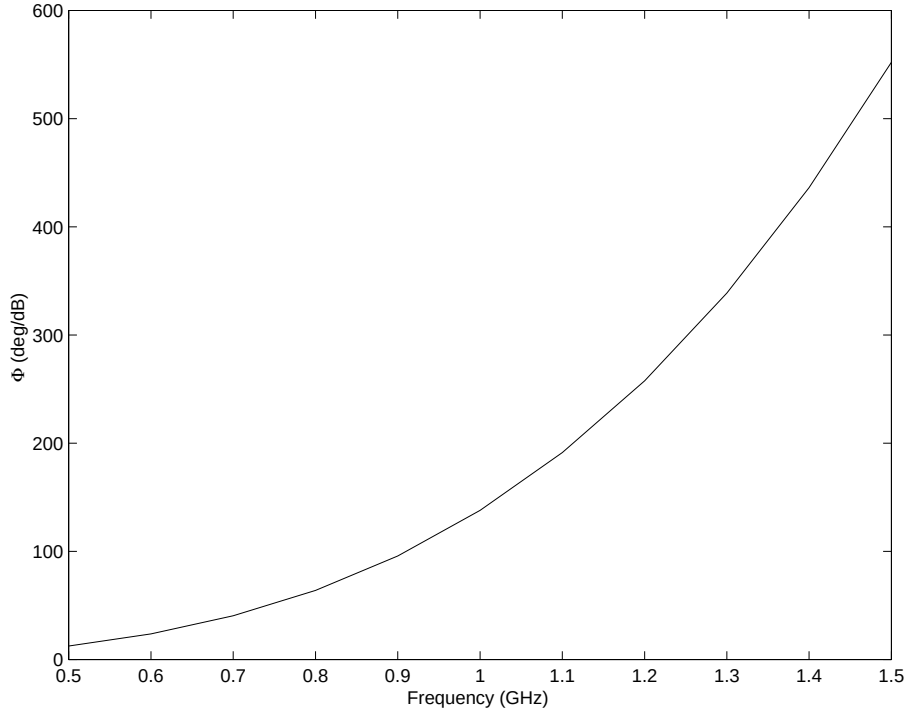


Figure 4.10: Phase Shift (degrees per dB of attenuation) for a saturated ferrite. The attenuation, $\alpha$ (dB/m), consists solely of metallic contribution.

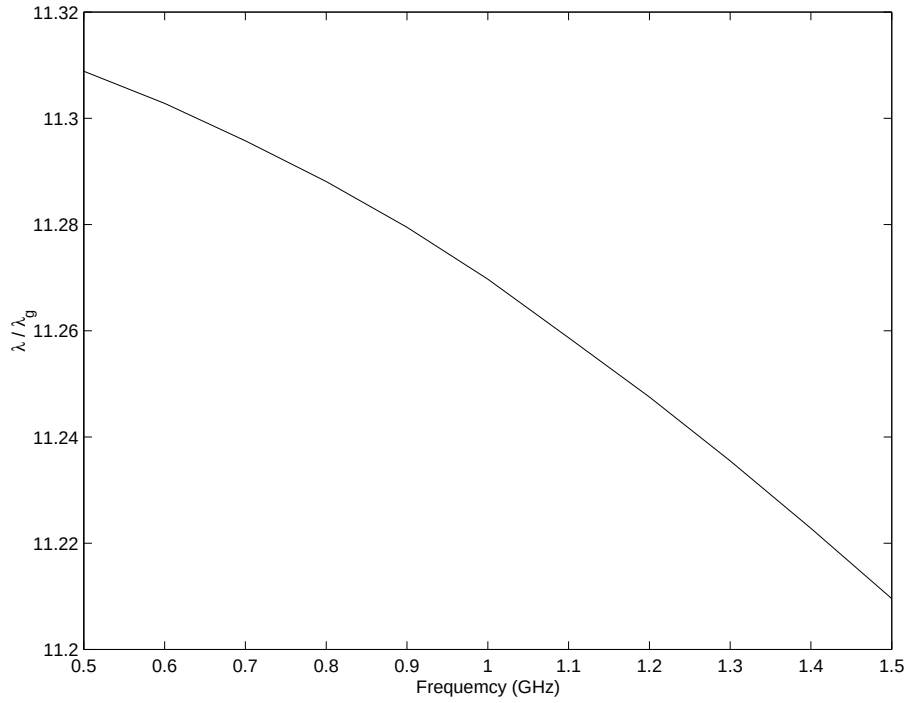


Figure 4.11: $\lambda/\lambda_g$ against frequency.

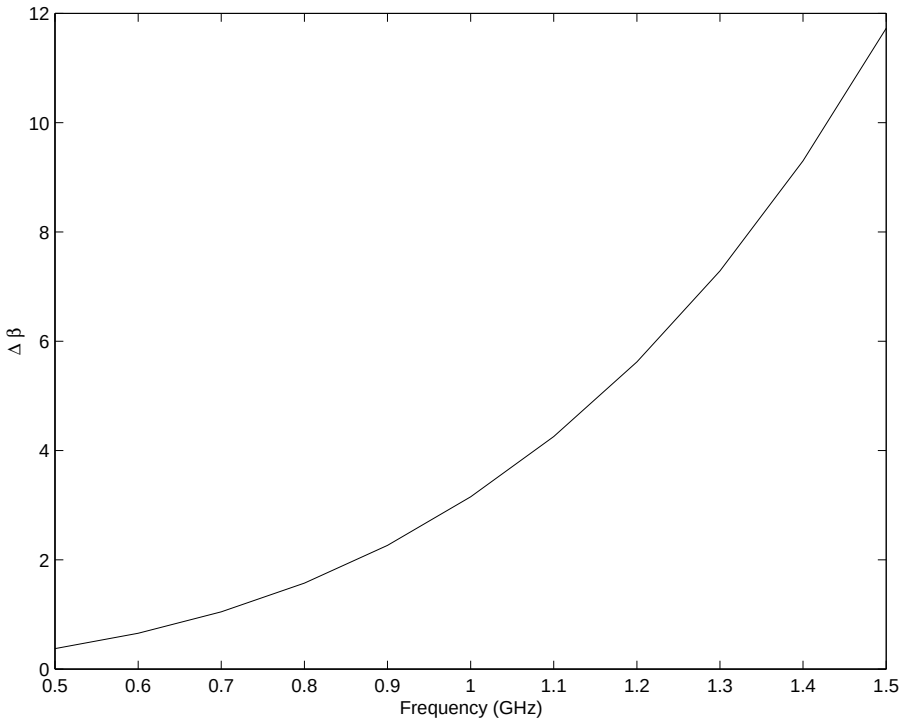


Figure 4.12: $\Delta\beta$ against frequency.

The resistivity of the metal helix and waveguide are both $2.5 \times 10^{-6}$ $\Omega$ cm. Figure 4.13 shows how the phase shift varies for different values of helical resistivities. The graph indicates that an increase in helical resistivity leads to a decrease in phase shift. These values are shown in table 4.2. Figure 4.14 shows how the phase shift varies for different values of the waveguide resistivity. These values are shown in table 4.3. Therefore, in both cases, an increase in helical or waveguide resistivity leads to a decrease in phase shift. However, the change is much greater in the variation of helical resistivity than in the variation of waveguide resistivity. The explanation for these requires consideration of equation (2.68). This is reproduced here.

$$\alpha = -\frac{\sqrt{\pi\mu_0 f}}{\Upsilon}\ \left[a\ \sqrt{\rho_1}\ \left(|H_{\theta 1}(a)|^2 + |H_{z1}(a)|^2 + |H_{\theta 2}(a)|^2 + |H_{z2}(a)|^2\right) + d\ \sqrt{\rho_2}\ \left(|H_{\theta 4}(d)|^2 + |H_{z4}(d)|^2\right)\right], \tag{4.7}$$

where

$$\Upsilon = \int_0^a rS_1 dr + \int_a^b rS_2 dr + \int_b^c rS_3 dr + \int_c^d rS_4 dr.$$

Firstly, an increase in helical or waveguide resistivity, ($\rho_1$ or $\rho_2$), leads to an increase in $\alpha$. An increase in $\alpha$ implies that over a length of 1 metre, the wave is attenuated to a greater extent. Therefore, there is a decrease in the length over which the wave is attenuated by 1 dB. As this length decreases, the phase shift also decreases. Secondly, the change in $\alpha$ is much greater in the variation of helical resistivity than in the variation of waveguide resistivity. In equation (4.7), the magnetic field components that are calculated are all expressed as Bessel functions. These field components are greater in quantity nearer the origin. Therefore,

$$|H_{\theta 1}(a)|^2 + |H_{z1}(a)|^2 + |H_{\theta 2}(a)|^2 + |H_{z2}(a)|^2 > |H_{\theta 4}(d)|^2 + |H_{z4}(d)|^2 .$$

A variation in the helical resistivity, $\rho_1$, leads to a greater variation in $\alpha$ than a corresponding variation in the waveguide resistivity, $\rho_2$.

So far, the discussion of the attenuation coefficient has been restricted to the case where $\varepsilon_f$ and $\mu_f$ have been real quantities - $\mu_f$ and $\varepsilon_f$ being the permeability and permittivity of the ferrite. The

losses have consisted solely from metallic ones: the waveguide and the helix. The values of $\mu_f$ and $\varepsilon_f$ can be extended to be complex quantities. Firstly, $\mu_f$ is kept as a real quantity and $\varepsilon_f$ takes the form

$$\varepsilon_f = \varepsilon_f \left(1 - \tan(\delta)i\right), \tag{4.8}$$

where $\tan(\delta)$ is the dielectric loss tangent. A large value of $\tan(\delta)$ represents a lossy material. At a frequency value of 1.5 GHz, a variation in $\tan(\delta)$ is shown in figure 4.15. The graph also shows that increasing the value of $\tan(\delta)$ increases the value of $\alpha$.

The analysis can be extended to include the effect of damping in the structure. This is achieved by replacing the expressions of $\mu$ and $\kappa$ to include the damping constant $x$. Previously, the expressions of $\mu$ and $\kappa$ were

$$\kappa = -\frac{\omega\gamma M_0}{\gamma^2 H_0^2 - \omega^2}$$

and

$$\mu = \mu_0 + \chi,$$

where

$$\chi = \frac{\gamma^2 H_0 M_0}{\gamma^2 H_0^2 - \omega^2}.$$

$\kappa$ and $\mu$ can be written in complex quantities to give a representation of the damping,

$$\chi = \chi' - i\,\chi'',$$

$$\kappa = \kappa' - i\,\kappa'',$$

where

$$\chi' = \frac{\gamma^2 M_0 H_0 \left[\gamma^2 H_0^2 - \omega^2\left(1 - x^2\right)\right]}{\left[\gamma^2 H_0^2 - \omega^2\left(1 + x^2\right)\right]^2 + 4\gamma^2 H_0^2 \omega^2 x^2},$$

$$\chi'' = \frac{\gamma M_0 \omega x \left[\gamma^2 H_0^2 + \omega^2\left(1 + x^2\right)\right]}{\left[\gamma^2 H_0^2 - \omega^2\left(1 + x^2\right)\right]^2 + 4\gamma^2 H_0^2 \omega^2 x^2},$$

$$\kappa' = \frac{-\omega\gamma M_0 \left[\gamma^2 H_0^2 - \omega^2\left(1 + x^2\right)\right]}{\left[\gamma^2 H_0^2 - \omega^2\left(1 + x^2\right)\right]^2 + 4\gamma^2 H_0^2 \omega^2 x^2},$$

$$\kappa'' = \frac{-2\gamma^2 M_0 H_0 \omega^2 x \left[\gamma^2 H_0^2 + \omega^2 (1+x^2)\right]}{\left[\gamma^2 H_0^2 - \omega^2 (1+x^2)\right]^2 + 4\gamma^2 H_0^2 \omega^2 x^2}.$$

By allowing $x$ to take different values, an insight into how damping will affect the loss in the structure can be obtained. Letting

$$t = \log_{10}(x) \qquad \Rightarrow \qquad x = 10^t,$$

then as $t \to -\infty$, $x \to 0$, the effect of damping is decreased until an undamped system is achieved. Figure 4.16 shows how the attenuation coefficient $\alpha$ varies for different values of $t$. As the value of $t$ decreases, the graph approaches the undamped system, as expected.

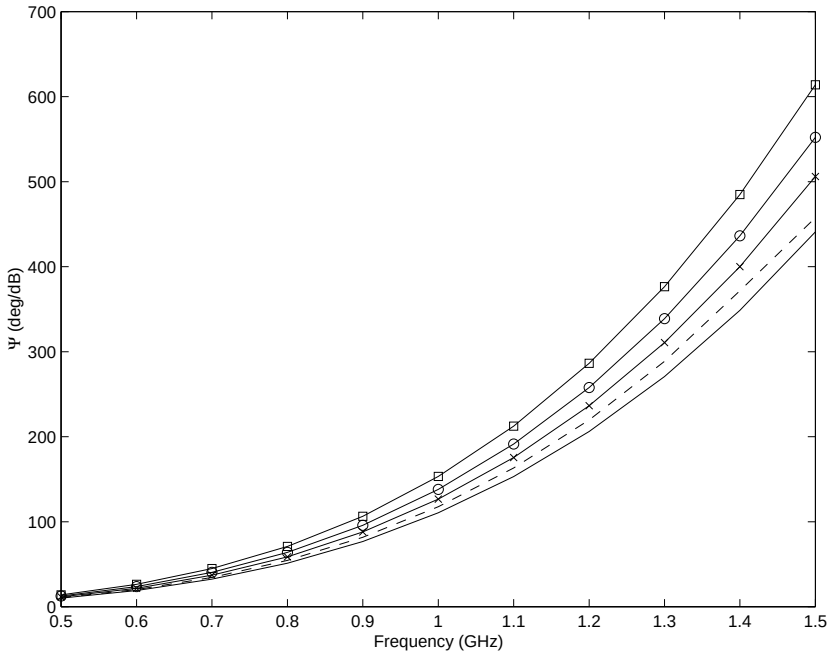


Figure 4.13: Phase Shift against frequency for variation in helical resistivity. $\rho_1 = 2\times\ 10^{-6}\ \Omega\ cm$ (squared line), $2.5\times\ 10^{-6}\ \Omega\ cm$ (circled line), $3\times\ 10^{-6}\ \Omega\ cm$ (crossed line), $3.5\times\ 10^{-6}\ \Omega\ cm$ (dashed line), $4\times\ 10^{-6}\ \Omega\ cm$ (straight line). The attenuation, $\alpha$ (dB/m), consists solely of metallic loss.

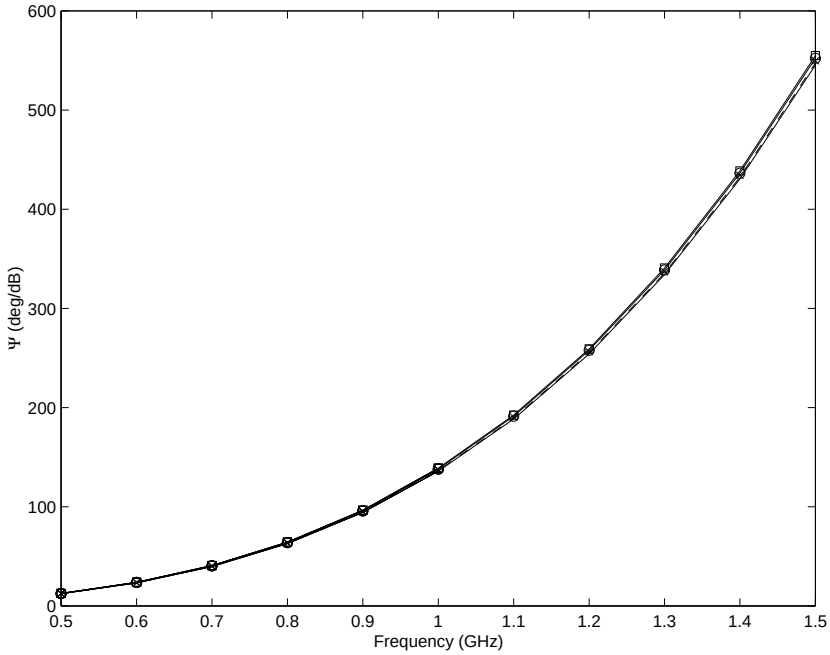


Figure 4.14: Phase Shift against frequency for variation in waveguide resistivity. $\rho_1 = 2\times\ 10^{-6}\ \Omega\ cm$ (squared line), $2.5\times\ 10^{-6}\ \Omega\ cm$ (circled line), $3\times\ 10^{-6}\ \Omega\ cm$ (crossed line), $3.5\times\ 10^{-6}\ \Omega\ cm$ (dashed line), $4\times\ 10^{-6}\ \Omega\ cm$ (straight line). The attenuation, $\alpha$ (dB/m), consists solely of metallic loss.

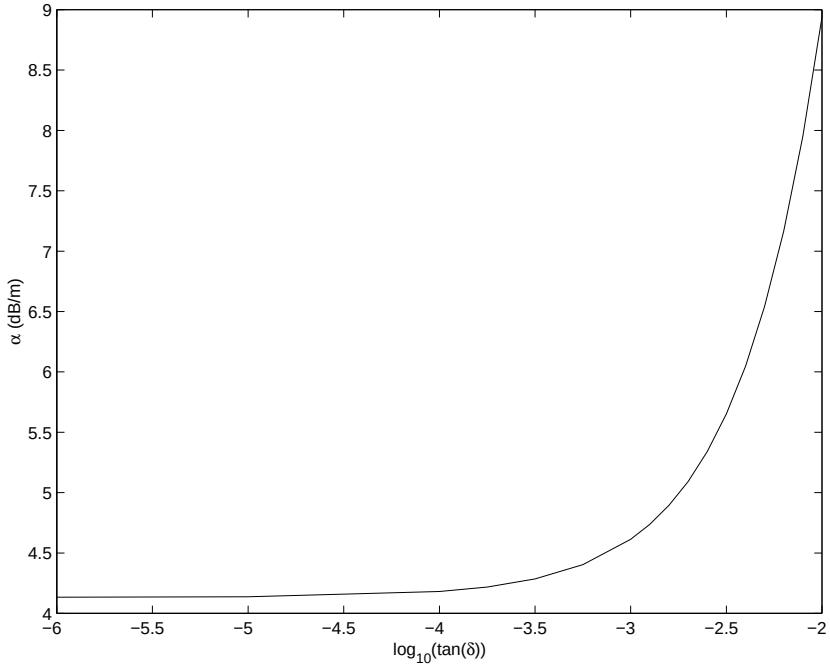


Figure 4.15: Attenuation coefficient against dielectric loss tangent at a frequency of 1.5 GHz, ($\mu$ and $\kappa$ are real, $\varepsilon$ is constant).

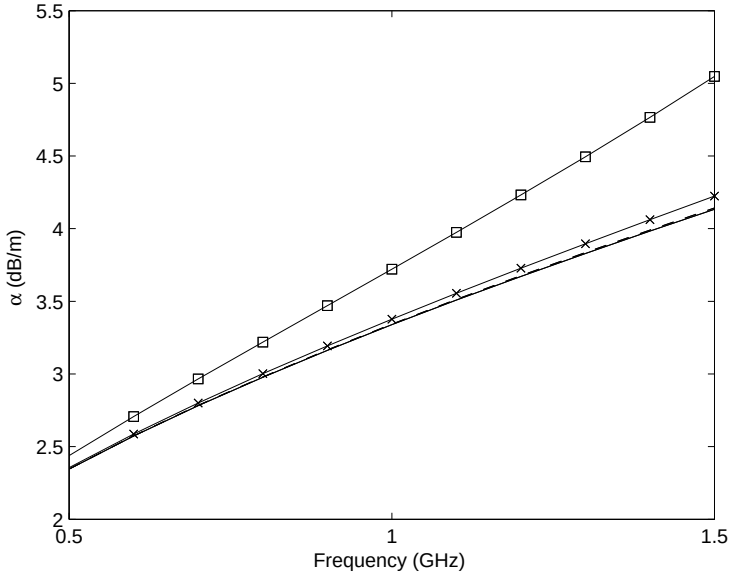


Figure 4.16: Attenuation coefficient against frequency for different values of $t$. The undamped system (solid line), $t = -4$ (dashed line), $t = -3$ (crossed line) and $t = -2$ (squared line).

| Freq (GHz) | Φ (deg/dB) ($2\times 10^{-6}$ Ω cm) | Φ (deg/dB) ($2.5\times 10^{-6}$ Ω cm) | Φ (deg/dB) ($3\times 10^{-6}$ Ω cm) | Φ (deg/dB) ($3.5\times 10^{-6}$ Ω cm) | Φ (deg/dB) ($4\times 10^{-6}$ Ω cm) |
|---|---|---|---|---|---|
| 0.5 | 13.9252 | 12.5529 | 11.5259 | 10.7195 | 10.0641 |
| 0.6 | 26.2876 | 23.6938 | 21.7533 | 20.2298 | 18.9917 |
| 0.7 | 44.8939 | 40.4581 | 37.1405 | 34.5362 | 32.4202 |
| 0.8 | 70.9978 | 63.9717 | 58.7183 | 54.5954 | 51.2462 |
| 0.9 | 106.3851 | 95.8385 | 87.9554 | 81.7703 | 76.7469 |
| 1 | 153.2462 | 138.0242 | 126.6507 | 117.7296 | 110.4859 |
| 1.1 | 212.5083 | 191.3546 | 175.5557 | 163.1672 | 153.1106 |
| 1.2 | 286.3518 | 257.7817 | 236.4533 | 219.7346 | 206.1665 |
| 1.3 | 376.4707 | 338.8163 | 310.7196 | 288.7036 | 270.8415 |
| 1.4 | 484.9534 | 436.3211 | 400.0515 | 371.6424 | 348.6006 |
| 1.5 | 613.9407 | 552.2024 | 506.1833 | 457.7877 | 440.9385 |

Table 4.2: Phase shift against frequency for variation in helix resistivity.

| Freq (GHz) | Φ (deg/dB) ($2\times 10^{-6}$ Ω cm) | Φ (deg/dB) ($2.5\times 10^{-6}$ Ω cm) | Φ (deg/dB) ($3\times 10^{-6}$ Ω cm) | Φ (deg/dB) ($3.5\times 10^{-6}$ Ω cm) | Φ (deg/dB) ($4\times 10^{-6}$ Ω cm) |
|---|---|---|---|---|---|
| 0.5 | 12.6416 | 12.5529 | 12.4737 | 12.4018 | 12.3356 |
| 0.6 | 23.8585 | 23.6938 | 23.5468 | 23.4133 | 23.2903 |
| 0.7 | 40.7338 | 40.4581 | 40.2121 | 39.9884 | 39.7825 |
| 0.8 | 64.3975 | 63.9717 | 63.5916 | 63.246 | 62.9277 |
| 0.9 | 96.4594 | 95.8385 | 95.2841 | 94.7798 | 94.3153 |
| 1 | 138.8912 | 138.0242 | 137.2496 | 136.545 | 135.8956 |
| 1.1 | 192.5155 | 191.3546 | 190.3171 | 189.3729 | 188.5024 |
| 1.2 | 259.2856 | 257.7817 | 256.437 | 255.2128 | 254.0838 |
| 1.3 | 340.7083 | 338.8163 | 337.1237 | 335.5821 | 334.1599 |
| 1.4 | 438.6416 | 436.3211 | 434.2442 | 432.3516 | 430.6048 |
| 1.5 | 554.984 | 552.2024 | 549.7115 | 547.4407 | 545.3438 |

Table 4.3: Phase shift against frequency for variation in waveguide resistivity.

## 4.3 Variation of Parameters

This section deals with the affect of varying certain parameters of the helical structure. One of the assumptions of the sheath helix model is that p << $\lambda$. The pitch angle is related to the pitch by the relation: $\tan(\psi) = \frac{p}{2\pi a}$. Therefore,

$$2\pi a \tan(\psi) << \lambda \qquad \Rightarrow \qquad 2\pi a \tan(\psi) << \frac{c}{f}.$$

The variation of the length parameters will alter the nature of the structure. For example, if the helical radius $a$ is decreased, then the proportion of ferrite in the structure will be increased.

This section considers the same helical structure but with two different geometrical properties. The first is a structure where the thickness of the ferrite is greater than that of helical radius. Figure 4.17 shows a cross section of the structure with this property.

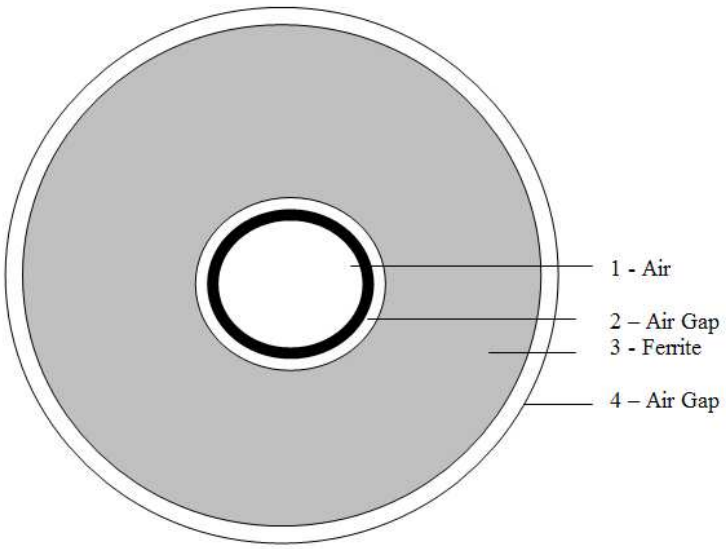


Figure 4.17: Cross-section of helical structure.

Table 4.4 shows the dimension that are initially used in the structure. Dispersion curves representing the forward and backward waves are given in figure 4.19. The phase shift in degrees per quarter wavelength is shown in figure 4.20. The difference in the forward and backward propagation

| Parameter | Symbol | Numerical Value |
|---|---|---|
| Helical radius | $a$ | 1 mm |
| Ferrite (inner radius) | $b$ | $a$ + 0.001 mm |
| Ferrite (outer radius) | $c$ | $b$ + 10 mm |
| Waveguide radius | $d$ | $c$ + 0.001 mm |
| Pitch angle | $\psi$ | 9.5° |
| Saturation Magnetisation | $4\pi M_s$ | 0.068 T |
| Applied Magnetic Field | $H_0$ | 55 kA $m^{-1}$ |

Table 4.4: Dimensions of helical structure,

constant increases as the frequency increases. This is due to the increase in $\kappa$ as the frequency approaches the GMR frequency, 1.9 GHz. The increase in $\kappa$ also corresponds to an increase in phase shift. The tensor permeability matrix is given by

$$\mathbf{M} = \begin{pmatrix} \mu & 0 & i\kappa \\ 0 & \mu_0 & 0 \\ -i\kappa & 0 & \mu \end{pmatrix}.$$

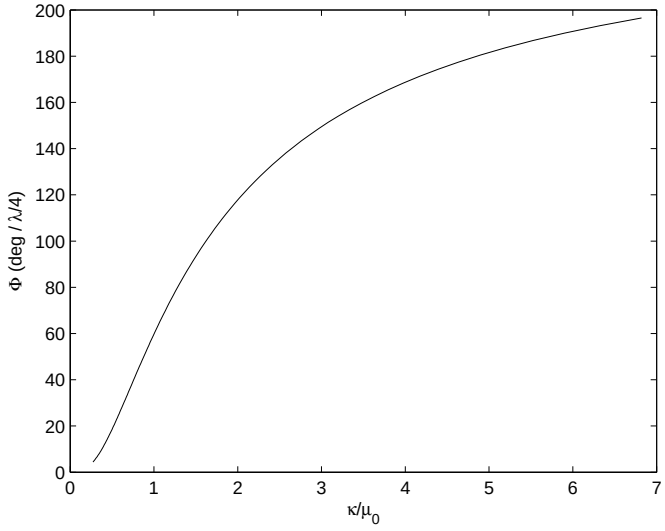


Figure 4.18: Phase shift against $\kappa$

**The increased off-diagonal components of the tensor permeability matrix M lead to an increase in non-reciprocal behaviour and thus an increased phase shift. This point can be illustrated if the example in the previous section is considered, with parameters given in table 4.1. If the phase shift is plotted against $\kappa$, figure 4.18 is obtained. As the frequency increases and approaches GMR, the value ok $\kappa$ increases (figure 4.4), $\Delta\beta$ also increases (figure 4.12). Thus increasing $\kappa$ increases the non-reciprocal behavior of the device.**

The first variation considered was that of the thickness of the air gap between the metal helix and the ferrite. When this air gap is altered, the other regions maintain their original thickness. For example, the thickness of the ferrite is kept constant at 10 mm. Altering the air gap does not affect the thickness of the ferrite. This results in the following; as the thickness of the air gap increases or decreases the cross-sectional area of the helical structure increases or decreases, respectively. Figure 4.21 shows how the size of the air gap is altered without affecting the thickness of other regions.

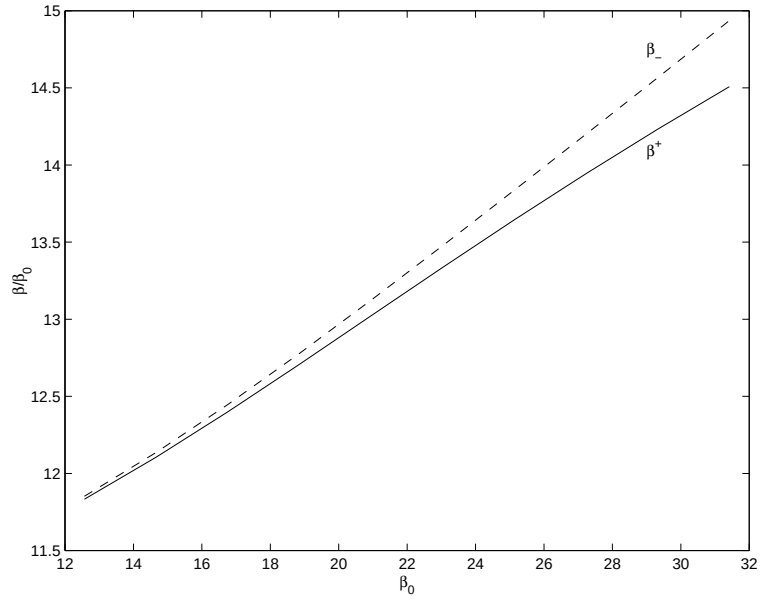


Figure 4.19: Dispersion curves for forward ($\beta^+$) and backward ($\beta_-$) waves.

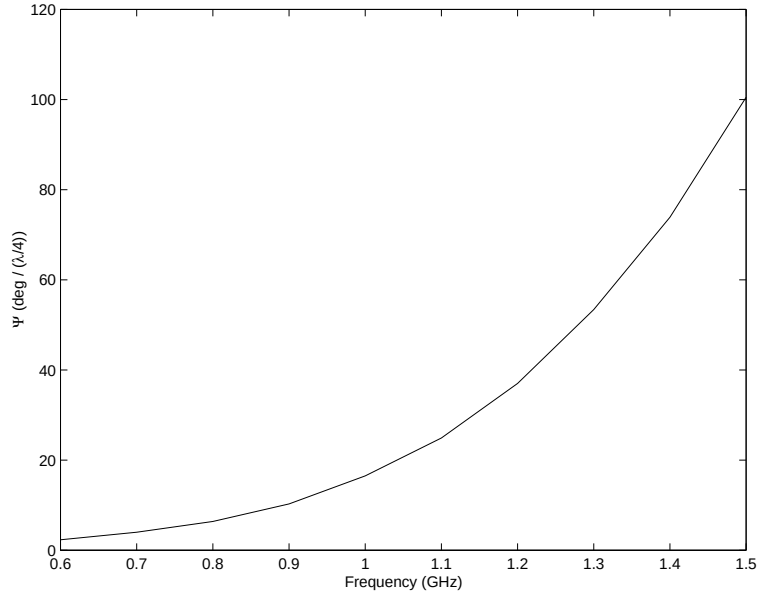


Figure 4.20: Phase shift against frequency

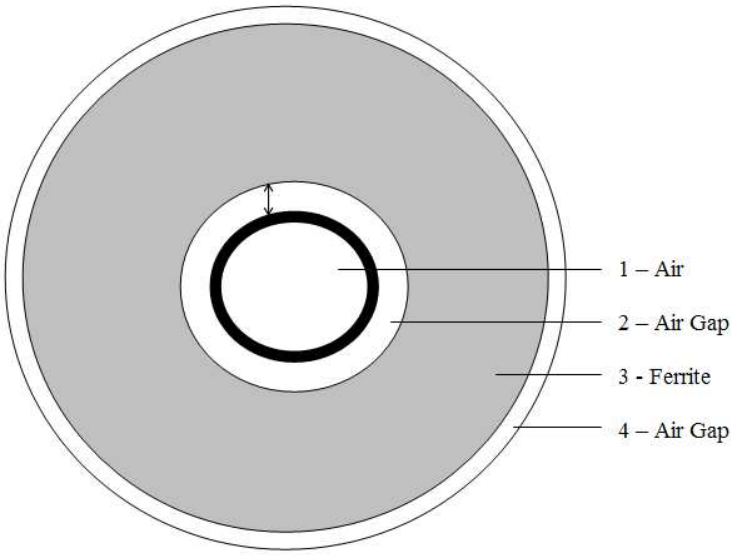


Figure 4.21: Cross-section of Helical Structure

When the air gap between the helix and the ferrite is altered, the resulting dispersion curves are shown in figure 4.22. The phase shifts per ($\lambda/4$) are shown in figure 4.23. An increase in the air gap leads to a decrease in the propagation constants; (both $\beta^+$ and $\beta_-$), as well as a decrease in the phase shift. Also, as the air gap increased, the dispersion decreases.

The effect of varying ferrite thickness is shown in figure 4.24. Figure 4.25 shows the phase shift per ($\lambda/4$). The graphs show minimal changes for ferrite thicknesses of 1 cm, 2 cm, 3 cm, 4 cm and 5 cm . The graphs appear to be on top of one another as the phase shift is so minute. However, by setting the ferrite thickness at 2 mm, the phase shift was less than that of the other values. Therefore, an increased quantity of ferrite in the structure leads to an increase in phase shift. This behaviour continues until such a quantity of ferrite is used beyond which additional ferrite shows

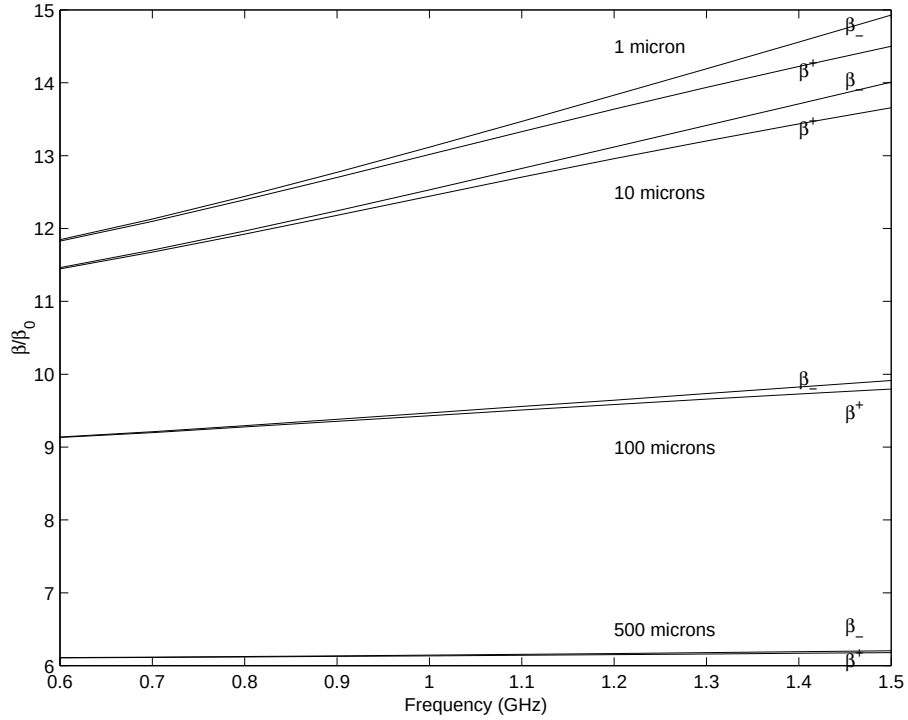


Figure 4.22: Dispersion curves for forward ($\beta^+$) and backward ($\beta_-$) waves for variation in the air gap between helix and ferrite.

minimal changes to the ferrite. Thus, increasing the ferrite thickness from 2 mm to 1 cm causes the phase shift to increase. The difference in phase shift is minimal if the thickness of the ferrite exceeds 1 cm.

When the air gap between the ferrite and the waveguide is varied, the phase shift per ($\lambda/4$) is not affected, (see figure 4.26). Again, the phase shift is not affected by the thickness of this air gap.

Therefore, a structure corresponding to the parameters of table 4.4 gives the following results:

1. Altering the thickness of the air gap between the helix and ferrite causes a change in the propagation constants, and phase shift.

2. Altering the thickness of the ferrite causes a minimal change in the propagation constants, and phase shift.

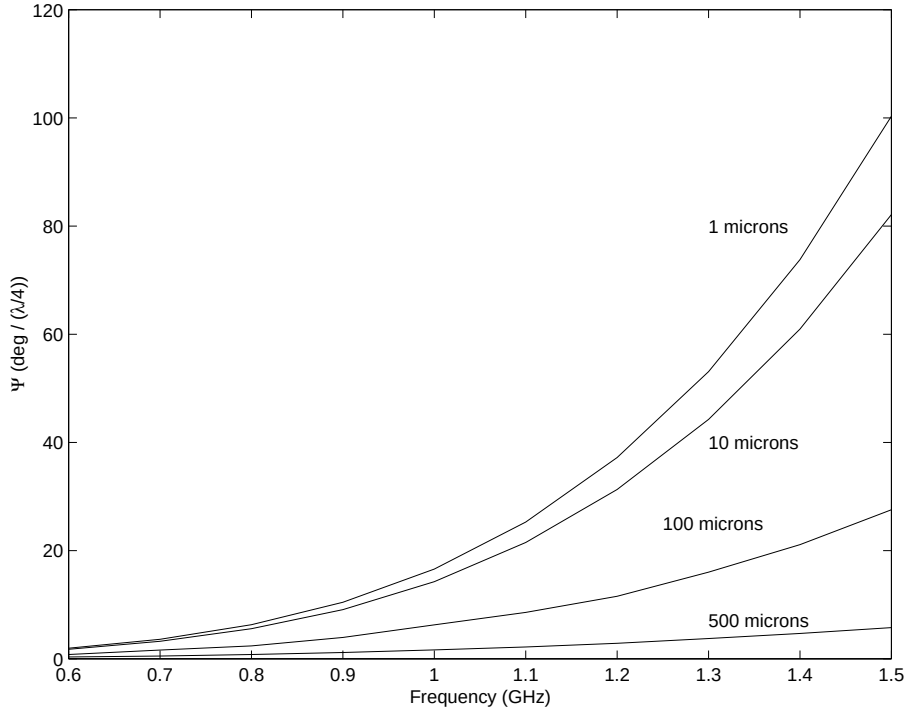


Figure 4.23: Phase shift for variation in the air gap between helix and ferrite.

3. Altering the thickness of the air gap between the ferrite and waveguide causes no change in the propagation constants, and phase shift.

A possible reason for this is that all the quantities that are being calculated (propagation constants, phase shifts and others) are affected by the magnitude of the electric and magnetic field components in each region. The expressions for these are Bessel functions in the air regions, and Confluent Hypergeometric functions in the ferrite. The Bessel functions are such that a slight increase or decrease close to the origin has a greater effect on the function than one further away from the origin. Therefore, in this geometry, changes in the air gap close to the helix produces a greater effect than ones which are further away from the centre (such as in the ferrite or the air gap between the ferrite and the waveguide).

Figure 4.27 shows the propagation constants for different values of ferrite permittivity. Figure 4.29 shows how the phase shift of a wave travelling through this helical structure varies with the

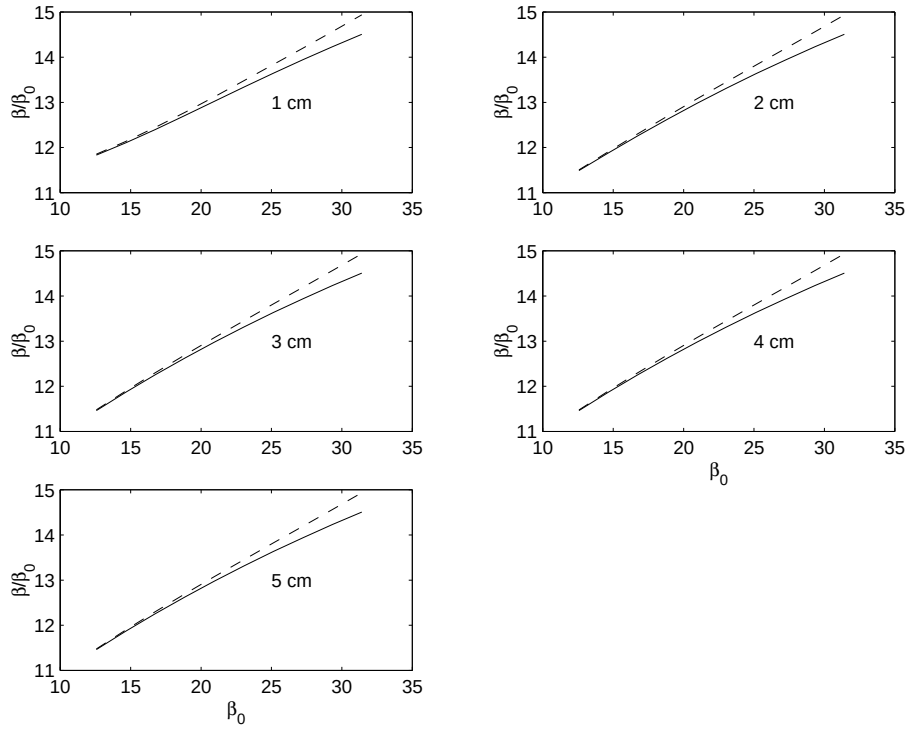


Figure 4.24: Dispersion curves for forward ($\beta^+$) and backward ($\beta_-$) waves for variation in ferrite thickness. The solid line represents forward wave and the dashed line represents the backward wave.

permittivity of the ferrite, $\varepsilon_f$. The graphs show that an increase in $\varepsilon_f$ results in an increase in phase shift. This can be understood by considering the expression for phase shift. The phase shift is obtained by equation (4.1) - showing that the term $\sqrt{\varepsilon_f}$ affects the phase shift. Increasing the ferrite permittivity leads to an increase in phase shift. Figure 4.28 shows how the dispersion varies with frequency. The graph indicates that a larger value of ferrite permittivity results in a greater dispersion.

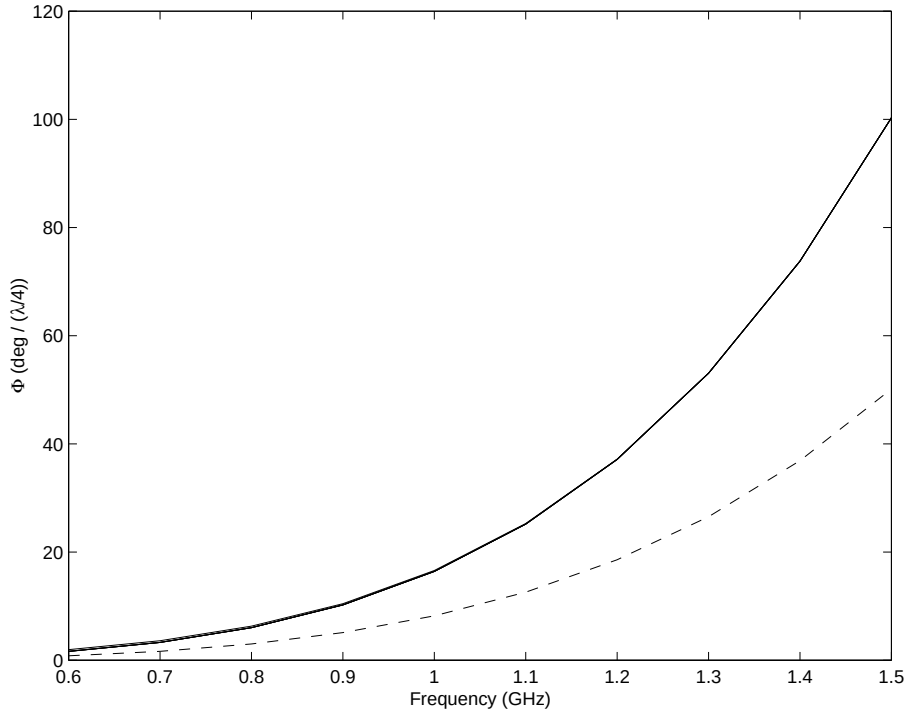


Figure 4.25: Phase shift for variation in ferrite thickness. The solid lines are for a ferrite of thickness: 1 cm, 2 cm, 3 cm, 4 cm and 5 cm. The dashed line represents a ferrite of thickness 2 mm.

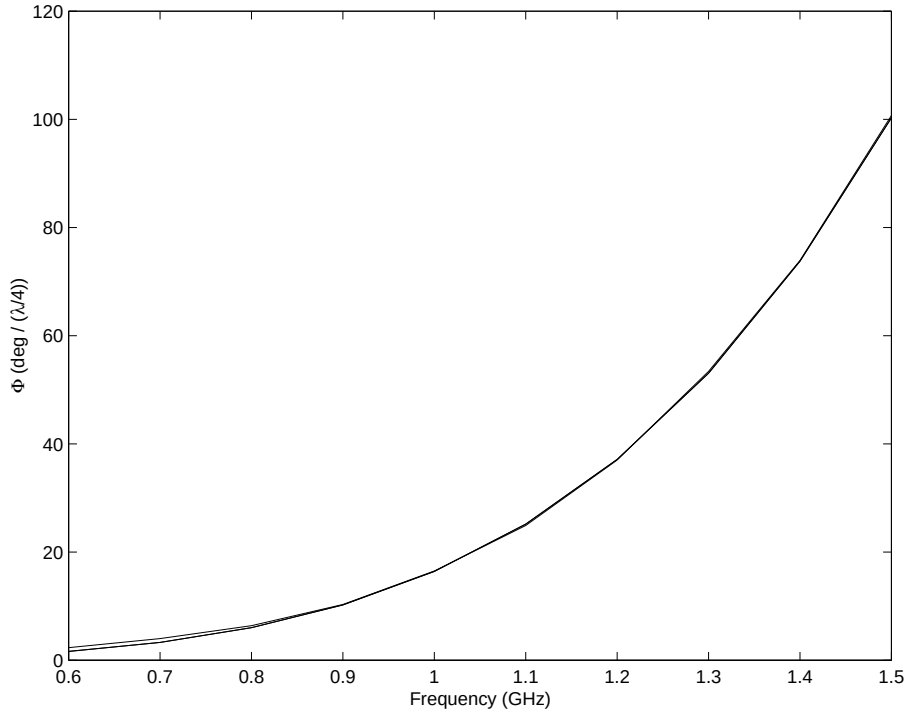


Figure 4.26: Phase shift for variation in the air gap between ferrite and metal waveguide. The air gaps are 1 micron, 10 microns and 100 microns.

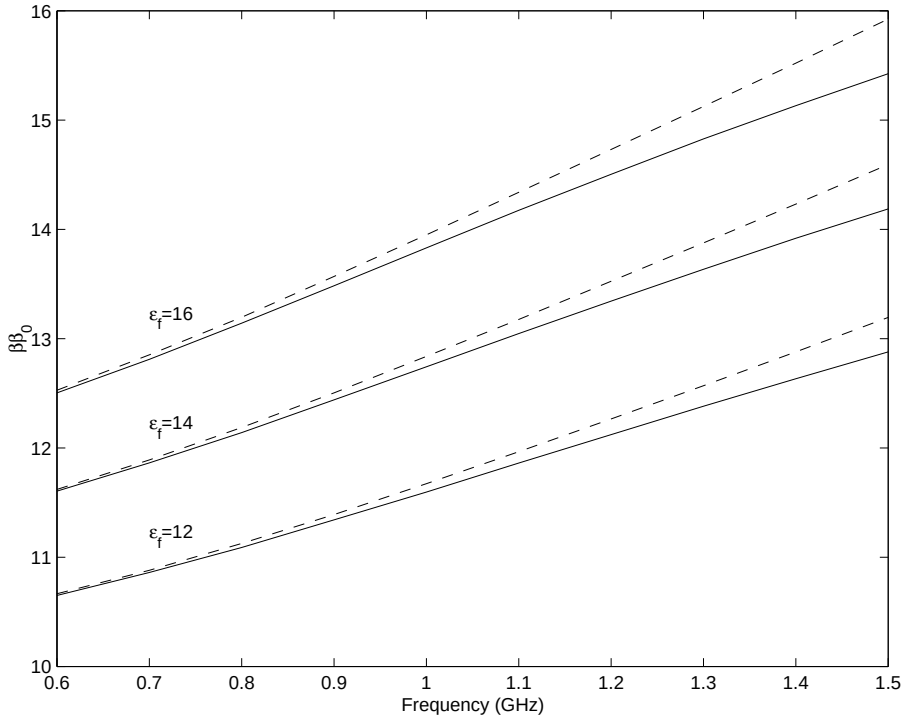


Figure 4.27: Dispersion curves against frequency for variation in ferrite permittivity. The propagation constant in the forward direction (solid line) and backward direction (dashed line).

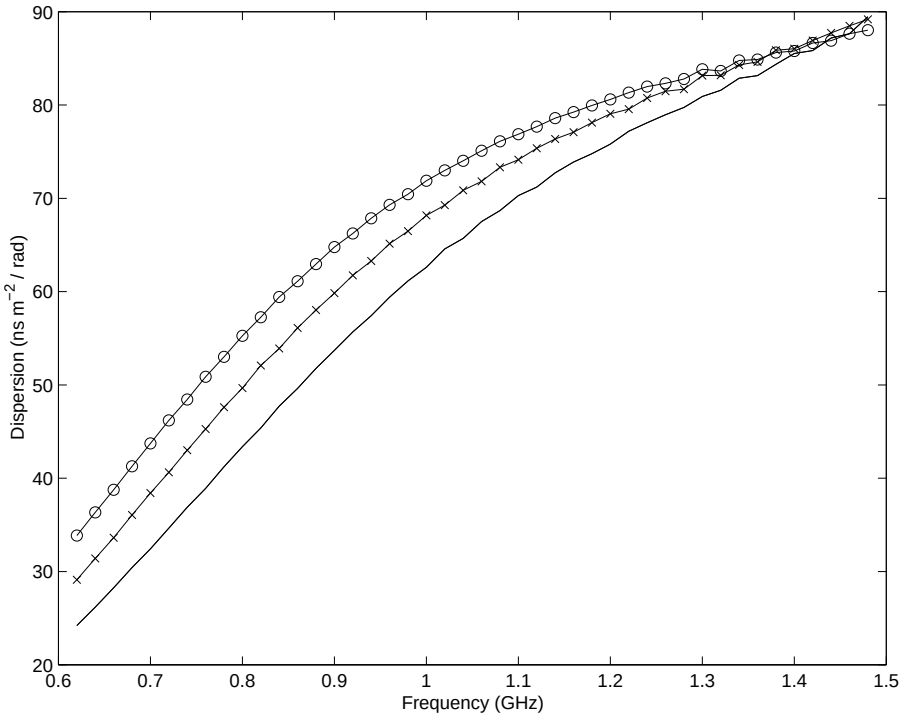


Figure 4.28: Dispersion against frequency for variation in ferrite permittivity. The solid line represents $\varepsilon_f = 12$, the crossed line represents $\varepsilon_f = 14$ and the circled line represents $\varepsilon_f = 16$.

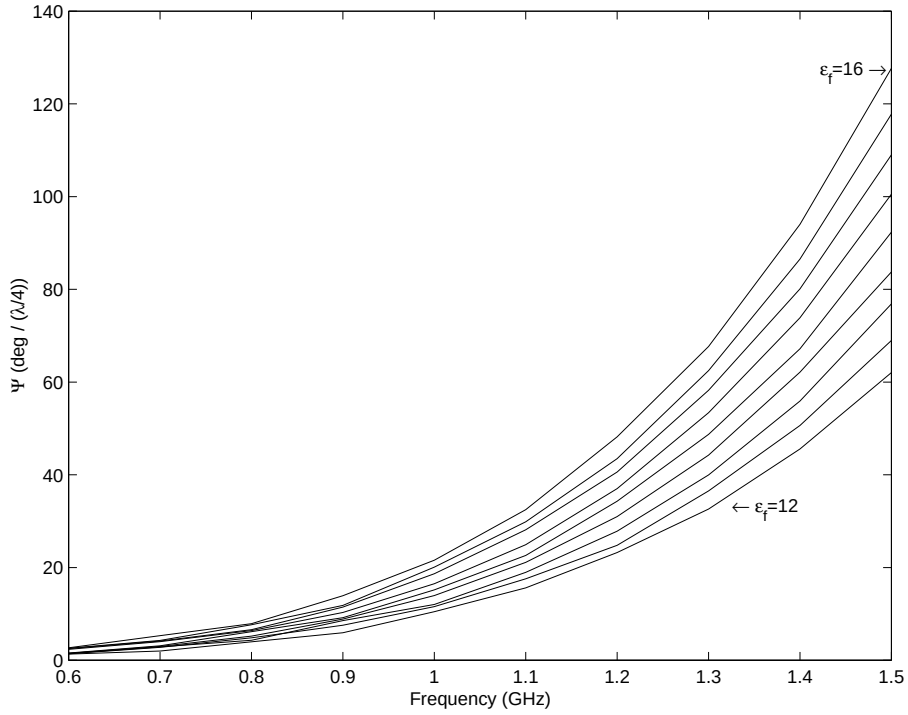


Figure 4.29: Phase shift against frequency for variation in relative permittivity of ferrite. The graphs increase in ferrite permittivity from 12 to 16 in increments of 0.5.

Gilmor [19] and Lopez [21] both showed that as the permittivity of the dielectric supports increases, the conductor loss increases. This is also true when the dielectric rods are replaced with a ferrite tube. In order to explain this, it is necessary to consider the equation for conductor loss

$$\alpha = -\frac{\sqrt{\pi\mu_0 f}}{\Upsilon}\ \left[a\ \sqrt{\rho_1}\ \left(|H_{\theta 1}(a)|^2 + |H_{z1}(a)|^2 + |H_{\theta 2}(a)|^2 + |H_{z2}(a)|^2\right) + d\ \sqrt{\rho_2}\ \left(|H_{\theta 4}(d)|^2 + |H_{z4}(d)|^2\right)\right] \tag{4.9}$$

where

$$\Upsilon = \int_0^a rS_1 dr + \int_a^b rS_2 dr + \int_b^c rS_3 dr + \int_c^d rS_4 dr. \tag{4.10}$$

As the permittivity increases, the magnetic field on the helix will also increase. As the magnetic field on the helix increases the conductor loss also increases. Figure 4.30 shows that as the permittivity of the ferrite ($\varepsilon_f$) increases, the conductor loss on the helix increases. The conductor loss consists of the metallic loss on the helix and the waveguide. As the permittivity increases, a greater proportion of the metallic loss arises from the helix, as shown in figure 4.31.

An increase in permittivity leads to the energy being concentrated around the helix. This can be shown by considering the integrals

$$I_1 = \int_0^a rS_1 dr \qquad \text{and} \qquad I_2 = \int_a^b rS_2 dr. \tag{4.11}$$

$I_1$ calculates the energy that is in the inside of the helix and $I_2$ calculates the energy that is in the air gap between the helix and ferrite. Graphs of how $I_1$ and $I_2$ against the variation in ferrite permittivity are given in figures 4.32 and 4.33. These graphs show that increasing the permittivity of the ferrite increases the values of $I_1$ and $I_2$, (thus the energy on the helix increases).

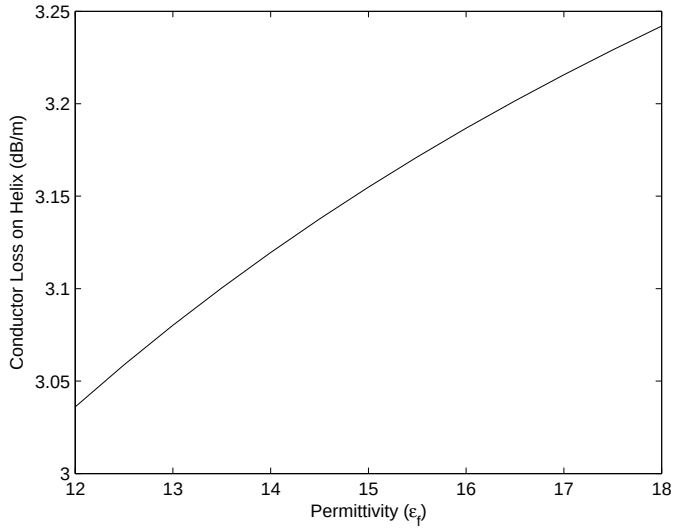


Figure 4.30: Conductor Loss on Helix

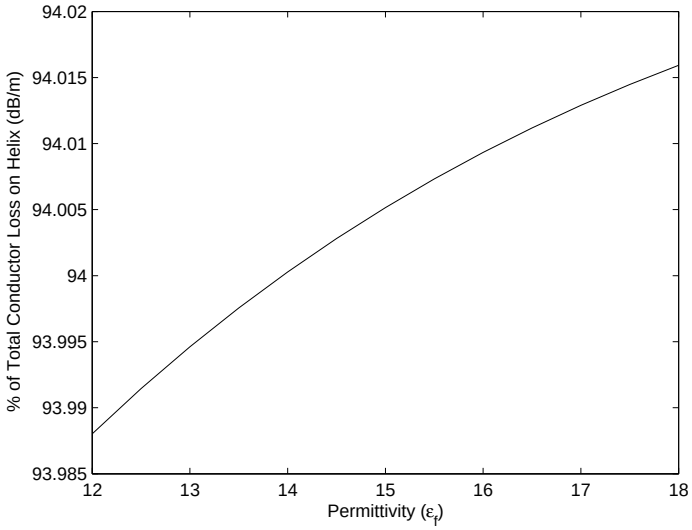


Figure 4.31: Percentage of Conductor Loss on Helix

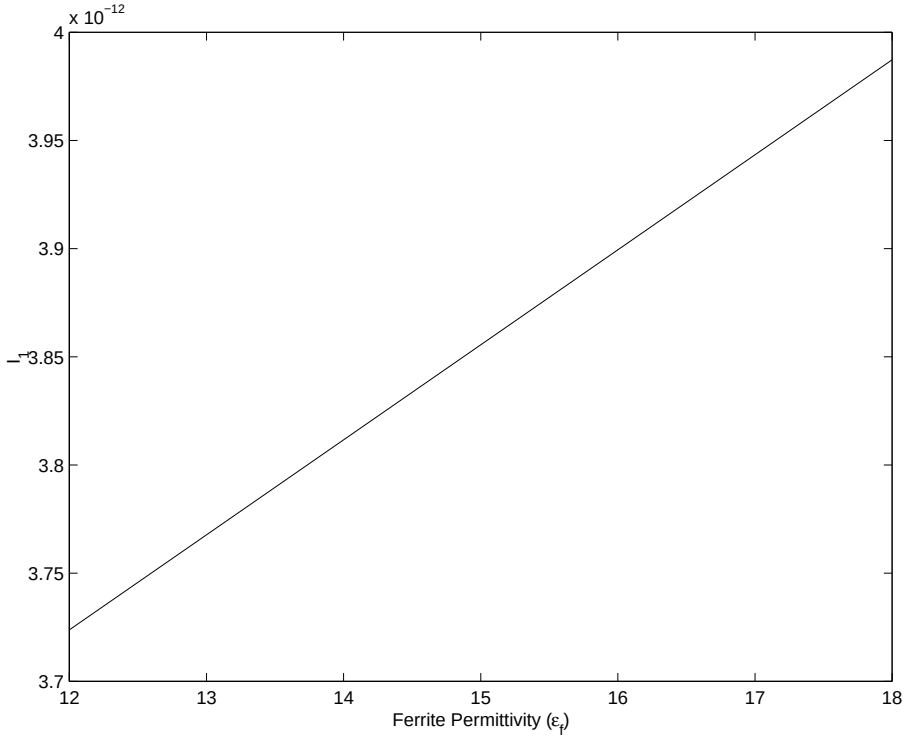


Figure 4.32: $I_1$ against variation in ferrite permittivity.

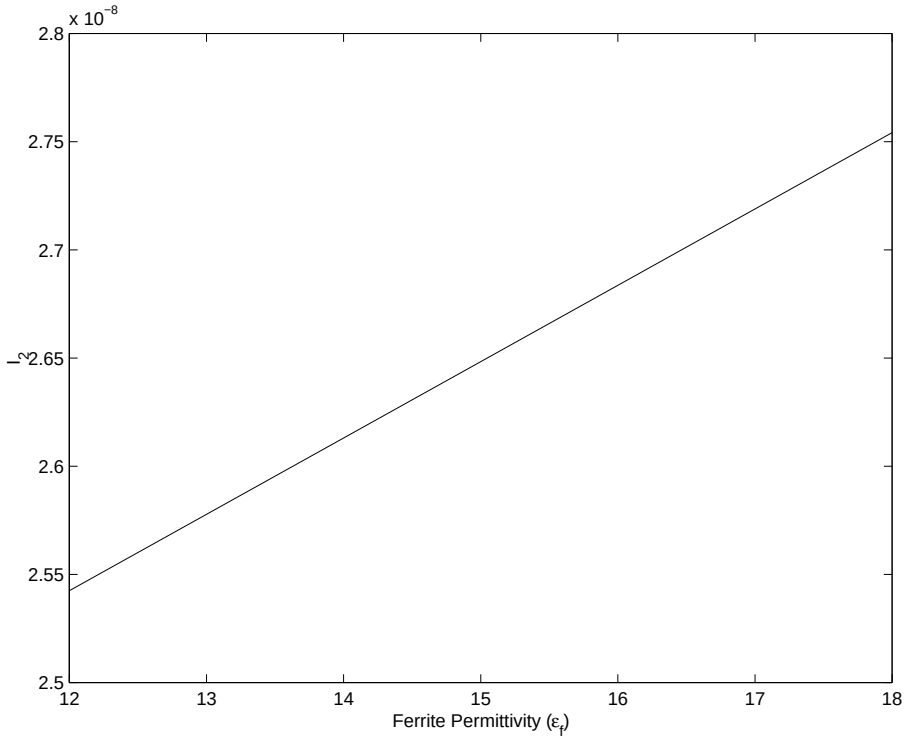


Figure 4.33: $I_2$ against variation in ferrite permittivity.

Another variable that can be altered is the pitch angle, $\psi$. Figure 4.34 shows the dispersion curves for varying pitch angles. As the pitch angle is increased, the propagation constant decreases and the dispersion decreases. Figure 4.35 shows the graphs corresponding to phase shift for different values of helical pitch angles. As the pitch angle is increased, the phase shift per $(\lambda/4)$ decreases. This can be explained in the following way; as the pitch angle increases, the helical pitch increases, (as $\tan(\psi)$ = p/2$\pi$ a). Therefore, the distance between each helical winding increases. As the distance between each helical winding increase, then for a given length L, there will be less helical windings. The helix plays an important part in slowing down the wave and producing a desired propagation constant $\beta$, both in the forward and reverse directions. Due to this, an increased in pitch angle decreases the phase shift for a given length, as shown in figure 4.35.

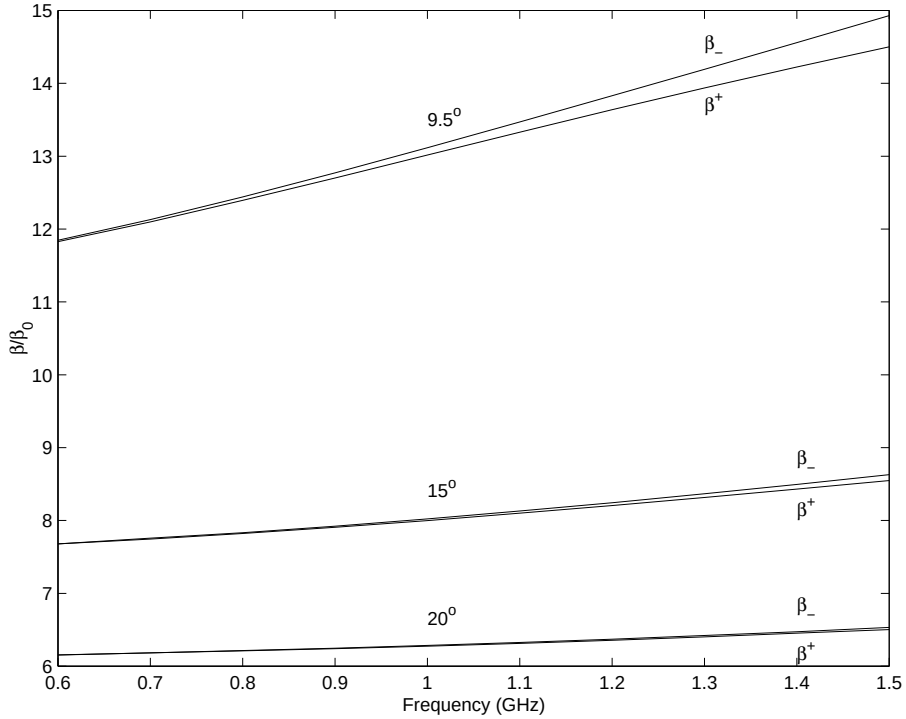


Figure 4.34: Dispersion curves for forward ($\beta^+$) and backward ($\beta_-$) waves for variation in helix pitch angle.

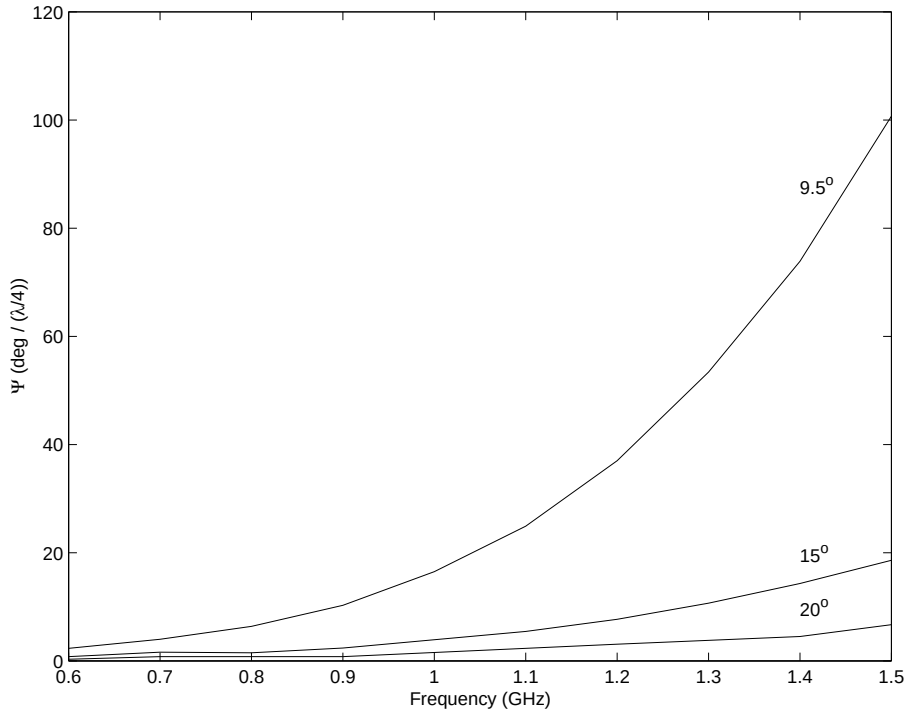


Figure 4.35: Phase shift for variation in pitch angle.

The section continues by considering a structure where the thickness of the ferrite is smaller than that of the helical radius. Figure 4.36 shows a cross section of the structure with this property. The dimensions of this structure are given in table 4.5

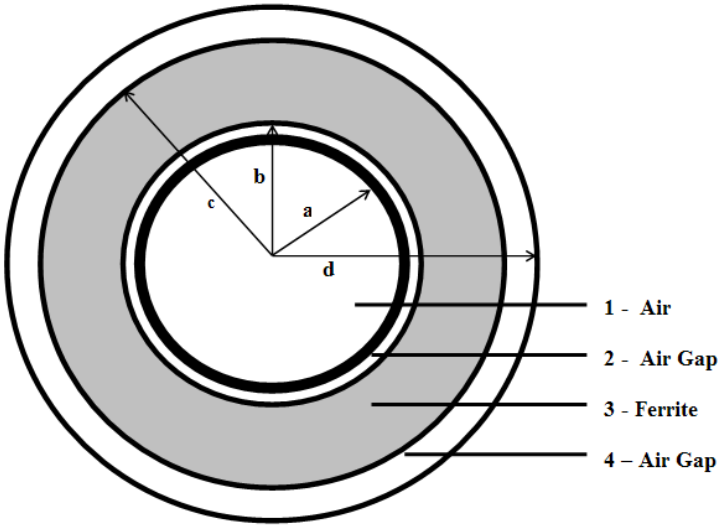


Figure 4.36: Cross-section of helical structure

| Parameter | Symbol | Numerical Value |
|---|---|---|
| Helical radius | $a$ | 10 mm |
| Ferrite (inner radius) | $b$ | $a$ + 0.001 mm |
| Ferrite (outer radius) | $c$ | $b$ + 5 mm |
| Waveguide radius | $d$ | $c$ + 0.001 mm |
| Pitch angle | $\psi$ | 10° |
| Saturation Magnetisation | $4\pi M_s$ | 0.068 T |
| Applied Magnetic Field | $H_0$ | 55 kA $m^{-1}$ |

Table 4.5: Dimensions of helical structure

Figure 4.37 shows how the phase shift varies with frequency for different thicknesses of ferrite. As the thickness of the ferrite increases, the shape of the graph is maintained (a sine curve); the

increase in the maxima decreases and the the decrease in the minima also decreases. Secklemann [27] plotted the graph of frequency against phase shift for a similar helical structure. The graph has the same shape as figure 4.38. A positive phase shift indicates a change in the phase angle in a counter-clockwise direction and a negative phase shift indicates a change in the phase angle in a clockwise direction.

Figures 4.8 and 4.37 both consider the phase shift of similar helical structures against frequency. The difference in the shapes of these graphs can be explained if the expression for calculating the phase shift is considered, equation (4.1). The shape of the graph is governed by the polarising function, $P$, which is given by,

$$P(\omega) = \sin\left(\frac{\omega}{c}\sqrt{\varepsilon_f}\, l_0\right) \qquad \text{with} \qquad l_0 \approx 2\pi r_0,$$

where $c$ is the velocity of light in free space, $\varepsilon_f$ is the effective relative dielectric constant for the ferrite and $r_0$ is the radius of of the helix. The frequency range that has been considered was 0.5 GHz - 1.85 GHz and the relative permittivity of the ferrite was 14.5. Figure 4.8 considered a structure of helix radius 1.465 mm and figure 4.37 considered a helix radius of 1 cm. The polarising function against frequency for different helical radii is shown in figure 4.39. Therefore, the behaviour of the phase shift against frequency is determined largely by the polarising function. For a specific permittivity and frequency range, the shape of the polarising function, and thus the phase shift, is governed by the radius of the helix. The maximum and minimum phase shift is obtained when

$$\sin\left(\frac{\omega}{c}\sqrt{\varepsilon_f}\, 2\pi r_0\right) = \pm 1.$$

A maxima is reached when the following equation is satisfied:

$$\frac{\omega}{c}\sqrt{\varepsilon_f}\, 2\pi r_0 = (4N-3)\,\frac{\pi}{2}, \text{ where } N\epsilon\mathbb{N}.$$

This is obtained at radii values of

$$r = (4N-3)\,\frac{c}{4\omega\sqrt{\varepsilon_r}}.$$

The minima is reached when the following equation is satisfied:

$$\frac{\omega}{c}\sqrt{\varepsilon_f}\,2\pi r_0 = (4N-1)\,\frac{\pi}{2},\ \text{ where } N\epsilon\mathbb{N}.$$

This is obtained at radii values of

$$r = (4N-1)\,\frac{c}{4\omega\sqrt{\varepsilon_r}}.$$

Therefore, depending on the frequency range, the ferrite permittivity and the helical radius, the range of the polarising function may not be the full sine curve.

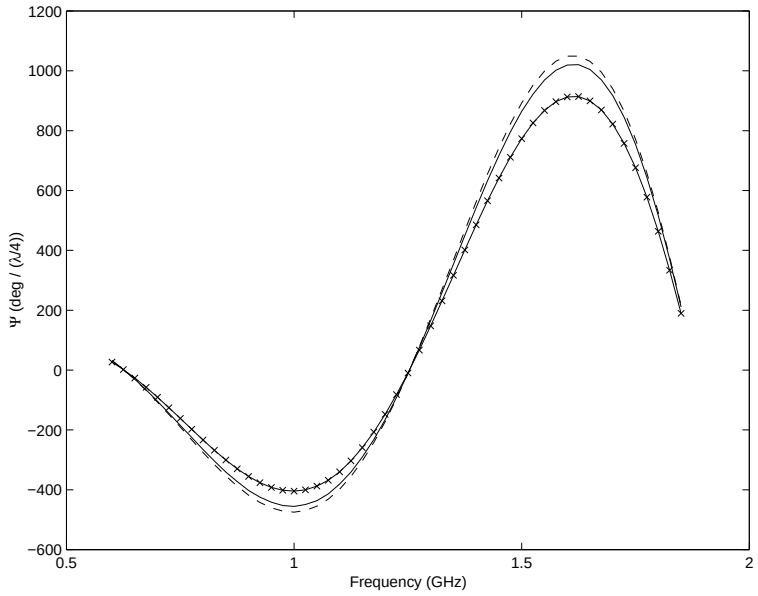


Figure 4.37: Phase shift against frequency for variations in ferrite thickness. A ferrite of thickness 1 mm (crossed line), 3 mm (straight line) and 5 mm (dashed line) are shown.

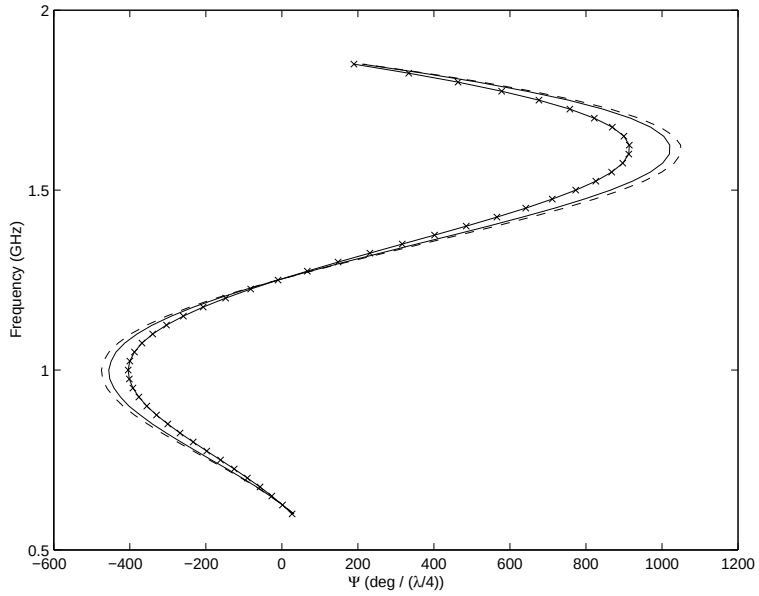


Figure 4.38: Frequency against phase shift for variations in ferrite thickness. A ferrite of thickness 1 mm (crossed line), 3 mm (straight line) and 5 mm (dashed line) are shown.

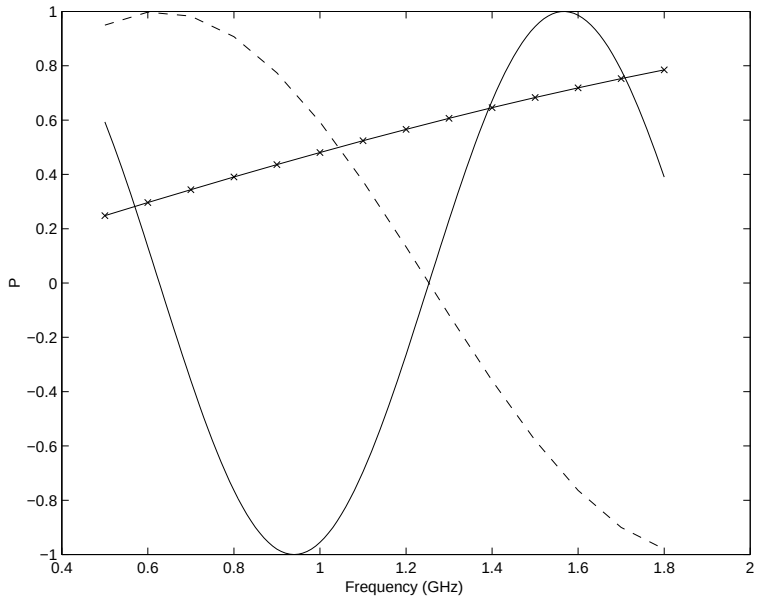


Figure 4.39: Polarising against frequency for variations in helical radii. A helix of radius 1 mm (crossed line), 5 mm (dashed line) and 10 mm (solid line) are all shown.

## 4.4 Variation of Applied Magnetic Field

This section considers the case where the applied field $H_0$ is varied. The equations for $\mu$ and $\kappa$ show that changing $H_0$ changes the value of $\mu$ and $\kappa$. The equations for $\mu$ and $\kappa$ are given below.

$$\mu = 1 - \frac{\gamma^2 H_0 M_0}{\gamma^2 H_0^2 - \omega^2} \qquad \text{and} \qquad \kappa = \frac{|\gamma|\,\omega M_0}{\gamma^2 H_0^2 - \omega^2}. \tag{4.12}$$

Both $\mu$ and $\kappa$ approach a singularity at

$$\omega = \gamma H_0, \tag{4.13}$$

where the frequency at the value of $\omega$ is the frequency of GMR. Equation (4.13) shows that the frequency at which GMR occurs is proportional to the applied magnetic field. Figure 4.40 shows

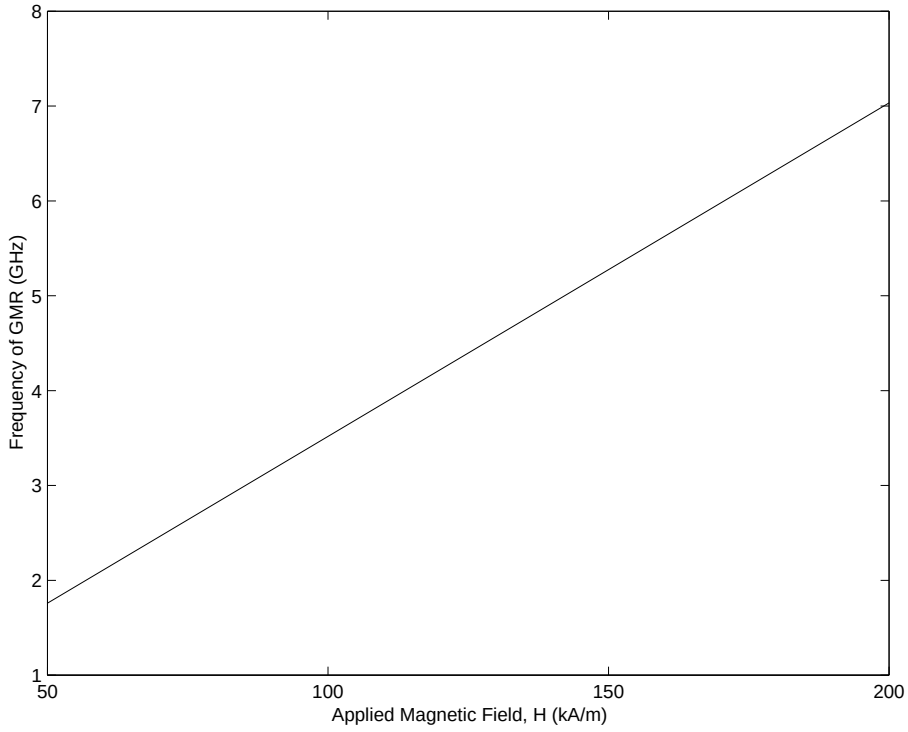


Figure 4.40: Frequency of GMR against Applied Magnetic Field.

how the frequency of GMR varies with the applied magnetic field.

The previous section considered the case where the applied field $H_0$ was 55 kA m$^{-1}$. This section considers cases where the applied field is changed to $H_1$=100 kA m$^{-1}$ and $H_2$=150 kA m$^{-1}$. The

frequencies of GMR associated with these applied fields are 3.52 GHz and 5.28 GHz. The phase shifts at these applied fields are give in figures 4.41 - 4.43. The shapes of the graphs are determined

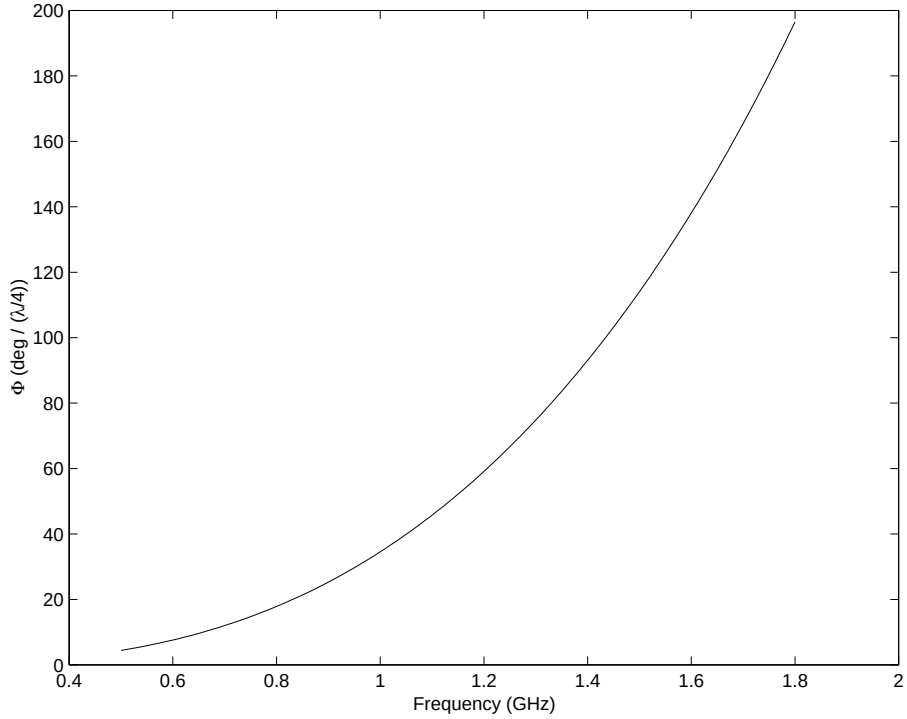


Figure 4.41: Phase shift per quarter wavelength against frequency for an applied magnetic field of 55 kA $m^{-1}$.

by the shape of the Polarisation function $P$.

$$P = \sin\left(\frac{\omega}{c}\sqrt{\varepsilon_f}2\pi r_0\right). \tag{4.14}$$

Figure 4.44 shows how the polarisation function varies with frequency. Equation (4.14) can be used to determine at which frequencies (for a given radius and permittivity) the phase shift changes sign. The sin function changes sign at $\pi$. Therefore,

$$\frac{\omega}{c}\sqrt{\varepsilon_f}\, 2\pi r_0 = \pi. \tag{4.15}$$

The frequency associated with this is 4.28 GHz. Figure 4.44 shows that at 4.28 GHz the phase shift changes sign.

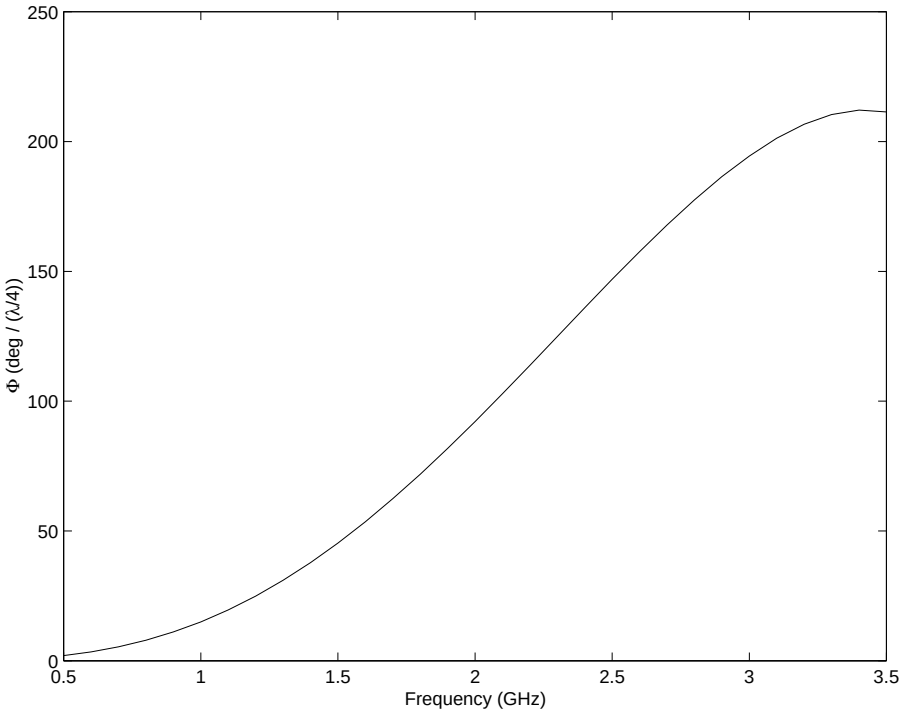


Figure 4.42: Phase shift per quarter wavelength against frequency for an applied magnetic field of 100 kA $m^{-1}$.

If a particular frequency range is chose 0.5 GHz - 1.8 GHz, a comparison of the phase shifts can be made for different applied magnetic fields.

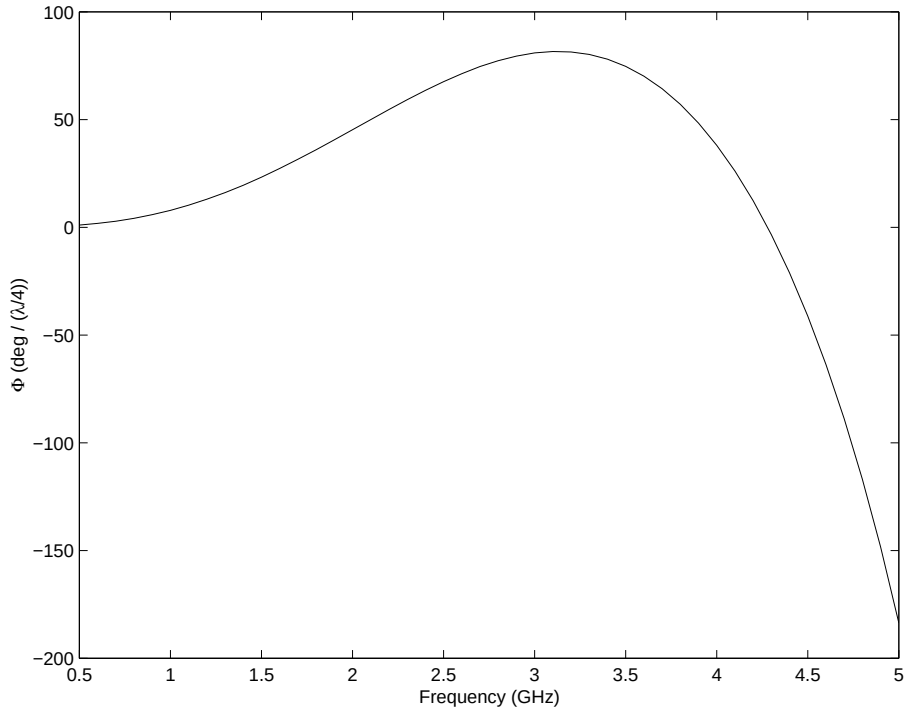


Figure 4.43: Phase shift per quarter wavelength against frequency for an applied magnetic field of 150 kA $m^{-1}$.

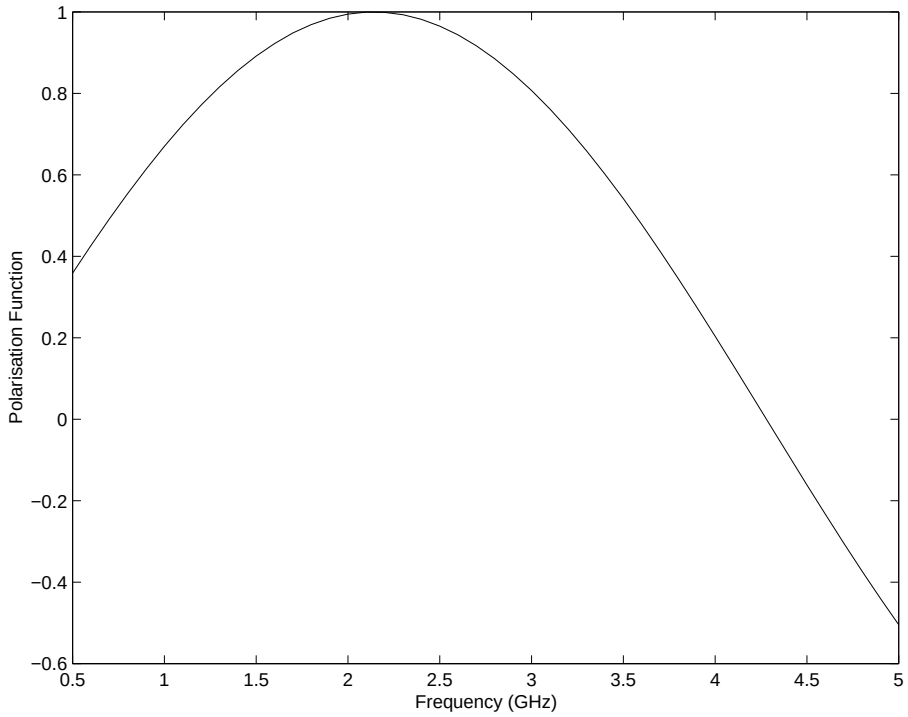


Figure 4.44: Polarisation function against frequency.

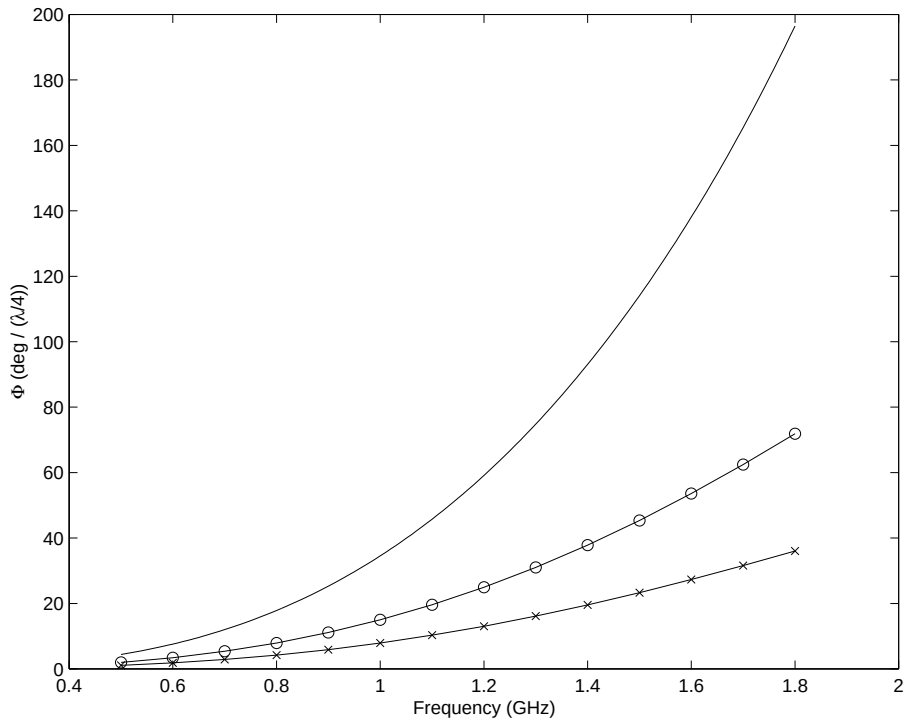


Figure 4.45: Phase shift per quarter wavelength against frequency for varying applied magnetic fields, $H_0$=55 kA$m^{-1}$ (solid line), $H_1$=100 kA$m^{-1}$ (circled line), and $H_2$=150 kA$m^{-1}$ (crossed line).

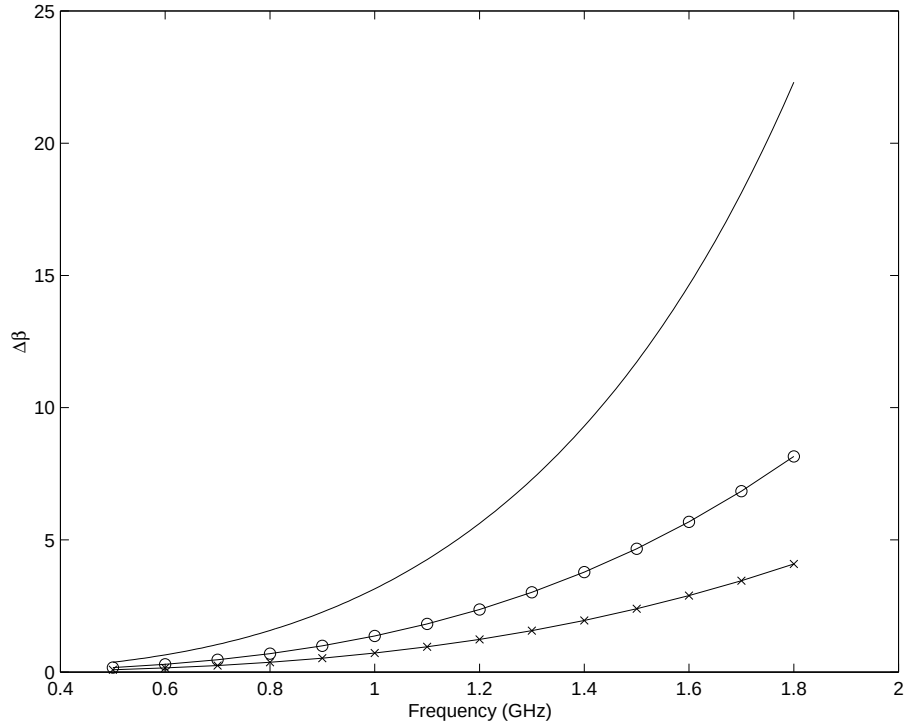


Figure 4.46: $\Delta\beta$ against frequency, $H_0$=55 kA$m^{-1}$ (solid line), $H_1$=100 kA$m^{-1}$ (circled line), and $H_2$=150 kA$m^{-1}$ (crossed line).

## 4.5 Comparison to a Dielectric

The above discussion considered the case of a helical structure where a ferrite was modelled between the helix and waveguide. The analysis of section 4.1 considered a structure which had the same dimensions as Duan et al [22]. If the same structure was analysed with dielectric tubes in the region between the helix and waveguide (using the same method as Duan et al) a comparison of attenuation coefficients can be done.

The permittivity of a dielectric single rod was 6.5. Three such rods were placed between the helix and the waveguide. These rods are modelled as an assumed distributed layer of dielectric between the helix and the waveguide.

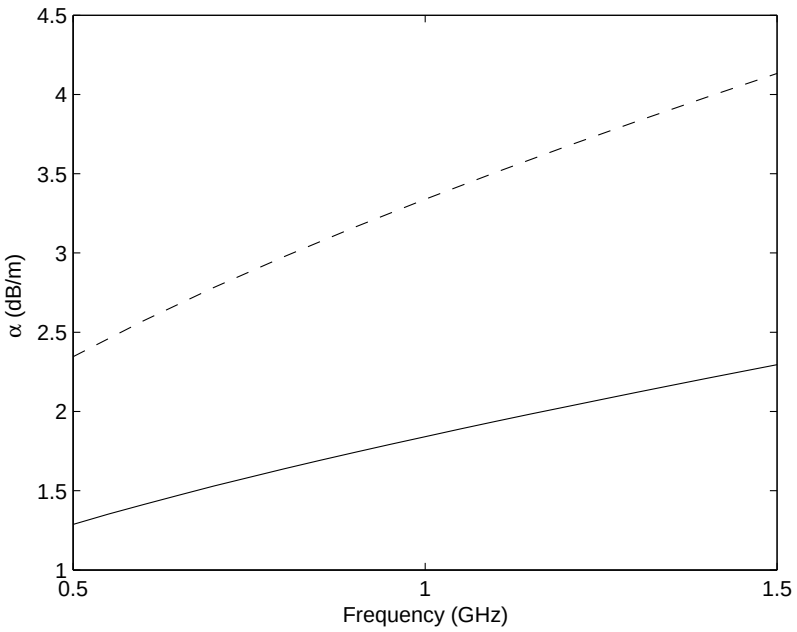


Figure 4.47: Attenuation coefficient against frequency. A comparison of structure containing dielectric (solid line) with ferrite (dashed line).

Figure 4.47 shows that the loss in the structure comprising a ferrite is higher than the one with a dielectric. The increased conductor loss in the structure containing a ferrite is due primarily to

difference in value of permittivity (the ferrite being 14.5 and the effective permittivity of a dielectric layer 1.79). Figure 4.47 suggests that ferrite could be employed as an alternative in a TWT, without incurring excessive loss. Presently, 10-20 dB of attenuation is typically employed in a TWT to prevent oscillation.

## 4.6 Summary

This chapter used the current model to investigate certain properties of the helical structure shown in figure 4.1. An important aspect in helical devices lies in minimising dispersion and maximising the phase shift. The variations in different parameters show the extent to which these quantities are affected. An analysis of the size of the air gaps within the structure has not been considered by previous authors. The attenuation coefficient for a ferrite loaded helical structure is also absent from previous work. This present study calculates the phase shift and attenuation coefficients of the model. The chapter discusses the behaviour of the phase shift in relation to the other variables.

The investigation extended the area of study to include cases where the ferrite was partially magnetised. In latched devices where a ferrite is not completely magnetised, this additional modification of the model improves the accuracy and reliability of it. Greene and Sandy [42] and [43] derived equations for losses in partially magnetised ferrites. The inclusion of these equations within the current model had not been considered previously. The chapter also discusses the possibility of using a ferrite or dielectric in phase shifter and TWTs.

# Chapter 5

# Conclusion

In this concluding chapter, the work that been done will be reviewed and analysed in greater detail. The main results from the previous chapter will be expanded upon and explained further. This chapter also discusses various ways of how the investigation can be extended.

## 5.1 Review

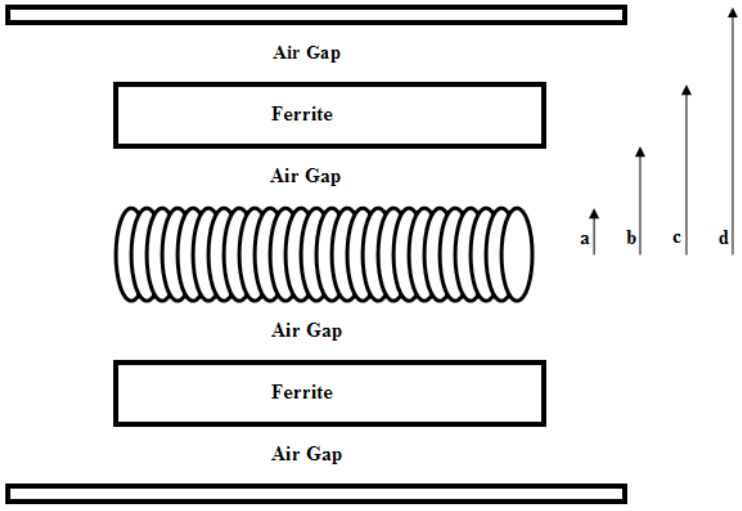


Figure 5.1: Helical structure

Figure 5.1 shows the helical structure that was analysed when a wave travels through it. A metal helix was surrounded by a ferrite tube. This was further enclosed within a waveguide wall. The structure was modelled with an air gap between the helix and the ferrite tube and also between the ferrite tube and the metal waveguide. The metal helix was of radius of $a$, the ferrite tube had an inner radius of $b$ and outer radius of $c$. The metal waveguide had radius $d$, where $a < b < c < d < e$.

When a wave travels through a structure, quantities such as phase shift and attenuation coefficient are useful to determine the applicability of the device. The effect on these quantities by varying many different parameters was analysed. Therefore, by setting the parameters at certain values, the efficiency of the device can be greatly enhanced. The way in which the variation of certain parameters affected the behaviour of the wave is presented here.

In every situation, an increase in frequency led to an increase in the phase shift and attenuation coefficient. As the frequency is increased, the frequency approaches that of GMR and thus the value of $\kappa$ increases. The amount of phase shift depends on the value of $\kappa$, as $\kappa$ represents the degree of non-reciprocal behaviour of the ferrite. Thus an increase in frequency led to an increase in phase shift. Equation (4.7) shows the expression of $\alpha$. In this equation, only the conductor loss is considered. The equation shows that as the frequency increases, the value of $\alpha$ also increases.

Previous authors who have investigated helical structures, have not analysed the effect of air gaps surrounding the ferrite. The variation in the thickness of the air gap between the helix and the ferrite produced more significant changes in the propagation constants and the phase shifts than variation in other parameters. Figures 4.22 showed that as the thickness of the air gap between the helix and ferrite increases, both the dispersion and propagation constant decrease. However, figure 4.23 shows that increasing the air thickness leads to a decrease in phase shift. Whist it is always desirable to decrease the quantity of dispersion and increase the amount of phase shift within a structure, it is not always possible to achieve both of these things. The variation in the air gap thickness between the helix and ferrite shows this.

The purpose of the helix is to act as a delay line; it decreases the value of the propagation constant in the structure. It also allows the structure to be more compact, (as a helix is wound and not a straight transmission line). Figure 4.34 showed that as the pitch angle increases, the propagation constant and dispersion both decrease. However, an increase in phase shift is achieved by decreasing the pitch angle. As with the previously mentioned parameter, it was not possible to reduce the dispersion and increase the phase shift simultaneously.

Tables 4.2 and 4.3 showed how altering the resistivity of the helix and waveguide affected the phase shift. In both cases, an increase in the resistivity led to a decrease in the phase shift. In these cases, the phase shift was measured in $deg/dB$, where this quantity represents the number of degrees that the wave will be rotated over a length when the wave is attenuated by 1 dB. This length is determined by considering the losses in the metal helix and waveguide, and thus altering the resistivities of the helix or waveguide will alter the phase shift. As the propagation constant is not affected by the resistivity of the helix or waveguide, altering these did not affect the propagation constants and dispersion. If the phase shift is expressed as $deg/(\lambda/4)$ or $deg/(\lambda_g/4)$, where $\lambda$ and $\lambda_g$ denote the free space wavelength and electrical wavelength respectively, altering the resistivities of either the waveguide or helix will not affect the phase shifts.

In many applications, it is desirable to increase the amount of phase shift. The phase shift is given by

$$\triangle\Phi = \triangle\beta \; P \; L \; \sqrt{\varepsilon_f}, \tag{5.1}$$

where $\Phi$ is given in radians per length. $P$ is the polarising function and is calculated by,

$$P(\omega) = \sin\left(\frac{\omega}{c}\sqrt{\varepsilon_f}\, l_0\right) \qquad \text{with} \qquad l_0 \approx 2\pi r_0,$$

where $c$ is the velocity of light in free space, $\varepsilon_f$ is the effective relative dielectric constant for the ferrite and $r_0$ is the radius of of the helix. $L$ is the length over which the phase shift is measured. Figure 4.28 shows that an increase in ferrite permittivity leads to a slight increase in dispersion. Figure

4.29 shows that an increase in ferrite permittivity corresponds to an increase in phase shift. Again, an increase in phase shift is accompanied with an increase in dispersion. However, as the ferrite permittivity increases, the increase in phase shift is greater than the slight increase in dispersion.

As mentioned in section 4.3, the range of possible phase shift values is determined by the behavior of the polarising function; which is a sine function. Depending on the frequency range, the ferrite permittivity and the helical radius, the range of the polarising function may not be the full sine curve. The helical structure in figure 4.1 achieved the maximum phase shift at a frequency of,

$$f = \frac{c/r}{8\pi\sqrt{\varepsilon_f}}.$$

The minimum phase shift was achieved at a frequency of,

$$f = \frac{3c/r}{8\pi\sqrt{\varepsilon_f}}.$$

However, these expressions are true if the full range of frequency values correspond to only one maximum and minimum value.

The investigation considered cases where the applied field was varied. As the applied field increases, the frequency corresponding to GMR increases. Equation (5.2) shows that the frequency corresponding to GMR is proportional to the applied magnetic field $H_0$. Figure 4.40 shows this relationship.

$$\omega = \gamma H_0, \tag{5.2}$$

Let the frequency that corresponds to GMR $f_{GMR}$. As the increase in the applied field $H_0$ leads to the increase $f_{GMR}$, a particular frequency $f_0$ which is initially below $f_{GMR}$, will be further and further away from the $f_{GMR}$ as the applied field is increased. The phase shift corresponding to $f_0$ will decrease as applied filed is increased. An explanation of this can be found in section 4.4.

The attenuation coefficient for a helical structure similar to the one considered in Duan et al [22] was compared to the one in figure 4.1. The structure in [22] replaced the ferrite in figure 4.1

with three dielectric rods. These rods were modelled as an assumed distributed layer of dielectric between the helix and the waveguide. Figure 4.47 showed that the loss in the structure comprising a ferrite was higher than the one with the dielectric rods. The increased conductor loss in the structure containing a ferrite is due primarily to the difference in the value of permittivity (the ferrite being 14.5 and the effective permittivity of a dielectric layer being 1.79). Figure 4.47 suggests that ferrite could be employed as an attenuator in a TWT without incurring excessive loss. Presently, 10-20 dB of attenuation is typically employed in a TWT to prevent oscillation. Therefore, with 10-20 dB of attenuation being present in a helical device, the forward wave is attenuated by 10-20 dB whilst the backward wave is attenuated by 20-40 dB. A ferrite lends itself to these devices as they allow a wave to pass with little absorption in the forward direction, but with much more absorption in the reverse direction.

The present investigation has extended the previously published work in many ways. These are:

1. The present model incorporates the air gaps within the helical structure. When a helix is placed inside the ferrite tube, a gap (even a very minute one) is present. The same is true when the ferrite is placed inside the metal waveguide.

2. The attenuation coefficient of this helical structure is calculated.

3. Both the loss contributed to by the metal and ferrite can be modelled.

The above extensions are particularly important in the construction of the helical device. When the helix is placed inside the ferrite, a very small gap will be present between the helix and the ferrite. The present study shows that a variation in the size of this air gap affects the propagation constant, attenuation constant and phase shift of the structure. For the first time, the attenuation coefficient has been calculated for this device. This was used to produce the phase shift for this structure. Although the phase shift can be represented in different ways, the phase shift in degrees per dB of attenuation is the figure of merit for this quantity.

The next section considers how the present investigation can be extended and further work that can be undertaken.

## 5.2 Further Work

This section discusses how the thesis can be extended. One way of furthering the investigation is by changing the modelling assumptions that were used. Another way is by improving various methods that were used in the current study.

The investigation considered the case of an axisymmetric wave - i.e. where $\partial/\partial\theta = 0$ or $n = 0$. As yet, the case of $n = 1$ has not been investigated. Appendix B.1 derives full expressions for all the **E** and **H** field components. The system of equations are transferred into a matrix equation. Although the investigation did not produce results for the case of $n = 1$, further work can produce a working program of this case.

One assumption that was used throughout the investigation, was to model the helical structure using the sheath helix. As mentioned in section 1.7, a helix can be modelled using the sheath helix or the tape helix. The tape helix model yields a greater level of accuracy than the sheath helix one. Section 1.7.2 describes the tape helix model. The tape helix models a more realistic helix as it incorporates a gap between each helical winding into the model, whereas the sheath helix models the helix as an anisotropic cylinder. The sheath helix assumes each winding as *infinitely thin*, whereas the tape helix takes the thickness of each winding into consideration. Some of the assumptions that are used in the tape helix model are:

• A reasonable current distribution is assumed [16].

• $E_{||}$, the total electric field in the direction of the tape as a function of $\phi$ and $z$ at $r = a$, is calculated in terms of the assumed current distribution [16].

• $E_{||}$ is set to equal zero along the centreline of the tape [16].

The last assumption satisfies the the boundary conditions on $E$ approximately [16]. The approximation is good for narrow tapes.

One assumption that was made use of throughout the research was that the magnetic field in

the structure was known. Although this assumption has been used by many authors, the model's accuracy will be improved if the exact value for the magnetic field inside the structure is known. One way of obtaining this is to use a numerical package that gives the values of the magnetic field inside structures. However, if an analytical approach is to be maintained, use can be made of *demagnetisation factors*. Demagnetisation factors can be used to calculate the magnetic field inside of a ferrite if the applied external field is known. Demagnetisation factors can only be calculated exactly for ellipsoidal shapes; shapes such as disks and rods are approximated by a suitable ellipsoidal shape [4]. The use of demagnetisation factors concerning a ferrite tube will have to be derived before employing it into this particular investigation. Zheng et al [45] attempted to experimentally determine demagnetisation factors for nonellipsoidal geometries. This can be used with other resources in an attempt to derive expressions for demagnetisation factors for a ferrite tube.

The ferrite was assumed to be biased azimuthally. The ferrite can also be biased longitudinally or transversely. Waldron [46] - [50] investigated a longitudinally biased structure. These different directions of ferrite biasings can also be considered. In reality, a ferrite can be biased in *any* direction. A permeability matrix corresponding to a ferrite being biased in any direction was first formulated by Tyras [51]. Below is a partial derivation of a method that can be used in an attempt to solve this problem. The method is similar to the one derived in chapter 2.

$$\mathbf{B} = \mathbf{MH}, \qquad \text{where} \qquad \mathbf{M} = \begin{pmatrix} \mu_1 & \mu_2 & \mu_3 \\ \mu_4 & \mu_5 & \mu_6 \\ \mu_7 & \mu_8 & \mu_9 \end{pmatrix}, \qquad \Rightarrow \qquad \begin{bmatrix} B_r \\ B_\theta \\ B_z \end{bmatrix} = \begin{bmatrix} \mu_1 & \mu_2 & \mu_3 \\ \mu_4 & \mu_5 & \mu_6 \\ \mu_7 & \mu_8 & \mu_9 \end{bmatrix} \begin{bmatrix} H_r \\ H_\theta \\ H_z \end{bmatrix}. \tag{5.3}$$

The matrix **M** can be expressed as,

$$
\begin{aligned}
\mu_1 &= \mu + (\mu_0 - \mu)\ \sin^2(\phi)\ \cos^2(\theta), \\
\mu_2 &= \tfrac{\mu_0-\mu}{2}\ \sin^2(\phi)\ \sin(2\theta) + i\kappa\ \cos(\phi), \\
\mu_3 &= \tfrac{\mu_0-\mu}{2}\ \sin(2\phi)\ \cos(\theta) - i\kappa\ \sin(\phi)\ \sin(\theta), \\
\mu_4 &= \tfrac{\mu_0-\mu}{2}\ \sin^2(\phi)\ \sin(2\theta) - i\kappa\ \cos(\phi), \\
\mu_5 &= \mu + (\mu_0 - \mu)\ \sin^2(\theta)\ \sin^2(\phi), \\
\mu_6 &= \tfrac{\mu_0-\mu}{2}\ \sin(2\phi)\ \sin(\theta) + i\kappa\ \sin(\phi)\ \cos(\theta), \\
\mu_7 &= \tfrac{\mu_0-\mu}{2}\ \sin(2\phi)\ \cos(\theta) + i\kappa\ \sin(\phi)\ \sin(\theta), \\
\mu_8 &= \tfrac{\mu_0-\mu}{2}\ \sin(2\phi)\ \sin(\theta) - i\kappa\ \sin(\phi)\ \cos(\theta), \\
\mu_9 &= \mu_0 - (\mu_0 - \mu)\ \sin^2(\phi).
\end{aligned}
$$

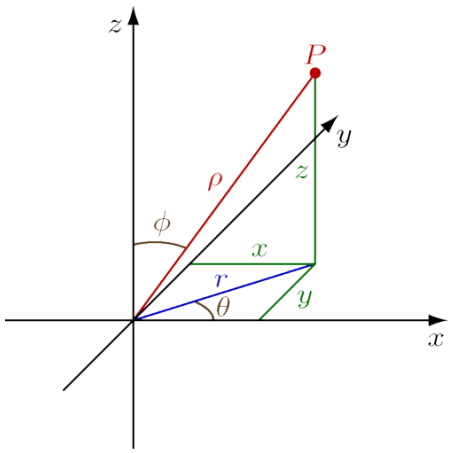


with respect to the following co-ordinate system where

P represents the direction of magnetisation.

Tyras considered the case where the direction of magnetisation was in the x-z plane, ($\theta = 0$). However, the method can be extended to consider the case where P can vary in the 3 dimensional plane. In order to facilitate calculations, it is necessary to diagonalise matrix **M**. The eigenvalues of **M** with their corresponding eigenvectors are given by,

$$
\begin{aligned}
&\lambda_1 = \mu + \kappa && (\cos(\theta)\cos(\phi) + i\ \sin(\theta),\ \cos(\phi)\sin(\theta) - i\ \cos(\theta),\ -\sin(\phi))^T, \\
&\lambda_2 = \mu - \kappa && (\cos(\theta)\cos(\phi) - i\ \sin(\theta),\ \cos(\phi)\sin(\theta) + i\ \cos(\theta),\ -\sin(\phi))^T, \\
&\lambda_3 = \mu_0 && (\cos(\theta)\sin(\phi),\ \sin(\theta)\sin(\phi),\ \cos(\phi))^T.
\end{aligned}
$$

Normalising the eigenvectors gives a matrix

$$
\mathbf{P} = \frac{1}{\sqrt{2}} \begin{pmatrix}
\cos(\phi)\cos(\theta) - i\ \sin(\theta) & \cos(\phi)\sin(\theta) + i\ \cos(\theta) & -\sin(\phi) \\
\cos(\phi)\cos(\theta) + i\ \sin(\theta) & \cos(\phi)\sin(\theta) - i\ \cos(\theta) & -\sin(\phi) \\
\sqrt{2}\ \cos(\theta)\sin(\phi) & \sqrt{2}\ \sin(\theta)\sin(\phi) & \sqrt{2}\ \cos(\phi)
\end{pmatrix},
$$

such that,

$$\mathbf{PMP}^{-1} = \begin{pmatrix} \lambda_1 & 0 & 0 \\ 0 & \lambda_2 & 0 \\ 0 & 0 & \lambda_3 \end{pmatrix}.$$

Transforming the $\mathbf{B}$ and $\mathbf{H}$ fields into the new co-ordinate system gives,

$$\mathbf{B}' = \mathbf{PB}, \quad \mathbf{H}' = \mathbf{PH},$$

where $\mathbf{B}'$ and $\mathbf{H}'$ represent the fields and $\nabla'$ represents the $\nabla$ in the new co-ordinate system. Therefore,

$$\begin{bmatrix} B'_x \\ B'_y \\ B'_z \end{bmatrix} = \begin{bmatrix} \lambda_1 & 0 & 0 \\ 0 & \lambda_2 & 0 \\ 0 & 0 & \lambda_3 \end{bmatrix} \begin{bmatrix} H'_x \\ H'_y \\ H'_z \end{bmatrix} \quad \Rightarrow \quad B'_x = \lambda_1 H'_x, \ B'_y = \lambda_2 H'_y, \text{ and } B'_z = \lambda_3 H'_z.$$

The aim is to obtain the equation,

$$\left(\nabla_t^2 + p^2\right)\left(\nabla_t^2 + q^2\right) E_z = 0, \quad \text{and} \quad \left(\nabla_t^2 + r^2\right)\left(\nabla_t^2 + s^2\right) H_z = 0, \tag{5.4}$$

where $p$, $q$, $r$ and $s$ are constants. Then $\nabla_t^2$ can be replaced by its cylindrical polar co-ordinate representation,

$$\nabla_t^2 = \frac{\partial^2}{\partial r^2} + \frac{1}{r}\frac{\partial}{\partial r} + \frac{1}{r^2}\frac{\partial}{\partial \theta^2}.$$

This will give solutions in the $'$ co-ordinate system. The solutions can be transformed into the original co-ordinate system.

The same helical structure can be investigated using a computer simulated package. However, the analytical method has some advantages over a computer simulated approach. These are:

1. Analytical expressions can be used to predict behavioural patterns. Computer simulations do not allow this.

2. Computer simulations usually take longer time than calculating solutions to analytical expressions for the corresponding problem.

An analytical method can be used to obtain an insight into how to optimise the structure - minimising dispersion and loss and maximising phase shift. This was used extensively in chapter 4 where the results from the program were explained using the expressions obtained in chapter 2. Analytical and numerical methods are generally obtained faster than those generated from a simulation package. The results from a computer simulation can be useful in verifying the theoretical results.

The results in this investigation can be compared with practical measurements. An outline of how practical measurements can be obtained is given here. Yang *et al* [52] obtained experimental results for a copper helix surrounded by a ferrite helix. Although the present research modelled a metal helix surrounded by a ferrite tube enclosed in a metal waveguide, some factors are common experimentally to both investigations and so can be used.

A copper helix surrounded by a ferrite tube enclosed in a metal waveguide can be held in place by PTFE supports. Different sizes of PTFE (polytetrofluroethylene) supports can maintain the metal helix, ferrite tube and metal waveguide coaxially within a central cavity and also keep them in the centre of the cavity.

The azimuthal biasing can be achieved by wrapping a wire around the ferrite and applying a current to it, (as shown in figure 5.2). If there are N turns of wire, then Ampere's Law gives a relationship between the magnetic field and current.

$$H = \frac{NI}{2\pi r}, \tag{5.5}$$

where $r$ is the radius of the ferrite tube. The RF signal signal can be applied to the system along the power cables. The network analyser (Agilent) can be used to obtain $S_{21}$ readings.

Initially, it is necessary to calibrate the system. Therefore, if the two cables are connected together, and no current is flowing in the metal turns, then a value for the loss of the apparatus can

be obtained. As the current is then applied to the turns, a biasing field $H_{DC}$ is produced. Equation (5.5) shows that H is proportional to I. If a large current is required to be produced, the the relation

$$I = \frac{dQ}{dt}, \tag{5.6}$$

that current is the rate of change of charge can be used. If a large charge is sent over a very small time, then a large current can be produced (and thus a large biasing field can be generated). This idea is used extensively by authors (such as Gibson *et al* [53]).

The phase and magnitude of S21 can be used to obtain the insertion loss and propagation constant. The insertion loss (IL) (in dB) is given by,

$$IL = -20 \log_{10} |S_{21}| . \tag{5.7}$$

In order to obtain the propagation constant $\beta$, it is necessary to make two identical structures of different lengths $L_1$ and $L_2$. Letting the phase of $S_{21}$ of the structure which of length $L_1$ to be denoted by $S_{21}^1$, and the phase of $S_{21}$ of the structure of length $L_2$ to be denoted by $S_{21}^2$, the propagation constant $\beta$ is given by,

$$\beta = \frac{S_{21}^2 - S_{21}^1}{L_2 - L_1}. \tag{5.8}$$

To obtain the propagation constant $\beta$ in the reverse direction, a signal can be sent in the opposite directions. By obtaining the value of $\beta$ and the insertion loss, practical measurements can be obtained to compare with the theoretical results obtained.

The above are some ways of extending the investigation on the helical structure in figure 5.1. A metal helix surrounded by a ferrite helix would be a very useful structure for investigation. Kompfner [26] showed the advantage of using a ferrite helix over a ferrite cylinder. By investigating this double helical structure, this can be used to enhance TWTs and non reciprocal absorbers. When a magnetic field is applied to a ferrite helix, each individual part of the ferrite will be biased at different directions. The results from equation (5.4) can be used to derive expressions for each part of the ferrite helix.

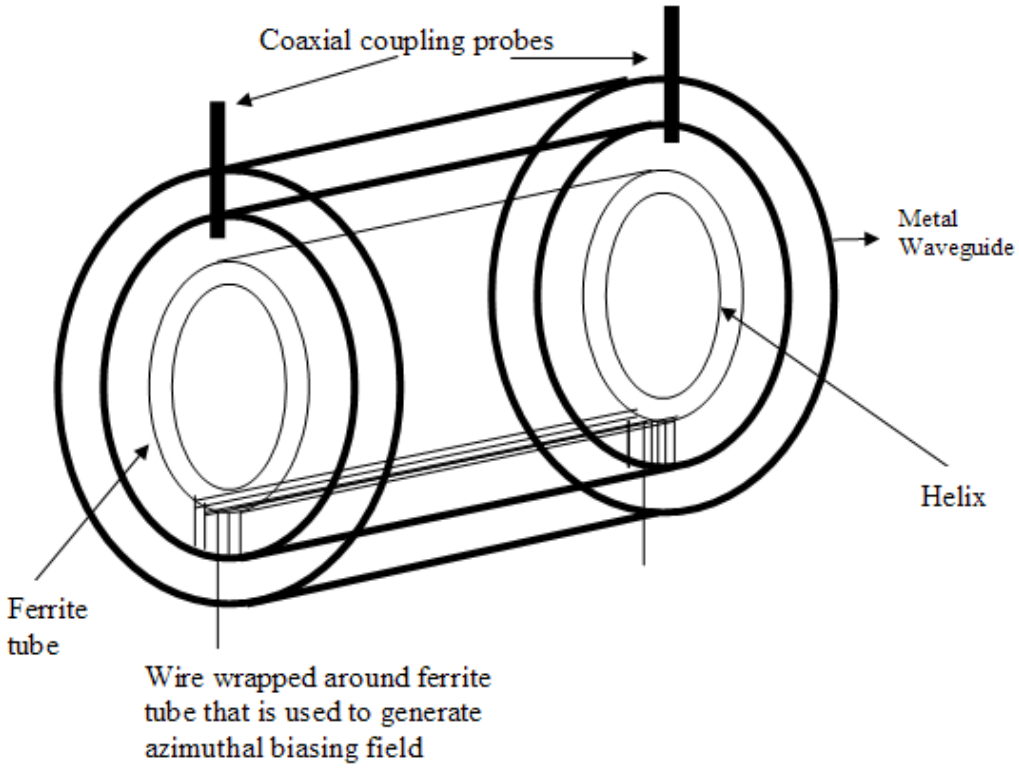


Figure 5.2: Experimental Setup

The present investigation can be considered as an intermediate step on the way to analysing a metal helix surrounded by a ferrite helix.

# Appendix A

# The Wave Equation

This chapter derives the wave equation. Substituting $\mathbf{B} = \mu\mathbf{H}$into Maxwell's equations give

$$\nabla \cdot \mathbf{E} = 0, \quad \nabla \cdot \mathbf{H} = 0, \quad \nabla \wedge \mathbf{E} = -\mu \frac{\partial \mathbf{H}}{\partial t}, \quad \nabla \wedge \mathbf{H} = \varepsilon \frac{\partial \mathbf{E}}{\partial t}. \tag{A.1}$$

Taking the curl of

$$\nabla \wedge \mathbf{E} = -\mu \frac{\partial \mathbf{H}}{\partial t} \qquad \text{and} \qquad \nabla \wedge \mathbf{H} = \varepsilon \frac{\partial \mathbf{E}}{\partial t}$$

gives,

$$\nabla \wedge (\nabla \wedge \mathbf{E}) = -\mu \frac{\partial}{\partial t} \nabla \wedge \mathbf{H} = -\mu\varepsilon \frac{\partial^2 \mathbf{E}}{\partial t^2} \qquad \text{and} \qquad \nabla \wedge (\nabla \wedge \mathbf{H}) = \varepsilon \frac{\partial}{\partial t} \nabla \wedge \mathbf{E} = -\mu\varepsilon \frac{\partial^2 \mathbf{H}}{\partial t^2}$$

Using the vector identity,

$$\nabla \wedge \nabla \wedge \mathbf{A} = \nabla (\nabla \cdot \mathbf{A}) - \nabla^2 \mathbf{A},$$

gives

$$\nabla \left( \nabla \cdot \begin{bmatrix} \mathbf{E} \\ \mathbf{H} \end{bmatrix} \right) - \nabla^2 \begin{bmatrix} \mathbf{E} \\ \mathbf{H} \end{bmatrix} = -\mu\varepsilon \frac{\partial^2}{\partial t^2} \begin{bmatrix} \mathbf{E} \\ \mathbf{H} \end{bmatrix}.$$

Using the relations $\nabla \cdot \mathbf{E} = 0$ and $\nabla \cdot \mathbf{H} = 0$ give,

$$\nabla^2 \begin{bmatrix} \mathbf{E} \\ \mathbf{H} \end{bmatrix} = \mu\varepsilon \frac{\partial^2}{\partial t^2} \begin{bmatrix} \mathbf{E} \\ \mathbf{H} \end{bmatrix}.$$

Letting $c = \frac{1}{\sqrt{\mu\varepsilon}}$, the wave equation is arrived at:

$$\nabla^2 \begin{bmatrix} \mathbf{E} \\ \\ \mathbf{H} \end{bmatrix} = \frac{1}{c^2} \frac{\partial^2}{\partial t^2} \begin{bmatrix} \mathbf{E} \\ \\ \mathbf{H} \end{bmatrix}.$$

# Appendix B

# The Governing Equations for Electromagnetic Waves in the Ferrite

## B.1 Azimuthal Biasing

### B.1.1 The Governing Equation

If the ferrite is biased circumferentially, the following equation can be set up.

$$\mathbf{B} = \mathbf{M}\mathbf{H}, \qquad \mathbf{M} = \begin{pmatrix} \mu & 0 & -i\kappa \\ 0 & \mu_0 & 0 \\ i\kappa & 0 & \mu \end{pmatrix}. \tag{B.1}$$

Equations (B.1) can be rewritten as,

$$\begin{bmatrix} B_r \\ B_\theta \\ B_z \end{bmatrix} = \begin{bmatrix} \mu & 0 & -i\kappa \\ 0 & \mu_0 & 0 \\ i\kappa & 0 & \mu \end{bmatrix} \begin{bmatrix} H_r \\ H_\theta \\ H_z \end{bmatrix}. \tag{B.2}$$

Therefore, (B.2) can be expanded,

$$B_r = \mu H_r - i\kappa H_z, \quad B_\theta = \mu_0 H_\theta, \quad B_z = i\kappa H_r + \mu H_z. \tag{B.3}$$

The governing equations are Mazwell's equations,

$$\nabla \cdot \mathbf{H} = 0, \qquad \nabla \cdot \mathbf{E} = 0, \qquad \nabla \wedge \mathbf{H} = i\omega\varepsilon_f \mathbf{E}, \qquad \nabla \wedge \mathbf{E} = -i\omega\mu\mathbf{H}. \tag{B.4}$$

Expressing (B.4) in cylindrical polar coordinates give;

$$\begin{aligned}
(\nabla \wedge \mathbf{H})_r &= \tfrac{1}{r}\tfrac{\partial H_z}{\partial \theta} - \tfrac{\partial H_\theta}{\partial z} &&= i\omega\varepsilon_f\, E_r, \\
(\nabla \wedge \mathbf{H})_\theta &= \tfrac{\partial H_r}{\partial z} - \tfrac{\partial H_z}{\partial r} &&= i\omega\varepsilon_f\, E_\theta, \\
(\nabla \wedge \mathbf{H})_z &= \tfrac{\partial H_\theta}{\partial r} + \tfrac{H_\theta}{r} - \tfrac{1}{r}\tfrac{\partial H_r}{\partial \theta} &&= i\omega\varepsilon_f\, E_z, \\
(\nabla \wedge \mathbf{E})_r &= \tfrac{1}{r}\tfrac{\partial E_z}{\partial \theta} - \tfrac{\partial E_\theta}{\partial z} &&= -i\omega B_r = -i\omega\left(\mu H_r - i\kappa H_z\right), \\
(\nabla \wedge \mathbf{E})_\theta &= \tfrac{\partial E_r}{\partial z} - \tfrac{\partial E_z}{\partial r} &&= -i\omega B_\theta = -i\omega\left(\mu_0 H_\theta\right), \\
(\nabla \wedge \mathbf{E})_z &= \tfrac{\partial E_\theta}{\partial r} + \tfrac{E_\theta}{r} - \tfrac{1}{r}\tfrac{\partial E_r}{\partial \theta} &&= -i\omega B_z = -i\omega\left(i\kappa H_r + \mu H_z\right).
\end{aligned} \tag{B.5}$$

Writing $E_\theta$, $H_\theta$, $E_r$ and $H_r$ in terms of $E_z$ and $H_z$,

$$k_{0f}^2 E_r = -\frac{i\omega\mu_0}{r}\frac{\partial H_z}{\partial \theta} - i\beta\frac{\partial E_z}{\partial r}, \tag{B.6}$$

$$k_c^2 H_r = \frac{i\omega\varepsilon_f}{r}\frac{\partial E_z}{\partial \theta} - i\beta\frac{\partial H_z}{\partial r} + i\omega^2\varepsilon_f\,\kappa H_z, \tag{B.7}$$

$$k_c^2 E_\theta = -\frac{i\beta}{r}\frac{\partial E_z}{\partial \theta} + i\omega\mu\frac{\partial H_z}{\partial r} - i\beta\omega\kappa H_z, \tag{B.8}$$

$$k_{0f}^2 H_\theta = -\frac{i\beta}{r}\frac{\partial H_z}{\partial \theta} - i\omega\varepsilon_f\,\frac{\partial E_z}{\partial r}, \tag{B.9}$$

where $k_{0f}^2 = \omega^2\mu_0\varepsilon_f - \beta^2$ and $k_c^2 = \omega^2\mu\varepsilon_f - \beta^2$. These equations can be rearranged to give the following equations,

$$E_z'' + \frac{1}{r}E_z' + k_{0f}^2\left(1 - \frac{n^2}{r^2 k_c^2}\right)E_z = \frac{i\beta n}{\omega\varepsilon r}\left(\frac{k_{0f}^2}{k_c^2} - 1\right)H_z' - \frac{i\omega\kappa n}{r}\frac{k_{0f}^2}{k_c^2}H_z, \tag{B.10}$$

$$H_z'' + \frac{1}{r}H_z' + \left(k_c^2 - \frac{\omega^2\kappa^2\varepsilon}{\mu} - \frac{\beta\kappa}{\mu r} - \frac{n^2\mu_0 k_c^2}{r^2\mu k_{0f}^2}\right)H_z = \frac{i\beta n}{\omega\mu r}\left(1 - \frac{k_c^2}{k_{0f}^2}\right)E_z' + \frac{i\omega\varepsilon\kappa n}{\mu r}E_z. \tag{B.11}$$

where $'$ and $''$ are the first and second derivatives respectively with respect to $r$.

### B.1.2 Solutions to the Governing Equations

**The case when n = 0**

If $n = 0$, equations (B.10) and (B.11) can be rearranged to give the following equations,

$$E_z'' + \frac{E_z'}{r} - k_f^2 E_z = 0, \qquad \text{where } k_f^2 = \beta^2 - \omega^2 \mu_0 \varepsilon_f \tag{B.12}$$

$$H_z'' + \frac{H_z'}{r} - \left( k_1^2 + \frac{\omega^2 \kappa^2 \varepsilon}{\mu} + \frac{\beta \kappa}{\mu r} \right) H_z = 0 \qquad \text{where } k_1^2 = \beta^2 - \omega^2 \mu \varepsilon_f. \tag{B.13}$$

Equation (B.12) can be solved to give,

$$E_z = A I_0(k_f r) + B K_0(k_f r) \tag{B.14}$$

where $A$ and $B$ are constants. Equation (B.13) can be solved to give,

$$H_z = C\, e^{-\sqrt{\frac{k_1^2 \mu + \omega^2 \varepsilon_f \kappa^2}{\mu}}\, r}\, M\left( \frac{\sqrt{k_1^2 \mu + \omega^2 \varepsilon_f \kappa^2}\sqrt{\mu} + \beta\kappa}{2\sqrt{k_1^2 \mu + \omega^2 \varepsilon_f \kappa^2}\sqrt{\mu}}, 1, 2\sqrt{\frac{k_1^2 \mu + \omega^2 \varepsilon_f \kappa^2}{\mu}}\, r \right) +$$

$$D\, e^{-\sqrt{\frac{k_1^2 \mu + \omega^2 \varepsilon_f \kappa^2}{\mu}}\, r}\, U\left( \frac{\sqrt{k_1^2 \mu + \omega^2 \varepsilon_f \kappa^2}\sqrt{\mu} + \beta\kappa}{2\sqrt{k_1^2 \mu + \omega^2 \varepsilon_f \kappa^2}\sqrt{\mu}}, 1, 2\sqrt{\frac{k_1^2 \mu + \omega^2 \varepsilon_f \kappa^2}{\mu}}\, r \right)$$

where $C$ and $D$ are constants and $M(x, y, z)$ and $U(x, y, z)$ are Kummer functions[1]. Substituting these into (B.6) - (B.9) give expressions for $E_r$, $E_\theta$, $H_r$ and $H_\theta$. Chapter 2 gave expressions for the electric and magnetic field components in air at $n = 0$. Using the same notation as section 2.6.3, the field components in region 3 (ferrite) can be written below:

[1]Refer to Appendix (C.2) for further details of these functions.

$$
\begin{aligned}
E_{z31} &= I_0\left(k_f r\right), & E_{z32} &= K_0\left(k_f r\right), \\
E_{z33} &= 0, & E_{z34} &= 0, \\
H_{z31} &= 0, & H_{z32} &= 0, \\
H_{z33} &= e^{-\sqrt{\frac{\eta}{\mu}}\,r}\, M\left(\tfrac{\sqrt{\eta}\sqrt{\mu}+\beta\kappa}{2\sqrt{\eta}\sqrt{\mu}}, 1, 2\sqrt{\tfrac{\eta}{\mu}}r\right), & H_{z34} &= e^{-\sqrt{\frac{\eta}{\mu}}\,r}\, U\left(\tfrac{\sqrt{\eta}\sqrt{\mu}+\beta\kappa}{2\sqrt{\eta}\sqrt{\mu}}, 1, 2\sqrt{\tfrac{\eta}{\mu}}r\right), \\
H_{\theta 31} &= \tfrac{i\omega\varepsilon_f}{k_f} I_1\left(k_f r\right), & H_{\theta 32} &= -\tfrac{i\omega\varepsilon_f}{k_f} K_1\left(k_f r\right), \\
H_{\theta 33} &= 0, & H_{\theta 34} &= 0, \\
E_{r31} &= \tfrac{i\beta}{k_f} I_1\left(k_f r\right), & E_{r32} &= -\tfrac{i\beta}{k_f} K_1\left(k_f r\right), \\
E_{r33} &= 0, & E_{r34} &= 0, \\
E_{\theta 31} &= 0, & E_{\theta 32} &= 0, \\
H_{r31} &= 0, & H_{r32} &= 0,
\end{aligned}
$$

$$E_{\theta 33} = -\frac{i\omega\mu}{k_1^2}\left(-\sqrt{\frac{\eta}{\mu}}e^{-\sqrt{\frac{\eta}{\mu}}\,r}\,M\left(\frac{\sqrt{\eta}\sqrt{\mu}+\beta\kappa}{2\sqrt{\eta}\sqrt{\mu}},1,2\sqrt{\frac{\eta}{\mu}}\,r\right)\right)$$
$$-\frac{i\omega\mu}{k_1^2}\frac{\sqrt{\eta\mu}+\beta\kappa}{2\sqrt{\eta\mu}\,r}e^{-\sqrt{\frac{\eta}{\mu}}}\left[M\left(\frac{\sqrt{\eta}\sqrt{\mu}+\beta\kappa}{2\sqrt{\eta}\sqrt{\mu}}+1,1,2\sqrt{\frac{\eta}{\mu}}\,r\right)-M\left(\frac{\sqrt{\eta}\sqrt{\mu}+\beta\kappa}{2\sqrt{\eta}\sqrt{\mu}},1,2\sqrt{\frac{\eta}{\mu}}\,r\right)\right]$$
$$+\frac{i\omega\beta\kappa}{k_1^2}\left(e^{-\sqrt{\frac{\eta}{\mu}}\,r}\,M\left(\frac{\sqrt{\eta}\sqrt{\mu}+\beta\kappa}{2\sqrt{\eta}\sqrt{\mu}},1,2\sqrt{\frac{\eta}{\mu}}r\right)\right),$$
$$E_{\theta 34} = -\frac{i\omega\mu}{k_1^2}\left(-\sqrt{\frac{\eta}{\mu}}e^{-\sqrt{\frac{\eta}{\mu}}\,r}\,U\left(\frac{\sqrt{\eta}\sqrt{\mu}+\beta\kappa}{2\sqrt{\eta}\sqrt{\mu}},1,2\sqrt{\frac{\eta}{\mu}}\,r\right)\right)$$
$$-\frac{i\omega\mu}{k_1^2}\left(\frac{\sqrt{\eta\mu}+\beta\kappa}{2\sqrt{\eta\mu}\,r}e^{-\sqrt{\frac{\eta}{\mu}}}\left[\frac{\sqrt{\eta\mu}+\beta\kappa}{2\sqrt{\eta\mu}}U\left(\frac{\sqrt{\eta}\sqrt{\mu}+\beta\kappa}{2\sqrt{\eta}\sqrt{\mu}}+1,1,2\sqrt{\frac{\eta}{\mu}}\,r\right)-U\left(\frac{\sqrt{\eta}\sqrt{\mu}+\beta\kappa}{2\sqrt{\eta}\sqrt{\mu}},1,2\sqrt{\frac{\eta}{\mu}}\,r\right)\right]\right)$$
$$+\frac{i\omega\beta\kappa}{k_1^2}\left(e^{-\sqrt{\frac{\eta}{\mu}}\,r}\,U\left(\frac{\sqrt{\eta}\sqrt{\mu}+\beta\kappa}{2\sqrt{\eta}\sqrt{\mu}},1,2\sqrt{\frac{\eta}{\mu}}r\right)\right),$$

$$H_{r33} = \frac{i\beta}{k_1^2}\left(-\sqrt{\frac{\eta}{\mu}}e^{-\sqrt{\frac{\eta}{\mu}}\,r}\,M\left(\frac{\sqrt{\eta}\sqrt{\mu}+\beta\kappa}{2\sqrt{\eta}\sqrt{\mu}},1,2\sqrt{\frac{\eta}{\mu}}\,r\right)\right)+$$
$$\frac{i\beta}{k_1^2}\left(\frac{\sqrt{\eta\mu}+\beta\kappa}{2\sqrt{\eta\mu}\,r}e^{-\sqrt{\frac{\eta}{\mu}}}\left[M\left(\frac{\sqrt{\eta}\sqrt{\mu}+\beta\kappa}{2\sqrt{\eta}\sqrt{\mu}}+1,1,2\sqrt{\frac{\eta}{\mu}}\,r\right)-M\left(\frac{\sqrt{\eta}\sqrt{\mu}+\beta\kappa}{2\sqrt{\eta}\sqrt{\mu}},1,2\sqrt{\frac{\eta}{\mu}}\,r\right)\right]\right)$$
$$-\frac{i\omega^2\kappa\varepsilon_f}{k_1^2}\left(e^{-\sqrt{\frac{\eta}{\mu}}\,r}\,M\left(\frac{\sqrt{\eta}\sqrt{\mu}+\beta\kappa}{2\sqrt{\eta}\sqrt{\mu}},1,2\sqrt{\frac{\eta}{\mu}}r\right)\right),$$
$$H_{r34} = \frac{i\beta}{k_1^2}\left(-\sqrt{\frac{\eta}{\mu}}e^{-\sqrt{\frac{\eta}{\mu}}\,r}\,U\left(\frac{\sqrt{\eta}\sqrt{\mu}+\beta\kappa}{2\sqrt{\eta}\sqrt{\mu}},1,2\sqrt{\frac{\eta}{\mu}}\,r\right)\right)+$$
$$\frac{i\beta}{k_1^2}\left(\frac{\sqrt{\eta\mu}+\beta\kappa}{2\sqrt{\eta\mu}\,r}e^{-\sqrt{\frac{\eta}{\mu}}}\left[\frac{\sqrt{\eta\mu}+\beta\kappa}{2\sqrt{\eta\mu}}U\left(\frac{\sqrt{\eta}\sqrt{\mu}+\beta\kappa}{2\sqrt{\eta}\sqrt{\mu}}+1,1,2\sqrt{\frac{\eta}{\mu}}\,r\right)-U\left(\frac{\sqrt{\eta}\sqrt{\mu}+\beta\kappa}{2\sqrt{\eta}\sqrt{\mu}},1,2\sqrt{\frac{\eta}{\mu}}\,r\right)\right]\right)$$
$$-\frac{i\omega^2\kappa\varepsilon_f}{k_1^2}\left(e^{-\sqrt{\frac{\eta}{\mu}}\,r}\,U\left(\frac{\sqrt{\eta}\sqrt{\mu}+\beta\kappa}{2\sqrt{\eta}\sqrt{\mu}},1,2\sqrt{\frac{\eta}{\mu}}r\right)\right),$$

where $\eta = k_1^2\mu + \omega^2\varepsilon_f\kappa^2$.

The above expressions were used in the MATLAB programs, which were used to find the propagation constant, $\beta$, and also in the MAPLE programs, which were used to find the attenuation coefficient, $\alpha$.

**The case when $n = 1$**

This section deals with the case where $n = 1$. Although Veselov et al [54] considered this case before, his expressions and method were very ambiguous and the majority of his method was ommitted. A full derivation is given here, beginning from the governing equation and ending at full and clear expressions for each component of the electric and magnetic fields in the ferrite. These expressions can be used to write a program (similar to the one written for $n = 0$) that can be used to obtain values of the propagation constant, $\beta$.

In the ferrite, at $n = 1$, the governing equations are,

$$E_z'' + \frac{1}{r}E_z' + k_0^2\left(1 - \frac{1}{r^2k_c^2}\right)E_z = \frac{i\beta}{\omega\varepsilon r}\left(\frac{k_0^2}{k_c^2} - 1\right)H_z' - \frac{i\omega\kappa}{r}\frac{k_0^2}{k_c^2}H_z, \tag{B.15}$$

$$H_z'' + \frac{1}{r}H_z' + \left(k_c^2 - \frac{\omega^2\kappa^2\varepsilon}{\mu} - \frac{\beta\kappa}{\mu r} - \frac{\mu_0 k_c^2}{r^2\mu k_0^2}\right)H_z = \frac{i\beta}{\omega\mu r}\left(1 - \frac{k_c^2}{k_0^2}\right)E_z' + \frac{i\omega\varepsilon\kappa}{\mu r}E_z. \tag{B.16}$$

where $'$ and $''$ are the first and second derivative respectively with respect to $r$. For convenience, the equations will be transformed in terms of $x = k_c r$. This gives,

$$E_z'' + \frac{E_z'}{x} + \frac{k_0^2}{k_c^2}\left(1 - \frac{1}{x^2}\right)E_z = \frac{i\beta}{\omega\varepsilon x}\left(\frac{k_0^2}{k_c^2} - 1\right)H_z' - \frac{i\omega\kappa}{x}\frac{k_0^2}{k_c^3}H_z, \tag{B.17}$$

$$H_z'' + \frac{H_z'}{x} + \left(1 - \frac{\omega^2\kappa^2\varepsilon}{k_c^2\mu} - \frac{\beta\kappa}{\mu k_c x} - \frac{\mu_0 k_c^2}{x^2\mu k_0^2}\right)H_z = \frac{i\beta}{\omega\mu x}\left(1 - \frac{k_c^2}{k_0^2}\right)E_z' + \frac{i\omega\varepsilon\kappa}{\mu k_c x}E_z. \tag{B.18}$$

where $'$ and $''$ are the first and second derivative respectively with respect to $x$. Equations (B.17) and (B.18) can be rewritten as,

$$E_z'' + \frac{E_z'}{x} + A\left(1 - \frac{1}{x^2}\right)E_z + \frac{B}{x}H_z' + \frac{C}{x}H_z = 0, \tag{B.19}$$

$$H_z'' + \frac{H_z'}{x} + \left(P + \frac{Q}{x} + \frac{R}{x^2}\right)H_z + \frac{S}{x}E_z' + \frac{T}{x}E_z = 0, \tag{B.20}$$

where

$$A = \frac{k_0^2}{k_c^2},\ B = \frac{i\beta}{\omega\varepsilon}(1 - A),\ C = i\omega\kappa\frac{A}{k_c},$$

$$P = 1 - \frac{\omega^2\kappa^2\varepsilon}{k_c^2\mu},\ Q = -\frac{\beta\kappa}{\mu k_c},\ R = -\frac{\mu_0}{\mu A},\ S = \frac{i\beta}{\omega\mu}\left(\frac{1}{A} - 1\right),\ T = -\frac{i\omega\varepsilon\kappa}{\mu k_c}.$$

Using the method of Frobenius [55], and let

$$E_z = \sum_{m=0}^{\infty} e_m x^{m+r}, \qquad H_z = \sum_{m=0}^{\infty} h_m x^{m+r}. \tag{B.21}$$

The first and second derivatives of (B.21) with respect to $x$ give,

$$E_z' = \sum_{m=0}^{\infty}(m+r)e_m x^{m+r-1}, \;\; H_z' = \sum_{m=0}^{\infty}(m+r)h_m x^{m+r-1}, \tag{B.22}$$

$$E_z'' = \sum_{m=0}^{\infty}(m+r)(m+r-1)e_m x^{m+r-2}, \;\; H_z'' = \sum_{m=0}^{\infty}(m+r)(m+r-1)h_m x^{m+r-2}. \tag{B.23}$$

Substituting (B.21), (B.22) and (B.23) into (B.19) gives,

$$\sum_{m=0}^{\infty}\left\{\left[(m+r)^2 e_m - Ae_m + B(m+r)h_m\right]x^{m+r-2} + Ae_m x^{m+r} + Ch_m x^{m+r-1}\right\} = 0, \tag{B.24}$$

$$\sum_{m=0}^{\infty}\left\{\left[(m+r)^2 h_m + Rh_m + S(m+r)e_m\right]x^{m+r-2} + \left[Qh_m + Te_m\right]x^{m+r-1} + Ph_m x^{m+r} = 0\right\}, \tag{B.25}$$

Rearranging (B.24) gives,

$$\sum_{m=0}^{\infty}\left[(m+r)^2 e_m - Ae_m + B(m+r)h_m\right]x^{m+r-2} + C\sum_{m=0}^{\infty} h_m x^{m+r-1} + A\sum_{m=0}^{\infty} e_m x^{m+r} = 0. \tag{B.26}$$

Expanding (B.26)

$$\left[r^2 e_0 - Ae_0 + Brh_0\right]x^{r-2} + \left[(r+1)^2 e_1 - Ae_1 + B(r+1)h_1 + Ch_0\right]x^{r-1} +$$

$$\sum_{m=2}^{\infty}\left[(m+r)^2 e_m - Ae_m + B(m+r)h_m + Ch_{m-1} + Ae_{m-2}\right]x^{m+r-2} = 0. \tag{B.27}$$

Rearranging (B.25) gives,

$$\sum_{m=0}^{\infty}\left\{\left[(m+r)^2 h_m + Rh_m + S(m+r)e_m\right]x^{m+r-2} + \left[Qh_m + Te_m\right]x^{m+r-1} + Ph_m x^{m+r}\right\} = 0. \tag{B.28}$$

Expanding (B.28)

$$\left[r^2 h_0 + Rh_0 + Sre_0\right]x^{r-2} + \left[(r+1)^2 h_1 + Rh_1 + S(r+1)e_1 + Qh_0 + Te_0\right]x^{r-1} +$$

$$\sum_{m=2}^{\infty}\left[(m+r)^2 h_m + Rh_m + S(m+r)e_m + Qh_{m-1} + Te_{m-1} + Ph_{m-2}\right]x^{m+r-2} = 0. \tag{B.29}$$

The lowest degree of $x$ in the equations is $x^{r-2}$ and is satisfied by the equations,

$$r^2 e_0 - A e_0 + B r h_0 = 0 \quad \text{and} \quad r^2 h_0 + R h_0 + S r e_0 = 0, \tag{B.30}$$

which can be re-written as,

$$\begin{pmatrix} r^2 - A & Br \\ Sr & r^2 + R \end{pmatrix} \begin{pmatrix} e_0 \\ h_0 \end{pmatrix} = \begin{pmatrix} 0 \\ 0 \end{pmatrix}. \tag{B.31}$$

In order to obtain a non-trivial solution, the determinant

$$\begin{vmatrix} r^2 - A & Br \\ Sr & r^2 + R \end{vmatrix} = 0, \quad \Rightarrow \quad (r^2 - A)(r^2 + R) - BSr^2 = 0, \quad \Rightarrow \quad r^4 + (R - A - BS)r^2 + BR = 0, \tag{B.32}$$

which solves to give $r_{1,2} = \pm\sqrt{\frac{\mu_0}{\mu}}$ and $r_{3,4} = \pm 1$. As $n = 1$, $|r_1 - r_2|$ is not an integer, and $|r_3 - r_4| \epsilon \mathbb{Z}$.

This gives

$$h_0 = -\frac{r^2 - A}{Br}\, e_0.$$

The next degree of $x$ in the equations is $x^{r-1}$ and is satisfied by the equations,

$$(r+1)^2 e_1 - A e_1 + B(r+1) h_1 + C h_0 = 0, \tag{B.33}$$

$$(r+1)^2 h_1 + R h_1 + S(r+1) e_1 + Q h_0 + T e_0 = 0. \tag{B.34}$$

By using the expression for $h_0$ gives, $e_1$ and $h_1$ as

$$e_1 = \frac{\left[BQ(r+1) - C(r+1)^2 - RC\right](A - r^2) + TB^2 r(r+1)}{Br\left[(r+1)^4 - (r+1)^2(A + SB - R) - RA\right]}\, e_0, \tag{B.35}$$

$$h_1 = \frac{Q(r(r+1) - A)^2 - Cr^2 S(r+1) - TBr(r+1)^2 + A(TBr - Q) + CAS(r+1)}{Br\left[(r+1)^4 - (r+1)^2(A + SB - R) - RA\right]}\, e_0. \tag{B.36}$$

The problem is now split into two cases, case 1, $r_{1,2,3}$ and case 2, $r_4$.

**Case 1: $r_{1,2} = \pm\sqrt{\frac{\mu_0}{\mu}}$ and $r_3 = 1$.**

Both summations in equations (B.27) and (B.29) must equal zero and so without loss of generality

the following equations are obtained, ($form \geq 2$)

$$e_m = \frac{[(m+r)^2+R][Ch_{m-1}+Ae_{m-2}] - B(m+r)[Qh_{m-1}+Te_{m-1}+Ph_{m-2}]}{BS(m+r)^2 - [(m+r)^2-A][(m+r)^2+R]}, \tag{B.37}$$

$$h_m = \frac{[(m+r)^2-A][Qh_{m-1}+Te_{m-1}+Ph_{m-2}] - S(m+r)[Ch_{m-1}+Ae_{m-2}]}{BS(m+r)^2 - [(m+r)^2-A][(m+r)^2+R]}. \tag{B.38}$$

By using the expressions for $e_0$, $e_1$, $h_0$ and $h_1$ with the above recurrence relations, it is possible to generate an expression for $E_z$ and $H_z$ in the ferrite.

**Case 2:** $r_4 = -1$**.**

As $r_3$ and $r_4$ differ by and integer, the series solutions corresponding to $r_4 = -1$ will take the form,

$$E_z = E_1 ln(x) + D_1 \quad \text{and} \quad H_z = H_1 ln(x) + B_1. \tag{B.39}$$

where

$$E_1 = \sum_{m=0}^{\infty} e_m x^{m+1}, \quad D_1 = \sum_{m=0}^{\infty} d_m x^{m-1}, \quad H_1 = \sum_{m=0}^{\infty} h_m x^{m+1}, \quad \text{and} \quad B_1 = \sum_{m=0}^{\infty} b_m x^{m-1}, \tag{B.40}$$

The first and second derivatives of (B.39) are given by,

$$E_z' = E_1' ln(x) + \frac{E_1}{x} + D_1', \quad H_z' = H_1' ln(x) + \frac{H_1}{x} + B_1', \tag{B.41}$$

$$E_z'' = E_1'' ln(x) + 2\frac{E_1'}{x} - \frac{E_1'}{x^2} + D_1'', \quad H_z'' = H_1'' ln(x) + 2\frac{H_1'}{x} - \frac{H_1'}{x^2} + B_1''. \tag{B.42}$$

Substituting (B.39) in (B.19),

$$\left[E_1'' + \frac{E_1'}{x} + A\left(1 - \frac{1}{x^2}\right)E_1 + \frac{B}{x}H_1' + \frac{C}{x}H_1\right] ln(x) +$$

$$\frac{2}{x}E_1' + D_1'' + \frac{D_1'}{x} + A\left(1 - \frac{1}{x^2}\right)D_1 + \frac{B}{x^2}H_1 + \frac{B}{x}B_1' + \frac{C}{x}B_1 = 0,$$

$E_1$ and $H_1$ are solutions to (B.19) so the coefficient of $\ln(x)$ is zero. Therefore,

$$\frac{2}{x}E_1' + \frac{B}{x^2}H_1 + D_1'' + \frac{D_1'}{x} + A\left(1 - \frac{1}{x^2}\right)D_1 + \frac{B}{x}B_1' + \frac{C}{x}B_1 = 0. \tag{B.43}$$

Substituting (B.39) in (B.20),

$$\left[H_1'' + \frac{H_1'}{x} + \left(P + \frac{Q}{x} + \frac{R}{x^2}\right)H_1 + \frac{S}{x}E_1' + \frac{T}{x}E_1\right] ln(x) +$$

$$\frac{2}{x}H_1' + \frac{S}{x^2}E_1 + B_1'' + \frac{B_1'}{x} + P\left(P + \frac{Q}{x} + \frac{R}{x^2}\right)B_1 + \frac{S}{x}D_1' + \frac{T}{x}D_1 = 0,$$

$E_1$ and $H_1$ are solutions to (B.20) so the coefficient of $\ln(x)$ is zero. Therefore,

$$\frac{2}{x}H_1' + \frac{S}{x^2}E_1 + B_1'' + \frac{B_1'}{x} + \left(P + \frac{Q}{x} + \frac{R}{x^2}\right)B_1 + \frac{S}{x}D_1' + \frac{T}{x}D_1 = 0. \tag{B.44}$$

The first and second derivatives of (B.40) are given by,

$$\begin{aligned}
E_1' &= \textstyle\sum_{m=0}^{\infty}(m+1)e_m x^m, & E_1'' &= \textstyle\sum_{m=0}^{\infty} m(m+1)e_m x^{m-1},\\
D_1' &= \textstyle\sum_{m=0}^{\infty}(m-1)d_m x^{m-2}, & D_1'' &= \textstyle\sum_{m=0}^{\infty}(m-1)(m-2)d_m x^{m-3},\\
H_1' &= \textstyle\sum_{m=0}^{\infty}(m+1)h_m x^m, & H_1'' &= \textstyle\sum_{m=0}^{\infty} m(m+1)h_m x^{m-1},\\
B_1' &= \textstyle\sum_{m=0}^{\infty}(m-1)b_m x^{m-2} \text{ and} & B_1'' &= \textstyle\sum_{m=0}^{\infty}(m-1)(m-2)b_m x^{m-3}.
\end{aligned} \tag{B.45}$$

Substituting (B.45) into (B.43)

$$2\sum_{m=0}^{\infty}(m+1)e_m x^{m-1} + B\sum_{m=0}^{\infty}h_m x^{m-3} + \sum_{m=0}^{\infty}(m-1)(m-2)d_m x^{m-3} + \sum_{m=0}^{\infty}(m-1)d_m x^{m-3} +$$

$$A\sum_{m=0}^{\infty}d_m x^{m-1} - A\sum_{m=0}^{\infty}d_m x^{m-3} + B\sum_{m=0}^{\infty}(m-1)b_m x^{m-3} + C\sum_{m=0}^{\infty}b_m x^{m-2} = 0.$$

This can be written in ascending powers of $x$.

$$\sum_{m=0}^{\infty}\left[B(h_m + (m-1)b_m) + \left((m-1)^2 - A\right)d_m\right]x^{m-3} + \sum_{m=0}^{\infty}Cb_m x^{m-2} + \sum_{m=0}^{\infty}\left[2(m+1)e_m + Ad_m\right]x^{m-1} = 0. \tag{B.46}$$

Expanding (B.46) gives

$$\left[B(h_0 - b_0) + (1-A)d_0\right]x^{-3} + \left[Bb_1 - Ad_1 + Cb_0\right]x^{-2} +$$

$$\sum_{m=2}^{\infty}\left[B(h_m + (m-1)b_m) + \left((m-1)^2 - A\right)d_m + Cb_{m-1} + 2(m-1)e_{m-2} + Ad_{m-2}\right]x^{m-3} = 0. \tag{B.47}$$

Substituting (B.45) into (B.44)

$$2\sum_{m=0}^{\infty}(m+1)h_m x^{m-1} + S\sum_{m=0}^{\infty}e_m x^{m-1} + \sum_{m=0}^{\infty}(m-1)(m-2)b_m x^{m-3} + \sum_{m=0}^{\infty}(m-1)b_m x^{m-3} +$$

$$P\sum_{m=0}^{\infty} b_m x^{m-1} + Q\sum_{m=0}^{\infty} b_m x^{m-2} + R\sum_{m=0}^{\infty} b_m x^{m-3} + S\sum_{m=0}^{\infty}(m-1)d_m x^{m-3} + T\sum_{m=0}^{\infty} d_m x^{m-2} = 0.$$

This can be written in ascending powers of $x$.

$$\sum_{m=0}^{\infty}\left[((m-1)^2+R)b_m + S(m-1)d_m\right]x^{m-3} + \sum_{m=0}^{\infty}\left[Qb_m + Td_m\right]x^{m-2} +$$

$$\sum_{m=0}^{\infty}\left[2(m+1)h_m + Se_m + Pb_m\right]x^{m-1} = 0. \tag{B.48}$$

Expanding (B.48) gives

$$\left[(1+R)b_0 - Sd_0\right]x^{-3} + \left[Rb_1 + Qb_0 + Td_0\right]x^{-2} +$$

$$\sum_{m=2}^{\infty}\left[((m-1)^2+R)b_m + S(m-1)d_m + Qb_{m-1} + Td_{m-1} + 2(m-1)h_{m-2} + Se_{m-2} + Pb_{m-2}\right]x^{m-3} = 0. \tag{B.49}$$

This gives the following equations,

$$B(h_0-b_0)+(1-A)d_0 = 0,\ \ (1+R)b_0 - Sd_0 = 0,\ \ Bb_1 - Ad_1 + Cb_0 = 0 \text{ and } Rb_1 + Qb_0 + Td_0 = 0, \tag{B.50}$$

which gives

$$b_0 = \frac{BSh_0}{SB-1-R+A+AR},\ \ d_0 = \frac{(1+R)Bh_0}{SB-1-R+A+AR}, \tag{B.51}$$

$$b_1 = -\frac{B(SQ+T+TR)h_0}{(SB-1-R+A+AR)R},\ \ d_1 = -\frac{B(SQB+TB+TRB-CSR)h_0}{(SB-1-R+A+AR)AR}. \tag{B.52}$$

The remaining terms can be calculated from equations (B.47) and (B.49), which can be expressed in the following form,

$$\begin{pmatrix} b_m \\ d_m \end{pmatrix} = \begin{pmatrix} B(m-1) & (m-1)^2 - A \\ (m-1)^2 + R & S(m-1) \end{pmatrix}^{-1} \begin{pmatrix} -\left(Bh_m + Cb_{m-1} + 2(m-1)e_{m-2} + Ad_{m-2}\right) \\ -\left(Qb_{m-1} + Td_{m-1} + 2(m-1)h_{m-2} + Se_{m-2} + Pb_{m-2}\right) \end{pmatrix}. \tag{B.53}$$

From the expressions of $E_z$ and $H_z$, it possible to calculate $E_\theta$ and $H_\theta$ from the expressions,

$$E_\theta = \frac{\sqrt{\omega^2\mu\varepsilon-\beta^2}\left[\frac{\beta}{x}E_z + i\omega\mu\frac{dH_z}{dx}\right] - i\beta\omega\kappa H_z}{\omega^2\mu\varepsilon-\beta^2} \quad \text{and} \quad H_\theta = \frac{\sqrt{\omega^2\mu\varepsilon-\beta^2}}{\omega^2\mu_0\varepsilon-\beta^2}\left[\frac{\beta}{x}H_z - i\omega\varepsilon\frac{dE_z}{dx}\right]. \quad \text{(B.54)}$$

Therefore, in the ferrite, the following expressions are obtained,

$$E_z = AE_1 + BE_2 + CE_3 + D\left(E_3 ln(x) + D_4\right), \quad \text{(B.55)}$$

$$H_z = AH_1 + BH_2 + CH_3 + D\left(H_3 ln(x) + B_4\right), \quad \text{(B.56)}$$

$$\begin{aligned} E_\theta \;=\; & \tfrac{\beta}{x\sqrt{\omega^2\mu\varepsilon-\beta^2}}\left(AE_1 + BE_2 + CE_3 + D\left(E_3 ln(x) + D_4\right)\right) \\ & + \tfrac{i\omega\mu}{\sqrt{\omega^2\mu\varepsilon-\beta^2}}\left(A\tfrac{dH_1}{dx} + B\tfrac{dH_2}{dx} + C\tfrac{dH_3}{dx} + D\left(\tfrac{dH_3}{dx}ln(x) + \tfrac{H_3}{x} + \tfrac{dB_4}{dx}\right)\right) \\ & - \tfrac{i\beta\omega\kappa}{\omega^2\mu\varepsilon-\beta^2}\left(AH_1 + BH_2 + CH_3 + D\left(H_3 ln(x) + B_4\right)\right), \end{aligned} \quad \text{(B.57)}$$

$$\begin{aligned} H_\theta \;=\; & \tfrac{\sqrt{\omega^2\mu\varepsilon-\beta^2}}{\omega^2\mu_0\varepsilon-\beta^2}\left[\tfrac{\beta}{x}\left(AH_1 + BH_2 + CH_3 + D\left(H_3 ln(x) + B_4\right)\right)\right] \\ & - \tfrac{\sqrt{\omega^2\mu\varepsilon-\beta^2}}{\omega^2\mu_0\varepsilon-\beta^2}\left[i\omega\varepsilon\left(A\tfrac{dE_1}{dx} + B\tfrac{dE_2}{dx} + C\tfrac{dE_3}{dx} + D\left(\tfrac{dE_3}{dx}ln(x) + \tfrac{E_3}{x} + \tfrac{dD_4}{dx}\right)\right)\right], \end{aligned} \quad \text{(B.58)}$$

where

$$E_1 = \sum_{k=0}^{\infty} e_k x^{k-\sqrt{\frac{\mu_0}{\mu}}}, \;\; E_2 = \sum_{k=0}^{\infty} e_k x^{k+\sqrt{\frac{\mu_0}{\mu}}}, \;\; E_3 = \sum_{k=0}^{\infty} e_k x^{k+1}, \;\; D_4 = \sum_{k=0}^{\infty} d_k x^{k-1},$$

$$H_1 = \sum_{k=0}^{\infty} h_k x^{k-\sqrt{\frac{\mu_0}{\mu}}}, \;\; H_2 = \sum_{k=0}^{\infty} h_k x^{k+\sqrt{\frac{\mu_0}{\mu}}}, \;\; H_3 = \sum_{k=0}^{\infty} h_k x^{k+1}, \;\; B_4 = \sum_{k=0}^{\infty} b_k x^{k-1},$$

where $A$, $B$, $C$ and $D$ are constants. Therefore, the following expressions in each region are obtained.

**Region 1 - Air**

$$E_{z1}(x) = a_1 J_1\left(\frac{k_0}{k_c}x\right), \quad H_{z1}(x) = c_1 J_1\left(\frac{k_0}{k_c}x\right), \quad \text{(B.59)}$$

$$E_{\theta 1}(x) = a_1\frac{\beta k_c}{xk_0^2}J_1\left(\frac{k_0}{k_c}x\right) + c_1\frac{i\omega\mu_0}{k_0}\left(J_0\left(\frac{k_0}{k_c}x\right) - \frac{k_c}{k_0 x}J_1\left(\frac{k_0}{k_c}x\right)\right), \quad \text{(B.60)}$$

$$H_{\theta 1}(x) = -a_1\frac{i\omega\varepsilon}{k_0}\left(J_0\left(\frac{k_0}{k_c}x\right) - \frac{k_c}{k_0 x}J_1\left(\frac{k_0}{k_c}x\right)\right) + c_1\frac{\beta k_c}{xk_0^2}J_1\left(\frac{k_0}{k_c}x\right), \quad \text{(B.61)}$$

where $a_1$ and $c_1$ are constants.

**Region 2 - Air**

$$E_{z2}(x) = a_2 J_1\left(\frac{k_0}{k_c}x\right) + b_2 Y_1\left(\frac{k_0}{k_c}x\right), \quad H_{z2}(x) = c_2 J_1\left(\frac{k_0}{k_c}x\right) + d_2 Y_1\left(\frac{k_0}{k_c}x\right), \tag{B.62}$$

$$\begin{aligned} E_{\theta 2}(x) &= a_2\tfrac{\beta k_c}{xk_0^2} J_1\left(\tfrac{k_0}{k_c}x\right) + b_2\tfrac{\beta k_c}{xk_0^2} Y_1\left(\tfrac{k_0}{k_c}x\right) + \\ &\quad c_2\tfrac{i\omega\mu_0}{k_0}\left(J_0\left(\tfrac{k_0}{k_c}x\right) - \tfrac{k_c}{k_0 x} J_1\left(\tfrac{k_0}{k_c}x\right)\right) + \\ &\quad d_2\tfrac{i\omega\mu_0}{k_0}\left(Y_0\left(\tfrac{k_0}{k_c}x\right) - \tfrac{k_c}{k_0 x} Y_1\left(\tfrac{k_0}{k_c}x\right)\right), \end{aligned} \tag{B.63}$$

$$\begin{aligned} H_{\theta 2}(x) &= -a_2\tfrac{i\omega\varepsilon}{k_0}\left(J_0\left(\tfrac{k_0}{k_c}x\right) - \tfrac{k_c}{k_0 x} J_1\left(\tfrac{k_0}{k_c}x\right)\right) \\ &\quad -b_2\tfrac{i\omega\varepsilon}{k_0}\left(Y_0\left(\tfrac{k_0}{k_c}x\right) - \tfrac{k_c}{k_0 x} Y_1\left(\tfrac{k_0}{k_c}x\right)\right) + \\ &\quad c_2\tfrac{\beta k_c}{xk_0^2} J_1\left(\tfrac{k_0}{k_c}x\right) + d_2\tfrac{\beta k_c}{xk_0^2} Y_1\left(\tfrac{k_0}{k_c}x\right), \end{aligned} \tag{B.64}$$

where $a_2$, $b_2$, $c_2$, and $d_2$ are constants.

**Region 3 - Ferrite**

$$E_z(x) = a_3 E_1 + b_3 E_2 + c_3 E_3 + d_3\left(E_3 ln(x) + D_4\right), \tag{B.65}$$

$$H_z(x) = a_3 H_1 + b_3 H_2 + c_3 H_3 + d_3\left(H_3 ln(x) + B_4\right), \tag{B.66}$$

$$\begin{aligned} &E_{\theta 3}(x) = a_3\left[\tfrac{\beta E_1}{x\sqrt{\omega^2\varepsilon\mu-\beta^2}} + \tfrac{i\omega\mu}{\sqrt{\omega^2\varepsilon\mu-\beta^2}}\tfrac{dH_1}{dx} - \tfrac{i\omega\beta\kappa H_1}{\omega^2\varepsilon\mu-\beta^2}\right] + b_3\left[\tfrac{\beta E_2}{x\sqrt{\omega^2\varepsilon\mu-\beta^2}} + \tfrac{i\omega\mu}{\sqrt{\omega^2\varepsilon\mu-\beta^2}}\tfrac{dH_2}{dx} - \tfrac{i\omega\beta\kappa H_2}{\omega^2\varepsilon\mu-\beta^2}\right] + \\ &c_3\left[\tfrac{\beta E_3}{x\sqrt{\omega^2\varepsilon\mu-\beta^2}} + \tfrac{i\omega\mu}{\sqrt{\omega^2\varepsilon\mu-\beta^2}}\tfrac{dH_3}{dx} - \tfrac{i\omega\beta\kappa H_3}{\omega^2\varepsilon\mu-\beta^2}\right] + \\ &d_3\left[\left[\tfrac{\beta E_3}{x\sqrt{\omega^2\varepsilon\mu-\beta^2}} + \tfrac{i\omega\mu}{\sqrt{\omega^2\varepsilon\mu-\beta^2}}\tfrac{dH_3}{dx} - \tfrac{i\omega\beta\kappa H_3}{\omega^2\varepsilon\mu-\beta^2}\right] ln(x) + \left[\tfrac{\beta D_4}{x\sqrt{\omega^2\varepsilon\mu-\beta^2}} + \tfrac{i\omega\mu}{\sqrt{\omega^2\varepsilon\mu-\beta^2}}\tfrac{dB_4}{dx} - \tfrac{i\omega\beta\kappa B_4}{\omega^2\varepsilon\mu-\beta^2}\right] + \tfrac{i\omega\mu H_3}{x\sqrt{\omega^2\varepsilon\mu-\beta^2}}\right], \end{aligned} \tag{B.67}$$

$$\begin{aligned} &H_{\theta 3}(x) = a_3\tfrac{\sqrt{\omega^2\varepsilon\mu-\beta^2}}{\omega^2\varepsilon\mu_0-\beta^2}\left[\tfrac{\beta}{x}H_1 - i\omega\varepsilon\tfrac{dE_1}{dx}\right] + b_3\tfrac{\sqrt{\omega^2\varepsilon\mu-\beta^2}}{\omega^2\varepsilon\mu_0-\beta^2}\left[\tfrac{\beta}{x}H_2 - i\omega\varepsilon\tfrac{dE_2}{dx}\right] + c_3\tfrac{\sqrt{\omega^2\varepsilon\mu-\beta^2}}{\omega^2\varepsilon\mu_0-\beta^2}\left[\tfrac{\beta}{x}H_3 - i\omega\varepsilon\tfrac{dE_3}{dx}\right] + \\ &d_3\tfrac{\sqrt{\omega^2\varepsilon\mu-\beta^2}}{\omega^2\varepsilon\mu_0-\beta^2}\left[\left[\tfrac{\beta}{x}H_3 - i\omega\varepsilon\tfrac{dE_3}{dx}\right] ln(x) + \left[\tfrac{\beta}{x}B_4 - i\omega\varepsilon\left(\tfrac{E_3}{x} - \tfrac{dD_4}{dx}\right)\right]\right], \end{aligned} \tag{B.68}$$

where

$$E_1 = \sum_{k=0}^{\infty} e_k x^{k-\sqrt{\frac{\mu_0}{\mu}}}, \quad E_2 = \sum_{k=0}^{\infty} e_k x^{k+\sqrt{\frac{\mu_0}{\mu}}}, \quad E_3 = \sum_{k=0}^{\infty} e_k x^{k+1}, \quad D_4 = \sum_{k=0}^{\infty} d_k x^{k-1},$$

$$H_1 = \sum_{k=0}^{\infty} h_k x^{k-\sqrt{\frac{\mu_0}{\mu}}}, \quad H_2 = \sum_{k=0}^{\infty} h_k x^{k+\sqrt{\frac{\mu_0}{\mu}}}, \quad H_3 = \sum_{k=0}^{\infty} h_k x^{k+1}, \quad B_4 = \sum_{k=0}^{\infty} b_k x^{k-1},$$

where $a_3$, $b_3$, $c_3$ and $d_3$ are constants.

**Region 4 - Air**

$$E_{z4}(x) = a_4 J_1\left(\frac{k_0}{k_c}x\right) + b_4 Y_1\left(\frac{k_0}{k_c}x\right), \quad H_{z4}(x) = c_4 J_1\left(\frac{k_0}{k_c}x\right) + d_4 Y_1\left(\frac{k_0}{k_c}x\right), \tag{B.69}$$

$$\begin{aligned} E_{\theta 2}(x) &= a_4 \tfrac{\beta k_c}{x k_0^2} J_1\left(\tfrac{k_0}{k_c}x\right) + b_4 \tfrac{\beta k_c}{x k_0^2} Y_1\left(\tfrac{k_0}{k_c}x\right) + \\ &\quad c_4 \tfrac{i\omega\mu_0}{k_0}\left(J_0\left(\tfrac{k_0}{k_c}x\right) - \tfrac{k_c}{k_0 x} J_1\left(\tfrac{k_0}{k_c}x\right)\right) + \\ &\quad d_4 \tfrac{i\omega\mu_0}{k_0}\left(Y_0\left(\tfrac{k_0}{k_c}x\right) - \tfrac{k_c}{k_0 x} Y_1\left(\tfrac{k_0}{k_c}x\right)\right), \end{aligned} \tag{B.70}$$

$$\begin{aligned} H_{\theta 2}(x) &= -a_4 \tfrac{i\omega\varepsilon}{k_0}\left(J_0\left(\tfrac{k_0}{k_c}x\right) - \tfrac{k_c}{k_0 x} J_1\left(\tfrac{k_0}{k_c}x\right)\right) \\ &\quad -b_4 \tfrac{i\omega\varepsilon}{k_0}\left(Y_0\left(\tfrac{k_0}{k_c}x\right) - \tfrac{k_c}{k_0 x} Y_1\left(\tfrac{k_0}{k_c}x\right)\right) + \\ &\quad c_4 \tfrac{\beta k_c}{x k_0^2} J_1\left(\tfrac{k_0}{k_c}x\right) + d_4 \tfrac{\beta k_c}{x k_0^2} Y_1\left(\tfrac{k_0}{k_c}x\right), \end{aligned} \tag{B.71}$$

where $a_4$, $b_4$, $c_4$, and $d_4$ are constants. The expressions for each region can be combined with the boundary conditions leads to the system of equations which can be written in matrix form.

$$\mathbf{A}.\,(a_1, a_2, a_3, a_4, b_2, b_3, b_4, c_1, c_2, c_3, c_4, d_2, d_3, d_4)^T = \mathbf{0}, \quad \text{where} \quad \mathbf{A} = \begin{pmatrix} A_{11} & \cdots & A_{114} \\ \vdots & \ddots & \vdots \\ A_{141} & \cdots & A_{1414} \end{pmatrix}. \tag{B.72}$$

The same method, as shown in section 2.8, can be used to generate the vaslues of $\beta$.

# Appendix C

# Mathematical Functions

This section considers the mathematical functions that have been used in the derivation of the governing equations. In air, the electric and magnetic fields can be expressed as Bessel functions, whilst in the ferrite, the fields are expressed as Confluent Hypergeometric functions [56]. Important properties of both of these sets of functions are given below.

## C.1 Bessel Functions

### C.1.1 Differential Equation

Bessel functions arise from solutions to differetntial equations. The most popular usage of Bessel functions are in the solutions of the wave equation in cylindrical polar coordinates. Here, the differential equation from which the Bessel functions arise are discussed.

Let $y$ be a function of $x$ that satisfies the following equation,

$$\frac{d^2y}{dx^2} + \frac{1}{x}\frac{dy}{dx} + \left[k^2 - \frac{n^2}{x^2}\right] y(x) = 0. \tag{C.1}$$

The general solution can be written as,

$$y = A\, J_n(kx) + B\, Y_n(kx), \tag{C.2}$$

where $A$ and $B$ are constants. $J_n$ and $Y_n$ are referred to as Bessel functions of the first and second kinds, respectively.

An alternative set of Bessel functions, referred to as *modified Bessel fucntions*, also exist. These are solutions to a slighly varied form of the original differential requation. Letting $y$ be a function of $x$ that satisfies the following equation,

$$\frac{d^2y}{dx^2} + \frac{1}{x}\frac{dy}{dx} - \left[k^2 + \frac{n^2}{x^2}\right] y(x) = 0. \tag{C.3}$$

The general solution can be written as,

$$y = C\, I_n(kx) + D\, K_n(kx), \tag{C.4}$$

where $C$ and $D$ are constants. $I_n$ and $K_n$ are the modified Bessel functions of the first and second kinds, respectively

### C.1.2 Derivatives

The Besssl functions that were used in this invesigation were of zero and first order. Their derivatives are given below.

$$\frac{d}{dx} I_0(kx) = k\, I_1(kx), \qquad \frac{d}{dx} K_0(kx) = -k\, K_1(kx), \tag{C.5}$$

$$\frac{d}{dx} I_1(kx) = k\, I_0(kx) - \frac{I_1(kx)}{x}, \qquad \frac{d}{dx} K_1(kx) = -k\, K_0(kx) - \frac{K_1(kx)}{x}, \tag{C.6}$$

$$\frac{d}{dx} J_0(kx) = -k\, J_1(kx), \qquad \frac{d}{dx} Y_0(kx) = -k\, Y_1(kx), \tag{C.7}$$

$$\frac{d}{dx} J_1(kx) = k\, J_0(kx) - \frac{J_1(kx)}{x}, \qquad \frac{d}{dx} Y_1(kx) = k\, Y_0(kx) - \frac{Y_1(kx)}{x}. \tag{C.8}$$

### C.1.3 The limit at 0 and $\infty$

The behaviour of these functions at 0 and $\infty$ have also been made use of. The centreline of the structure requires a knowledge of how the functions behave at 0. The behaviour at $\infty$ is improtant if a freely immersed helix (without a metal waveguide) is to be investigated.

Let $x \epsilon \mathbb{R}$, as $x \to 0$

$$I_0(x) \to 0, \qquad I_1(x) \to 0, \qquad K_0(x) \to \infty, \qquad K_1(x) \to \infty. \tag{C.9}$$

Let $x \epsilon \mathbb{R}$, as $x \to \infty$

$$I_0(x) \to \infty, \qquad I_1(x) \to \infty, \qquad K_0(x) \to 0, \qquad K_1(x) \to 0. \tag{C.10}$$

## C.2 Confluent Hypergeometric Functions

The governing equations for the behaviour of the wave in the ferrite can be solved to give expressions in terms of Confluent Hypergeometric Functions. Examples of these functions are Whittaker functions and Kummer functions. Both of these functions can be used to express the electric and magnetic field components in the ferrite.

### C.2.1 Whittaker Functions

Let $y$ be a function of $x$, and satisfy the following equation,

$$\frac{d^2y}{dx^2} + \left[\frac{\mu}{x} - \frac{1}{4} + \frac{1-4\nu^2}{4x^2}\right] y(x) = 0. \tag{C.11}$$

The solution can be written as,

$$y = a\, M(\mu, \nu, x) + b\, W(\mu, \nu, x), \tag{C.12}$$

where $M$ and $W$ are Whittaker functions and $a$ and $b$ are constants.

### C.2.2 Kummer Functions

Let $y$ be a function of $x$, and satisfy the following equation,

$$\frac{d^2y}{dx^2} + \left[\frac{\nu}{x} - 1\right] \frac{dy}{dx} - \mu y(x) = 0. \tag{C.13}$$

The solution can be written as,

$$y = c\,\mathcal{M}(\mu,\nu,x) + d\,\mathcal{U}(\mu,\nu,x), \tag{C.14}$$

where $\mathcal{M}$ and $\mathcal{U}$ are Kummer functions and $c$ and $d$ are constants.

### C.2.3 Relationship between Kummer and Whittaker Functions

The Kummer and Whittaker functions are related to each other by the following equations.

$$\mathcal{M}(\mu,\nu,z) = e^{z/2} z^{-\nu/2} M\left(\nu/2-\mu,(\nu-1)/2,z\right), \tag{C.15}$$

$$\mathcal{U}(\mu,\nu,z) = e^{z/2} z^{-\nu/2} W\left(\nu/2-\mu,(\nu-1)/2,z\right), \tag{C.16}$$

$$M\left(x,y,z\right) = e^{-z/2} z^{(1+2y)/2} \mathcal{M}(1/2+y-x,1+2y,z), \tag{C.17}$$

$$W\left(x,y,z\right) = e^{-z/2} z^{(1+2y)/2} \mathcal{U}(1/2+y-x,1+2y,z). \tag{C.18}$$

# Appendix D

# Computer Programs

## D.1 MATLAB

This section gives the codes that were used in the MATLAB program. Otto et al [57] provided a comprehensive understanding of the matlab commands that were used in these programs. The first code is for finding a real-valued propagation constant, and the second is for finding a complex-valued propagation constant.

### D.1.1 Real-Valued Propagation Constant

Below is the MATLAB code which generated the propagation coefficient in the cases where $\mu$ and $\varepsilon$ are both real-valued constants. The program generates a value for the determinant of the matrix[1].

[1]The matrix **A** was explained in chapter 2

```
function complete = f(beta);

i=sqrt(-1);

a=1.465/1000;

b=1.59/1000;

c=2.92/1000; d=c+(10^(-6)); psi=9.5*pi/180;


T=tan(psi);


omega=2*pi*1*10^9;


mu0=4*pi*10^(-7); e0=8.854188*10^(-12); beta0=omega*sqrt(mu0*e0);


gamma=2.21*10^(5); Ms=0.068; H=55000;

kappa=gamma*omega*Ms/(omega^2-gamma^2*H^2);

mu=mu0+(gamma^2*H*Ms)/(gamma^2*H^2-omega^2); ef=14.5*e0; er=1;

epsilonf=ef;
```

```
Hz31b=exp(-(-(omega^2*mu*epsilonf-beta^2)*mu+omega^2*ef*kappa^2)^(1/2)/mu^(1/2)*b)*
M(1/2*((-(omega^2*mu*epsilonf-beta^2)*mu+omega^2*ef*kappa^2)^(1/2)*mu^(1/2)+beta*kappa)/
(-(omega^2*mu*epsilonf-beta^2)*mu+omega^2*ef*kappa^2)^(1/2)/mu^(1/2),1,2*
(-(omega^2*mu*epsilonf-beta^2)*mu+omega^2*ef*kappa^2)^(1/2)/mu^(1/2)*b);

Hz31c=exp(-(-(omega^2*mu*epsilonf-beta^2)*mu+omega^2*ef*kappa^2)^(1/2)/mu^(1/2)*c)*
M(1/2*((-(omega^2*mu*epsilonf-beta^2)*mu+omega^2*ef*kappa^2)^(1/2)*mu^(1/2)+beta*kappa)/
(-(omega^2*mu*epsilonf-beta^2)*mu+omega^2*ef*kappa^2)^(1/2)/mu^(1/2),1,2*
(-(omega^2*mu*epsilonf-beta^2)*mu+omega^2*ef*kappa^2)^(1/2)/mu^(1/2)*c);

Hz32b=exp(-(-(omega^2*mu*epsilonf-beta^2)*mu+omega^2*ef*kappa^2)^(1/2)/mu^(1/2)*b)*
U(1/2*((-(omega^2*mu*epsilonf-beta^2)*mu+omega^2*ef*kappa^2)^(1/2)*mu^(1/2)+beta*kappa)/
(-(omega^2*mu*epsilonf-beta^2)*mu+omega^2*ef*kappa^2)^(1/2)/mu^(1/2),1,2*
(-(omega^2*mu*epsilonf-beta^2)*mu+omega^2*ef*kappa^2)^(1/2)/mu^(1/2)*b);

Hz32c=exp(-(-(omega^2*mu*epsilonf-beta^2)*mu+omega^2*ef*kappa^2)^(1/2)/mu^(1/2)*c)*
U(1/2*((-(omega^2*mu*epsilonf-beta^2)*mu+omega^2*ef*kappa^2)^(1/2)*mu^(1/2)+beta*kappa)/
(-(omega^2*mu*epsilonf-beta^2)*mu+omega^2*ef*kappa^2)^(1/2)/mu^(1/2),1,2*
(-(omega^2*mu*epsilonf-beta^2)*mu+omega^2*ef*kappa^2)^(1/2)/mu^(1/2)*c);
```

```
Et31b=(-i*omega*mu*(omega^2*ef*kappa^2/mu-(omega^2*mu*epsilonf-beta^2))^(1/2)*
M(1/2*((mu*(omega^2*ef*kappa^2-(omega^2*mu*epsilonf-beta^2)*mu))^(1/2)+beta*kappa)/
(mu*(omega^2*ef*kappa^2-(omega^2*mu*epsilonf-beta^2)*mu))^(1/2),1,
2*b*((omega^2*ef*kappa^2-(omega^2*mu*epsilonf-beta^2)*mu)/mu)^(1/2))/
exp(b*(omega^2*ef*kappa^2/mu-(omega^2*mu*epsilonf-beta^2))^(1/2))+1/2*i*omega*mu*
M(1/2*((mu*(omega^2*ef*kappa^2-(omega^2*mu*epsilonf-beta^2)*mu))^(1/2)+beta*kappa)/
(mu*(omega^2*ef*kappa^2-(omega^2*mu*epsilonf-beta^2)*mu))^(1/2)+1,1,
2*b*((omega^2*ef*kappa^2-(omega^2*mu*epsilonf-beta^2)*mu)/mu)^(1/2))/
(exp(b*(omega^2*ef*kappa^2/mu-(omega^2*mu*epsilonf-beta^2))^(1/2))*b)+1/2*i*omega*mu*
M(1/2*((mu*(omega^2*ef*kappa^2-(omega^2*mu*epsilonf-beta^2)*mu))^(1/2)+beta*kappa)/
(mu*(omega^2*ef*kappa^2-(omega^2*mu*epsilonf-beta^2)*mu))^(1/2)+1,1,
2*b*((omega^2*ef*kappa^2-(omega^2*mu*epsilonf-beta^2)*mu)/mu)^(1/2))*beta*kappa/
(exp(b*(omega^2*ef*kappa^2/mu-(omega^2*mu*epsilonf-beta^2))^(1/2))*
(mu*omega^2*ef*kappa^2-(omega^2*mu*epsilonf-beta^2)*mu^2)^(1/2)*b)-1/2*i*omega*mu*
M(1/2*((mu*(omega^2*ef*kappa^2-(omega^2*mu*epsilonf-beta^2)*mu))^(1/2)+beta*kappa)/
(mu*(omega^2*ef*kappa^2-(omega^2*mu*epsilonf-beta^2)*mu))^(1/2),1,
2*b*((omega^2*ef*kappa^2-(omega^2*mu*epsilonf-beta^2)*mu)/mu)^(1/2))/
(exp(b*(omega^2*ef*kappa^2/mu-(omega^2*mu*epsilonf-beta^2))^(1/2))*b)-1/2*i*omega*mu*
M(1/2*((mu*(omega^2*ef*kappa^2-(omega^2*mu*epsilonf-beta^2)*mu))^(1/2)+beta*kappa)/
(mu*(omega^2*ef*kappa^2-(omega^2*mu*epsilonf-beta^2)*mu))^(1/2),1,
2*b*((omega^2*ef*kappa^2-(omega^2*mu*epsilonf-beta^2)*mu)/mu)^(1/2))*beta*kappa/
(exp(b*(omega^2*ef*kappa^2/mu-(omega^2*mu*epsilonf-beta^2))^(1/2))*
(mu*omega^2*ef*kappa^2-(omega^2*mu*epsilonf-beta^2)*mu^2)^(1/2)*b)-i*omega*kappa*beta*
M(1/2*((mu*(omega^2*ef*kappa^2-(omega^2*mu*epsilonf-beta^2)*mu))^(1/2)+beta*kappa)/
```

```
(mu*(omega^2*ef*kappa^2-(omega^2*mu*epsilonf-beta^2)*mu))^(1/2),1,
2*b*((omega^2*ef*kappa^2-(omega^2*mu*epsilonf-beta^2)*mu)/mu)^(1/2))/
exp(b*(omega^2*ef*kappa^2/mu-(omega^2*mu*epsilonf-beta^2))^(1/2)))/
(omega^2*mu*epsilonf-beta^2);
```

```
Et31c=(-i*omega*mu*(omega^2*ef*kappa^2/mu-(omega^2*mu*epsilonf-beta^2))^(1/2)*
M(1/2*((mu*(omega^2*ef*kappa^2-(omega^2*mu*epsilonf-beta^2)*mu))^(1/2)+beta*kappa)/
(mu*(omega^2*ef*kappa^2-(omega^2*mu*epsilonf-beta^2)*mu))^(1/2),1,
2*c*((omega^2*ef*kappa^2-(omega^2*mu*epsilonf-beta^2)*mu)/mu)^(1/2))/
exp(c*(omega^2*ef*kappa^2/mu-(omega^2*mu*epsilonf-beta^2))^(1/2))+1/2*i*omega*mu*
M(1/2*((mu*(omega^2*ef*kappa^2-(omega^2*mu*epsilonf-beta^2)*mu))^(1/2)+beta*kappa)/
(mu*(omega^2*ef*kappa^2-(omega^2*mu*epsilonf-beta^2)*mu))^(1/2)+1,1,
2*c*((omega^2*ef*kappa^2-(omega^2*mu*epsilonf-beta^2)*mu)/mu)^(1/2))/
(exp(c*(omega^2*ef*kappa^2/mu-(omega^2*mu*epsilonf-beta^2))^(1/2))*c)+1/2*i*omega*mu*
M(1/2*((mu*(omega^2*ef*kappa^2-(omega^2*mu*epsilonf-beta^2)*mu))^(1/2)+beta*kappa)/
(mu*(omega^2*ef*kappa^2-(omega^2*mu*epsilonf-beta^2)*mu))^(1/2)+1,1,
2*c*((omega^2*ef*kappa^2-(omega^2*mu*epsilonf-beta^2)*mu)/mu)^(1/2))*beta*kappa/
(exp(c*(omega^2*ef*kappa^2/mu-(omega^2*mu*epsilonf-beta^2))^(1/2))*
(mu*omega^2*ef*kappa^2-(omega^2*mu*epsilonf-beta^2)*mu^2)^(1/2)*c)-1/2*i*omega*mu*
M(1/2*((mu*(omega^2*ef*kappa^2-(omega^2*mu*epsilonf-beta^2)*mu))^(1/2)+beta*kappa)/
(mu*(omega^2*ef*kappa^2-(omega^2*mu*epsilonf-beta^2)*mu))^(1/2),1,
2*c*((omega^2*ef*kappa^2-(omega^2*mu*epsilonf-beta^2)*mu)/mu)^(1/2))/
(exp(c*(omega^2*ef*kappa^2/mu-(omega^2*mu*epsilonf-beta^2))^(1/2))*c)-1/2*i*omega*mu*
M(1/2*((mu*(omega^2*ef*kappa^2-(omega^2*mu*epsilonf-beta^2)*mu))^(1/2)+beta*kappa)/
(mu*(omega^2*ef*kappa^2-(omega^2*mu*epsilonf-beta^2)*mu))^(1/2),1,
2*c*((omega^2*ef*kappa^2-(omega^2*mu*epsilonf-beta^2)*mu)/mu)^(1/2))*beta*kappa/
(exp(c*(omega^2*ef*kappa^2/mu-(omega^2*mu*epsilonf-beta^2))^(1/2))*
(mu*omega^2*ef*kappa^2-(omega^2*mu*epsilonf-beta^2)*mu^2)^(1/2)*c)-i*omega*kappa*beta*
M(1/2*((mu*(omega^2*ef*kappa^2-(omega^2*mu*epsilonf-beta^2)*mu))^(1/2)+beta*kappa)/
```

```
(mu*(omega^2*ef*kappa^2-(omega^2*mu*epsilonf-beta^2)*mu))^(1/2),1,
2*c*((omega^2*ef*kappa^2-(omega^2*mu*epsilonf-beta^2)*mu)/mu)^(1/2))/
exp(c*(omega^2*ef*kappa^2/mu-(omega^2*mu*epsilonf-beta^2))^(1/2)))/
(omega^2*mu*epsilonf-beta^2);
```

```
Et32b=(-i*omega*mu*(omega^2*ef*kappa^2/mu-(omega^2*mu*epsilonf-beta^2))^(1/2)*
U(1/2*((mu*(omega^2*ef*kappa^2-(omega^2*mu*epsilonf-beta^2)*mu))^(1/2)+beta*kappa)/
(mu*(omega^2*ef*kappa^2-(omega^2*mu*epsilonf-beta^2)*mu))^(1/2),1,
2*b*((omega^2*ef*kappa^2-(omega^2*mu*epsilonf-beta^2)*mu)/mu)^(1/2))/
exp(b*(omega^2*ef*kappa^2/mu-(omega^2*mu*epsilonf-beta^2))^(1/2))+1/4*i*omega*mu*
U(1/2*((mu*(omega^2*ef*kappa^2-(omega^2*mu*epsilonf-beta^2)*mu))^(1/2)+beta*kappa)/
(mu*(omega^2*ef*kappa^2-(omega^2*mu*epsilonf-beta^2)*mu))^(1/2)+1,1,
2*b*((omega^2*ef*kappa^2-(omega^2*mu*epsilonf-beta^2)*mu)/mu)^(1/2))/
(exp(b*(omega^2*ef*kappa^2/mu-(omega^2*mu*epsilonf-beta^2))^(1/2))*b)+1/2*i*omega*mu*
U(1/2*((mu*(omega^2*ef*kappa^2-(omega^2*mu*epsilonf-beta^2)*mu))^(1/2)+beta*kappa)/
(mu*(omega^2*ef*kappa^2-(omega^2*mu*epsilonf-beta^2)*mu))^(1/2)+1,1,
2*b*((omega^2*ef*kappa^2-(omega^2*mu*epsilonf-beta^2)*mu)/mu)^(1/2))*beta*kappa/
(exp(b*(omega^2*ef*kappa^2/mu-(omega^2*mu*epsilonf-beta^2))^(1/2))*
(mu*omega^2*ef*kappa^2-(omega^2*mu*epsilonf-beta^2)*mu^2)^(1/2)*b)+1/4*i*omega*mu*
U(1/2*((mu*(omega^2*ef*kappa^2-(omega^2*mu*epsilonf-beta^2)*mu))^(1/2)+beta*kappa)/
(mu*(omega^2*ef*kappa^2-(omega^2*mu*epsilonf-beta^2)*mu))^(1/2)+1,1,
2*b*((omega^2*ef*kappa^2-(omega^2*mu*epsilonf-beta^2)*mu)/mu)^(1/2))*beta^2*kappa^2/
(exp(b*(omega^2*ef*kappa^2/mu-(omega^2*mu*epsilonf-beta^2))^(1/2))*
(mu*omega^2*ef*kappa^2-(omega^2*mu*epsilonf-beta^2)*mu^2)*b)-1/2*i*omega*mu*
U(1/2*((mu*(omega^2*ef*kappa^2-(omega^2*mu*epsilonf-beta^2)*mu))^(1/2)+beta*kappa)/
(mu*(omega^2*ef*kappa^2-(omega^2*mu*epsilonf-beta^2)*mu))^(1/2),1,
2*b*((omega^2*ef*kappa^2-(omega^2*mu*epsilonf-beta^2)*mu)/mu)^(1/2))/
(exp(b*(omega^2*ef*kappa^2/mu-(omega^2*mu*epsilonf-beta^2))^(1/2))*b)-1/2*i*omega*mu*
U(1/2*((mu*(omega^2*ef*kappa^2-(omega^2*mu*epsilonf-beta^2)*mu))^(1/2)+beta*kappa)/
```

```
(mu*(omega^2*ef*kappa^2-(omega^2*mu*epsilonf-beta^2)*mu))^(1/2),1,
2*b*((omega^2*ef*kappa^2-(omega^2*mu*epsilonf-beta^2)*mu)/mu)^(1/2))*beta*kappa/
(exp(b*(omega^2*ef*kappa^2/mu-(omega^2*mu*epsilonf-beta^2))^(1/2))*
(mu*omega^2*ef*kappa^2-(omega^2*mu*epsilonf-beta^2)*mu^2)^(1/2)*b)-i*omega*kappa*beta*
U(1/2*((mu*(omega^2*ef*kappa^2-(omega^2*mu*epsilonf-beta^2)*mu))^(1/2)+beta*kappa)/
(mu*(omega^2*ef*kappa^2-(omega^2*mu*epsilonf-beta^2)*mu))^(1/2),1,
2*b*((omega^2*ef*kappa^2-(omega^2*mu*epsilonf-beta^2)*mu)/mu)^(1/2))/
exp(b*(omega^2*ef*kappa^2/mu-(omega^2*mu*epsilonf-beta^2))^(1/2)))/
(omega^2*mu*epsilonf-beta^2);
```

```
Et32c=(-i*omega*mu*(omega^2*ef*kappa^2/mu-(omega^2*mu*epsilonf-beta^2))^(1/2)*
U(1/2*((mu*(omega^2*ef*kappa^2-(omega^2*mu*epsilonf-beta^2)*mu))^(1/2)+beta*kappa)/
(mu*(omega^2*ef*kappa^2-(omega^2*mu*epsilonf-beta^2)*mu))^(1/2),1,
2*c*((omega^2*ef*kappa^2-(omega^2*mu*epsilonf-beta^2)*mu)/mu)^(1/2))/
exp(c*(omega^2*ef*kappa^2/mu-(omega^2*mu*epsilonf-beta^2))^(1/2))+1/4*i*omega*mu*
U(1/2*((mu*(omega^2*ef*kappa^2-(omega^2*mu*epsilonf-beta^2)*mu))^(1/2)+beta*kappa)/
(mu*(omega^2*ef*kappa^2-(omega^2*mu*epsilonf-beta^2)*mu))^(1/2)+1,1,
2*c*((omega^2*ef*kappa^2-(omega^2*mu*epsilonf-beta^2)*mu)/mu)^(1/2))/
(exp(c*(omega^2*ef*kappa^2/mu-(omega^2*mu*epsilonf-beta^2))^(1/2))*c)+1/2*i*omega*mu*
U(1/2*((mu*(omega^2*ef*kappa^2-(omega^2*mu*epsilonf-beta^2)*mu))^(1/2)+beta*kappa)/
(mu*(omega^2*ef*kappa^2-(omega^2*mu*epsilonf-beta^2)*mu))^(1/2)+1,1,
2*c*((omega^2*ef*kappa^2-(omega^2*mu*epsilonf-beta^2)*mu)/mu)^(1/2))*beta*kappa/
(exp(c*(omega^2*ef*kappa^2/mu-(omega^2*mu*epsilonf-beta^2))^(1/2))*
(mu*omega^2*ef*kappa^2-(omega^2*mu*epsilonf-beta^2)*mu^2)^(1/2)*c)+1/4*i*omega*mu*
U(1/2*((mu*(omega^2*ef*kappa^2-(omega^2*mu*epsilonf-beta^2)*mu))^(1/2)+beta*kappa)/
(mu*(omega^2*ef*kappa^2-(omega^2*mu*epsilonf-beta^2)*mu))^(1/2)+1,1,
2*c*((omega^2*ef*kappa^2-(omega^2*mu*epsilonf-beta^2)*mu)/mu)^(1/2))*beta^2*kappa^2/
(exp(c*(omega^2*ef*kappa^2/mu-(omega^2*mu*epsilonf-beta^2))^(1/2))*
(mu*omega^2*ef*kappa^2-(omega^2*mu*epsilonf-beta^2)*mu^2)*c)-1/2*i*omega*mu*
U(1/2*((mu*(omega^2*ef*kappa^2-(omega^2*mu*epsilonf-beta^2)*mu))^(1/2)+beta*kappa)/
(mu*(omega^2*ef*kappa^2-(omega^2*mu*epsilonf-beta^2)*mu))^(1/2),1,
2*c*((omega^2*ef*kappa^2-(omega^2*mu*epsilonf-beta^2)*mu)/mu)^(1/2))/
(exp(c*(omega^2*ef*kappa^2/mu-(omega^2*mu*epsilonf-beta^2))^(1/2))*c)-1/2*i*omega*mu*
U(1/2*((mu*(omega^2*ef*kappa^2-(omega^2*mu*epsilonf-beta^2)*mu))^(1/2)+beta*kappa)/
```

```
(mu*(omega^2*ef*kappa^2-(omega^2*mu*epsilonf-beta^2)*mu))^(1/2),1,
2*c*((omega^2*ef*kappa^2-(omega^2*mu*epsilonf-beta^2)*mu)/mu)^(1/2))*beta*kappa/
(exp(c*(omega^2*ef*kappa^2/mu-(omega^2*mu*epsilonf-beta^2))^(1/2))*
(mu*omega^2*ef*kappa^2-(omega^2*mu*epsilonf-beta^2)*mu^2)^(1/2)*c)-i*omega*kappa*beta*
U(1/2*((mu*(omega^2*ef*kappa^2-(omega^2*mu*epsilonf-beta^2)*mu))^(1/2)+beta*kappa)/
(mu*(omega^2*ef*kappa^2-(omega^2*mu*epsilonf-beta^2)*mu))^(1/2),1,
2*c*((omega^2*ef*kappa^2-(omega^2*mu*epsilonf-beta^2)*mu)/mu)^(1/2))/
exp(c*(omega^2*ef*kappa^2/mu-(omega^2*mu*epsilonf-beta^2))^(1/2)))/
(omega^2*mu*epsilonf-beta^2);
```

```
A=zeros(14);


A(1,1)= I(0,sqrt(beta^2-beta0^2)*a)*T;

A(1,8)=-i*omega*mu0*I(1,sqrt(beta^2-omega^2*e0*mu0)*a)/sqrt(beta^2-omega^2*e0*mu0);;


A(2,2)=I(0,sqrt(beta^2-beta0^2)*a)*T;

A(2,5)=K(0,sqrt(beta^2-beta0^2)*a)*T;

A(2,9)=-i*omega*mu0/(beta^2-beta0^2)^(1/2)*I(1,(beta^2-beta0^2)^(1/2)*a);

A(2,12)=omega*mu0/(beta^2-beta0^2)^(1/2)*K(1,(beta^2-beta0^2)^(1/2)*a)*i;


A(3,1)=I(0,sqrt(beta^2-beta0^2)*a);

A(3,2)=-I(0,sqrt(beta^2-beta0^2)*a);

A(3,5)=-K(0,sqrt(beta^2-beta0^2)*a);

A(3,8)=i*omega*mu0*I(1,sqrt(beta^2-omega^2*e0*mu0)*a)/sqrt(beta^2-omega^2*e0*mu0)*T;

A(3,9)=-i*omega*mu0/(beta^2-beta0^2)^(1/2)*I(1,(beta^2-beta0^2)^(1/2)*a)*T;

A(3,12)=(omega*mu0/(beta^2-beta0^2)^(1/2)*K(1,(beta^2-beta0^2)^(1/2)*a)*i)*T;


A(4,1)=-i*omega*e0*I(1,(beta^2-omega^2*mu0*e0)^(1/2)*a)*(beta^2-omega^2*mu0*e0)^(1/2)/

(-beta^2+omega^2*mu0*e0);

A(4,2)=-(-i*omega*e0*sqrt(beta^2-beta0^2)*I(1,sqrt(beta^2-beta0^2)*a)/(-beta^2+beta0^2));

A(4,5)=-(i*omega*e0*sqrt(beta^2-beta0^2)*K(1,sqrt(beta^2-beta0^2)*a)/(-beta^2+beta0^2));

A(4,8)=I(0,sqrt(beta^2-beta0^2)*a)*T;

A(4,9)=-I(0,sqrt(beta^2-beta0^2)*a)*T;

A(4,12)=-K(0,sqrt(beta^2-beta0^2)*a)*T;
```

```
% Ez2

A(5,2)=I(0,sqrt(beta^2-beta0^2)*b);

A(5,5)=K(0,sqrt(beta^2-beta0^2)*b);

% -Ez3

A(5,3)=-I(0,sqrt(beta^2-omega^2*ef*mu0)*b);

A(5,6)=-K(0,sqrt(beta^2-omega^2*ef*mu0)*b);

% Etheta 2

A(6,9)=-i*omega*mu0/(beta^2-beta0^2)^(1/2)*I(1,(beta^2-beta0^2)^(1/2)*b);

A(6,12)=i*omega*mu0/(beta^2-beta0^2)^(1/2)*K(1,(beta^2-beta0^2)^(1/2)*b);

% -Etheta 3

A(6,10)=-Et31b;

A(6,13)=-Et32b;

% Hz2

A(7,9)=I(0,sqrt(beta^2-beta0^2)*b);

A(7,12)=K(0,sqrt(beta^2-beta0^2)*b);

% -Hz3

A(7,10)=-Hz31b; A(7,13)=-Hz32b;
```

```
% Htheta 2
A(8,2)=(-i*omega*e0*sqrt(beta^2-beta0^2)*I(1,sqrt(beta^2-beta0^2)*b)/
(beta0^2)-beta^2);
A(8,5)=(i*omega*e0*sqrt(beta^2-beta0^2)*K(1,sqrt(beta^2-beta0^2)*b)/
(beta0^2)-beta^2);

% -Htheta 3
A(8,3)=i*omega*ef*I(1,sqrt(beta^2-omega^2*ef*mu0)*b)*sqrt(beta^2-omega^2*ef*mu0)/
(omega^2*ef*mu0-beta^2);
A(8,6)=-i*omega*ef*K(1,sqrt(beta^2-omega^2*ef*mu0)*b)*sqrt(beta^2-omega^2*ef*mu0)/
(omega^2*ef*mu0-beta^2);

% Ez3
A(9,3)=I(0,sqrt(beta^2-omega^2*ef*mu0)*c);
A(9,6)=K(0,sqrt(beta^2-omega^2*ef*mu0)*c);
% -Ez4
A(9,4)=-I(0,sqrt(beta^2-beta0^2)*c);
A(9,7)=-K(0,sqrt(beta^2-beta0^2)*c);

% Etheta3
A(10,10)=Et31c; A(10,13)=Et32c;
% -Etheta4
A(10,11)=-(-i*omega*mu0/(beta^2-beta0^2)^(1/2)*I(1,(beta^2-beta0^2)^(1/2)*c));
A(10,14)=-(i*omega*mu0/(beta^2-beta0^2)^(1/2)*K(1,(beta^2-beta0^2)^(1/2)*c));
```

```
% Hz3

A(11,10)=Hz31c; A(11,13)=Hz32c;

% -Hz4

A(11,11)=-I(0,sqrt(beta^2-beta0^2)*c);

A(11,14)=-K(0,sqrt(beta^2-beta0^2)*c);


% Htheta3

A(12,3)=-i*omega*ef*I(1,sqrt(beta^2-omega^2*ef*mu0)*c)*sqrt(beta^2-omega^2*ef*mu0)/

(omega^2*ef*mu0-beta^2);

A(12,6)=i*omega*ef*K(1,sqrt(beta^2-omega^2*ef*mu0)*c)*sqrt(beta^2-omega^2*ef*mu0)/

(omega^2*ef*mu0-beta^2);


% -Htheta4

A(12,4)=-(-i*omega*e0*sqrt(beta^2-beta0^2)*I(1,sqrt(beta^2-beta0^2)*c)/(beta0^2-beta^2));

A(12,7)=-(i*omega*e0*sqrt(beta^2-beta0^2)*K(1,sqrt(beta^2-beta0^2)*c)/(beta0^2-beta^2));


A(13,4)=I(0,sqrt(beta^2-beta0^2)*d);

A(13,7)=K(0,sqrt(beta^2-beta0^2)*d);

A(14,11)=I(1,sqrt(beta^2-beta0^2)*d);

A(14,14)=-K(1,sqrt(beta^2-beta0^2)*d);


complete=(det(A));

return;
```

```
function I = I(x,y);

I = mfun('BesselI',x,y);

return;


function K = K(x,y);

K = mfun('BesselK',x,y);

return;


function M = M(x,y,z);

M = mfun('KummerM',x,y,z);

return;


function U = U(x,y,z);

U = mfun('KummerU',x,y,z);

return;
```

The determinant in the above case consisted of a purely imaginary number. By taking the imaginary component of determinant, a $\beta$ value satisfying the equation

$$f(\beta) = 0$$

is sought. An iterative method that was used to obtain an increased accuracy in $\beta$ was the bisection method[2]. A MATLAB code for the bisection method is given below.

```
% Let dp = number of decimal points of solution of f(x)=0
% Let a and b be the interval containing a root of f(x)=0


while round(a*10^dp)~=round(b*10^dp)
   c=(a+b)/2;
   if f(a)*f(c)<0, b=c; end;
   if f(b)*f(c)<0, a=c; end;
end;
```

### D.1.2 Complex-Valued Propagation Constant

The case dealing with complex-valued values of $\mu$ and $\varepsilon$ has a separate MATLAB code. This code gave a complex-valued propagation constant. The iterative method that was used to increase the accuracy of the answers generated was Newton's Method[3].

[2]The bisection method was introduced in chapter 2

[3]Newton's Method was explained in chapter 2

```
function complete = fci;

x=;

y=;


for it=1:5

J=[dfx(x,y),dfy(x,y);dgx(x,y),dgy(x,y)];


H=-inv(J)*[f(x,y);g(x,y)];

x=x+H(1);

y=y+H(2);


disp(['At iteration' num2str(it)])

x

y

end;


comp=1;


return;
```

```
function out = dfx(x,y)

h=10^(-2);  out=(f(x+h,y)-f(x,y))/(h);

return


function out = dfy(x,y)

k=10^(-2);  out=(f(x,y+k)-f(x,y))/(k);

return


function out = dgx(x,y)

h=10^(-2);  out=(g(x+h,y)-g(x,y))/(h);

return


function out = dgy(x,y)

k=10^(-2);  out=(g(x,y+k)-g(x,y))/(k);

return


function f=f(x,y)

f=real(sk2(x+y*i));

return;


function g=g(x,y)

g=imag(sk2(x+y*i));

return;
```

```
function complete = sk2(beta);

i=sqrt(-1);

a=1.465/1000;

b=1.59/1000;

c=2.92/1000;

d=c+(10^(-6));

psi=9.5*pi/180;

T=tan(psi);

omega=2*pi*freq*10^9;


mu0=4*pi*10^(-7);

e0=8.854188*10^(-12);

beta0=omega*sqrt(mu0*e0);


gamma=2.21*10^(5); Ms=0.068; H=55000;

kappa=gamma*omega*Ms/(omega^2-gamma^2*H^2);

mu=mu0+(gamma^2*H*Ms)/(gamma^2*H^2-omega^2); ef=14.5*e0;

mu=mu*(1+i/1000); ef=ef*(1+i/1000); er=1; epsilonf=ef;
```

```
Hz31b=exp(-(-(omega^2*mu*epsilonf-beta^2)*mu+omega^2*ef*kappa^2)^(1/2)/mu^(1/2)*b)*
M(1/2*((-(omega^2*mu*epsilonf-beta^2)*mu+omega^2*ef*kappa^2)^(1/2)*mu^(1/2)+beta*kappa)/
(-(omega^2*mu*epsilonf-beta^2)*mu+omega^2*ef*kappa^2)^(1/2)/mu^(1/2),1,
2*(-(omega^2*mu*epsilonf-beta^2)*mu+omega^2*ef*kappa^2)^(1/2)/mu^(1/2)*b);

Hz31c=exp(-(-(omega^2*mu*epsilonf-beta^2)*mu+omega^2*ef*kappa^2)^(1/2)/mu^(1/2)*c)*
M(1/2*((-(omega^2*mu*epsilonf-beta^2)*mu+omega^2*ef*kappa^2)^(1/2)*mu^(1/2)+beta*kappa)/
(-(omega^2*mu*epsilonf-beta^2)*mu+omega^2*ef*kappa^2)^(1/2)/mu^(1/2),1,
2*(-(omega^2*mu*epsilonf-beta^2)*mu+omega^2*ef*kappa^2)^(1/2)/mu^(1/2)*c);

Hz32b=exp(-(-(omega^2*mu*epsilonf-beta^2)*mu+omega^2*ef*kappa^2)^(1/2)/mu^(1/2)*b)*
U(1/2*((-(omega^2*mu*epsilonf-beta^2)*mu+omega^2*ef*kappa^2)^(1/2)*mu^(1/2)+beta*kappa)/
(-(omega^2*mu*epsilonf-beta^2)*mu+omega^2*ef*kappa^2)^(1/2)/mu^(1/2),1,
2*(-(omega^2*mu*epsilonf-beta^2)*mu+omega^2*ef*kappa^2)^(1/2)/mu^(1/2)*b);

Hz32c=exp(-(-(omega^2*mu*epsilonf-beta^2)*mu+omega^2*ef*kappa^2)^(1/2)/mu^(1/2)*c)*
U(1/2*((-(omega^2*mu*epsilonf-beta^2)*mu+omega^2*ef*kappa^2)^(1/2)*mu^(1/2)+beta*kappa)/
(-(omega^2*mu*epsilonf-beta^2)*mu+omega^2*ef*kappa^2)^(1/2)/mu^(1/2),1,
2*(-(omega^2*mu*epsilonf-beta^2)*mu+omega^2*ef*kappa^2)^(1/2)/mu^(1/2)*c);
```

```
Et31b=(-i*omega*mu*(omega^2*ef*kappa^2/mu-(omega^2*mu*epsilonf-beta^2))^(1/2)*
M(1/2*((mu*(omega^2*ef*kappa^2-(omega^2*mu*epsilonf-beta^2)*mu))^(1/2)+beta*kappa)/
(mu*(omega^2*ef*kappa^2-(omega^2*mu*epsilonf-beta^2)*mu))^(1/2),1,
2*b*((omega^2*ef*kappa^2-(omega^2*mu*epsilonf-beta^2)*mu)/mu)^(1/2))/
exp(b*(omega^2*ef*kappa^2/mu-(omega^2*mu*epsilonf-beta^2))^(1/2))+1/2*i*omega*mu*
M(1/2*((mu*(omega^2*ef*kappa^2-(omega^2*mu*epsilonf-beta^2)*mu))^(1/2)+beta*kappa)/
(mu*(omega^2*ef*kappa^2-(omega^2*mu*epsilonf-beta^2)*mu))^(1/2)+1,1,
2*b*((omega^2*ef*kappa^2-(omega^2*mu*epsilonf-beta^2)*mu)/mu)^(1/2))/
(exp(b*(omega^2*ef*kappa^2/mu-(omega^2*mu*epsilonf-beta^2))^(1/2))*b)+1/2*i*omega*mu*
M(1/2*((mu*(omega^2*ef*kappa^2-(omega^2*mu*epsilonf-beta^2)*mu))^(1/2)+beta*kappa)/
(mu*(omega^2*ef*kappa^2-(omega^2*mu*epsilonf-beta^2)*mu))^(1/2)+1,1,
2*b*((omega^2*ef*kappa^2-(omega^2*mu*epsilonf-beta^2)*mu)/mu)^(1/2))*beta*kappa/
(exp(b*(omega^2*ef*kappa^2/mu-(omega^2*mu*epsilonf-beta^2))^(1/2))*
(mu*omega^2*ef*kappa^2-(omega^2*mu*epsilonf-beta^2)*mu^2)^(1/2)*b)-1/2*i*omega*mu*
M(1/2*((mu*(omega^2*ef*kappa^2-(omega^2*mu*epsilonf-beta^2)*mu))^(1/2)+beta*kappa)/
(mu*(omega^2*ef*kappa^2-(omega^2*mu*epsilonf-beta^2)*mu))^(1/2),1,
2*b*((omega^2*ef*kappa^2-(omega^2*mu*epsilonf-beta^2)*mu)/mu)^(1/2))/
(exp(b*(omega^2*ef*kappa^2/mu-(omega^2*mu*epsilonf-beta^2))^(1/2))*b)-1/2*i*omega*mu*
M(1/2*((mu*(omega^2*ef*kappa^2-(omega^2*mu*epsilonf-beta^2)*mu))^(1/2)+beta*kappa)/
(mu*(omega^2*ef*kappa^2-(omega^2*mu*epsilonf-beta^2)*mu))^(1/2),1,
2*b*((omega^2*ef*kappa^2-(omega^2*mu*epsilonf-beta^2)*mu)/mu)^(1/2))*beta*kappa/
(exp(b*(omega^2*ef*kappa^2/mu-(omega^2*mu*epsilonf-beta^2))^(1/2))*
(mu*omega^2*ef*kappa^2-(omega^2*mu*epsilonf-beta^2)*mu^2)^(1/2)*b)-i*omega*kappa*beta*
M(1/2*((mu*(omega^2*ef*kappa^2-(omega^2*mu*epsilonf-beta^2)*mu))^(1/2)+beta*kappa)/
(mu*(omega^2*ef*kappa^2-(omega^2*mu*epsilonf-beta^2)*mu))^(1/2),1,
```

```
2*b*((omega^2*ef*kappa^2-(omega^2*mu*epsilonf-beta^2)*mu)/mu)^(1/2))/
exp(b*(omega^2*ef*kappa^2/mu-(omega^2*mu*epsilonf-beta^2))^(1/2)))/
(omega^2*mu*epsilonf-beta^2);
```

```
Et31c=(-i*omega*mu*(omega^2*ef*kappa^2/mu-(omega^2*mu*epsilonf-beta^2))^(1/2)*
M(1/2*((mu*(omega^2*ef*kappa^2-(omega^2*mu*epsilonf-beta^2)*mu))^(1/2)+beta*kappa)/
(mu*(omega^2*ef*kappa^2-(omega^2*mu*epsilonf-beta^2)*mu))^(1/2),1,
2*c*((omega^2*ef*kappa^2-(omega^2*mu*epsilonf-beta^2)*mu)/mu)^(1/2))/
exp(c*(omega^2*ef*kappa^2/mu-(omega^2*mu*epsilonf-beta^2))^(1/2))+1/2*i*omega*mu*
M(1/2*((mu*(omega^2*ef*kappa^2-(omega^2*mu*epsilonf-beta^2)*mu))^(1/2)+beta*kappa)/
(mu*(omega^2*ef*kappa^2-(omega^2*mu*epsilonf-beta^2)*mu))^(1/2)+1,1,
2*c*((omega^2*ef*kappa^2-(omega^2*mu*epsilonf-beta^2)*mu)/mu)^(1/2))/
(exp(c*(omega^2*ef*kappa^2/mu-(omega^2*mu*epsilonf-beta^2))^(1/2))*c)+1/2*i*omega*mu*
M(1/2*((mu*(omega^2*ef*kappa^2-(omega^2*mu*epsilonf-beta^2)*mu))^(1/2)+beta*kappa)/
(mu*(omega^2*ef*kappa^2-(omega^2*mu*epsilonf-beta^2)*mu))^(1/2)+1,1,
2*c*((omega^2*ef*kappa^2-(omega^2*mu*epsilonf-beta^2)*mu)/mu)^(1/2))*beta*kappa/
(exp(c*(omega^2*ef*kappa^2/mu-(omega^2*mu*epsilonf-beta^2))^(1/2))*
(mu*omega^2*ef*kappa^2-(omega^2*mu*epsilonf-beta^2)*mu^2)^(1/2)*c)-1/2*i*omega*mu*
M(1/2*((mu*(omega^2*ef*kappa^2-(omega^2*mu*epsilonf-beta^2)*mu))^(1/2)+beta*kappa)/
(mu*(omega^2*ef*kappa^2-(omega^2*mu*epsilonf-beta^2)*mu))^(1/2),1,
2*c*((omega^2*ef*kappa^2-(omega^2*mu*epsilonf-beta^2)*mu)/mu)^(1/2))/
(exp(c*(omega^2*ef*kappa^2/mu-(omega^2*mu*epsilonf-beta^2))^(1/2))*c)-1/2*i*omega*mu*
M(1/2*((mu*(omega^2*ef*kappa^2-(omega^2*mu*epsilonf-beta^2)*mu))^(1/2)+beta*kappa)/
(mu*(omega^2*ef*kappa^2-(omega^2*mu*epsilonf-beta^2)*mu))^(1/2),1,
2*c*((omega^2*ef*kappa^2-(omega^2*mu*epsilonf-beta^2)*mu)/mu)^(1/2))*beta*kappa/
(exp(c*(omega^2*ef*kappa^2/mu-(omega^2*mu*epsilonf-beta^2))^(1/2))*
(mu*omega^2*ef*kappa^2-(omega^2*mu*epsilonf-beta^2)*mu^2)^(1/2)*c)-i*omega*kappa*beta*
M(1/2*((mu*(omega^2*ef*kappa^2-(omega^2*mu*epsilonf-beta^2)*mu))^(1/2)+beta*kappa)/
(mu*(omega^2*ef*kappa^2-(omega^2*mu*epsilonf-beta^2)*mu))^(1/2),1,
```

```
2*c*((omega^2*ef*kappa^2-(omega^2*mu*epsilonf-beta^2)*mu)/mu)^(1/2))/
exp(c*(omega^2*ef*kappa^2/mu-(omega^2*mu*epsilonf-beta^2))^(1/2)))/
(omega^2*mu*epsilonf-beta^2);
```

```
Et32b=(-i*omega*mu*(omega^2*ef*kappa^2/mu-(omega^2*mu*epsilonf-beta^2))^(1/2)*
U(1/2*((mu*(omega^2*ef*kappa^2-(omega^2*mu*epsilonf-beta^2)*mu))^(1/2)+beta*kappa)/
(mu*(omega^2*ef*kappa^2-(omega^2*mu*epsilonf-beta^2)*mu))^(1/2),1,
2*b*((omega^2*ef*kappa^2-(omega^2*mu*epsilonf-beta^2)*mu)/mu)^(1/2))/
exp(b*(omega^2*ef*kappa^2/mu-(omega^2*mu*epsilonf-beta^2))^(1/2))+1/4*i*omega*mu*
U(1/2*((mu*(omega^2*ef*kappa^2-(omega^2*mu*epsilonf-beta^2)*mu))^(1/2)+beta*kappa)/
(mu*(omega^2*ef*kappa^2-(omega^2*mu*epsilonf-beta^2)*mu))^(1/2)+1,1,
2*b*((omega^2*ef*kappa^2-(omega^2*mu*epsilonf-beta^2)*mu)/mu)^(1/2))/
(exp(b*(omega^2*ef*kappa^2/mu-(omega^2*mu*epsilonf-beta^2))^(1/2))*b)+
1/2*i*omega*mu*U(1/2*((mu*(omega^2*ef*kappa^2-(omega^2*mu*epsilonf-beta^2)*mu))^(1/2)+
beta*kappa)/(mu*(omega^2*ef*kappa^2-(omega^2*mu*epsilonf-beta^2)*mu))^(1/2)+1,1,
2*b*((omega^2*ef*kappa^2-(omega^2*mu*epsilonf-beta^2)*mu)/mu)^(1/2))*beta*kappa/
(exp(b*(omega^2*ef*kappa^2/mu-(omega^2*mu*epsilonf-beta^2))^(1/2))*(mu*omega^2*ef*kappa^2
-(omega^2*mu*epsilonf-beta^2)*mu^2)^(1/2)*b)+1/4*i*omega*mu*
U(1/2*((mu*(omega^2*ef*kappa^2-(omega^2*mu*epsilonf-beta^2)*mu))^(1/2)+beta*kappa)/
(mu*(omega^2*ef*kappa^2-(omega^2*mu*epsilonf-beta^2)*mu))^(1/2)+1,1,
2*b*((omega^2*ef*kappa^2-(omega^2*mu*epsilonf-beta^2)*mu)/mu)^(1/2))*beta^2*kappa^2/
(exp(b*(omega^2*ef*kappa^2/mu-(omega^2*mu*epsilonf-beta^2))^(1/2))*
(mu*omega^2*ef*kappa^2-(omega^2*mu*epsilonf-beta^2)*mu^2)*b)-1/2*i*omega*mu*
U(1/2*((mu*(omega^2*ef*kappa^2-(omega^2*mu*epsilonf-beta^2)*mu))^(1/2)+beta*kappa)/
(mu*(omega^2*ef*kappa^2-(omega^2*mu*epsilonf-beta^2)*mu))^(1/2),1,
2*b*((omega^2*ef*kappa^2-(omega^2*mu*epsilonf-beta^2)*mu)/mu)^(1/2))/
(exp(b*(omega^2*ef*kappa^2/mu-(omega^2*mu*epsilonf-beta^2))^(1/2))*b)-1/2*i*omega*mu*
U(1/2*((mu*(omega^2*ef*kappa^2-(omega^2*mu*epsilonf-beta^2)*mu))^(1/2)+beta*kappa)/
```

```
(mu*(omega^2*ef*kappa^2-(omega^2*mu*epsilonf-beta^2)*mu))^(1/2),1,
2*b*((omega^2*ef*kappa^2-(omega^2*mu*epsilonf-beta^2)*mu)/mu)^(1/2))*beta*kappa/
(exp(b*(omega^2*ef*kappa^2/mu-(omega^2*mu*epsilonf-beta^2))^(1/2))*
(mu*omega^2*ef*kappa^2-(omega^2*mu*epsilonf-beta^2)*mu^2)^(1/2)*b)-i*omega*kappa*beta
*U(1/2*((mu*(omega^2*ef*kappa^2-(omega^2*mu*epsilonf-beta^2)*mu))^(1/2)+beta*kappa)/
(mu*(omega^2*ef*kappa^2-(omega^2*mu*epsilonf-beta^2)*mu))^(1/2),1,
2*b*((omega^2*ef*kappa^2-(omega^2*mu*epsilonf-beta^2)*mu)/mu)^(1/2))/
exp(b*(omega^2*ef*kappa^2/mu-(omega^2*mu*epsilonf-beta^2))^(1/2)))/
(omega^2*mu*epsilonf-beta^2);
```

```
Et32c=(-i*omega*mu*(omega^2*ef*kappa^2/mu-(omega^2*mu*epsilonf-beta^2))^(1/2)*
U(1/2*((mu*(omega^2*ef*kappa^2-(omega^2*mu*epsilonf-beta^2)*mu))^(1/2)+beta*kappa)/
(mu*(omega^2*ef*kappa^2-(omega^2*mu*epsilonf-beta^2)*mu))^(1/2),1,
2*c*((omega^2*ef*kappa^2-(omega^2*mu*epsilonf-beta^2)*mu)/mu)^(1/2))
/exp(c*(omega^2*ef*kappa^2/mu-(omega^2*mu*epsilonf-beta^2))^(1/2))+1/4*i*omega*mu*
U(1/2*((mu*(omega^2*ef*kappa^2-(omega^2*mu*epsilonf-beta^2)*mu))^(1/2)+beta*kappa)/
(mu*(omega^2*ef*kappa^2-(omega^2*mu*epsilonf-beta^2)*mu))^(1/2)+1,1,
2*c*((omega^2*ef*kappa^2-(omega^2*mu*epsilonf-beta^2)*mu)/mu)^(1/2))/
(exp(c*(omega^2*ef*kappa^2/mu-(omega^2*mu*epsilonf-beta^2))^(1/2))*c)+1/2*i*omega*mu*
U(1/2*((mu*(omega^2*ef*kappa^2-(omega^2*mu*epsilonf-beta^2)*mu))^(1/2)+beta*kappa)/
(mu*(omega^2*ef*kappa^2-(omega^2*mu*epsilonf-beta^2)*mu))^(1/2)+1,1,
2*c*((omega^2*ef*kappa^2-(omega^2*mu*epsilonf-beta^2)*mu)/mu)^(1/2))*beta*kappa/
(exp(c*(omega^2*ef*kappa^2/mu-(omega^2*mu*epsilonf-beta^2))^(1/2))*
(mu*omega^2*ef*kappa^2-(omega^2*mu*epsilonf-beta^2)*mu^2)^(1/2)*c)+1/4*i*omega*mu*
U(1/2*((mu*(omega^2*ef*kappa^2-(omega^2*mu*epsilonf-beta^2)*mu))^(1/2)+beta*kappa)/
(mu*(omega^2*ef*kappa^2-(omega^2*mu*epsilonf-beta^2)*mu))^(1/2)+1,1,
2*c*((omega^2*ef*kappa^2-(omega^2*mu*epsilonf-beta^2)*mu)/mu)^(1/2))*beta^2*kappa^2/
(exp(c*(omega^2*ef*kappa^2/mu-(omega^2*mu*epsilonf-beta^2))^(1/2))*
(mu*omega^2*ef*kappa^2-(omega^2*mu*epsilonf-beta^2)*mu^2)*c)-1/2*i*omega*mu*
U(1/2*((mu*(omega^2*ef*kappa^2-(omega^2*mu*epsilonf-beta^2)*mu))^(1/2)+beta*kappa)/
(mu*(omega^2*ef*kappa^2-(omega^2*mu*epsilonf-beta^2)*mu))^(1/2),1,
2*c*((omega^2*ef*kappa^2-(omega^2*mu*epsilonf-beta^2)*mu)/mu)^(1/2))/
(exp(c*(omega^2*ef*kappa^2/mu-(omega^2*mu*epsilonf-beta^2))^(1/2))*c)-1/2*i*omega*mu*
U(1/2*((mu*(omega^2*ef*kappa^2-(omega^2*mu*epsilonf-beta^2)*mu))^(1/2)+beta*kappa)/
(mu*(omega^2*ef*kappa^2-(omega^2*mu*epsilonf-beta^2)*mu))^(1/2),1,
```

```
2*c*((omega^2*ef*kappa^2-(omega^2*mu*epsilonf-beta^2)*mu)/mu)^(1/2))*beta*kappa/
(exp(c*(omega^2*ef*kappa^2/mu-(omega^2*mu*epsilonf-beta^2))^(1/2))*
(mu*omega^2*ef*kappa^2-(omega^2*mu*epsilonf-beta^2)*mu^2)^(1/2)*c)-i*omega*kappa*beta*
U(1/2*((mu*(omega^2*ef*kappa^2-(omega^2*mu*epsilonf-beta^2)*mu))^(1/2)+beta*kappa)/
(mu*(omega^2*ef*kappa^2-(omega^2*mu*epsilonf-beta^2)*mu))^(1/2),1,
2*c*((omega^2*ef*kappa^2-(omega^2*mu*epsilonf-beta^2)*mu)/mu)^(1/2))/
exp(c*(omega^2*ef*kappa^2/mu-(omega^2*mu*epsilonf-beta^2))^(1/2)))/
(omega^2*mu*epsilonf-beta^2);
```

```
A=zeros(14);

A(1,1)= I(0,sqrt(beta^2-beta0^2)*a)*T;

A(1,8)=-i*omega*mu0*I(1,sqrt(beta^2-omega^2*e0*mu0)*a)/sqrt(beta^2-omega^2*e0*mu0);


A(2,2)=I(0,sqrt(beta^2-beta0^2)*a)*T;

A(2,5)=K(0,sqrt(beta^2-beta0^2)*a)*T;

A(2,9)=-i*omega*mu0/(beta^2-beta0^2)^(1/2)*I(1,(beta^2-beta0^2)^(1/2)*a);

A(2,12)=omega*mu0/(beta^2-beta0^2)^(1/2)*K(1,(beta^2-beta0^2)^(1/2)*a)*i;


A(3,1)=I(0,sqrt(beta^2-beta0^2)*a);

A(3,2)=-I(0,sqrt(beta^2-beta0^2)*a);

A(3,5)=-K(0,sqrt(beta^2-beta0^2)*a);

A(3,8)=i*omega*mu0*I(1,sqrt(beta^2-omega^2*e0*mu0)*a)/sqrt(beta^2-omega^2*e0*mu0)*T;

A(3,9)=-i*omega*mu0/(beta^2-beta0^2)^(1/2)*I(1,(beta^2-beta0^2)^(1/2)*a)*T;

A(3,12)=(omega*mu0/(beta^2-beta0^2)^(1/2)*K(1,(beta^2-beta0^2)^(1/2)*a)*i)*T;


A(4,1)=-i*omega*e0*I(1,(beta^2-omega^2*mu0*e0)^(1/2)*a)*(beta^2-omega^2*mu0*e0)^(1/2)

/(omega^2*mu0*e0-beta^2);

A(4,2)=-(-i*omega*e0*sqrt(beta^2-beta0^2)*I(1,sqrt(beta^2-beta0^2)*a)/(beta0^2-beta^2));

A(4,5)=-(i*omega*e0*sqrt(beta^2-beta0^2)*K(1,sqrt(beta^2-beta0^2)*a)/(beta0^2-beta^2));

A(4,8)=I(0,sqrt(beta^2-beta0^2)*a)*T;

A(4,9)=-I(0,sqrt(beta^2-beta0^2)*a)*T;

A(4,12)=-K(0,sqrt(beta^2-beta0^2)*a)*T;
```

```
A(5,2)=I(0,sqrt(beta^2-beta0^2)*b);

A(5,5)=K(0,sqrt(beta^2-beta0^2)*b);


A(5,3)=-I(0,sqrt(beta^2-omega^2*ef*mu0)*b);

A(5,6)=-K(0,sqrt(beta^2-omega^2*ef*mu0)*b);


A(6,9)=-i*omega*mu0/(beta^2-beta0^2)^(1/2)*I(1,(beta^2-beta0^2)^(1/2)*b);

A(6,12)=i*omega*mu0/(beta^2-beta0^2)^(1/2)*K(1,(beta^2-beta0^2)^(1/2)*b);


A(6,10)=-Et31b; A(6,13)=-Et32b;


A(7,9)=I(0,sqrt(beta^2-beta0^2)*b);

A(7,12)=K(0,sqrt(beta^2-beta0^2)*b);


A(7,10)=-Hz31b; A(7,13)=-Hz32b;


A(8,2)=(-i*omega*e0*sqrt(beta^2-beta0^2)*I(1,sqrt(beta^2-beta0^2)*b)/(beta0^2-beta^2));

A(8,5)=(i*omega*e0*sqrt(beta^2-beta0^2)*K(1,sqrt(beta^2-beta0^2)*b)/(beta0^2-beta^2));


A(8,3)=i*omega*ef*I(1,sqrt(beta^2-omega^2*ef*mu0)*b)*sqrt(beta^2-omega^2*ef*mu0)/

(omega^2*ef*mu0-beta^2);

A(8,6)=-i*omega*ef*K(1,sqrt(beta^2-omega^2*ef*mu0)*b)*sqrt(beta^2-omega^2*ef*mu0)/

(omega^2*ef*mu0-beta^2);
```

```
A(9,3)=I(0,sqrt(beta^2-omega^2*ef*mu0)*c);

A(9,6)=K(0,sqrt(beta^2-omega^2*ef*mu0)*c);

A(9,4)=-I(0,sqrt(beta^2-beta0^2)*c);

A(9,7)=-K(0,sqrt(beta^2-beta0^2)*c);


A(10,10)=Et31c;

A(10,13)=Et32c;

A(10,11)=-(-i*omega*mu0/(beta^2-beta0^2)^(1/2)*I(1,(beta^2-beta0^2)^(1/2)*c));

A(10,14)=-(i*omega*mu0/(beta^2-beta0^2)^(1/2)*K(1,(beta^2-beta0^2)^(1/2)*c));


A(11,10)=Hz31c;

A(11,13)=Hz32c;

A(11,11)=-I(0,sqrt(beta^2-beta0^2)*c);

A(11,14)=-K(0,sqrt(beta^2-beta0^2)*c);


A(12,3)=-i*omega*ef*I(1,sqrt(beta^2-omega^2*ef*mu0)*c)*sqrt(beta^2-omega^2*ef*mu0)/

(omega^2*ef*mu0-beta^2);

A(12,6)=i*omega*ef*K(1,sqrt(beta^2-omega^2*ef*mu0)*c)*sqrt(beta^2-omega^2*ef*mu0)/

(omega^2*ef*mu0-beta^2);

A(12,4)=-(-i*omega*e0*sqrt(beta^2-beta0^2)*I(1,sqrt(beta^2-beta0^2)*c)/(beta0^2-beta^2));

A(12,7)=-(i*omega*e0*sqrt(beta^2-beta0^2)*K(1,sqrt(beta^2-beta0^2)*c)/(beta0^2-beta^2));
```

```
A(13,4)=I(0,sqrt(beta^2-beta0^2)*d);

A(13,7)=K(0,sqrt(beta^2-beta0^2)*d);

A(14,11)=I(1,sqrt(beta^2-beta0^2)*d);

A(14,14)=-K(1,sqrt(beta^2-beta0^2)*d);


complete=(det(A));


return;


function I = I(x,y);

I = mfun('BesselI',x,y);

return;


function K = K(x,y);

K = mfun('BesselK',x,y);

return;


function M = M(x,y,z);

M = mfun('KummerM',x,y,z);

return;


function U = U(x,y,z);

U = mfun('KummerU',x,y,z);

return;
```

## D.2 MAPLE

MAPLE was used to obtain the value of the attenuation coefficient. Richards [58] provided a comprehensive understanding of the commands that were used in this program. The code that was used is written below.

```
Ez1:= r-> BesselI(0, k*r);


Hz1:= r-> c1*BesselI(0, k*r);


Er1:= r->I*beta*BesselI(1, k*r)/k;


Hr1:= r-> c1*I*beta*BesselI(1,k*r)/k;


Et1:=r-> -I*omega*mu0*c1*BesselI(1, k*r)/k;


Ht1:=r-> I*omega*e0*BesselI(1, k*r)/k;


Ez2:= r-> a2*BesselI(0, k*r)+b2* BesselK(0, k*r);


Hz2:= r->c2*BesselI(0, k*r)+d2* BesselK(0, k*r);


Er2:= r-> I*beta*(a2*BesselI(1, k*r)-b2* BesselK(1, k*r)) /k;


Hr2:= r-> I*beta*(c2*BesselI(1, k*r)-d2* BesselK(1, k*r)) /k;
```

```
Et2:=r-> -I*omega*mu0*(c2*BesselI(1, k*r)-d2* BesselK(1, k*r))/k;

Ht2:=r-> I*omega*e0*(a2*BesselI(1, k*r)-b2* BesselK(1, k*r)) /k;

Ez4:= r-> a4*BesselI(0,k*r)+b4* BesselK(0,k*r);

Hz4:= r-> c4*BesselI(0,k*r)+d4* BesselK(0,k*r);

Er4:= r-> I*beta*(a4*BesselI(1,k*r)-b4* BesselK(1,k*r))/k;

Hr4:= r-> I*beta*(c4*BesselI(1,k*r)-d4* BesselK(1,k*r))/k;

Et4:=r-> -I*omega*mu0*(c4*BesselI(1,k*r)-d4* BesselK(1,k*r))/k;

Ht4:=r-> I*omega*e0*(a4*BesselI(1,k*r)-b4* BesselK(1,k*r))/k;
```

```
a:=1.465/1000;

b:=1.59/1000;

c:=2.92/1000;

d:=c+10^(-6);

T:=tan(9.5*evalf(Pi)/180);

mu0:= 4*evalf(Pi)*10^(-7);

mud:=mu0;e0:= 8.85*10^(-12);

ef:= 14.5*e0;

f:= 10^9;

omega:=2*evalf(Pi)*f;

beta:=;


g:=2.21*10^(5); Ms:=0.068; H:=55000;


kappa:=g*omega*Ms/(omega^2-g^2*H^2);

mu:=mu0+(g^2*H*Ms)/(g^2*H^2-omega^2);


k:=sqrt(beta^2-omega^2*e0*mu0);

kf:=sqrt(beta^2-omega^2*ef*mu0);

kc:=sqrt(beta^2-omega^2*ef*mu);


M:=(x,y,z)->evalf(KummerM(x,y,z));

U:=(x,y,z)->evalf(KummerU(x,y,z)) ;
```

```
Ez3:= r-> a3*BesselI(0,kf*r)+b3* BesselK(0,kf*r);


Er3:= r-> I*beta*(a3*BesselI(1,kf*r)-b3* BesselK(1,kf*r))/kf;

Ht3:=r-> I*omega*ef*(a3*BesselI(1,kf*r)-b3* BesselK(1,kf*r))/kf;



Hz31:=r->

exp(-(-(omega^2*mu*ef-beta^2)*mu+omega^2*ef*kappa^2)^(1/2)/mu^(1/2)*r)*

M(1/2*((-(omega^2*mu*ef-beta^2)*mu+omega^2*ef*kappa^2)^(1/2)*mu^(1/2)+beta*kappa)/

(-(omega^2*mu*ef-beta^2)*mu+omega^2*ef*kappa^2)^(1/2)/mu^(1/2),1,2*

(-(omega^2*mu*ef-beta^2)*mu+omega^2*ef*kappa^2)^(1/2)/mu^(1/2)*r);


Hz32:=r->

exp(-(-(omega^2*mu*ef-beta^2)*mu+omega^2*ef*kappa^2)^(1/2)/mu^(1/2)*r)*

U(1/2*((-(omega^2*mu*ef-beta^2)*mu+omega^2*ef*kappa^2)^(1/2)*mu^(1/2)+beta*kappa)/

(-(omega^2*mu*ef-beta^2)*mu+omega^2*ef*kappa^2)^(1/2)/mu^(1/2),1,2*

(-(omega^2*mu*ef-beta^2)*mu+omega^2*ef*kappa^2)^(1/2)/mu^(1/2)*r);


Hz3:= r-> c3*Hz31(r)+ d3*Hz32(r) ;
```

```
Et31:=b->
(-i*omega*mu*(omega^2*ef*kappa^2/mu-(omega^2*mu*ef-beta^2))^(1/2)*
M(1/2*((mu*(omega^2*ef*kappa^2-(omega^2*mu*ef-beta^2)*mu))^(1/2)+beta*kappa)/
(mu*(omega^2*ef*kappa^2-(omega^2*mu*ef-beta^2)*mu))^(1/2),1,2*b*((omega^2*ef*kappa^2
-(omega^2*mu*ef-beta^2)*mu)/mu)^(1/2))/exp(b*(omega^2*ef*kappa^2/mu-
(omega^2*mu*ef-beta^2))^(1/2))+1/2*i*omega*mu*M(1/2*((mu*(omega^2*ef*kappa^2-
(omega^2*mu*ef-beta^2)*mu))^(1/2)+beta*kappa)/(mu*(omega^2*ef*kappa^2-
(omega^2*mu*ef-beta^2)*mu))^(1/2)+1,1,2*b*((omega^2*ef*kappa^2-(omega^2*mu*ef-beta^2)
*mu)/mu)^(1/2))/(exp(b*(omega^2*ef*kappa^2/mu-(omega^2*mu*ef-beta^2))^(1/2))*b)+
1/2*i*omega*mu*M(1/2*((mu*(omega^2*ef*kappa^2-(omega^2*mu*ef-beta^2)*mu))^(1/2)+
beta*kappa)/(mu*(omega^2*ef*kappa^2-(omega^2*mu*ef-beta^2)*mu))^(1/2)+1,1,2*b*
((omega^2*ef*kappa^2-(omega^2*mu*ef-beta^2)*mu)/mu)^(1/2))*beta*kappa/
(exp(b*(omega^2*ef*kappa^2/mu-(omega^2*mu*ef-beta^2))^(1/2))*(mu*omega^2*ef*kappa^2
-(omega^2*mu*epsilonf-beta^2)*mu^2)^(1/2)*b)-1/2*i*omega*mu*M(1/2*
((mu*(omega^2*ef*kappa^2-(omega^2*mu*ef-beta^2)*mu))^(1/2)+beta*kappa)/(mu*
(omega^2*ef*kappa^2-(omega^2*mu*ef-beta^2)*mu))^(1/2),1,2*b*((omega^2*ef*kappa^2
-(omega^2*mu*ef-beta^2)*mu)/mu)^(1/2))/(exp(b*(omega^2*ef*kappa^2/mu
-(omega^2*mu*ef-beta^2))^(1/2))*b)-1/2*i*omega*mu*M(1/2*((mu*(omega^2*ef*kappa^2
-(omega^2*mu*ef-beta^2)*mu))^(1/2)+beta*kappa)/(mu*(omega^2*ef*kappa^2
-(omega^2*mu*ef-beta^2)*mu))^(1/2),1,2*b*((omega^2*ef*kappa^2-(omega^2*mu*ef-beta^2)
*mu)/mu)^(1/2))*beta*kappa/(exp(b*(omega^2*ef*kappa^2/mu-(omega^2*mu*ef-beta^2))^(1/2))
*(mu*omega^2*ef*kappa^2-(omega^2*mu*ef-beta^2)*mu^2)^(1/2)*b)-i*omega*kappa*beta*
M(1/2*((mu*(omega^2*ef*kappa^2-(omega^2*mu*ef-beta^2)*mu))^(1/2)+beta*kappa)/
(mu*(omega^2*ef*kappa^2-(omega^2*mu*ef-beta^2)*mu))^(1/2),1,2*b*
```

```
((omega^2*ef*kappa^2-(omega^2*mu*ef-beta^2)*mu)/mu)^(1/2))/exp(b*(omega^2*ef*kappa^2/mu-
(omega^2*mu*ef-beta^2))^(1/2)))/(omega^2*mu*ef-beta^2);
```

```
Et32:=b->
(-i*omega*mu*(omega^2*ef*kappa^2/mu-(omega^2*mu*ef-beta^2))^(1/2)*
U(1/2*((mu*(omega^2*ef*kappa^2-(omega^2*mu*ef-beta^2)*mu))^(1/2)+beta*kappa)/
(mu*(omega^2*ef*kappa^2-(omega^2*mu*ef-beta^2)*mu))^(1/2),1,
2*b*((omega^2*ef*kappa^2-(omega^2*mu*ef-beta^2)*mu)/mu)^(1/2))/exp(b*(omega^2*ef*kappa^2
/mu-(omega^2*mu*ef-beta^2))^(1/2))+1/4*i*omega*mu*U(1/2*((mu*(omega^2*ef*kappa^2
-(omega^2*mu*ef-beta^2)*mu))^(1/2)+beta*kappa)/(mu*(omega^2*ef*kappa^2
-(omega^2*mu*ef-beta^2)*mu))^(1/2)+1,1,2*b*((omega^2*ef*kappa^2-(omega^2*mu*ef-beta^2)
*mu)/mu)^(1/2))/(exp(b*(omega^2*ef*kappa^2/mu-(omega^2*mu*ef-beta^2))^(1/2))*b)+
1/2*i*omega*mu*U(1/2*((mu*(omega^2*ef*kappa^2-(omega^2*mu*ef-beta^2)*mu))^(1/2)+
beta*kappa)/(mu*(omega^2*ef*kappa^2-(omega^2*mu*ef-beta^2)*mu))^(1/2)+1,1,2*b*
((omega^2*ef*kappa^2-(omega^2*mu*ef-beta^2)*mu)/mu)^(1/2))*beta*kappa/
(exp(b*(omega^2*ef*kappa^2/mu-(omega^2*mu*ef-beta^2))^(1/2))*(mu*omega^2*ef*kappa^2
-(omega^2*mu*ef-beta^2)*mu^2)^(1/2)*b)+1/4*i*omega*mu*U(1/2*((mu*(omega^2*ef*kappa^2
-(omega^2*mu*ef-beta^2)*mu))^(1/2)+beta*kappa)/(mu*(omega^2*ef*kappa^2-(omega^2*mu*ef
-beta^2)*mu))^(1/2)+1,1,2*b*((omega^2*ef*kappa^2-(omega^2*mu*ef-beta^2)*mu)/mu)^(1/2))
*beta^2*kappa^2/(exp(b*(omega^2*ef*kappa^2/mu-(omega^2*mu*ef-beta^2))^(1/2))*
(mu*omega^2*ef*kappa^2-(omega^2*mu*ef-beta^2)*mu^2)*b)-1/2*i*omega*mu*
U(1/2*((mu*(omega^2*ef*kappa^2-(omega^2*mu*ef-beta^2)*mu))^(1/2)+beta*kappa)/
(mu*(omega^2*ef*kappa^2-(omega^2*mu*ef-beta^2)*mu))^(1/2),1,2*b*((omega^2*ef*kappa^2
-(omega^2*mu*ef-beta^2)*mu)/mu)^(1/2))/(exp(b*(omega^2*ef*kappa^2/mu-
(omega^2*mu*ef-beta^2))^(1/2))*b)-1/2*i*omega*mu*U(1/2*((mu*(omega^2*ef*kappa^2
-(omega^2*mu*ef-beta^2)*mu))^(1/2)+beta*kappa)/(mu*(omega^2*ef*kappa^2
-(omega^2*mu*ef-beta^2)*mu))^(1/2),1,2*b*((omega^2*ef*kappa^2-(omega^2*mu*ef-beta^2)*mu)
/mu)^(1/2))*beta*kappa/(exp(b*(omega^2*ef*kappa^2/mu-(omega^2*mu*ef-beta^2))^(1/2))
```

```
*(mu*omega^2*ef*kappa^2-(omega^2*mu*ef-beta^2)*mu^2)^(1/2)*b)-i*omega*kappa*beta
*U(1/2*((mu*(omega^2*ef*kappa^2-(omega^2*mu*ef-beta^2)*mu))^(1/2)+beta*kappa)/
(mu*(omega^2*ef*kappa^2-(omega^2*mu*ef-beta^2)*mu))^(1/2),1,2*b*((omega^2*ef*kappa^2
-(omega^2*mu*ef-beta^2)*mu)/mu)^(1/2))/exp(b*(omega^2*ef*kappa^2/mu
-(omega^2*mu*ef-beta^2))^(1/2)))/(omega^2*mu*ef-beta^2);


 Et3 := r-> c3*Et31(r)+d3*Et32(r) ;
```

```
Hr3:=r->
1/2*I*beta^2*d3*KummerU(1/2*(3*(kc^2*mu+omega^2*ef*kappa^2)^(1/2)*mu^(1/2)+beta*kappa)/
((kc^2*mu+omega^2*ef*kappa^2)^(1/2)*mu^(1/2)),1,2*(kc^2*mu+omega^2*ef*kappa^2)^(1/2)*r/
mu^(1/2))*kappa/(exp((kc^2*mu+omega^2*ef*kappa^2)^(1/2)*r/mu^(1/2))*kc^2*mu^(1/2)*r*
(kc^2*mu+omega^2*ef*kappa^2)^(1/2))-1/2*I*beta*d3*
KummerU(1/2*((kc^2*mu+omega^2*ef*kappa^2)^(1/2)*mu^(1/2)+beta*kappa)/
((kc^2*mu+omega^2*ef*kappa^2)^(1/2)*mu^(1/2)),1,2*(kc^2*mu+omega^2*ef*kappa^2)^(1/2)*r
/mu^(1/2))*omega^2*ef*kappa^2/(exp((kc^2*mu+omega^2*ef*kappa^2)^(1/2)*r/mu^(1/2))*kc^2*r*
(kc^2*mu+omega^2*ef*kappa^2))+1/2*I*beta*c3*KummerM(1/2*(3*(kc^2*mu+omega^2*ef*kappa^2)
^(1/2)*mu^(1/2)+beta*kappa)/((kc^2*mu+omega^2*ef*kappa^2)^(1/2)*mu^(1/2)),1,2*(kc^2*mu+
omega^2*ef*kappa^2)^(1/2)*r/mu^(1/2))*omega^2*ef*kappa^2/(exp((kc^2*mu+omega^2*ef*
kappa^2)^(1/2)*r/mu^(1/2))*kc^2*r*(kc^2*mu+omega^2*ef*kappa^2))-1/2*I*beta^2*d3*
KummerU(1/2*((kc^2*mu+omega^2*ef*kappa^2)^(1/2)*mu^(1/2)+beta*kappa)/((kc^2*mu+omega^2*
ef*kappa^2)^(1/2)*mu^(1/2)),1,2*(kc^2*mu+omega^2*ef*kappa^2)^(1/2)*r/mu^(1/2))*kappa/
(exp((kc^2*mu+omega^2*ef*kappa^2)^(1/2)*r/mu^(1/2))*kc^2*mu^(1/2)*r*(kc^2*mu+omega^2*ef
*kappa^2)^(1/2))-I*mu*omega^2*ef*kappa*d3*KummerU(1/2*((kc^2*mu+omega^2*ef*kappa^2)^(1/2)
*mu^(1/2)+beta*kappa)/((kc^2*mu+omega^2*ef*kappa^2)^(1/2)*mu^(1/2)),1,2*(kc^2*mu+omega^2*
ef*kappa^2)^(1/2)*r/mu^(1/2))/(exp((kc^2*mu+omega^2*ef*kappa^2)^(1/2)*r/mu^(1/2))*
(kc^2*mu+omega^2*ef*kappa^2))-1/2*I*mu*beta*d3*KummerU(1/2*((kc^2*mu+omega^2*ef*kappa^2)
^(1/2)*mu^(1/2)+beta*kappa)/((kc^2*mu+omega^2*ef*kappa^2)^(1/2)*mu^(1/2)),1,2*(kc^2*mu+
omega^2*ef*kappa^2)^(1/2)*r/mu^(1/2))/(exp((kc^2*mu+omega^2*ef*kappa^2)^(1/2)*r/mu^(1/2))
*r*(kc^2*mu+omega^2*ef*kappa^2))+1/2*I*beta^2*c3*KummerM(1/2*(3*(kc^2*mu+omega^2*ef*
kappa^2)^(1/2)*mu^(1/2)+beta*kappa)/((kc^2*mu+omega^2*ef*kappa^2)^(1/2)*mu^(1/2)),1,
2*(kc^2*mu+omega^2*ef*kappa^2)^(1/2)*r/mu^(1/2))*kappa/(exp((kc^2*mu+omega^2*ef*kappa^2)
^(1/2)*r/mu^(1/2))*kc^2*mu^(1/2)*r*(kc^2*mu+omega^2*ef*kappa^2)^(1/2))-I*mu*omega^2*ef
```

```
*kappa*c3*KummerM(1/2*((kc^2*mu+omega^2*ef*kappa^2)^(1/2)*mu^(1/2)+beta*kappa)/
((kc^2*mu+omega^2*ef*kappa^2)^(1/2)*mu^(1/2)),1,2*(kc^2*mu+omega^2*ef*kappa^2)^(1/2)*r/
mu^(1/2))/(exp((kc^2*mu+omega^2*ef*kappa^2)^(1/2)*r/mu^(1/2))*(kc^2*mu+omega^2*ef*
kappa^2))-I*(kc^2*mu+omega^2*ef*kappa^2)^(1/2)*beta*c3*KummerM(1/2*((kc^2*mu+omega^2*ef
*kappa^2)^(1/2)*mu^(1/2)+beta*kappa)/((kc^2*mu+omega^2*ef*kappa^2)^(1/2)*mu^(1/2)),1,
2*(kc^2*mu+omega^2*ef*kappa^2)^(1/2)*r/mu^(1/2))/(exp((kc^2*mu+omega^2*ef*kappa^2)^(1/2)
*r/mu^(1/2))*kc^2*mu^(1/2))-1/2*I*beta*c3*KummerM(1/2*((kc^2*mu+omega^2*ef*kappa^2)^(1/2)
*mu^(1/2)+beta*kappa)/((kc^2*mu+omega^2*ef*kappa^2)^(1/2)*mu^(1/2)),1,2*(kc^2*mu+omega^2
*ef*kappa^2)^(1/2)*r/mu^(1/2))*omega^2*ef*kappa^2/(exp((kc^2*mu+omega^2*ef*kappa^2)^(1/2)
*r/mu^(1/2))*kc^2*r*(kc^2*mu+omega^2*ef*kappa^2))-I*omega^4*ef^2*kappa^3*c3*KummerM(1/2*
((kc^2*mu+omega^2*ef*kappa^2)^(1/2)*mu^(1/2)+beta*kappa)/((kc^2*mu+omega^2*ef*kappa^2)
^(1/2)*mu^(1/2)),1,2*(kc^2*mu+omega^2*ef*kappa^2)^(1/2)*r/mu^(1/2))/(exp((kc^2*mu+omega^2
*ef*kappa^2)^(1/2)*r/mu^(1/2))*kc^2*(kc^2*mu+omega^2*ef*kappa^2))-I*(kc^2*mu+omega^2*ef*
kappa^2)^(1/2)*beta*d3*KummerU(1/2*((kc^2*mu+omega^2*ef*kappa^2)^(1/2)*mu^(1/2)+
beta*kappa)/((kc^2*mu+omega^2*ef*kappa^2)^(1/2)*mu^(1/2)),1,2*(kc^2*mu+omega^2*ef*
kappa^2)^(1/2)*r/mu^(1/2))/(exp((kc^2*mu+omega^2*ef*kappa^2)^(1/2)*r/mu^(1/2))*kc^2*mu
^(1/2))-1/2*I*beta^2*c3*KummerM(1/2*((kc^2*mu+omega^2*ef*kappa^2)^(1/2)*mu^(1/2)+beta
*kappa)/((kc^2*mu+omega^2*ef*kappa^2)^(1/2)*mu^(1/2)),1,2*(kc^2*mu+omega^2*ef*kappa^2)
^(1/2)*r/mu^(1/2))*kappa/(exp((kc^2*mu+omega^2*ef*kappa^2)^(1/2)*r/mu^(1/2))*kc^2*mu
^(1/2)*r*(kc^2*mu+omega^2*ef*kappa^2)^(1/2))-I*omega^4*ef^2*kappa^3*d3*KummerU(1/2*
((kc^2*mu+omega^2*ef*kappa^2)^(1/2)*mu^(1/2)+beta*kappa)/((kc^2*mu+omega^2*ef*kappa^2)
^(1/2)*mu^(1/2)),1,2*(kc^2*mu+omega^2*ef*kappa^2)^(1/2)*r/mu^(1/2))/(exp((kc^2*mu+
omega^2*ef*kappa^2)^(1/2)*r/mu^(1/2))*kc^2*(kc^2*mu+omega^2*ef*kappa^2))+1/4*I*beta*d3*
KummerU(1/2*(3*(kc^2*mu+omega^2*ef*kappa^2)^(1/2)*mu^(1/2)+beta*kappa)/((kc^2*mu+omega^2
*ef*kappa^2)^(1/2)*mu^(1/2)),1,2*(kc^2*mu+omega^2*ef*kappa^2)^(1/2)*r/mu^(1/2))*omega^2
```

```
*ef*kappa^2/(exp((kc^2*mu+omega^2*ef*kappa^2)^(1/2)*r/mu^(1/2))*kc^2*r*(kc^2*mu+omega^2
*ef*kappa^2))+1/4*I*mu*beta*d3*KummerU(1/2*(3*(kc^2*mu+omega^2*ef*kappa^2)^(1/2)*mu^(1/2)
+beta*kappa)/((kc^2*mu+omega^2*ef*kappa^2)^(1/2)*mu^(1/2)),1,2*(kc^2*mu+omega^2*ef*
kappa^2)^(1/2)*r/mu^(1/2))/(exp((kc^2*mu+omega^2*ef*kappa^2)^(1/2)*r/mu^(1/2))*r*(kc^2*mu
+omega^2*ef*kappa^2))-1/2*I*mu*beta*c3*KummerM(1/2*((kc^2*mu+omega^2*ef*kappa^2)^(1/2)*mu
^(1/2)+beta*kappa)/((kc^2*mu+omega^2*ef*kappa^2)^(1/2)*mu^(1/2)),1,2*(kc^2*mu+omega^2*ef*
kappa^2)^(1/2)*r/mu^(1/2))/(exp((kc^2*mu+omega^2*ef*kappa^2)^(1/2)*r/mu^(1/2))*r*(kc^2*mu
+omega^2*ef*kappa^2))+1/2*I*mu*beta*c3*KummerM(1/2*(3*(kc^2*mu+omega^2*ef*kappa^2)^(1/2)*
mu^(1/2)+beta*kappa)/((kc^2*mu+omega^2*ef*kappa^2)^(1/2)*mu^(1/2)),1,2*(kc^2*mu+omega^2*
ef*kappa^2)^(1/2)*r/mu^(1/2))/(exp((kc^2*mu+omega^2*ef*kappa^2)^(1/2)*r/mu^(1/2))*r*(kc^2
*mu+omega^2*ef*kappa^2))+1/4*I*beta^3*d3*KummerU(1/2*(3*(kc^2*mu+omega^2*ef*kappa^2)
^(1/2)*mu^(1/2)+beta*kappa)/((kc^2*mu+omega^2*ef*kappa^2)^(1/2)*mu^(1/2)),1,2*(kc^2*mu+
omega^2*ef*kappa^2)^(1/2)*r/mu^(1/2))*kappa^2/(exp((kc^2*mu+omega^2*ef*kappa^2)^(1/2)*r/
mu^(1/2))*kc^2*mu*r*(kc^2*mu+omega^2*ef*kappa^2));
```

```
Et1(a)+Ez1(a)*T=0; solve(%,c1); c1:= %;

Et2(a)+Ez2(a)*T=0; solve(%,b2); b2:= %;

Ez1(a)-Et1(a)*T=Ez2(a)-Et2(a)*T;  solve(%,c2);c2:=%;

Ht1(a)+Hz1(a)*T= Ht2(a)+Hz2(a)*T; solve(%,d2);d2:=%;

Ez2(b)=Ez3(b);solve(%,a3);a3:=%; Ht2(b)=Ht3(b);solve(%,b3);b3:=%;

Et2(b)=Et3(b);solve(%,c3);c3:=%; Hz2(b)=Hz3(b);solve(%,d3);d3:=%;

Ez4(c)=Ez3(c);solve(%,a4);a4:=%; Ht4(c)=Ht3(c);solve(%,b4);b4:=%;

Et4(c)=Et3(c);solve(%,c4);c4:=%; Hz4(c)=Hz3(c);solve(%,d4);d4:=%;

Et4(d)=0;solve(%,a2);a2:=%;
Hr1c:=x-> subs(I=-I, Hr1(x)); Ht1c:=x-> subs(I=-I, Ht1(x));

Hr2c:=x-> subs(I=-I, Hr2(x)); Ht2c:=x-> subs(I=-I, Ht2(x));

Hr3c:=x-> subs(I=-I, Hr3(x)); Ht3c:=x-> subs(I=-I, Ht3(x));

Hr4c:=x-> subs(I=-I, Hr4(x)); Ht4c:=x-> subs(I=-I, Ht4(x));


S1:= Er1(r)*Ht1c(r)-Et1(r)*Ht1c(r);


S2:= Er2(r)*Ht2c(r)-Et2(r)*Ht2c(r);


S3:= Er3(r)*Ht3c(r)-Et3(r)*Ht3c(r);


S4:= Er4(r)*Ht4c(r)-Et4(r)*Ht4c(r);
```

```
P1:= int(r*S1,r=0a);

P2:= int(r*S2,r=ab);

P3:= int(r*S3,r=bc);

P4:= int(r*S4,r=cd);


rho1:=2.5*10^(-8);

rho2:=rho1;

rho4:= rho1;

Rs1:=sqrt(evalf(Pi)*mu0*f*rho1);

Rs2:=sqrt(evalf(Pi)*mu0*f*rho2);

Rs4:=sqrt(evalf(Pi)*mu0*f*rho4);


PL1:=   Rs1/2*( ( abs(Hz1(a)) )^2 + (abs(Ht1(a)))^2 )+

        Rs2/2*((abs(Hz2(a)) )^2 + (abs(Ht2(a)))^2 );


PL2:=   Rs4/2*( ( abs(Hz4(d)) )^2 + (abs(Ht4(d)))^2 );


alpha:= (a*PL1+d*PL2)/(P1+P2+P3+P4);
```

# Bibliography


[1] LINKHART, D., *Microwave Circulator Design*, The Artech House Microwave Library 1989.

[2] GRANT, I.S. and PHILLIPS, W.R., *Electromagnetism*, John Wiley & Sons and Ltd 1990.

[3] BADEN-FULLER, A.J., *An introduction to the use of ferrite and garnet materials at microwave and optical frequencies*, Electronics and Communication Engineering Journal, Vol. 7, Issue 2, pp. 72-80, April 1995.

[4] BADEN-FULLER, A.J., *Ferrites at microwave Frequencies*, IEE Electromagnetic Waves 1987.

[5] POLDER, P., *On the Theory of Ferromagnetic Resonance*, Philosophical Magazine, Vol. 40, pp. 99-115, 1949.

[6] HELSZAJN, J., *Microwave Engineering: Passive, Active and NON-Reciprocal Circuits*, McGraw-Hill Book Company 1992.

[7] JASPER, L. J. *Effects of a Gyromagnetic Material in a Double-Coupled Helix Traveling-Wave Tube*. IEEE Transactions on Electron Devices, Vol. 17, No. 4, pp. 353-365, April 1970.

[8] SUHL, H. and WALKER, L.R., *Part II - Transverse Magnetisation and the Non-Reciprocal Helix*, Bell System Technical Journal, Vol. 33, pp. 939-986, March 1954.

[9] RAMO, S., WHINNERY, J. R. and DAUZER, T.V. *Fields and Waves in Communication Electronics*. John Whiley & Sons. Inc. 1993.

[10] RAMO, S., WHINNERY, J. R. and DAUZER, T.V. *Fields and Waves in Communication Electronics*. John Whiley & Sons. Inc. 1993.

[11] VENDIK, I.B., PLESKACHEV, V. and VENDIK, O.G., *Figure of Merit and Limiting Characteristics of Tunable Ferroelevtric Microwave Devices*, Progress In Electromagnetics Research Symposium, Vol. 1, No. 3, pp. 327-330, August 2005.

[12] ADAM, J.D., DAVIS, L.E., DIONNE, G.E., SCHLOEMANN and E.F., STIZZER, S.N., *Ferrite Devices and Materials*, IEEE Transactions on Microwave Theory and Technique, Vol. 50, No. 3, pp. 721-740, March 2002.

[13] COLLINS, R.E., *Foundations for Microwave Engineering*, IEEE/OUP Series on Electromagnetic Wave Theory, 2000.

[14] PIERCE, J. and Field, L.M., *Travelling-Wave Tubes*. Proceedings of the IRE., Vol. 35, pp. 108-111, February 1947.

[15] Thales Electron Devices, GmbH.

[16] WATKINS, D.A., *Topics in Electromagnetic Wave*, John Wiley & Sons, Inc., New York, 1958.

[17] SENSIPER, S., *Electromagnetic Wave Propagation on Helical Structures (A Review and Survey of Recent Progress)*, Proceedings of the IRE, Vol. 43, Issue 2, pp. 149-161, February 1955.

[18] CORUM, K. L. and CORUM, J. F., *RF Coils, Helical Resonators and Voltage Magnification by Coherent Spatial Modes*. Telecommunications in Modern Satellite, Cable and Broadcasting Service, 2001. Vol. 1, pp. 339 - 348, September 2001.

[19] GILMOUR, A.S., GILLETTE, M.R. and CHEN, J., *Theoretical and Experimental TWT Helix Loss Determination*, IEEE Transactions on Electron Devices, Vol. ED-26, No. 10, pp. 1581-1588, October 1979.

[20] BRYANT, J.R. and WHITE, E.J., *Attenuation and Power-Handling Capability of Helical Radio-Frequency Lines*, Electronic Communications, pp. 278-282, December 1954.

[21] LOPES D. T. and MOTTA C. C., *Loss Tape-Helix Analysis of Slow-Wave Structures*, Centro Tecnologico da Marinha em Sao Paulo - CTMSP - 05508-900 Sao Paulo, SP, Brazil. pp. 222 - 225, 2005.

[22] DUAN, Z., GONG, Y., WANG, W., BASU, B.N. and WEI, Y., *Accurate tape analysis of the attenuator-coated helical slow-wave structure*, IEEE Transactions on Electron Devices, Vol. 53, No. 4, pp. 903-909, April 2006.

[23] D'AGOSTINO, S., EMMA, F. and PAOLONI, C., *Accurate Analysis of helix slow-wave structure*, IEEE Transactions on Electron Devices, Vol. 45, No. 7, pp. 1605-1613, July 1998.

[24] SWIFTHOOK, D. T. and MOTTA, C. C., *Dispersion Curves for a Helix in a Glass Tube*, The Institution of Electrical Engineers. December 1958.

[25] DUAN, Z., GONG, Y., WANG, W., BASU, B.N. and WEI, Y., *Investigation into the Effect of Dielectric Loss on RF Characteristics of Helical SWS*, International Journal of Infrared and Millimeter Waves, Vol. 29, No. 1, pp. 23-34, 2008.

[26] COOK, J.S., KOMPFNER, R. and SUHL, H., *Nonreciprocal Loss in Traveling-Wave Tubes Using Ferrite Attenuators*, Bell Telephone Labs. Murray Hill, N.J. (Correspondance), July 1954.

[27] SECKELMANN, R., *Phase-Shift Characteristics of Helical Phase Shifters*, IEEE Transactions on Microwave Theory and Techniques, Vol. MTT-14, No. 1, pp. 24-28, January 1966.

[28] IVANOV, E.P. and KOSTEV, K.G., *Propagation in Helical Line with Latching Ferrite Medium*, Microwave Conference, pp. 503-507, September 1975.

[29] IVANOV, E.P., *Analytical Study of Helical Latching Ferrite Phase Structure*, Microwave Conference, pp. 221-225, September 1978.

[30] ORLANDO, A., *Analysis of Circularly Non-Symmetric Modes in Helical Line Externally Loaded by Athimuthally Magentized Hollow Ferrite Cylinder*, Institute Technologio de Aeronautica (ITA) Microwave Department, 12228-900- Sāo José dos Campos- SP, Brazil, Asia Ferrite Microwave Conference, 1997.

[31] KAI, S. and CHAKRABORTI, N. B., *Finite-element analysis of helical phase shifters*, IRE Proceedings, Vol. 132, Part H, No. 4, pp. 176-177, July 1985.

[32] WALDRON, R.A., *FERRITES - An Introduction for Microwave Engineers*, D. Van Nostrand Company Ltd 1964.

[33] BILLINGHAM, J. and KING, A.C., *Wave Motion*. Cambridge University Press 2000.

[34] DUAN, Z., GONG, Y., WANG, W. and WEI, Y., *Theoretical Determination of TWT Helix Loss*,

[35] MANNALLM G. and KENWOOD, M., *Pure Mathematics: No. 3*, Heinemann Modular Mathematics for London AS & A-level, Heinemann 1996.

[36] HAMMING, R.W.,*Numerical Methods for Scientists and Engineers*, Dover Publications, 1987.

[37] JAIN, P. K. and BASU, B. N., *A Theory of the Attenuator-Coated Helical Slow-Wave Structure of a Travelling-Wave Tube* IEEE Transactions on Electron Devices, Vol. 35, No. 10, pp. 1750-1757, October 1988.

[38] CHERNIN, D., ANTONSEN, T.M. Jr. and LEVUSH, B. *Exact Treatment of the Dispersion and Beam Interaction Impedance of a thin Tape Helix surrounded by a Radically Stratified Dielectric*, IEEE Transactions Electron Devices, , Vol. ED-46, No. 7, pp. 1472-1483, July 1999.

[39] DAYTON, J.A. Jr., MEARINI, G.T., CHEN, H. and KORY, C.L., *Diamond-Studded Helical Traveling Wave Tube*, IEEE Transactions Electron Devices, Vol. ED-52, No. 2, pp. 695-701, May 2005.

[40] BOXER, A.S., HERSHENOV, S., LANDRY, E.F.,*A High-Power Coaxial Ferrite Phase Shifter (Correspondence)*, IRE Transactions on Microwave Theory and Techniques, Vol. 9, N0. 6, November 1961.

[41] CHE, W., YUNG, E. K., CHEN, S. and WEN, J., *Improved Analysis of Nonreciprocal Remanence Ferrite Phase Shifter in Grooved Waveguide*. IEEE Transactions on Microwave Theory and Techniques, pp. 1912-1918, August 2002.

[42] GREENE, J.J. and SANDY, F., *Microwave Characterization of Partially Magnetized Ferrites*, IEEE Transactions on Microwave Theory and Techniques, Vol. MTT-22, No. 6, pp. 641-645, June 1974.

[43] GREENE, J.J. and SANDY, F., *A Catalog of Low Power Loss Parameters and High Power Thresholds for Partially Magnetized Ferrites*, IEEE Transactions on Microwave Theory and Techniques, Vol. MTT-22, No. 6, pp. 645-651, June 1974.

[44] KRUPKA, J., *Improved Analysis of Nonreciprocal Remanence Ferrite Phase Shifter in Grooved Waveguide*, IEEE Transactions on Microwave Theory and Techniques, Vol. 50, No. 8, pp. 1912-1918, August 2002.

[45] ZHENG, G., PARDAVI-HORVATH, M., HUANG, X., KESZERi, B. and VANDLIK, J., *Experimental determination of an effective demagnetization factor for nonellipsoidal geometries*, Journal of Applied Physics, Vol. 79, No. 8, pp. 5742-5744, June 2009.

[46] WALDRON, R.A., *Electromagnetic Wave Propagating in a cylindrical waveguide containing gyromagnetic media - Part I*, Journal of the British Institution of Radio Engineers, Vol. 18, No. 10, pp. 597-612, October 1958.

[47] WALDRON, R.A., *Electromagnetic Wave Propagating in a cylindrical waveguide containing gyromagnetic media - Part II*, Journal of the British Institution of Radio Engineers, Vol. 18, No. 11, pp. 677-690, November 1958.

[48] WALDRON, R.A., *Electromagnetic Wave Propagating in a cylindrical waveguide containing gyromagnetic media - Part III*, Journal of the British Institution of Radio Engineers, Vol. 18, No. 12, pp. 733-746, December 1958.

[49] WALDRON, R.A., *Erratum: Electromagnetic Wave Propagating in a cylindrical waveguide containing gyromagnetic media*, Journal of the British Institution of Radio Engineers, Vol. 18, No. 12, pp. 746, December 1958.

[50] WALDRON, R.A., *Erratum: Electromagnetic Wave Propagating in a cylindrical waveguide containing gyromagnetic media - Part II*, Journal of the British Institution of Radio Engineers, Vol. 18, No. 12, pp. 746, December 1958.

[51] TYRAS, G., *The Permeability Matrix for a Ferrite Medium Magnetized at an Arbitrary Direction and its Eigenvalues (Correspondence).* IRE Transactions on Microwave Theory and Technique, pp. 176-177, January 1959.

[52] YANG, C.P, SMITH, P.A, DOLMAN, G, BUTTON, T.W. and CRUICKSHANK, D, *Helical Ferrite Devicesfor Non-Reciprocal Applications*, Ferroelectrics, January 2009.

[53] ZAFAR, J., HAIGH, A., MORGAN, I., ABUELMA'ATTI, A., KHAIRUDDIN, I., and GIBSON, A.A.P. *Variable Toroidal Ferrite Phase Shifters*, IET Microwaves, Antennas and Propagation, pp. 242-249, Issue 2, Volume 3, 2009.

[54] VESELOV, G.I., VORONINA, G.G., PLATONOV, N.I. and SEMENOV. S.G., *Theory of Waveguide Structures with Azimuthally Magnetized Ferrite Medium*, Proceedings of the $5^{th}$ Colloquium on Microwave Communication, pp. 385-394, 1974.

[55] KING, A.C., BILLINGHAM, J. and OTTO, S.R., *Differential Equations: Linear, Nonlinear, Ordinary, Partial*, CAmbridge University Press 2003.

[56] ABRAMOVITZ, M. and STEGUN, I.A., *Handbook of Mathematical Functions*, Dover Publication Inc. 1965.

[57] OTTO, S.R. and DENIER, J.P., *An Introduction to Programming and Numerical Methods in MATLAB*, Springer 2005.

[58] RICHARDS, D., *Advanced Mathematical Methods with Maple*, Cambridge University Press 2001.